

NATIONAL AND KAPODISTRIAN UNIVERSITY OF ATHENS

FACULTY OF GEOLOGY AND GEOENVIRONMENT

*Mineralogical, Petrographical and Geochemical Study of the
Stypsi
Porphyry-Epithermal System, Lesvos Island, Greece*

Argyrios Periferakis

Athens

2019

NATIONAL AND KAPODISTRIAN UNIVERSITY OF ATHENS

SCHOOL OF SCIENCES

FACULTY OF GEOLOGY AND GEOENVIRONMENT

*Mineralogical, Petrographical and Geochemical Study of the
Stypsi
Porphyry-Epithermal System, Lesvos Island, Greece*

Argyrios Periferakis

Examination Committee

Dr. Panagiotis Voudouris

Professor, National and Kapodistrian University of Athens, Faculty of Geology and Geoenvironment

Dr. Andreas Magganas

Professor, National and Kapodistrian University of Athens, Faculty of Geology and Geoenvironment

Dr. Vasileios Melfos

Associate Professor, Aristotle University of Thessaloniki, School of Geology

2019

To my parents

TABLE OF CONTENTS

Table of Contents.....	pg. 3-7
List of Tables.....	pg. 8
List of Figures.....	pg. 9-15
Acknowledgments.....	pg. 16-17
Foreword.....	pg. 18
Abstract.....	pg. 19
Materials and Methods.....	pg. 20
Chapter 1: The Geochemistry of Granitoids and their Relationship to Metallogeny...	pg. 21-27
1.1: Geochemical Classification of Granitoids	pg. 21-24
1.1.1: Geochemical Differences between I-type and S-type Granitoids	pg. 23
1.1.2: Aluminium Saturation Index and Granitoid Classification	pg. 24
1.2: Geotectonic Classification of Granitoids	pg. 24-25
1.3: Granitoids and Metallogeny	pg. 25-27
1.3.1: Sources of Metals in Magmas	pg. 25-26
1.3.2: Effects of Crystal Fractionation in the Metal Supply of Magmas	pg. 26-27
Chapter 2: The Main Characteristics and the Nature of Porphyry Ore Deposits.....	pg. 28-46
2.1: Geological Framework of Porphyry Deposits	pg. 28-29
2.2: Classification Scheme of Porphyry Deposits	pg. 30-34
2.2.1: Porphyry Au Deposits	pg. 31
2.2.2: Porphyry Cu Deposits	pg. 32
2.2.3: Porphyry Mo Deposits, Porphyry Sn Deposits and Porphyry W Deposits	pg. 32-34
2.3: Hydrothermal Alteration and Mineralisation	pg. 34-35
2.3.1: Spatial distribution of alteration zones	pg. 34-35
2.3.2: Temporal relationships between alteration types	pg. 35
2.4: Hydrothermal Veins in Porphyry Systems	pg. 36-40
2.4.1: Classification of Veins and Description of Vein Types	pg. 36-40
I. Veins associated with potassic alteration	pg. 37-38

II. Veins associated with sodic and/or calcic alteration	pg. 38
III. Veins associated with strong hydrolytic alteration	pg. 38-39
IV. Quartz veins lacking wall rock alteration	pg. 39
V. Late stage veins, low temperature veins and distal veins	pg. 39-40
2.4.2: Crosscutting Relationships of Veins and Relative Mineralisation and Alteration Ages	pg. 40
2.5: Spatial Distribution of Igneous and Hydrothermal Features	pg. 40-43
2.5.1: Distribution of Grade and Metal Ratios	pg. 41
2.5.2: Depth of Porphyry Systems and Correlation with Palaeosurface	pg. 41-42
2.5.3: Geometry of Ore Bodies	pg. 42
2.5.4: Metal Zoning Patterns	pg. 42
2.5.5: Structural Style of Porphyry Deposits	pg. 43
2.6: Variables Affecting the Formation of Porphyry Systems	pg.43-45
2.7: Genesis of Porphyry Systems	pg. 45-46
Chapter 3: The Main Characteristics and the Nature of Epithermal Ore Deposits.....	pg. 47-60
3.1: Low Sulfidation Epithermal Deposits	pg. 51-54
3.1.1: Volcanotectonic Setting of Low Sulfidation Deposits	pg. 52-53
3.1.2: Chemical Composition of Low Sulfidation Hydrothermal Fluids	pg. 53
3.1.3: Sources of Low Sulfidation Hydrothermal Fluids	pg. 53-54
3.2: Intermediate Sulfidation Epithermal Deposits	pg. 55-56
3.2.1: Volcanotectonic Setting of Intermediate Sulfidation Deposits	pg. 55
3.2.2: Chemical Composition of Intermediate Sulfidation Hydrothermal Fluids	pg. 55-56
3.3.3: Sources of Intermediate Sulfidation Hydrothermal Fluids	pg. 56
3.3: High Sulfidation Epithermal Deposits	pg. 57-60
3.3.1: Volcanotectonic Setting of High Sulfidation Deposits	pg. 57-58
3.3.2: Chemical Composition of High Sulfidation Hydrothermal Fluids	pg. 58
3.3.3: Sources of High Sulfidation Hydrothermal Fluids	pg. 58-60
3.4: Range of Compositions of Hydrothermal Fluids in Active Hydrothermal Systems	pg. 60
Chapter 4: Crystallography and Mineral Chemistry of Molybdenite.....	pg. 61-71
4.1 Occurrence and Geochemistry of Molybdenite	pg. 62-63
4.2 Trace Elements in Molybdenite	pg. 63-69

4.2.1: Rhenium Enrichment in Molybdenite	pg. 63-69
I. Sources and Controls of Re enrichment in molybdenite	pg. 64-66
II. Rhenium heterogeneity in molybdenite and polytypism	pg. 66-67
III. Rhenium content relative to the mineralisation stage of porphyry deposits	pg. 67
IV. Rhenium content and alteration style in porphyry deposits	pg. 68-69
4.2.2: Other Trace Elements in Molybdenite	pg. 69-71
I. Tungsten in molybdenite	pg. 70
II. Niobium and selenium in molybdenite	pg. 70
III. Tellurium in molybdenite	pg. 70
IV. Other trace elements in molybdenite	pg. 70-71
Chapter 5: Tectonic Activity in the Aegean Sea	pg. 72-80
5.1: The Geological History of the Hellenides	pg. 72-74
5.2: The Terranes and the Ophiolite Belts of the Hellenides	pg. 74-80
Chapter 6: Geology of Lesvos Island	pg. 81-88
6.1: Autochthonous Basement Unit	pg. 82-83
6.2: Allochthonous Ophiolites	pg. 83-84
6.3: Tertiary Volcanic Sequence	pg. 84-86
6.3.1: Skoutaros Unit	pg. 84
6.3.2: Acid Volcanics Unit	pg. 84-85
6.3.3: Sikaminea Unit	pg. 84
6.3.4: Mytilene Unit	pg. 84-86
6.3.5: Hypabyssal Intrusions	pg. 86
6.4: Post-Meiocene Sediments	pg. 86-88
Chapter 7: Field Observations and Geology of the Study Area	pg. 89-97
7.1: Geology of the Study Area	pg. 89-91
7.2: Veins and Alterations of the Stypsi Area	pg. 91-97
Chapter 8: Whole Rock and Bulk Rock Geochemistry	pg. 98-128
8.1: Interpretation of Geochemical Data	pg. 98-125
8.1.1: Geochemical Classification Plots	pg. 98-111
8.1.2: Harker Variation Plots	pg. 112-115
8.1.3: Larsen Variation Plots	pg. 116-119

8.1.4: Magma Series and Magma Calc/Alkali Indices	pg. 119-121
8.1.5: Geotectonic Discrimination Plots	pg. 121-124
8.1.6: Spider Plots	pg. 124-125
8.2: Bulk Ore Geochemistry	pg. 125-129
Chapter 9: Petrography and Ore Mineralogy	pg. 129-138
9.1: Petrographical Description	pg. 129-130
9.2: Ore Mineralogy	pg. 130-138
9.2.1: Sulfides	pg. 131-137
9.2.2: Sulfosalts and Oxides	pg. 137-138
Chapter 10: Discussion and Conclusions	pg. 139-141
Appendix I: Terminology Used in the Description of Porphyry Deposits	pg. 142
Appendix II: Mineralogy of Standard Alterations in Porphyry Systems	pg. 143-144
Appendix III: Distinguishing Features of Porphyry Systems' Alterations	pg. 145-146
Appendix IV: Breccia Formation and Significance in Porphyry Systems	pg. 147
Appendix V: Hydrothermal Fluid Geochemistry	pg. 148-155
V.1: Sulfide as a Ligand	pg. 148-149
V.2: Chloride as a Ligand	pg. 149-152
V.2.1: Copper Partition Coefficient and its Relation to Chloride	pg. 150-151
V.2.2: Aluminum Partition Coefficient and its Relation to Chloride	pg. 151
V.2.3: Molybdenum and Wolfram Partition Coefficients and their Relation to Chloride	pg. 151-152
V.3: Fluorine as a Ligand	pg. 152-155
V.3.1: Wolfram and Molybdenum Partition Coefficients and their Relation to Fluorine	pg. 153
V.3.2: Uranium and Thorium Partition Coefficients and their Relation to Fluorine	pg. 153
V.4: The Case of Au	pg. 154-155
V.5: A Concise View on the Controls of Ore Deposition	pg. 155
Appendix VI: Quartz Textures in Epithermal Veins	pg. 156-163
VI.1: Origins of Quartz Textures	pg. 158-159
VI.2: Implications of the Presence of Specific Quartz Textures	pg. 159-163

Appendix VII: Determination of Molybdenite's Crystal Structure and Details on Polytypism	pg. 164-169
VII.1: Determination of Molybdenite's Crystal Structure	pg. 164-165
VII.2: Polytypism in Molybdenite	pg. 165-169
VII.2.1: Polytypism and Sulfidation States	pg. 165-166
VII.2.2: Synthesis Studies of Molybdenite	pg. 166-167
VII.2.3: Polytypism in Relation to the Structural Energy of the Crystal Lattice	pg. 167
VII.2.4: Polytypism and Crystal Growth Mechanisms	pg. 167-168
VII.2.5: Polytypism in Relation to the Presence of Impurities	pg. 168
VII.2.6: Polytypism and Recrystallisation	pg. 169
Appendix VIII: Molybdenite in Greek Ore Deposits	pg. 170-172
Appendix IX: The Alpine Orogeny	pg. 173-180
IX.1: Interpretation of the Alpine Orogeny	pg. 173-175
IX.2: The Mountain Belt of the European Alps	pg. 175-180
IX.2.1: Rock Types of the Alpine Geological Setting	pg. 179
IX.2.2: The Alpine Nappes	pg. 179
IX.2.3: The Creation of the Alpine Mountain Range	pg. 180
Appendix X: Tectonics of the Central and Eastern Mediterranean Region	pg. 181-184
X.1: Tectonic Setting	pg. 182-183
X.2: Tectonic Reconstruction	pg. 184
References	pg. 185-212

LIST OF TABLES¹

Table 1.1: S-I-A-M Granitoid Characteristics	pg. 22
Table 1.2: Some Geochemical Differences between Fractionated S-type and I-type Granitoids	pg. 23
Table 1.3: Aluminium Saturation Index and Granitoid Classification	pg. 24
Table 2.1: Subtypes of Porphyry Mo Deposits and Major Characteristics	pg. 33
Table 2.2: First Descriptions of Typical Veins of Porphyry Deposits	pg. 36
Table 2.3: Spatial Relationships between Porphyry Intrusions	pg. 41
Table 4.1: Correlation between Molybdenites' Re Contents and Origin	pg. 65
Table 8.1: Geochemical Analyses Results of Fresh Samples	pg. 103-105
Table 8.2: Geochemical Analyses Results of Altered Samples	pg. 106-111
Table 8.3: Rittmann Magma Series Index Calculation Table	pg. 119
Table 8.4: Calc/alkaline Index Calculation Table	pg. 121
Table 9.1: Molybdenite Microanalyses Data and Chemical Formula	pg. 134-135
Table 9.2: Sphalerite Microanalyses Data and Chemical Formula	pg. 136
Table 9.3: Galena Microanalyses Data and Chemical Formula	pg. 137
Table Ap. II: Mineralogy of Standard Alterations in Porphyry Systems	pg. 143-144
Table Ap. III: Distinguishing Features of Porphyry Systems' Alterations	pg. 145-146
Table Ap. VI: Classification of Epithermal Quartz Textures	pg. 160
Table Ap. VII: Structural and Chemical Parametres of MS _n Layer Sulfides	pg. 168
Table Ap. VIII.1: Major Molybdenite Bearing Greek Ore Deposits and Prospects	pg. 170-171
Table Ap. VIII.2: Molybdenite Categories According to Rhenium Content in Greek Ore Deposits	pg. 173

¹ Table numbering is not sequential, as tables are numbered according to the chapters in which they are included.

LIST OF FIGURES²

Figure 2.1: The global distribution of porphyry deposits, which coincides with the Phanerozoic igneous provinces and the known orogenic belts (from Seedorff *et al.*, 2005).pg. 29

Figure 3.1: Model distribution of epithermal Au deposits in age-depth-space for the last 250 Ma of Earth history (age is shown on the X axis and depth on the Y axis; maximum age is 250 Ma and maximum depth is 20 Km), assuming that the number of the deposits on the current database (1164) represents all such deposits in the current database. Deposits enter the diagram at the upper right source region (star) at the rate of 562 deposits per m.y. and migrate (diffuse) across the diagram through time. Of the ~ 307000 deposits that formed over Phanerozoic time, about 20 % (63000) are preserved in the crust (42700 of those < 250 Ma in age are represented here), while 83 % have been removed by uplift and erosion. The gradual deepening of the maximum number of deposits with increasing time results from the loss of large numbers of deposits to erosion (from Kesler & Wilkinson, 2009).pg. 47

Figure 3.2: Schematic continental margin-scale sections illustrating selected volcanotectonic settings for high sulfidation, intermediate sulfidation, and low sulfidation epithermal deposits. a) Neutral stress to mildly extensional arc (e.g., Yanacocha, Peru). b) Compressive back arc during arc volcanism (e.g., Potosí, Bolivia). c) Compressive arc with subducted volcanism (e.g., El Indio). d) Extensional arc (e.g., Bodie, California or El Peñón, Chile). e) Extensional back arc during arc volcanism (e.g., Cerro Vanguardia, Argentina). f) Extensional back arc during transition from subduction-related to rift-related bimodal magmatism (e.g., Cripple Creek, Colorado). g) Extensional continental margin following cessation of subduction and advent of transform faulting (e.g., Bullfrog, Nevada). h) Compressive tectonism linked to transform fault boundary (e.g., McLaughlin, California). i) Restricted postcollisional magmatism during collision-induced slab breakoff and compressive tectonism (e.g., Porgera, Papua New Guinea). j) Extension due to tectonic collapse following continental collision (e.g., Baley, Russia) (from Sillitoe & Hedenquist, 2003).pg. 49

Figure 3.3: Schematic sections of end-member volcanotectonic settings and associated epithermal and related mineralization types. a) Calc-alkaline volcanic arc with neutral to mildly extensional stress state showing relationships between high- and intermediate-sulfidation epithermal and porphyry deposits (note that the complete spectrum need not be present everywhere). Early magmatic volatiles are absorbed into ground water within the volcanic edifice (shown here as a stratovolcano, but it may also be a dome setting) to produce acidic fluid for lithocap generation, over and/or supra-adjacent to the causative intrusion. Later, less acidic intermediate-sulfidation fluid gives rise to intermediate-sulfidation mineralization, both adjacent to and distal from the advanced argillic lithocap. Where the intermediate-sulfidation fluid flows through the leached lithocap environment, it evolves to a high-sulfidation fluid (Einaudi *et al.*, 2003) to produce high-sulfidation veins or disseminated mineralization, depending on the nature of the structural and lithological permeability. The high-sulfidation fluid may evolve back to intermediate-sulfidation stability during late stages, supported by paragenetic relationships and lateral transitions of high- to intermediate-sulfidation mineralogy. b) Rift with bimodal volcanism and low-sulfidation deposits. Deep neutralization of magmatic volatiles, typically reduced, results in a low-sulfidation fluid for shallow low-sulfidation vein and/or disseminated mineralization and related sinter formation (from Sillitoe & Hedenquist, 2003).pg. 50

Figure 3.4: The relationship between pressure, temperature and depth for a magmatic vapour expanding to the surface through a fracture array, in relation to the scale and geologic elements of a typical high sulfidation deposit. At the surface, rapid open system cooling occurs due to atmospheric intrusions and mixing with shallow groundwater or perched layers of condensate to produce a solfataric environment (from Henley & Burger, 2011).pg. 59

Figure 4.1: Spatial distributions of 3R/Re relationships for a hypothetical porphyry Cu deposit in cross section. To the left there is the hypothetical configuration of vein types and to the right the corresponding 3R and Re contents analogies (after Newberry, 1979b).pg. 68

Figure 4.2: A diagrammatic representation of 3R/Re relations in porphyry deposits during the various stages of molybdenite deposition and alteration (after Newberry, 1979b).pg. 69

Figure 5.1: A schematic scenario for regional extension within the Aegean. a) Regional extension initiated in the Oligocene-Miocene (~ 35 - 22 my ago) in a ~ 023° trend. b) Extension taking place in the Central Aegean while the NW Aegean

² Figure numbering is not sequential as figures are numbered according to the chapters in which they are included.

undergoes shortening. The resultant couple forced the west Aegean to rotate 30° clockwise. This semi-coherent block rotation was aided by thermal weakening of the inner margins and the pre-existing zones of weakness near the Mid-Cycladic and Scutari-Pec Lineaments. The Mid-Cycladi lineament acted as a continental fracture zone, which extended in length as it accommodated the rotation of the West Aegean block. The East Aegean block rotated about 19° counterclockwise during this period, although in a less coherent way than the West Aegean. c) At about 3 my ago, the West Aegean block rotated to such a position that it was more mechanically favourable to form new grabens trending WNW-ESE, than to continue reactivating pre-existing structures. These grabens caused the cessation of the Mid-Cycladic Lineament's activity and the splitting of the West Aegean block into two portions. The SE portion was coupled with a SW portion of the East Aegean block to form the Central Aegean block (from Walcott & White, 1998).....pg. 75

Figure 5.2: The terranes of the Hellenides, from H₁ to H₉ as described by Papanikolaou (1989, 1997). The oceanic terranes are characterised by even numbers and the continental terranes by odd numbers (from Papanikolaou, 2009).pg. 76

Figure 5.3: The main ophiolite outcrops of the Hellenides are distinguished in four different groups, the oceanic terranes H₂, H₄, H₆ and H₈. The quadrangles represent locations with characteristic transects for each terrane (from Papanikolaou, 2009).pg. 78

Figure 5.4: A schematic representation of the palaeogeographic organisation of the terranes in the Hellenides, with a reference to the location of the main tectonic units of the Hellenides belonging to each terrane (from Papanikolaou, 2009).pg. 79

Figure 5.5: Compiled lithospheric-scale cross-section of the Aegean region from the Balkan foreland to the African passive margin. This section is based upon surface geological observations as well as geophysical data. The Moho depth is taken from Bohnhoff *et al.* (2001), Papanikolaou *et al.* (2004), Kuhleemann *et al.* (2004) and Tirel *et al.* (2004). The geometry of the contact between the upper and the lower plate in the subduction zone is taken from the research of Li *et al.* (2003). The base of the lithosphere has been set at approximately 100 Km. For the part of the Moesian Platform and Srednogorie, this cross-section is based on that published by the TRANSMED team (Papanikolaou *et al.*, 2004). In the rest of the cross-section, new data have been used from Gautier & Brun (1994a, 1994b), Burg *et al.* (1996), Ricou *et al.* (1998), and Jolivet & Patriat (1999), Chamot-Rooke *et al.* (2005), Bonev *et al.* (2006), and Brun & Sokoutis (2007). The principal difference between the cross-section presented here and the cross-section presented by the TRANSMED team, is the emphasis on crustal extension given here, during the formation of the Aegean Sea in the Oligocene and Miocene (from Jolivet & Brun, 2010).pg. 80

Figure 6.1: The location of Lesvos Island in the NE Aegean Sea, in relation to the Hellenic trench, the modern volcanic arc of the Aegean and the North Anatolia fault (from Vamvoukakis, 2009).pg. 81

Figure 6.2: The geological structure of Lesvos Island according to the synthesis of existing data, as presented in this Thesis. The geological boundaries are those of Hecht (1970, 1972a, 1972b, 1973, 1974a, 1974b, 1975). The grouping of lithologies into tectonic units is modified after Pe-Piper (1978, 1980a, 1980b) and Pe-Piper & Piper (1992, 1993). The faults and their orientations are based on Hecht (1970, 1972a, 1972b, 1973, 1974, 1975), Voudouris & Alfieris (2005) and Chatzipetros *et al.* (2013).pg. 87-88

Figure 7.1: Simplified geological map of central Lesvos Island. The study area of Stypsi Therma is indicated by the blue rectangle. The large fault running from Stypsi all the way to Megala Therma, trending NNE, is clearly visible. The geological boundaries are those of Hecht (1970, 1972a, 1973, 1974b) and the grouping of lithologies into units is modified after Pe-Piper & Piper (1992, 1993). The faults and their orientations are taken from Hecht (1973, 1974b) and Voudouris & Alfieris (2005).pg. 90-91

Figure 7.2: (a) Simplified geological map of the Stypsi area (after Voudouris *et al.*, 2019). (b) Simplified alteration map of the Stypsi area, demonstrating the surface distribution of hydrothermal alteration zones and the location of the porphyry-epithermal prospect (after Voudouris *et al.*, 2019).pg. 92-93

Figure 7.3: (a) Loose stockwork of black banded quartz veins crosscutting the microgranite porphyry. (b) Linear black quartz veins stockwork inside sericitically altered microgranite porphyry. (c) Black quartz veins inside the microgranite porphyry, which has been affected by Na-Ca alteration. (d) D veins inside sericitically altered Lower Lavas.pg. 93

Figure 7.4: (a, b, c) D vein stockwork inside Lower Lavas affected by sericitic alteration, on the banks of the numerous streams to the South of Stypsi. (d) Black banded quartz veins in clasts inside a stream, with visible signs of Na-Ca alteration, as evidenced by the greenish colour of the rock.pg. 94

Figure 7.5: (a, b) D veins quartz stockwork in situ on the bank of one of the numerous streams crosscutting the area. (c) Black banded quartz veins inside the microgranite porphyry, which is affected by Na-Ca alteration. (d) Relatively fresh subvolcanite to the SE of Stypsi.pg. 95/97

Figure 7.6: (a) Panoramic view of the silica cup which is to the East of Stypsi. The photo has been taken 400 m directly South of the silica cup. (b) View of the silica cup with the village of Stypsi to the West. The photo is taken roughly 150 m to the West of the aforementioned location. (c) Panoramic view of the sericitic alteration of the Skoutaros Lavas, below the silica cup. This photo is taken 70 m to the West of the silica cup, facing towards SW. (d). Panoramic view of the silica cup and the surrounding area, illustrating the transition between the lithocap and the underlying sericitic alteration. This photo is taken roughly 250 m West of Stypsi.pg. 95/97

Figure 7.7: (a) Weak D veins stockwork inside sericitically altered Lower Lavas, about 400 m SSE of the village of Stypsi. (b) Weathered propylitic alteration roughly 600 m SSE of Stypsi. (c) Relatively fresh Upper Lavas, about 100 m to the NE of the silica cup, by the road. (d) The transition between sericitic and phyllic alteration, inside the Skoutaros Lavas, 200 m SSW of Stypsi.pg. 96-97

Figure 8.1: Geochemical classification plots. (a) TAS geochemical classification plot, where the samples from the Skoutaros Unit plot into the basaltic andesite, basaltic trachyandesite and trachyandesite fields, the samples from the Sikaminea Unit plot into the trachyte-trachydacite field, and the samples from the microgranite porphyry plot into the rhyolite field (after le Bas *et al.*, 1986). (b) TAS geochemical classification plot, where it can be observed that the samples from the Skoutaros Unit (blue circles) plot into the basaltic andesite and trachyandesite fields, the samples from the Sikaminea Unit (purple rectangles) plot into the dacite and rhyolite fields, and the samples from the microgranite porphyry (green triangles) plot into the rhyolite field (after Cox *et al.*, 1979). (c) TAS geochemical classification plot, where it can be observed that the samples from the Skoutaros Unit (blue circles) are classified as basaltic trachyandesites, trachyandesites and andesites. The samples from the Sikaminea Unit (purple rectangles) are classified as trachydacite, and the samples of the microgranite porphyry (green triangles) are plotted as rhyolites (after Middlemost, 1994). (d) Jensen Cation Plot, where the samples from the Skoutaros Unit plot into the basalt and andesite fields, those from the Sikaminea Unit plot into the dacite field, and the samples from the microgranite porphyry plots into the rhyolite field (after Jensen, 1976).pg. 99

Figure 8.2: Geochemical Classification Plots. (a) A/CNK versus A/NK geochemical classification plot, where the samples from the Skoutaros Unit (blue circles) and the Sikaminea Unit (purple rectangles) are classified as either metaluminous or peraluminous, and the samples from the microgranite porphyry (green triangles) plot into the peraluminous field (after Shand, 1943). (b) R1-R2 geochemical classification plot, where the samples from the Skoutaros Unit are classified as andesite-basalts and andesites, those from the Sikaminea Unit as dacite and rhyodacite and those from the microgranite porphyry as rhyodacites (after de la Roche *et al.*, 1980). (c) Co versus Th geochemical classification plot where all the samples plot into the high-K calc-alkaline and shoshonite series field, exhibiting a basaltic to andesitic affinity (after Hastie *et al.*, 2007). (d) AFM geochemical classification plot where all the samples plot into the calc-alkaline series field (after Irvine & Baragar, 1971).pg. 100

Figure 8.3: Geochemical classification plots. (a) (Zr/TiO₂) versus SiO₂ geochemical classification plot, where the samples from the Skoutaros Unit (blue circles) plot into the trachyandesite and andesite fields, those from the Sikaminea Units (purple rectangles) plot into the rhyodacite/dacite field as well as those from the microgranite porphyry (green triangles), which are however more acidic and as such are plotted closer to the rhyolite field (after Floyd & Winchester, 1978). (b) (Nb/Y) versus (Zr/TiO₂) geochemical classification plot, where the samples from the Skoutaros Unit are plotted as andesites and the samples from the Sikaminea Unit are plotted as trachyandesites. The samples from the microgranite porphyry are plotted as rhyodacite and rhyolite (after Floyd & Winchester, 1978). (c) Nb/Y versus Zr/Ti geochemical classification plot, where the samples from the Skoutaros Unit are plotted as dacites, andesites and basaltic andesites. The samples from the Sikaminea Unit are plotted as trachyandesites, and those from the microgranite porphyry plot into the rhyolite/dacite field (modified by Pearce, 1996). (d) SiO₂ versus K₂O geochemical classification plot, where all the samples plot into the shoshonite series, with the exception of one sample from the Skoutaros Unit, which plots into the high-K calc-alkaline series field (after Peccerillo & Taylor, 1976).pg. 101

Figure 8.4: Harker binary plots of SiO₂ versus main elements. (a) Binary plot of SiO₂ versus Al₂O₃ (after Harker, 1909). (b) Binary plot of SiO₂ versus CaO (after Harker, 1909). In both plots there is a distinct negative trend, which is expected in this case, where all the igneous rocks occur following the fractional crystallisation of a common magma source.pg. 112

Figure 8.5: Harker binary plots of SiO₂ versus main elements. (a) Binary plot of SiO₂ versus FeO. In this plot, the trend is negative, an expected result in this case, as mentioned above (after Harker, 1909). (b) Binary plot of SiO₂ versus K₂O, where

the distinct positive trend corroborates the aforementioned conclusions for a common magmatic source (after Harker, 1909).
.....pg. 113

Figure 8.6: Harker binary plots of SiO₂ versus main elements. (a) Binary plot of SiO₂ versus MgO (after Harker, 1909). (b) Binary plot of SiO₂ versus MnO (after Harker, 1909). In both plots the trend is negative, which is explained by the fractional crystallisation of a common magma source.pg. 113

Figure 8.7: Harker binary plots of SiO₂ versus main elements. (a) Binary plot of SiO₂ versus Na₂O (after Harker, 1909). The trend is distinctly positive as in most cases of fractional crystallisation (after Harker, 1909). (b) Binary plot of SiO₂ versus TiO₂, where the trend is, expectedly, distinctly negative (after Harker, 1909).pg. 114

Figure 8.8: Harker binary plots of SiO₂ versus trace elements. (a) Binary plot of SiO₂ versus Sr. The trend is positive as in most cases of fractional crystallisation (after Harker, 1909). (b) Binary plot of SiO₂ versus V. The trend is distinctly positive, as V decreases with increasing SiO₂ content (after Harker, 1909).pg. 115

Figure 8.9: Harker binary plots of SiO₂ versus trace elements. (a) Binary plot of SiO₂ versus Ba (after Harker, 1909). (b) Binary plot of SiO₂ versus Y (after Harker, 1909). In both plots there is a distinct clustering of the samples from the Skoutaros Unit (blue circles) on one side and from the Sikaminea Unit (purple rectangles) and microgranite porphyry (green triangles) on the other side.pg. 115

Figure 8.10: Harker binary plots of SiO₂ versus trace elements. (a) Binary plot of SiO₂ versus Rb, where a clear positive trend can be observed (Harker, 1909). (b) Binary plot of SiO₂ versus Zr, where there is a loosely defined positive trend (after Harker, 1909).pg. 115

Figure 8.11: Larsen binary plots of Larsen Index versus main elements. (a) Binary plot of L.I. versus Al₂O₃. The trend is negative with increasing L.I. (after Larsen, 1938). (b) Binary plot of L.I. versus K₂O. The trend is positive with increasing L.I. (after Larsen, 1938). (c) Binary plot of L.I. versus Na₂O. There is a vague positive trend for the samples of the Skoutaros and the Sikaminea Units (after Larsen, 1938). (d) Binary plot of L.I. versus SiO₂. The trend is clear and distinctly positive (after Larsen, 1938).pg. 116-117

Figure 8.12: Larsen binary plots of Larsen Index versus main elements. (a) Binary plot of L.I. versus CaO. The trend is distinctly negative (after Larsen, 1938). (b) Binary plot of L.I. versus FeO. The trend is expectedly negative (after Larsen, 1938). (c) Binary plot of L.I. versus MgO. The trend is clearly negative with increasing L.I. (after Larsen, 1938). (d) Binary plot of L.I. versus TiO₂. The trend is again distinctly negative (after Larsen, 1938).pg. 118-119

Figure 8.13: Binary plot of Rittmann Series Index versus SiO₂. The distinct clustering of samples reveals the existence of three different types of igneous rocks. In particular, the proximity of the Sikaminea Unit Samples (purple rectangles) and the microgranite porphyry samples (green triangles) indicates their similar geochemical affinities (after Rittmann, 1957).pg. 120

Figure 8.14: Binary plot of SiO₂ versus [CaO/(Na₂O + K₂O)]. (a) The plot, where the positions of the samples relative to the axes and to each other are presented. (b) The same plot with the least squares lines drawn for the three sample populations and the projection on the x axis for each one, corresponding to the value 1 of the y axis (after Christiansen & Lipman, 1972).pg. 121

Figure 8.15: Geotectonic discrimination plots. (a) Ta/Yb versus Th/Yb plot. Most samples plot into the oceanic arcs field, while one sample from the Skoutaros Unit plots into the active continental margins field (after Gorton & Schandl, 2000). (b) Ta versus Th plot, where all the samples plot into the active continental margins field (after Schandl & Gorton, 2002). (c) Ta/Hf versus Th/Hf plot, where all the samples plot again into the active continental margin field (after Schandl & Gorton, 2002). (d) Yb versus Th/Ta plot. Most samples plot into the oceanic arcs field, and one sample from the Skoutaros Unit plots into the active continental margins field (after Gorton & Schandl, 2000).pg. 122

Figure 8.16: Geotectonic discrimination plots. (a) Nb/Yb versus Th/Yb, where all the samples plot into the volcanic array series (after Pearce, 2008). (b) Nb/Yb versus TiO₂/Yb plot, where the samples from the microgranite porphyry plot away from the basalt fields, whereas the other samples, which have a basaltic component, plot nearer the basalt fields. Their slight scattering may be attributed to slight alteration or weathering (after Pearce, 2008).pg. 123

Figure 8.17: Geotectonic discrimination plots. (a) Hf versus (3 · Ta) versus (Rb/30) ternary plot, where all the samples plot into the volcanic arc field. The one exception is the sample from Sikamina Unit (the other one is not plotted because no Hf analysis is available) which due to slight weathering plots in the boundary with Group 3: post-collision calc-alkaline

intrusions. Group 2 corresponds to syn-collision peraluminous intrusions, while WP corresponds to within plate rocks (after Harris *et al.*, 1986). (b) Multivariate geotectonic discrimination plot of $R_1 = 4 \cdot Si - 11 \cdot (Na + K) - 2 \cdot (Fe + Ti)$ versus $R_2 = 6 \cdot Ca + 2 \cdot Mg + Al$. All the fresh samples plot in the pre-plate collision field, whereas the samples from the microgranite porphyry plot into the syn-collision field. This in effect indicates that they postdate the rest of the volcanics, a fact confirmed by the geochemical classification, Harker plots and magma series indices mentioned above (after Batchelor & Bowden, 1985).pg. 123

Figure 8.18: Primitive mantle normalised plot, for the fresh samples from the Skoutaros Unit (blue circles), Sikaminea Unit (purple rectangles) and the microgranite porphyry (green triangles). The microgranite porphyry samples exhibit the most negative anomaly in Nb and Ti, and the most positive ones in K, La, Ce, Pr, Zr, Eu, Dy, Y, Yb and Lu. In general, such a pattern is in conformity with the geochemical and the geotectonic classification of the volcanic rocks, and supports the conclusion that the microgranite porphyry is a more fractionated, later product, of the same magmatic source (after Sun & McDonough, 1989).pg. 124

Figure 8.19: REE chondrite normalised plot, for both the fresh samples from the Skoutaros Unit (blue circles), Sikaminea Unit (purple rectangles) and the microgranite porphyry (green triangles). The Skoutaros Unit are more enriched in all elements compared to those of the Sikaminea Unit, while the microgranite porphyry samples have a similar geochemical signature to the Skoutaros lavas. All samples exhibit enrichment in LREE in comparison to HREE (after Boynton, 1984).pg. 125

Figure 8.20: Bulk ore analyses plots. (a) Au versus Pb plot where the positive correlation is evident. (b) Au versus Sn plots where the positive correlation is more evident than in the previous diagramme.pg. 126

Figure 8.21: Bulk ore analyses plots. (a) Au versus Se plot where the positive correlation is evident. (b) Au versus Zn plot where the positive correlation is more evident than in the previous diagramme.pg. 126

Figure 8.22: Bulk ore analyses plots. (a) Binary plot of Cu versus Au, where the positive correlation is evident for some samples. (b) Binary plot of Cu versus Mo where the the positive correlation is evident for most of the samples.pg. 126

Figure 8.23: Bulk ore analyses plots. (a) Binary plot of Cu versus Bi, where the positive correlation is evident for some samples. (b) Binary plot of Cu versus Mo where the the positive correlation is evident for most of the samples.pg. 127

Figure 8.24: Bulk ore analyses plots. (a) Binary plot of Cu versus Se, where the positive correlation is evident for the majority of the samples. (b) Binary plot of Se versus Sn where the the positive correlation is evident for most of the samples.pg. 127

Figure 8.25: Bulk ore analyses plots. (a) Binary plot of Se versus Bi, where the positive correlation is evident for some samples. (b) Binary plot of Se versus Te where the the positive correlation is evident for the majority of the samples.pg. 128

Figure 8.26: Bulk ore analyses plots. (a) Binary plot of Te versus Zn, where the positive correlation is evident for some samples. (b) Binary plot of Zn versus Sn where the the positive correlation is evident for most of the samples.pg. 128

Figure 8.27: Bulk ore analyses plots. (a) Binary plot of Mo versus Au, where the positive correlation is evident for some samples. (b) Binary plot of Mo versus Re where the the positive correlation is evident for some samples.pg. 128

Figure 9.1: Photomicrographs of veins, associated hydrothermal alteration and gangue minerals, from the Stypsi system. (a, b, c) Quartz veins with granular quartz within K-feldspar altered microgranite porphyry. (d, e) Quartz + actinolite veinlets from the Na-Ca alteration of the microgranite porphyry. (f) Quartz + pyrite + epidote veinlets within the microgranite porphyry. (g, h, i) Banded quartz vein with granular quartz and botryoidal textures within K-feldspar, albite and actinolite altered trachyandesite. Metallic minerals occur in the marginal and central parts of the vein. Pyrite associated with actinolite ± chlorite occurs mostly in the centre of the veins and also crosscuts quartz in the veins, thus suggesting late deposition. (j) Sericitisation, which has overprinted an earlier alteration event. (k) Granular quartz vein with molybdenite + pyrite + chalcopyrite + molybdenite. (l) D-type veinlet associated with phyllic alteration. The mineral abbreviations are as follows: Fld: feldspar; Act: actinolite; Ep: epidote; Py: pyrite; Chl: chlorite; Cal: calcite; Ser: sericite; and are taken after Whitney & Evans (2010). Photomicrographs e, f, g, i and l are taken under PPL and the rest under XPL.pg. 130

Figure 9.2: Back scattered electron images of molybdenite from the second stage of mineralisation of the Stypsi deposit. (a) Electron microprobe mapping of Mo distribution within the molybdenite grains (after Voudouris *et al.*, 2019). (b) Electron microprobe mapping of Re distribution within the molybdenite grains (after Voudouris *et al.*, 2019).pg. 132

Figure 9.3: Back scattered electron images of molybdenite from the second stage of mineralisation of the Stypsi deposit. (a) Electron microprobe mapping of W distribution within the molybdenite grains (after Voudouris <i>et al.</i> , 2019). (b) Electron microprobe mapping of the relief of molybdenite grains (after Voudouris <i>et al.</i> , 2019).....	pg. 133
Figure 9.4: Back scattered electron image of molybdenite grains from the second stage of mineralisation of the Stypsi deposit.....	pg. 137
Figure 9.5: Mo versus Re correlation plot based on the EPMA data, as presented in Table 9.1, from the molybdenite of the samples from Stypsi.....	pg. 138
Figure 9.6: Photomicrographs of opaque mineral assemblages inside porphyry-type quartz (Qzt) veins. (a) and (b), sphalerite (Sph) in contact with pyrite (Py); (c) galena (Gln) in contact with pyrite (py); (d) and (e), sphalerite (Sph) inside pyrite (Py); (f) Fahlores (Fhl) inside pyrite (Py). Mineral abbreviations are taken after Whitney & Evans (2010).....	pg. 138
Figure VI.1: Interpretation of stages in the formation of various replacement quartz textures. The top row represents original forms of calcite. The middle row shows initial stage of replacement of calcite by quartz. The bottom row shows various quartz textures, formed after complete replacement of calcite (from Dong <i>et al.</i> , 1999).....	pg. 159
Figure VI.2: Schematic representation of the primary quartz textures in epithermal systems, along with their particular morphological characteristics (from Dong <i>et al.</i> , 1999).....	pg. 161
Figure VI.3: Schematic representation of the recrystallisation and replacement quartz textures in epithermal systems, along with their particular morphological characteristics (from Dong <i>et al.</i> , 1999).....	pg. 162
Figure VII.1: A schematic representation of the arrangement of atoms in a molybdenite crystal. This is the structure of the 2H polytype as polytypism was recognised after the first crystalligraphical study of molybdenite (after Dickinson & Pauling, 1923).....	pg. 165
Figure VII.2: A schematic representation of the crystal structure of the two molybdenite polytypes. The 2H polytype is comprises two different «types» of crystal structures, with slight differences. For the purposes of this study, no distinction between 2H ₁ and 2H ₂ polytypes is made. Instead they are referred to collectively as 2H polytypes (from Newberry, 1979a).....	pg. 166
Figure VIII.1: A schematic map of Greece, where all the molybdenite occurrences are presented, according to deposit type and location (from Voudouris <i>et al.</i> , 2013a).....	pg. 171
Figure IX.1: The neotectonic regime of the Alpine System where the major active microplates are presented, based mainly on Bogdanoff <i>et al.</i> (1964), Choubert (1968), Stöcklin (1968), McKenzie (1970) and Ryan <i>et al.</i> (1971). Key to symbols: triangles: volcanoes of Quaternary and Holocene age; circles: epicentres of earthquakes deeper than 100 Km; arrows: slip directions of plates with respect to the Eurasian plate; dashed lines: contours on Benioff zone in hundreds of kilometres. Key to abbreviations: AS: Alboran Sea; AT: Anatolian Transform; BS: Balearic Sea; HT: Hellenic Trench; IS: Ionian Sea; LS: Ligurian Sea; LVS: Levantine Sea; TS: Tyrrhenian Sea (from Dewey <i>et al.</i> , 1973).....	pg. 174
Figure IX.2: A representation of the position of Africa relative to Europe, at 180 my, 148 my, 80 my, 63 my, 53 my, 9 my and present. In A through F, the dashed and hachured lines are the outline of Africa, taken as present-day shoreline, before and after the continents rotation, as determined by palaeomagnetic data. The arrows are finite slip vectors representing the simplest path Africa could have taken to move from its position, relative to Europe, at 180 my, to successive positions at 148 my, 80 my and so on (from Dewey <i>et al.</i> , 1973).....	pg. 175
Figure IX.3: An early schematic outline of the Alpine System of Europe, North Africa and the Middle East, in Transverse Mercator Projection, showing the main zones and structures, based mainly on the earlier works of Bogdanoff <i>et al.</i> (1964), Choubert (1968) and Stöcklin (1968) (from Dewey <i>et al.</i> , 1973).....	pg. 176
Figure IX.4: A modern tectonic map of the Western and Central Alps, showing the major tectonic units. Site A, B and C correlate to the corresponding transects in Figure IX.5. Key to abbreviations of fault names: Br: Brenner; Si: Simplon; En: Engadine; In: Insubric; Gi: Giudicarie; Pu: Pustertal; Ga: Gailtal; La: Lavanttal (from Pfiffner, 2005).....	pg. 177
Figure IX.5: Three profiles through the Alpine Mountain Range, illustrating the deep structure of the orogen. The profile sites A, B and C, are those shown in Figure IX.4. (a) Transect through the Western Alps of France and Italy. (b) Transect	

through the Central Alps of Switzerland and Italy. (c) Transect through the Eastern Alps of Austria and Italy (from Pfiffner, 2005).....pg. 188

Figure X.1: Outline map delineating the main ophiolite suture zones, and showing the locations of studies concerned mainly with the Palaeozoic and Mesozoic development of the Eastern Mediterranean region. Key to numbers (each number corresponds to a study): 1: Smith (1993); 2: Himmerkus *et al.* (2006); 3: Yanev (2003); 4: Romano *et al.* (2006); 5: Robertson (2002); 6: Karamata (2006); 7: Kazmin & Tikhonova (2006); 8: Gardosh & Druckman (2006); 9: Danelian *et al.* (2006); 10: Rassios & Moores (2006); 11: Koller *et al.* (2006); 12: Garfunkel (2006); 13: Rizaoglu *et al.* (2006); 14: Morris *et al.* (2006); 15: Sharp & Robertson (1998); 16: Rice *et al.* (2006); 17: Rimmelé *et al.* (2006). Studies 1 to 7 cover the whole area (from Robertson & Mountrakis, 2006).....pg. 182

Figure X.2: Outline map delineating the main neotectonic features and presenting the locations of studies mainly concerning the Cenozoic-recent tectonic development of the Eastern Mediterranean region. Key to numbers (each number corresponds to a study): 1: Degnan & Robertson (2006); 2: Doutsos *et al.* (1993); 3: Vamvaka *et al.* (2006); 4: Muceku *et al.* (2006); 5: Westaway (2006); 6: Alçiçek *et al.* (2006); 7: Boulton *et al.* (2006); 8: Pavlides *et al.* (2006); 9: Mountrakis *et al.* (2006); 10: Tranos *et al.* (2006). Papazachos *et al.* (2006) cover the whole area (from Robertson & Mountrakis, 2006).....pg. 183

ACKNOWLEDGEMENTS

Firstly, I want to thank sincerely my supervisor, Professor Dr. Panagiotis Voudouris, who assigned to me this very interesting and challenging research topic, and helped me through to the completion of this Thesis from the very beginning. I am thankful to have been entrusted with the continuation of a research began by him many years earlier in 1999. I also want to mention my sincere gratitude to him, for he has been a constant source of inspiration and has imbued me with the passion for geology in general, and mineralogy and ore deposits in particular, which is necessary to pursue a research in such demanding disciplines. Also, fieldwork with him, in various places and countries, was an unforgettable experience. I am proud to have been his student and friend.

I must also thank Constantinos Mavrogonatos, PhD candidate in the Faculty of Geology and Geoenvironment, for his constant assistance and interest in the progress of my Thesis and for being genuinely and selflessly available to support me in personal and scientific problems. This Thesis would not have been completed without his help.

I also thank the other two members of the advisory committee, Associate Professor Dr. Vasileios Melfos, and Professor Dr. Andreas Magganas, the former for performing fluid inclusion analyses of selected samples and the latter for his insight on igneous rocks petrology and petrography.

At this point, I must also mention that I owe sincere gratitude to Dr. Christos Papatrechas, Economic Geology Department, Institute of Geology and Mineral Exploration, for he has constantly helped me though my undergraduate and postgraduate studies. Equally important was the help and support of my close and esteemed friend Natalia Papatrecha, whom has always been by my side, since the beginning of our studies back in 2010.

Since this Thesis is the cumulative result of many years of hard work in understanding and making the connections between the different disciplines of geology, I feel the need to thank, albeit briefly, those people who have helped me in this «journey of knowledge»:

- Dr. Christos Sideris, (ret.) Assistant Professor of Tectonic Geology, who during my first year as an undergraduate student made the world of geology not only interesting but also accessible to me.
- Dr. Charalambos Kranis, Assistant Professor of Neotectonics and Tectonic Geology, for his superb teaching on the subject of Neotectonics and Petroleum Geology.
- Dr. Dimitrios Papanikolaou, Emeritus Professor of Tectonic Geology, for his insights on matters of tectonic geology and particularly for his very interesting lessons, which I consider myself privileged to have attended, on geology of Greece.
- Dr. Panagiotis Pomonis, Associate Professor of Igneous Rocks Petrology, for teaching me the basics of studying rock forming minerals in thin section and of igneous rocks petrology.

- Dr. Athanasios Katerinopoulos, Emeritus Professor of Mineralogy, for sparking my interest in the marvellous world of minerals.
- Dr. Christos Koumelis, Emeritus Professor of Crystallography, for his priceless lectures on crystallography, physics and mathematics related to geology. These last three years, he took the time to teach me on many diverse matters and as such illuminated many hitherto unknown fields of study for me. I am honoured and indebted to him, for his kind interest and for the books which he gave me.
- Georgios Panagos, who taught me mathematics, physics and chemistry, during my high school years and who showed me how to think and understand the ways of science. Everything that I have thus far achieved might have been impossible if I had not known him.

From my fellow students, I thank in particular Maria Vlachomitrou, who supported me during difficult times, and without whose support I may have abandoned this research at an early stage. I must also mention Stamatis Xydous, now a Ph.D candidate at the Agricultural University of Athens, for the many hours we passed studying, in our mutual effort to complete our MSc theses.

In addition, I am eternally grateful to my beloved aunt and uncle, Sonia Loukaki and Miltiadis Papantonakis, who provided me and Constantinos Mavrogonatos with accommodation during our stay in Lesvos, to conduct fieldwork. I will never forget their sublime hospitality and their heartfelt generosity.

The support of my friends has been very important during those years. As such, I thank Nikolaos Paresoglou, Panagiotis Chatzidimitriou, Nikolaos Chamouridis and Spyrangellos Georgatos-Garcia, for the happy times we had together, their advice and their support.

Since a part of this Thesis was written during my mandatory service in the Hellenic Navy, in the Aegean Naval Command, where I am still stationed, I feel the need to thank first and foremost Warrant Officer Athanasios Bafatakis, for his help, understanding and kind interest in me. I am also thankful for the help of Warrant Officer Konstantinos Rentos, Chief Petty Officer Georgios Tsalapinas, Ensign Panagiotis Tsagiannis, Lieutenant Ioannis Papakonstantinou and Captain Charalambos Vlachos. During these last months, being in the 5th branch of the Aegean Naval Command has been a memorable experience.

Last but not least, I must thank my family in general and my parents in particular, for their constant psychological and financial support during all those years of study and academic endeavour. To them I owe everything that I have become.

Argyrios Periferakis,

Petty Officer 3rd Class, Aegean Naval Command

December 2019

FOREWORD

The present MSc Thesis was carried out within the framework of the Postgraduate Programme of Petrology-Mineralogy of the Department of Petrology and Mineralogy, Faculty of Geology and Geoenvironment, School of Sciences, National and Kapodistrian University of Athens, Greece. The topic of this Thesis was assigned to me by Associate Professor Panagiotis Voudouris in April 2016, who is my supervisor. The other two members of the three member committee are Professor Andreas Magganas and Associate Professor Vasileios Melfos.

The purpose of this MSc Thesis is the mineralogical and geochemical study of the porphyry-epithermal mineralisation at Stypsi, Lesvos Island, Greece. The initial phase of the work pertaining to this Thesis comprised the reading of relevant literature, which continued up to the completion of the Thesis. The samples presented in this Thesis were kindly provided by my supervisor, who had collected them in 1999, along with a preliminary alteration map of the prospect.

In the next stage, the samples were pulverised and sent for analyses at Bureau Veritas Labs, Vancouver, Canada. In addition, thin sections and polished sections were constructed and studied in detail under the microscope. Some selected polished sections were sent to Johanna Kolodziejczyk at the AGH University of Science and Technology in Krakow for microanalyses. Then the geochemical and microanalyses data were evaluated and interpreted for the completion of this Thesis.

Lastly, field work for the corroboration and supplementation of existing data was conducted in April 2018, in the study area, with the invaluable help of Constantinos Mavrogonatos, PhD Candidate at the Faculty of Geology and Geoenvironment. The samples collected are not presented in this Thesis since there was not enough time for evaluation of the analytical results.

Regarding the structure of this Thesis, I was opted to write it in three discrete parts. In the first part (Chapters 1 to 6) I have presented, as briefly as possible, the relevant theoretical background on the research subjects. In the second part (Chapters 7 to 10) I have presented the research results and the conclusions reached upon their evaluation. In the third part (Appendixes I to IX) I have placed all information which are related to the Chapters of the first part, but which would, in my judgement, be superfluous in the more brief theoretical analyses. The reader is referred to each Appendix by footnotes. Finally, before the main text I have placed a list of tables and a list of figures, which provides the pages and the description of all the tables and figures within the text.

ABSTRACT³

Lesvos Island comprises Lower Miocene, post-collisional volcanic to subvolcanic rocks with shoshonitic affinities overlying a metamorphic basement. The Stypsi porphyry-Cu-Mo-Au prospect is genetically related to a microgranite porphyry, which has intruded into trachyandesitic lavas of the Stypsi caldera. It comprises a stockwork of porphyry-style, black banded quartz- and quartz-actinolite veinlets associated with Na-Ca alteration, and a sericite-carbonate overprint related to IS epithermal quartz-carbonate veins. At higher topographic levels, a lithocap also hosts porphyry-style veinlets. Molybdenite, magnetite, pyrite, chalcopyrite, sphalerite, galena, bismuthinite and fahlores, are the metallic minerals of the porphyry mineralization. EPMA data indicate extremely high Re contents (up to 1.92 wt. %) in molybdenite, and low to moderate Fe contents (from 0.26 to 4.74 wt. %) in sphalerite. Fluid inclusion studies demonstrate coexistence of liquid- and vapor-rich inclusions in association with NaCl-bearing inclusions in the veinlets, suggesting that boiling occurred during the mineralization. Homogenization temperatures range between 344° and 510° C and salinities reach up to 44 % eq. NaCl. Bulk ore analyses revealed up to 843 ppm Cu, up to 76 ppm Mo, up to 0.5 ppm Au, up to 339 ppm Pb, up to 815 ppm Zn, up to 10 ppm Se, up to 4 ppm Te and Bi, and up to 23 ppm Sn. Quartz recrystallization from a silica gel is evidenced by botryoidal textures within banded quartz veinlets, a feature already described from porphyry-Au deposits. The late IS epithermal overprint, in the form of milky quartz-carbonate veins is controlled by NNE-trending faults, and extends further northwards to Megala Therma epithermal deposit, where fluorite in the veins and Au-Ag-Te enrichment occur.

Keywords: Lesvos Island, Stypsi-Megala Therma, porphyry-epithermal mineralization

³ This abstract was presented at the 8th Geochemistry Symposium, Manavgad, Turkey in May 2018.

MATERIALS AND METHODS

Sixty thin and polished sections of host rocks and sulfide mineralisation were studied by optical microscopy, and a JEOL JSM 5600 scanning electron microscope, equipped with back scattered imaging capabilities, at the Department of Mineralogy and Petrology, University of Athens.

XRF analyses of fresh and altered magmatic rocks from the study area were made at the Institute of Mineralogy and Petrology, University of Hamburg, Germany, using a Phillips PW 1220 instrument and international standards. Mineralised samples were analysed for their main and trace element content by modified (1:1:1 HNO₃:HCl:H₂O) Aqua Regia digestion Ultratrace ICP-MS analysis and Lithium Borate fusion coupled with ICP-MS analysis, in the Bureau Veritas Mineral Laboratories, Vancouver, Canada. The values of XRF analyses were utilised for SiO₂, Al₂O₃, MnO, MgO, CaO, Na₂O, Fe₂O₃, K₂O, TiO₂, P₂O₅, SO₃, Ba and Cr. The values of Aqua Regia digestion/ICP-MS analyses were utilised for Ag, As, Au, B, Be, Bi, Cd, Co, Cs, Cu, Ge, Hg, In, Mo, Li, Ni, Pb, Pd, Pt, Re, Sc, Se, Sb, Sn, Te, Tl and Zn. Finally, the values of Lithium Borate Fusion/ICP-MS were utilised for Ce, Dy, Er, Ey, Ga, Gd, Hf, Ho, La, Lu, Nb, Nd, Pr, Rb, Sm, Sr, Ta, Tb, Th, Tm, U, V, Y, Yb and Zr.

Molybdenite, sphalerite, galena, bismuthinite and fahlores, either disseminated or in veins in representative ore samples, were determined by a JEOL JXA-8230 Super Probe electron microprobe (EPMA) in the Critical Elements Laboratory at the Faculty of Geology, Geophysics, and Environmental Protection, AGH University of Science and Technology in Krakow. Operating conditions were: accelerating voltage 20 kV, beam current 20 nA, background time 10 sec and a beam diameter between 1 µm and 5 µm. The following wavelengths were used: CdL_α, InL_α, ZnK_α, CuK_α, SK_α, SnL_α, HgM_α, FeK_α, MnK_α, AgL_α, GaL_α, and GeL_α. Natural mineral standards (FeS₂) and synthetic standards (CdS, InAs, ZnS, Cu, SnS, HgTe, MnS, Ag, GaP, and GeS) were used for calibration. Average detection limits are Cd: 550 ppm, In: 230 ppm, Zn: 250 ppm, Cu: 200 ppm, S: 80 ppm, Sn: 100 ppm, Hg: 200 ppm, Fe: 100 ppm, Mn: 95 ppm, Ag: 90 ppm, Ga: 135 ppm, and Ge: 140 ppm.

CHAPTER 1: THE GEOCHEMISTRY OF GRANITOIDS AND THEIR RELATIONSHIP TO METALLOGENY

Geochemical Classification of Granitoids ~ Geotectonic Classification of Granitoids ~ Granitoids and Metallogeny

Granitoids are the most important plutonic rocks in the upper continental mantle. Since the term «**granitoids**» is used to describe a wide variety of rocks, it is to be expected that the origins and geochemical characteristics of granitoids will vary greatly (Winter, 2010).

In general, granitoids are related to crustal thickening by orogeny, either continental arc subduction or collision of sialic masses. However, it is possible in some cases for granitoids to postdate orogeny. Most often, there is some form of mantle involvement in the formation of granitoids (Winter, 2010).

1.1: GEOCHEMICAL CLASSIFICATION OF GRANITOIDS

It is possible to use many methods to classify granitoids, the simplest criterion being their mineralogical composition. It is also possible to use their chemical composition as a classification medium or their tectonic setting.

One of the most useful classification systems is the **S-I-A-M granitoid classification system**, whose origins can be traced to Chappell & White (1974). Based on their original discrimination between I-type and S-type granitoids, as well as subsequent additions, granitoids can be classified as follows:

- **I-type granitoids:** these are the granitoids whose composition suggests that they were derived by the partial melting of a mafic mantle-derived source material. Thereby their source material can be considered of igneous origin, being most probably a subcrustal underplate. Rocks of this category can either be weakly peraluminous or metaluminous. Their most common oxide is magnetite and they are hornblende-rich.
- **S-type granitoids:** the chemical composition of these granitoids suggests that they originated from partial melting of already peraluminous sedimentary rocks. Their most common oxide is ilmenite and they are biotite-rich, while most commonly containing cordierite.
- **M-type granitoids:** these granitoids are considered to have a direct magma source (White, 1979) and in this category includes the immature arc plutons and oceanic plagiogranites found in ophiolites. In effect this category represents the need for the existence of classification of island-arc granitoids.
- **A-type granitoids:** in this category all granitoids found in non-orogenic settings are included. They are mostly acidic and their chemical composition as well as their occurrence varies widely.

The aforementioned classification represents the fact that granitoids can originate from several source materials and each source material is reflected on the granitoid's chemical

composition. In the table below (Table 1.1), the main discriminating characteristics of different granitoid types are presented.

Table 1.1: S-I-A-M Granitoid Characteristics

Type	Abbreviation's Meaning	SiO ₂ (%)	$\frac{K_2O}{Na_2O}$	Ca, Sr	$\frac{A}{(C + N + K)}$	$\frac{Fe^{3+}}{Fe^{2+}}$	Cr, Ni	Notes	Petrogenesis
M	Mantle	46-70	Low	High	Low	Low	Low	Low Rb, Th, U/Low LIL and HFS	Subduction zone or ocean-intraplate/Mantle-derived
I	Igneous	53-76	Low	High in mafic rocks	Low (metaluminous to peraluminous)	Moderate	Low	High LIL to HFS ratio /Medium Rb, Th, U	Subduction zone or infrastructural (mafic to intermediate) igneous source
S	Sedimentary	65-74	High	Low	High (metaluminous)	Low	High	Variable LIL/HFS	Subduction zone or supracrustal sedimentary zone
A	Anorogenic	> 77	High Na ₂ O	Low	Variable (peralkaline)	Variable	Low	Low LIL to HFS ratio / High Fe to Mg ratio / High Ga to Al ratio	Anorogenic, stable craton or rift zone

Table data from White & Chappell (1983), Clarke (1992), and Whalen (1985)

The quantifiable geochemical characteristics of granitoids are related closely to the source material, since granitoids are an «image» of their source rocks (Chappell, 1979). The geochemical differences between source and granitoid depend upon the degree and particular characteristics of fractionation. The following general cases can be discerned:

- Partial melting of the source rocks with full restite-melt separation, in which case, following the partial melting of the source rocks, the resulting magma moves en masse forming a granite. There is consequently no fractionation of melt from the residual material. This is the case, where the chemical composition of the granitoid most closely resembles that of the source.
- Partial melting of the source rocks with no restite-melt fractionation, where the separation between restite and melt is not complete. As Chappell *et al.* (1987) assert, though not all the characteristics of the source are preserved, it is still possible to simulate the source's composition.
- Extraction of melt at the source and complete restite-melt separation, which leaves almost no possibility to estimate the source's original geochemical characteristics. Nevertheless, Chappell & Stefens (1988) postulate the some such characteristics are present in more mafic rocks.

Despite this apparently clear distinction between the different types of granitoids, it must be stressed that in reality, there are many cases where a granitoid may be a mixture of two types. In orogenic belts, there are frequently granitoids with both I-type and S-type characteristics. Also, granitoids displaying A-type geochemical attributes are not solely confined in anorogenic settings (Winter, 2010). In other words, the S-I-A-M classification scheme is an oversimplification in assuming that all granitoids will conform to these artificial boundaries.

Clarke (1992) has questioned the usefulness of the aforementioned classification, with the reasoning that it does not take into account variations in mantle reservoirs and mixings between mantle and crustal inputs.

1.1.1: Geochemical Differences between I-type and S-type Granitoids

The I-type and S-type granitoids represent the two extremes in the aforementioned classification and as such it is useful to examine their geochemical differences. S-type granites (in all cases but the most felsic rocks) are characterised by lower Na and Ca, in comparison to I-type granites. This phenomenon is caused by the chemical weathering of feldspars which leads to losses of Na and Ca. The clay component of the weathered sedimentary rocks supplies the excess Al. The following cases of granitoids can be distinguished:

- S-type granites which contain at least one mineral oversaturated in Al, with common examples being cordierite or muscovite.
- Less felsic I-type granites, containing hornblende, which are undersaturated in Al.
- Weakly Al-oversaturated I-type granites, which contain small amounts of secondary muscovite.

The weathering of sedimentary rocks also leads to losses of Sr, and this is reflected in S-type granites. O'Neil & Chappell (1977) suggest that possibly the best discrimination between felsic I-type and S-type granites lay in oxygen isotope values.

The continuing fractional crystallisation from a felsic granite melt, will affect only slightly the main element composition of the final granitoid, but will affect severely trace element content. Some geochemical differences between fractionated I-type and S-type granitoids are presented in the following table (Table 1.2).

Table 1.2: Some Geochemical Differences between Fractionated S-type and I-type Granitoids		
Element(s)	Fractionated S-type Granitoids	Fractionated I-type Granitoids
Y	Slight decrease	Dramatic increase
U	Slight increase	Slight Increase
Th	Decrease	Increase
LREE	Very low	Slight increase or decrease
HREE	Slight decrease	Dramatic increase
Data from Chappell <i>et al.</i> (1998)		

As S-type melts fractionate, the Al₂O₃ content increases, as well as phosphorus's solubility. As a consequence, S-type granites are characterised by an increased P-content and high Al₂O₃ content. The behaviour of REE and Th, under conditions of strong fractionation, is a function of the behaviour of accessory minerals, and of the phosphate phases in particular. The increased Y and HREE content in I-type melts indicates that no removal of accessory mineral containing these minerals took place, which means that these elements behave incompatibly. The differences between I-type and S-type granites are more pronounced in strongly fractionated rocks (Chappell *et al.*, 1998).

1.1.2: Aluminium Saturation Index and Granitoid Classification

Another way to classify granitoids, from a geochemical point of view, is to measure their Al saturation, according to the **Aluminium Saturation Index (ASI)** as proposed by Shand (1927) and modified by Zen (1986). The groups of granitoids according to this classification can be seen in the following table (Table 1.3).

Table 1.3: Aluminium Saturation Index Granitoid Classification

Granitoid Category	Alumina Molar Ratio	S-I-A-M Classification Correlation
Peralkaline	$Al_2O_3 < (Na_2O + K_2O)$	A-type granitoids
Peraluminous	$Al_2O_3 > (CaO + Na_2O + K_2O)$	S-type granitoids and some I-type granitoids
Metaluminous	$Al_2O_3 < (CaO + Na_2O + K_2O)$	Most mafic I-type granitoids and some S-type granitoids
Data from Chappell & White (1974) and Chappell (1999)		

In general, fractional crystallisation enriches the melt in H_2O , and causes it to become more strongly peraluminous, because of the existence of quartz and feldspars (Chappell *et al.*, 1998).

1.2: GEOTECTONIC CLASSIFICATION OF GRANITOIDS

The geotectonic classification of granitoids is considered by many researchers to be more useful than the geochemical one, as it provides the tectonic framework of their genesis and thus the associated genetic mechanism. Based on the tectonic setting on which they occur, granitoids are classified as follows (Pitcher, 1993; Winter, 2010):

- **Orogenic granitoids:** granitoids belonging to this category can be found in island arcs, in plate subduction settings. Their geochemical character moves from tholeiitic to calc-alkaline as the island arc becomes more mature. They originate from the melting of the mantle wedge and they correspond to the typical M-type granitoids, with some degree of hybridisation via interaction with the arc crust being not improbable. Also, in this category belong granitoids formed in continental arcs, which are formed from an original mantle source and subsequent assimilation of a crustal component. These are the I-type and S-type granitoids described in the previous chapter, with hybrid magmas being a common occurrence. Most orogenic granitoids are associated with culminations of metamorphism, magmatism and deformation.
- **Anorogenic granitoids:** these granitoids form in both oceanic and continental settings. In oceanic settings the most common are plagiogranites formed at mid-ocean ridges and those found in associated ocean islands. They occur via fractional crystallisation of basaltic magmas or remelting of deep mafic crust. Continental anorogenic granitoids occur in hotspots, such as the Yellowstone area. In such locations, the mantle plume supplies the heat necessary for crustal anatexis and the local generation of voluminous rhyolitic ignimbrites. There is, additionally, the partial

melting of the plume itself, which supplies a basaltic component. Thus, a bimodal basalt-rhyolite suite occurs.

- **Transitional granitoids:** such granitoids occur in orogenic belts after the compressive deformation activity has ceased. They are associated with a regional extensional setting, and have geochemical characteristics indicative of a crustal source.

1.3: GRANITOIDS AND METALLOGENY

In general, high temperature granitoids are more likely to be linked with mineral deposits, as they exhibit a great potential to undergo compositional changes. As Blevin & Chappell (1992) report, they are characterised by increased H₂O activity and concentrations of incompatible elements.

The distinction between high temperature and low temperature granitoids is made based upon the temperature of formation, which is deduced from zircon ages and the abundance and variation patterns of Zr. In particular high temperature granitoids are characterised by the absence of inherited zircons and low temperature granitoids by their presence (Chappell *et al.*, 1998).

1.3.1: Sources of Metals in Magmas

Different types of magmas are characterised by different metal contents, and these metals are acquired from a variety of pathways. Interactions with other magmas, interactions with the subducting slab and the magma's origins are the factors determining a magma's metal content. Then the different pathways of metal acquisition are:

- Mantle melting
- Mass transfer from the subducting slab
- Crust melting

As testified by Hedenquist & Lowenstern (1994), most of the Earth's siderophile⁴ elements are believed to be «locked away» into the planet's Fe-Ni core. As a consequence, their crustal abundances are much less than the abundances of the local bulk. However, as Lorand (1990) mentions, many of these siderophile elements are present in Fe-Ni sulfides in the upper mantle.

Transition metals and precious metal, with chalcophile tendencies, are also concentrated in these sulfides. Such elements are Cu, Pt, Pd and Au (Lorand, 1989). Hamlyn & Keays (1986) assert that this sulfur abundance has clear implications for the distribution of PGE-rich sulfide ores, which are associated with igneous layered intrusions. These sulfides are subsequently consumed during partial melting of the mantle, contributing metals to basaltic liquids. Liquids from partial melting of the mantle then ascend either in mid-ocean ridges or in subduction zones (MacLean, 1969).

⁴ The most siderophile elements are Sn, Mo, Au and PGE.

In any typical mid-ocean ridge setting, the erupted basalt will be more or less altered, and will be associated with oceanic sediments. This complex is then subducted below the continental crust, and melting of the mantle wedge beneath the volcanic arc is induced (Chappell *et al.*, 1998).

Gill (1980) has noted that of special interest are the elevated contents of Cl in arc magmas (700 - 2000 ppm). This is particularly interesting as there is not one single Cl-bearing phase in the mantle, meaning that the mantle lacks Cl. The facts presented above support the «Cl-recycling hypothesis», during subduction of the oceanic crust, which is altered by seawater, proposed by Ito *et al.* (1983).

Metals can be added to arc magmas through subduction, with the most striking examples being Zn and Cu, which are derived from the hydrothermal mineralisation of the subducted seafloor, as mentioned by Sillitoe (1972), Gill (1980) and Stoiper & Newman (1994). Hedenquist & Lowenstern (1994) have indicated that magmas can acquire metals, while «in transit», through the crust. A characteristic example is the case of Sn, which, as mentioned by Blevin & Chappell (1992), may be accumulated in reduced melts – produced in the presence of elemental C or Fe-sulfides – which are ideal from a geochemical point of view, for the accumulation of Sn.

Magmas with high concentrations of F are thought to have acquired such high contents from the meltdown of F-rich hydrous silicates. Such minerals contain, in many cases, significant amounts of Sn and Mo, so these metals are often associated with F in a number of deposits (Hedenquist & Lowenstern, 1994).

McInnes & Cameron (1994) mention yet another way of release of Cu and Au by the mantle wedge or by subducted slabs. This is caused by post-subduction partial melting of the uppermost parts – altered by seawater – of stalled (referred to also as «dead») slabs or the associated metasomatised – modified by subduction – mantle wedge. This process releases highly oxidised magmas and destabilises mantle sulfides, thereby releasing Cu and Au. The mantle melting events previously described can be triggered by cessation of subduction, which, according to Thompson (1995) is the result of island arc-island arc, continental arc-island arc, or continental arc-continental arc collision events. Sillitoe (1997) adds that it is possible to induce mantle melting by the transition from convergent to transform margins, or by the steepening and trenchward retreat of subducted slabs.

1.3.2: Effects of Crystal Fractionation in the Metal Supply of Magmas

In the vast majority of igneous systems, oxides and silicates are the first minerals to crystallise and, consequently, elements partitioning into such minerals – called **compatible elements** – will have their concentrations lowered in the melt. Elements that remain in the melt – called **incompatible elements** – will have increased concentrations. Hedenquist & Lowenstern (1994) mention that compatibility depends upon the crystal structure of the minerals, the composition of the melt and the oxidation state of the magma, and the P and T conditions of crystallisation.

Fe-oxides and Ti-oxides exhibit enrichment in Mo and Zn, and as a general rule, Mo and Zn tend to be in abundance in magmas containing rather small concentrations of the aforementioned oxides. As Lehmann (1982) and Candela (1989), postulate the low abundance of Fe-oxides and Ti-oxides in reduced rocks may also explain the enrichment of W and Sn in such minerals. Moreover, Candela (1989) has developed a model to explain the lack of Cu mineralisation associated with high silica granites. According to his research, the early crystallisation of pyrrhotite, which acts as a «sink» for Cu and probably Au, lowers their concentration in the melt. As Candela (1989) and Hedenquist & Lowenstern (1994) point out, due to molybdenum's higher incompatibility and its initial lower concentration, a high degree of crystal fractionation is necessary to produce the higher Mo/Cu ratio of high silica granites.

It must however be pointed out that, even after extensive crystallisation, metal concentrations in any magma are still less than those required to form porphyry-style ore deposits, by at least two or three orders of magnitude. This ascertainment led Hedenquist & Lowenstern (1994) to conclude that other processes are necessary to concentrate metals from magmas to ore deposits.

CHAPTER 2: THE MAIN CHARACTERISTICS AND THE NATURE OF PORPHYRY ORE DEPOSITS

Geological Framework of Porphyry Deposits ~ Classification Scheme of Porphyry Deposits ~ Hydrothermal Alteration and Mineralisation ~ Hydrothermal Veins in Porphyry Systems ~ Spatial Distribution of Igneous and Hydrothermal Features ~ Variables Affecting the Formation of Porphyry Systems ~ Genesis of Porphyry Systems

Porphyry ore deposits can be defined as magmatic-hydrothermal deposits, which are formed by the precipitation of sulfide and oxide ore minerals, from aqueous solutions at elevated temperatures. They are so named due to the porphyritic texture of the intrusive rocks with which they are associated, both spatially and genetically. These rocks are called **porphyries**, and their main distinguishing feature is their fine-grained groundmass⁵, which is related to their genesis (Seedorff *et al.*, 2005).

One of the main characteristics of these deposits is their large tonnage combined with a relatively low ore grade. Moreover, the ore minerals are found disseminated, either within narrow, closely spaced veins, and/or within the hydrothermally altered rock (Titley, 1966; Lowell & Guilbert, 1970). The exploitation of these deposits for the extraction of a host of metals is proof of their economic significance. In fact, they represent the most important inventories of Cu and Mo in a global level, while they are important sources of Au as well (Singer *et al.*, 2005).

As Hedenquist & Lowenstern (1994) have demonstrated, porphyry deposits form through pervasive veining and alteration of intermediate to acidic intrusions by magmatic-hydrothermal aqueous fluids which are exsolved from a subjacent magma reservoir. Marked contrasts in the permeability of rocks and structures at the sites of formation commonly exert powerful influences on the size and grade of the resulting porphyry deposit, because of the focusing and ponding of fluids.

2.1: GEOLOGICAL FRAMEWORK OF PORPHYRY DEPOSITS

In general, porphyry deposits are associated with magmatic arcs formed along convergent plate margins, as reported by Sillitoe (1972, 1976) and Sawkins (1990). However, this conclusion cannot always be upheld insofar as there are mentioned cases of porphyry deposits not associated with such a geological setting (Sillitoe, 1980, 2000). As demonstrated by Meyer (1981), owing to their broad spatial and temporal distribution, porphyry deposits can be a useful indicator for monitoring Earth's evolution.

The movement of fluids in the upper crust is regulated by hydrothermal systems, which are responsible for the convection of a large proportion of Earth's heat to the surface. Since these fluids are metal transporters, it follows that magmatic-hydrothermal deposits are the single

⁵ This type of groundmass is often referred to as «sugary» groundmass.

most important class of ore deposits (Cathles, 1981). According to Fournier (1987) the «lifespan» of such a system can be up to hundreds of thousands of years, and multiple intrusions are necessary to maintain the hydrothermal fluids' circulation and metal deposition. In addition, there must not only be a flow of hydrothermal fluid, but a focused flow, coupled with a proper metal precipitation mechanism. Generally, both porphyry and epithermal style ores require the existence of a hydrous magma (Richards, 2011).

If the main porphyry deposits are placed on a map (Figure 2.1) it can be seen that they outline the known Phanerozoic orogenic belts (Seedorff *et al.*, 2005). Archaean and Proterozoic porphyry deposits have also been discovered in Canada and Fennoscandia⁶ (Gaál & Isohanni, 1979; Wanhainen *et al.*, 2003) and there are also some probable Precambrian porphyry occurrences in Ontario and Finland, as reported by Gaál & Isohanni (1979) and Nunes and Ayres (1982).

From the above mentioned it is obvious that there is a predominance of Mesozoic and Cenozoic porphyry deposits, as has been reported many times (Meyer, 1981; Titley & Beane, 1981; Hunt, 1991). In examining the ensemble of the known porphyry deposits in the whole spectrum of the geological time scale, Burke & Kidd (1980) concluded that their distribution is largely uneven, since it is a function of numerous factors, most notably the uneven distribution of magmatism, which is related to changes in plate configuration (Seedorff *et al.*, 2005).

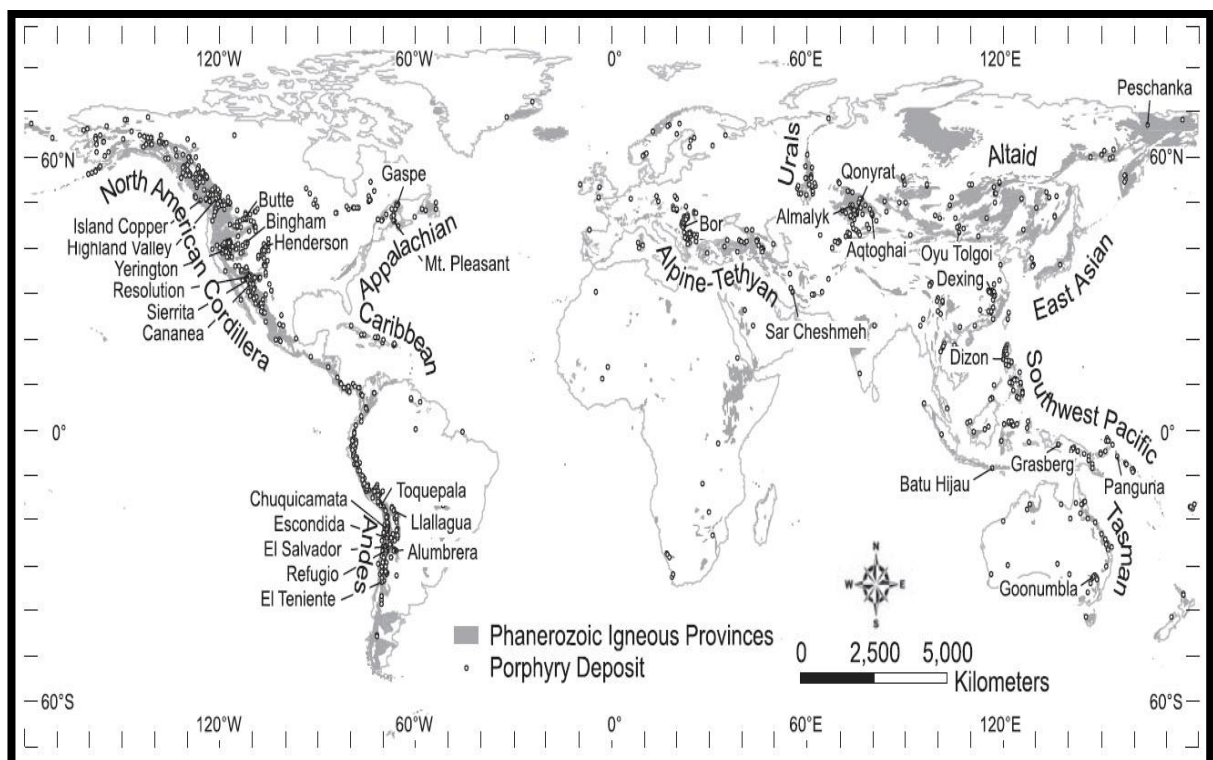


Figure 2.1: The global distribution of porphyry deposits, which coincides with the Phanerozoic igneous provinces and the known orogenic belts (from Seedorff *et al.*, 2005).

⁶ Most of these systems have small reported metal contents (Seedorff *et al.*, 2005).

2.2: CLASSIFICATION SCHEME OF PORPHYRY DEPOSITS

The most practical way to classify porphyry deposits is according to their different metal content, or, more accurately, their different ore metal ratios. In general, the relative proportions of ore metals (Cu, Mo, Au, Sn, W) in porphyry-type deposits are variable, but it is difficult to interpret the observed variations based on systematic criteria (Sillitoe, 1997). The metal ratios in such systems are most probably influenced by crustal magmatic processes, while hydrothermal alteration, inside the porphyry vein network, has not been observed to lead in intense fractionation of chemically similar metals, like Au and Cu. Based on this conclusion, the interpretation of the genesis and composition of such deposits must be found in the processes controlling the composition of the magmatic volatile phase.

The earliest efforts, for the classification of porphyry systems, based on their principal metal content lead into three classes: Cu-Mo porphyry ore deposits, Cu-Au-Mo porphyry ore deposits and Cu-Au porphyry ore deposits (Kesler, 1973; Kirkham & Sinclair, 1996). Despite being a major step, towards the classification of ore deposits, the many different morphologies of ore bodies do not depend upon metal contents, but rather upon tectonic settings and depth of emplacement. McMillan & Panteleyev (1980, 1995) distinguished three end members, terming them plutonic, volcanic and classic.

Modern classifications use quantitative geochemical data which can be used to form the clearest possible distinctions. Be that as it may, such a classification is characterised by the following shortcomings (Kesler, 1973; Seedorff *et al.*, 2005):

- Erosion rate and the nature of the host rocks, along with other factors, affect overall mean grades.
- Supergene processes preferentially enrich or deplete many metals, so the same deposit can present different characteristics depending upon the erosion profile.
- Classifications taking into account igneous features can be misleading even if the slightest alteration is present.
- The relative recovery rate of products and byproducts and the short term economic variations mean that the economic value of many deposits is not reflected by their classification.

In porphyry deposits, sulfur is the single most important element, since it is required for the precipitation of most of the economically important sulfides, like chalcopyrite and molybdenite. According to Hedenquist *et al.* (1998), the importance of sulfur is the direct result of the chalcophile nature of most economically important trace elements. Webster & Mandeville (2007) assert that the aforementioned minerals, as well as pyrite and anhydrite, reflect sulfur transport in hydrothermal fluids as reduced (sulfide) and oxidised (sulfate and sulfur dioxide) species.

This modern distinction of porphyry deposits, in porphyry Au, porphyry Cu, porphyry Mo, porphyry Sn and porphyry W deposits, represents the five possible different end members. However, in reality most deposits are characterised by at least two predominant metals. In each and every class of porphyry deposits the average grade of the major metal(s) exhibits an

enrichment of 10^2 to 10^3 times, compared to the average concentration in unmineralised rocks of similar composition (Seedorff *et al.*, 2005). In general, and despite variations in size, it can be attested that porphyry Cu deposits are larger than porphyry Mo and porphyry Au deposits, which are of similar mean size. Porphyry Sn deposits are typically smaller and porphyry W deposits are characterised by the smallest mean and maximum size (Seedorff *et al.*, 2005). These deposits are solely rhyodacitic porphyry Sn deposits and all known such deposits occur in Bolivia (Grant *et al.*, 1980).

2.2.1: Porphyry Au Deposits

The first porphyry Au deposits described were those from the Maricunga belt in Chile (Vila & Sillitoe, 1991) and later, more such deposits from Peru, Nevada and California were reported. The largest porphyry Au deposits are Grasberg, Bingham Canyon in the USA, and Far Southeast and Panguna in the Philippines. Between them they contain over 700 t of Au.

All porphyry Au deposits are dioritic porphyry Au deposits, and they form a continuum with porphyry Cu deposits. The host rocks of porphyry deposits are most often calc alkaline to high K calc alkaline or in some cases shoshonitic⁷ and are all of I-type (Sillitoe, 1997). However, Ishihara (1981) notes that there are contributions from oxidised subcrustal melts.

From a structural point of view, Sillitoe (1993a, 1997) has postulated that most large porphyry Au deposits conform to the general model of porphyry Cu deposits with little or no deviation. In addition to that, the Au mineralisation can either be confined exclusively to the stocks or disseminated in the host rocks, which can either be contemporaneous or older.

In the centre of the system the K-silicate alteration contains the Au and Cu mineralisation and grades outward to propylitic alteration. Frequently, sericitic alteration is found between K-silicate and propylitic alteration. Lithocaps are not always present, and their absence is indicative of deep erosion (Sillitoe, 1997). One characteristic feature of Au porphyry deposits is the presence of hydrothermal magnetite in the K-silicate alteration assemblages, which is indicative of the high oxidation state of parent magmas (Sillitoe, 1979). Where limestones are present, their impermeability is considered a major contributing factor for the localisation of large and potentially high grade mineralisations (Sillitoe, 1997).

In most of the large porphyry Au deposits, there is an appreciable amount of Cu present, as well as Mo-enriched haloes, which surround the outer parts of the orebodies. Although most porphyry Au deposits are genetically connected to fault systems there is no particular stress regime associated with their creation. The deep erosion in most cases of such porphyry systems makes difficult to pinpoint their original associated volcanic landform (Sillitoe, 1997).

⁷ This is the case of Bajo de la Alumbrera ore deposit in Argentina and Cadia Hill in Australia (Sillitoe, 1997).

2.2.2: Porphyry Cu Deposits

These deposits typically consist of sulfides that are both disseminated and located in veinlets. According to Gustafson & Hunt (1975) and Seo *et al.* (2009), individual copper deposits can be considered as crustal sulfur anomalies, commonly exceeding 10^9 tons of sulfur. There is no significant correlation between Pb and Cu content in general; however there is a trend of increasing Pb with increasing Cu content⁸ (Tarkian & Koopman, 1995). In addition, Economou-Eliopoulos & Economou (2000) report relatively high Pb and/or Pt contents in porphyry Cu (+ Au) intrusions, which may reflect the composition of the parent magma. This category consists of the following two subclasses:

- **Porphyry Cu deposits hosted by subalkaline rocks:** in this subclass belong the tonalitic-granodiorite Cu-(Au-Mo) deposits and the more silicic quartz-monzodiorite granitic porphyry Cu \pm Mo deposits.
- **Porphyry Cu deposits hosted by alkaline rocks:** in this subclass belong the monzonitic porphyry Cu-(Mo-Au) deposits and the silica-undersaturated syenitic porphyry Cu-(Au) deposits.

Porphyry Cu mineralisation is dominated by magmatic fluids in the early stage, although late meteoric water is not only common, but is perhaps critical in enhancing porphyry metal concentrations to ore grade (Titley & Beane, 1981; Hemley & Hunt, 1992).

2.2.3: Porphyry Mo Deposits, Porphyry Sn Deposits and Porphyry W Deposits

Porphyry Mo deposits exhibit enrichment in molybdenum, but it must be noted that according to Mutschler *et al.* (1999) and Sinclair (2007), the absolute amount of Mo contained in an average porphyry Mo deposit is similar to that in large porphyry Cu \pm (Au, Mo) deposits. This led Li & Audétat (2015) to conclude that porphyry Mo deposits can be regarded as standard porphyry deposits lacking Cu \pm Au. The world's largest Mo-rich and Mo-only porphyry deposits are clustered in the SW USA. These deposits include Bingham Canyon, Butte, Climax, Henderson and Questa (Singer *et al.*, 2005).

Regarding the specific nature of Mo enrichment in these deposits Pettke *et al.* (2010) have asserted the magma originating from a metasomatised mantle can be a major contributing factor in the formation of such deposits, and ore provinces in general. Molybdenum, like zinc, according to Hedenquist & Lowenstern (1994), is commonly enriched in magmas containing low abundances of Fe-oxides and Ti-oxides.

Mo-only porphyries are associated with very fractionated magmas, a fact which may explain the enrichment of Mo – an incompatible element – with very fractionated magmas (White *et al.*, 1981; Wallace, 1995; Sedorff & Einaudi, 2004a; Audétat, 2010). From a series of hydrothermal experiments (Candela & Holland, 1984; Kepler & Wyllie, 1991; Rempel *et al.*, 2006, 2008; Minubayeva & Seward, 2010) it was suggested that molybdic acid species

⁸ Tarkian *et al.* (1991) and Tarkian & Koopman (1995) mention that merenskyite, the main Pb-bearing mineral, is associated with chalcopyrite or bornite.

– such as H_2MoO_4 – are important for Mo transport in high temperature hydrothermal fluids. Hence, it can be concluded that selective precipitation of molybdenite from magmatic-hydrothermal fluids could also be an important factor in metal separation. According to Harry & Leeman (1995) in order to promote enrichment of incompatible ore metals, such as Mo, in residual melts, there is the need for a sustained mantle magma input to allow for the necessary protracted fractional crystallisation. According to Bingen & Stein (2003), sulfur limits hydrothermal mobility of Mo through saturation of molybdenite as a primary magmatic accessory mineral. So sulfur is an essential element for economically significant precipitation of molybdenite. Based on the aforementioned deductions, it can be seen that late-stage magmas are expected to exsolve the most Mo-rich fluids. Porphyry Mo deposits exhibit six subclasses, which are presented in the following table (Table 2.1).

Table 2.1: Subtypes of Porphyry Mo deposits and their Major Characteristics			
Porphyry Mo Deposit Subtype	Comments	Characteristic Examples	References
Alkalic monzonitic porphyry Mo \pm Au deposits	Very few examples of such deposits exist on a worldwide level	Three Rivers, USA; Central City, USA	Giles & Thompson (1972)
Alkalic syenitic porphyry Mo deposits	Few of these deposits have been studied comprehensively and their particular characteristics are not well known	Cave Peak, USA; Werner Bjerger, Greenland	Sharp (1979); Brooks <i>et al.</i> (1982)
Monzonitic-granitic porphyry Mo-Cu deposits	Those deposits are characterised by their rough parity between Mo and Cu contents. This subclass is geologically important as it represents a continuum with the monzodioritic-granitic porphyry Cu deposits. However, there are no distinctive igneous and hydrothermal features	Hall, USA; Buckingham, USA; Cumobabi, USA	Shaver (1991); Theodore <i>et al.</i> (1992); Scherkenbach <i>et al.</i> (1985)
Granitic porphyry Mo deposits	The mineralising intrusions which create this subclass are biotite granite porphyries.	Endako, Canada; Quartz Hill, USA; Thompson Creek, USA	Selby <i>et al.</i> (2000); Ashleman <i>et al.</i> (1997); Schmidt <i>et al.</i> (1983)
Trondhjemitic porphyry Mo deposits	This is a highly unusual class since the mineralising intrusions are not particularly silicic	Setting Net Lake, Canada; Trout Lake, Canada; Bald Hill, New Zealand	Ayres <i>et al.</i> (1982); Linnen <i>et al.</i> (1995); Bates (1989)
Rhyolitic porphyry Mo deposits	This subclass includes Climax type deposits and those transitional to them	Climax, USA; Henderson, USA Questa, USA; Pine Grove, USA	Wallace <i>et al.</i> (1968) Carten <i>et al.</i> (1988) Cline & Bodnar (1994) Keith <i>et al.</i> (1986)

Some porphyry molybdenum deposits show an increased enrichment in fluorine, and in these deposits fluorite and topaz are present in the ore zone. It is therefore assumed that fluorine must be very important in the transport of molybdenum in hydrothermal fluids and also in the enhancement of molybdenum's partition coefficient into hydrothermal fluids from silicate melts. However, there are numerous examples of other Mo rich deposits, such as Aldanac and Boss Mt in British Columbia, that contain no more fluorine than other porphyry copper deposits (Westra & Keith, 1981).

Porphyry Cu + Mo deposits of Siberia and Mongolia, which are of Caledonian/Hercynian to Mesozoic Age, are characterised by relatively small stocks and dykes. The Cu-Mo deposits in Armenia are considered to be similar in age and genesis to those in the Andes and the western Cordillera of North Africa (Pokalov, 1977). Relatively high Pb and/or Pt content in the porphyry Cu \pm Mo intrusions, may either be related to an early vein-type Cu mineralisation,

or is redistributed and concentrated by leaching, from an early stage stockwork mineralisation (Economou-Eliopoulos & Eliopoulos, 2000).

As for porphyry W deposits, there exist only rhyolitic porphyry W-Mo deposits and the only examples are located at New Brunswick. The Mount Pleasant deposit is the sole deposit to have been mined by modern methods (Kooiman *et al.*, 1986). Porphyry Sn deposits constitute only one subclass, the rhyodacitic porphyry Sn deposits. As mentioned before, all such deposits occur in Bolivia (Grant *et al.*, 1980), although some similarities are evident in the Majuba Hill deposit in Nevada (MacKenzie & Bookstrom, 1976).

2.3: HYDROTHERMAL ALTERATION AND MINERALISATION

Due to the nature of the processes which form the porphyry ore deposits, the host rocks undergo various degrees of hydrothermal alteration. Thus characteristic gangue mineral alteration assemblages are formed along with the ore minerals. The different alteration assemblages provide P-T constraints regarding ore deposition, and are the most prominent feature of a porphyry system in the field⁹.

As per Meyer & Hemley (1967) **alteration types** are defined as groups of mineral assemblages that formed in geochemically similar environments. Barton *et al.* (1991) distinguish between alteration types hosted by aluminosilicate rocks and alteration types hosted by carbonate and ultramafic rocks. Generally, it is possible to attribute specific alteration types to specific processes in the porphyry environment. These processes are volatile addition, hydrolysis, alkali exchange and silica addition¹⁰ (Seedorff *et al.*, 2005).

2.3.1. Spatial Distribution of Alteration Zones

The deep proximal part of porphyry systems is most commonly dominated by potassic alteration and the upper part is dominated by sericitic and advanced argillic alteration. In the flanks and distal areas of the system, propylitic and sodic-calcic alteration assemblages can be observed.

Potassic alteration is overlain by sericitic alteration narrowing to form a hood and then, possibly, overlain by fresh rock. This configuration is most evident in the Bajo de la Alumbrera, San Manuel, Henderson and Climax deposits (Lowell, 1968; Steininger, 1973, Grant *et al.*, 1980; Proffett, 2003a). This is the configuration of the **Climax type models** (Lowell & Guilbert, 1970).

In other systems, such as El Salvador, Batu Hijau and Grasberg (Gustafson & Hunt, 1975; Corn, 1975; Hedenquist *et al.*, 1998) there is extended advanced argillic alteration at shallow levels in the system, which is believed to have extended to the palaeosurface (Seedorff *et al.*, 2005). This is in effect the lithocap variant of these models. A detailed mapping of all the

⁹ The terminology used in describing porphyry deposits is provided in Appendix I.

¹⁰ A concise table on the main alteration types and their characteristics is provided in Appendixes II and III.

aforementioned deposits will result in potassic alteration ringed by hydrolytic alteration and in turn ringed by propylitic alteration.

There are also cases where the intense hydrolytic alteration extends upward, resembling an overall upright funnel. So, in such systems hydrolytic alteration penetrates deeply into older potassic alteration. A map of such deposits will depict a central region of hydrolytic alteration, ringed by potassic and then by propylitic alteration. This model corresponds to many of the world's largest porphyry Cu deposits, such as Butte, Chuquicamata, Escondida and Qonyrat (Meyer *et al.*, 1968; Kudryavtsev, 1996; Ossandón *et al.*, 2001; Padilla *et al.*, 2001).

In other cases, both sodic-calcic and potassic alteration zones are located in the centre of the system. Sodic-calcic alteration occupies a bell shaped volume beneath potassic alteration and fingerlike projections of sodic alteration extend up through the centre of the system. Mapping of such systems results in a central region characterised by prominent sodic alteration, ringed by potassic alteration and succeeded outward by sodic-calcic alteration. Both sericitic and propylitic alteration may be present only at higher levels (Seedorff *et al.*, 2005). Typical examples of such deposits are the Ann-Mason deposit and the Yerington mine (Carten, 1986; Dilles & Einaudi, 1992).

2.3.2: Temporal Relationships Between Alteration Types

As mentioned by Barton (2000) there is a cyclicity of hydrothermal events in porphyry systems which exists in many other types of igneous-related hydrothermal systems. The repetition of hydrothermal features is a direct consequence of the existence of multiple igneous intrusions. Seedorff *et al.* (2005) has concluded that hydrothermal features – such as vein types and alteration assemblages – are not timelines but rather parts of an evolving sequence, repeatable wholly or in part.

The most direct way to deduce the temporal relationships between different events is to observe crosscutting relationships. According to observations made in many porphyry systems, the potassic alteration forms earlier, followed by the sericitic alteration, which then extends downward following the temperature's decline. These field observations are in contrast with theoretical considerations which proposed that these two alteration types must be contemporaneous at some point in the system's evolution (Seedorff *et al.*, 2005). Regarding veins, since they are formed at different temperatures, and since high temperature veins are formed first, they will be cut and offset by veins of lower temperatures. In general, this crosscutting relationship where progressively higher temperature veins are cut by progressively lower temperature veins is termed a «**normal crosscutting relationship**» (Seedorff & Einaudi, 2004a; Seedorff *et al.*, 2005). Of course, and taking into account the cyclicity of hydrothermal features, there can be «**anomalous crosscutting relationships**» where lower temperature veins are cut by older higher temperature veins (Seedorff *et al.*, 2005). According to Seedorff & Einaudi (2004b) if all the crosscutting relationships are spatially plotted in a suitable matrix, the time-space-temperature dynamics of the system can be illustrated.

2.4: HYDROTHERMAL VEINS IN PORPHYRY SYSTEMS

As has been demonstrated in all studies regarding porphyry deposits, veins and breccias¹¹ form continuously throughout the life of porphyry systems. In fact, an appreciable amount of ore minerals occurs within them, as they represent the locus of hydrothermal fluid flux (Seedorff *et al.*, 2005). Titley *et al.* (1986), Muntean & Einaudi (2000, 2001) and Proffett (2003a, 2003b) have concluded that the specific characteristics of veins and breccias (mineralogy, textures, fluid inclusions, location, abundance and orientation) reflect the spatial and temporal evolution of flow of hydrothermal fluids, as well as the fluctuations of their chemical composition. It must be stressed that vein types were not all recognised at once, and this fact is reflected in the table below (Table 2.2), which provides the chronological order of each vein type's first description.

Table 2.2: First Descriptions of Typical Veins Types of Porphyry Deposits		
Vein Type(s)	Ore Deposit	Reference(s)
A-type, B-type and D-type veins	El Salvador, Chile	Gustafson & Hunt (1975)
Early biotite (EB)-type and C-type veins	El Salvador, Chile	Gustafson & Quiroga (1995)
M-type veins	Island Copper, Canada	Clark (1993); Arancibia & Clark (1996)
Banded quartz veinlets	Maricunga belt, Chile	Muntean & Einaudi (2000)

Apart from the aforementioned references, Meyer (1965), Meyer *et al.* (1968) and Brimhall (1977) had described several distinctive vein types from the pre-Main Stage at Butte. As Seedorff *et al.* (2005) point out, little of the existing vein terminology has been used for porphyry Mo, W or Sn deposits.

Vein dikes are also very important as they provide a link between magmatic and hydrothermal processes. At the Henderson deposit, Carten *et al.* (1988) described the typical mineralogy and texture of vein dikes. Euhedral crystals of quartz \pm biotite \pm molybdenite project inward from vein walls into an aplitic porphyry centre which may contain molybdenite grains. As the distance from the source stock increases, vein dikes may grade into open-space veins of coarse-grained quartz \pm fluorite (Seedorff *et al.*, 2005).

2.4.1: Classification of Veins and Description of Vein Types

Regarding the classification of veins it is customary to utilise descriptive criteria, such as morphology, texture and mineralogy of vein filling and alteration envelope(s) and orientation. As a general rule, it can be said that younger veins are formed at lower temperatures, although this does not apply to all cases. The association between wall rock alteration, via veinlet filling and associated alteration envelope, is evident (Seedorff *et al.*, 2005). Despite this, genetic relationships between ore minerals, gangue minerals and alteration assemblages

¹¹ The significance of breccias in porphyry systems is analysed in Appendix IV.

can be obscured by the reopening of early high temperature veins in later stages¹², as recorded by Rusk & Reed (2002) and Redmont *et al.* (2004). Below, the characteristics of main vein types are described in decreasing age, based on their spatial relationships within a system.

I. Veins associated with potassic alteration

Replacement and open-space veinlets, containing quartz, fluorite, molybdenite, K-feldspar and biotite are termed **veins with silicic and potassic envelopes** by Seedorff *et al.* (2005), and were first described by Carten *et al.* (1988) at Henderson. They do not contain any pyrite. The alteration veins of such envelopes vary according to the distance from the stocks. Near the apexes of the stocks the alteration haloes are zoned, with an inner silicic envelope (quartz + fluorite after feldspar and plagioclase) are enclosed by potassic envelopes (K-feldspar after plagioclase). Near the apex of the stocks there is usually not so much molybdenite, while many molybdenite grains can be found further from the stocks, where only the potassic alteration envelope can be observed (Seedorff *et al.*, 2005). These veins differ significantly from A-type and B-type veins.

In some shallow porphyry Cu deposits, Clode *et al.* (1999) report the existence of magnetite ± Cu-Fe sulfide veinlets, which exist within biotite alteration, and are collectively termed «**magnetite rich veinlets**» by Seedorff *et al.* (2005). These are cut by A-type quartz veinlets. According to Muntean & Einaudi (2000, 2001) these veinlets exhibit a variety of mineralogical and textural features. They range from hairline streaks of magnetite ± biotite with minor quartz and chalcopyrite and K-feldspar envelopes to sugary quartz veinlets with magnetite and chalcopyrite and no alteration envelopes. These last are termed «**A-type veinlets**» and cut other magnetite rich veinlets (Muntean & Einaudi, 2000, 2001).

According to Brimhall (1977) and Field *et al.* (2005), the earliest, highest temperature veins at many porphyry Cu deposits are **biotitic veinlets**, which are related to widespread potassic alteration of wall rocks. In some cases they are mineralised, containing magnetite and a host of sulfides.

Veinlets exhibiting mineralogical combinations of green biotite, K-feldspar, andalusite, muscovite, cordierite and corundum¹³, are collectively termed «**green mica veinlets**» by Seedorff *et al.* (2005). These veinlets have not been described at many porphyry deposits. Notable occurrences are at El Salvador, where Gustafson & Quiroga (1995) report the so-called **EB veinlets**, and at Butte and Los Pelambres, by Brimhall (1977) and Atkinson *et al.* (1996) respectively.

Similar to aforementioned veinlets, are the more complex **quartz bearing veinlets with biotite and sericite** (Seedorff *et al.*, 2005). These are also not often observed, and one notable example is at El Salvador, where they are reported as **C-type veins** by Gustafson & Quiroga

¹² In the special case of quartz veins, Penniston-Dorland (2001) reports that it is possible to study internal crystal growth and dissolution zones, so as to infer relative genetic relationships between minerals and alteration.

¹³ This mineral assemblage indicates formation at temperatures as high as ~ 600° C (Seedorff *et al.*, 2005).

(1995). They are characterised by the mineral assemblage muscovite + biotite \pm K-feldspar + andalusite. They are present both in the vein filling or the envelope, and, in stark contrast to green mica veinlets, corundum is absent (Seedorff *et al.*, 2005).

The **A-type veins**, as are known from the work of Gustafson & Hunt (1975), are termed «**sugary quartz veinlets**» by Seedorff *et al.* (2005), are observed in most porphyry Cu and Au deposits¹⁴. These are broadly contemporaneous with potassic alteration. These are described as granular assemblages of quartz (50 - 90 %), perthitic K-feldspar, anhydrite, bornite, chalcopyrite and rare biotite. The crystals of these minerals are randomly oriented and fringed by envelopes of K-feldspar, anhydrite, chalcopyrite, bornite, apatite, and rutile. As reported by Fournier (1999) these A-type veinlets lack centre lines or banding and their morphological appearance (they are irregular, discontinuous and segmented) suggest that they were formed under ductile conditions, indicating high temperature and high strain conditions.

II. Veins associated with sodic and/or calcic alteration

Clark (1993) terms veins dominated by magnetite, amphibole and plagioclase as **M-type veins**, so as to emphasise their high magnetite content. They are considered as being the earliest and highest temperature veins, in the deposits in which they occur (Seedorff *et al.*, 2005). These veins, which sometimes exhibit plagioclase alteration haloes, have been described in tonalitic-granodiorite porphyry Cu \pm (Au, Mo) deposits, such as Island Copper (Arancibia & Clark, 1996).

The spatial distribution of sodic and/or calcic alteration is controlled by **actinolite veinlets** which are characterised by temperatures of around 400° to 450° C. In rare occasions, quartz + plagioclase + actinolite veins are formed in their place (Battles & Barton, 1995; Carten, 1986). Finally, in some porphyry Cu deposits, **epidote veinlets** (containing also pyrite and quartz) control the distribution of sodic and/or calcic alteration (Dilles & Einaudi, 1992).

III. Veins associated with intense hydrolytic alteration

One rarely described category of veins is **greisen veins**, which are distinguished by the coarse grained white mica which predominantly fills them. They commonly exhibit textural and mineralogical changes, containing alternating assemblages of quartz \pm muscovite \pm sulfides. This type of greisen veins has been described by Williams and Forester (1995) for porphyry Cu and porphyry Mo deposits. One special subcategory is **pyritic greisen veins**, which can be observed in granite-hosted Mo-Cu porphyry deposits (Steeffel & Atkinson, 1984; Seedorff *et al.*, 2005). Also, it must be mentioned that greisen muscovite veins, such as those observed in the Highland Valley District, British Columbia, may represent deep levels of the system (Casselman *et al.*, 1995).

D-type veins, as described at the El Salvador deposit (Gustafson & Hunt, 1975), and termed alternatively by Seedorff *et al.* (2005) as «**veins with sericitic envelopes**», indicate moderate

¹⁴ It must be mentioned however that they are not reported from deposits hosted within strongly alkali host rocks (Seedorff *et al.*, 2005).

temperatures of formation. They are filled by pyrite ± quartz and at progressively deeper levels, tourmaline, calcite and anhydrite become abundant. Alteration haloes can either be monomineralic, meaning that they consist only of sericite, or consist of sericite + chlorite ± pyrite ± quartz ± anhydrite ± rutile ± sulfides (other than pyrite). It is also important to note that some researchers included in the definition of D veins minerals characteristic of advanced argillic alteration. So it is possible to regard the definition of D veins by Gustafson & Hunt (1975), which includes such minerals, as *sensu lato* **D veins**. In fact many researchers, namely Atkinson *et al.*, (1996), Seedorff & Einaudi (2004a) and Seedorff *et al.* (2005) are interested not so much on the mineral assemblages filling the veins as in the existence of the sericitic envelope.

IV. Quartz veins lacking wall rock alteration

The most important category of these veins is the so-called **B-type veins**, first described at the El Salvador deposit by Gustafson & Hunt (1975). These veins have only been reported in porphyry Cu deposits (Seedorff *et al.*, 2005), and are distinguished by continuous planar structures with internal banding. They are filled by coarse-grained quartz + molybdenite + chalcopyrite + anhydrite ± pyrite ± tourmaline.

According to Gustafson & Quiroga (1995) they are not characterised by alteration haloes, although in some cases, as in El Salvador, a K-feldspar ± albite ± biotite ± sericite ± corundum envelope is observed. It is therefore sometimes impossible to distinguish *sensu stricto* B-type veins and this is the reason why some researchers (e.g. Clode *et al.*, 1999) have adopted the terms «**AB-type veins**» and «**A-family veins**» for veins combining the characteristics of both A-type and B-type veins.

A most striking feature, described from porphyry Au deposits, in the Maricunga belt by Muntean & Einaudi (2000, 2001) is the **gray banded quartz veins**, which lack alteration envelopes. They contain dark gray bands and their dark colour is caused by abundant vapour-rich fluid inclusions and µm-sized grains of magnetite. That the bands are botryoidal and continuous through quartz veins suggests quartz crystallisation from a silica gel (Muntean & Einaudi, 2000, 2001; Seedorff *et al.*, 2005). Such banded quartz veinlets are reported from Northern Peru and also three such occurrences are reported from deposits in the USA (Muntean & Einaudi, 2000).

V. Late stage veins, low temperature veins and distal veins

At the distal edges of many porphyry systems, Gustafson & Hunt (1975), Koski & Cook (1982) and other researchers, have reported the existence of veins containing epidote + quartz + pyrite + chlorite + calcite, which are associated with propylitic alteration assemblages containing albite, epidote and chlorite.

Of special mention is the existence of **base metal veins** or **base metal lodes**, which are found in numerous porphyry deposits and may also contain precious metals. Some are transitional to D-type veins, such as the **proximal base lodes** (Meyer *et al.*, 1968). Seedorff *et al.* (2005) point out the importance of such veins, as they are spatially situated above and beyond the

bulk-tonnage ore bodies, and their mineralogy and metal ratios correlate fairly closely with the class of the underlying porphyry systems. As such, they are on their own quite important exploration targets.

Finally, it is important to note the existence of sulfide-poor veins without alteration envelopes, representing the final stages of a porphyry system. They have a quite distinctive mineralogy of carbonate ± silica minerals, and prehnite and zeolites which occur in more mafic rocks (Sillitoe & Gappe, 1984; Riedel *et al.*, 1996).

2.4.2: Crosscutting Relationships of Veins and Relative Mineralisation and Alteration Ages

In field study, as well as in hand and microscope specimens, veins cutting and offsetting one another can provide a more or less reliable guide for the relative ages of hydrothermal events. It must be stressed that when veins cut one another, without offset, then this may be due to selective mineral deposition or reopening of older veins (Meyer & Hemley, 1967).

As mentioned by Seedorff *et al.* (2005), a crosscutting relationship between veins establishes the relative ages of two events, at a single point in space. Some such relationships may be observed repeatedly in a porphyry system, yet be reversed in some parts of the systems, thereby providing important clues for the systems evolution.

It is equally important however to consider also the crosscutting relationships between veins and porphyry intrusions, which allows the relative dating of various hydrothermal events within the same system. If the age of an intrusion is known with high certainty then it is feasible to determine if a vein is formed before or after the intrusion, as Ballard *et al.* (2001) assert. So, in studying the aforementioned relative ages, it is possible to classify intrusions as **premineral**, if they are cut by all types of veins, **intramineral**, if they both cut off and are cut veins, and **postmineral**, if they cut off all veins (Seedorff *et al.*, 2005).

It must be mentioned that for a great number of deposits crosscutting relationships are poorly documented. However, for the proper estimation of a porphyry system's grade and tonnage it is important to record the geometry and relative age (relative to the mineralisation that is) of the porphyry intrusion.

2.5: SPATIAL DISTRIBUTION OF IGNEOUS AND HYDROTHERMAL FEATURES

Porphyry ore deposits have been studied for over 100 years, and their deposit and district-scale descriptions have resulted in the systematic recording of the spatial relationships between their different characteristics. One of the most important factors determining the subsequent development of a porphyry system is the relative position of the different porphyry intrusions. Also of primary importance is their relation to the magma chamber, from which intrusion and aqueous fluids ascend. Examples of different geometrical arrangements are provided below (Table 2.3).

Table 2.3: Spatial Relationships between Porphyry Intrusions		
Porphyry Intrusions' Geometrical Arrangement	Ore Deposit Examples	Refences
Successive intrusions emplaced at successively greater depths	Climax, USA; Pine Grove, USA	Wallace <i>et al.</i> (1968); White <i>et al.</i> (1981); Keith <i>et al.</i> (1986)
Successive intrusions emplaced at the same depth but derived from successively greater depths	Yerington, USA; Ann-Mason, USA	Carten (1986); Dilles (1987)
Intrusions emplaced side by side (sometimes along a trend)	Henderson USA; Mount Hope, USA; Bajo de la Alumbrera, Argentina	Carten <i>et al.</i> (1988b); Proffett (2003a, 2003b).
Successive cylindrical intrusions emplaced inside older intrusions	Santo Tomas II, Philippines ; Henderson, USA; Panguna, Papua New Guinea ; Goonumbla, Australia	Serafica & Baluda (1977); Carten <i>et al.</i> (1988); Clark (1990); Lickfold <i>et al.</i> (2003)

2.5.1: Distribution of Grade and Metal Ratios

At district scale, where ore bodies related to a batholith, occur in clusters, Carten *et al.* (1988) mention that individual mines or orebodies may be a composite of several ore-forming intrusive events. Langton & Williams (1982), Wilson *et al.* (2003), and Seedorff & Einaudi (2004b) have concluded that it is possible to use the relative distribution of ore grades and metal ratios so as to make genetic hypotheses. However, there are several conditions affecting the addition and subtraction of metals (Seedorff *et al.*, 2005). The principal determining factors are:

- Superposition of multiple veins' sets (Carten *et al.*, 1988)
- Local scale hypogene sulfidation and redistribution (Dilles & Einaudi, 1992)
- System-scale hypogene enrichment by an overprint of advanced argillic mineralisation (Titley & Marozas, 1995)
- Widespread hypogene depletion by sodic-calcic alteration (Proffett, 2003a)
- Supergene enrichment and depletion (Sillitoe, 2005)

The geologic controls on distribution can be illustrated by the detailed mapping of all the veins, breccias and the logging of hydrothermal minerals. Alteration-vein maps can also be used for exploration purposes, in locating the main ore body, like Carten *et al.* (1988b) and Proffett (2003a, 2003b) have demonstrated.

2.5.2: Depth of Porphyry Systems and Correlation with Palaeosurface

In studying a porphyry ore system it is important to ascertain the relative morphology of the palaeosurface and its position in relation to the ore bodies. It is possible to establish its level with relative certainty in most deposits (Sillitoe, 1994). In deposits which do not exhibit excessive tilting or deformation it is possible to estimate the level of the palaeosurface, as being slightly over the top of the orebody.

Examples of such systems are Bajo de la Alumbrera, Argentina (Proffett, 2003a), Bingham, USA (Einaudi, 1982) and Marte, Chile (Vila *et al.*, 1991). A special case is that of magmatic cupolas, which are the domal tops of evolving magma chambers. During the evolution of a batholith several cupolas may develop. Porphyry stocks and dykes commonly originate from such cupolas.

2.5.3: Geometry of Ore Bodies

There are many factors determining the shape of an ore body, such as the number of mineralising intrusions and their relative positions. Also the sequence and the relative positions of mineralising versus barren intrusions are important and the structural style of the deposit is also a contributing factor (Carten *et al.*, 1988; Proffett, 2003a; Seedorff & Einaudi, 2004b).

The precipitation of ore minerals in veins and disseminations can happen in one or many assemblages and be contemporary either with the potassic, the sericitic or the advanced argillic alteration, or any of these combinations (Seedorff & Einaudi, 2004b; Seedorff *et al.*, 2005). As demonstrated by Dilles & Einaudi (1992) it is possible for previously deposited Cu to be removed or redistributed by fluids associated with any of the aforementioned alteration types. There is no predominant type of geometry for the ore bodies, and there can be thick walled cylinders, inverted cups, inverted jars and domes. Different intrusions within the same system can display different geometries. The ore zones can be either distinct or overlapping (Seedorff *et al.*, 2005).

2.5.4: Metal Zoning Patterns

When examining a porphyry system, it is customary for the core of the system to contain the metal or metals from which the deposit is characterised, like Cu in porphyry Cu deposits. For metals such as Pb, Ag and Au it is customary to observe an outward and upward zonation with gradually increase metal contents (Seedorff *et al.*, 2005). However, Sillitoe (2000) has noted the Au content can be higher within the central Cu zone, in some porphyry Cu deposits.

One useful tool, which can be employed both as a zonal indicator and as a vector for Au potential, is the Ag/Au ratio. This ratio increases outward in most porphyry systems (Langton & Williams, 1982; Cox, 1985) and the highest Au grades are associated with the lowest Ag/Au ratios. Ag/Cu and Ag/Mo ratios probably increase towards the periphery of more felsic systems (Seedorff *et al.*, 2005).

The research by Seedorff & Einaudi (2004b) in the Henderson porphyry Mo deposit is an indication that in such systems Cu occurs in trace amounts – associated with sphalerite – outboard of Mo. W occurs as wolframite also outboard of Mo but inboard of Zn and Cu (Seedorff *et al.*, 2005). According to numerous researchers (Waterman & Hamilton, 1975; Sillitoe & Khan, 1977; John, 1978; Field *et al.*, 2005) the relative positions of Mo and Cu, in porphyry Cu deposits are variable.

2.5.5: Structural Style of Porphyry Deposits

It is to be expected that structural styles control, at least partly, the degree of involvement and timing of ingress of external fluids (Seedorff *et al.*, 2005). Depending upon the structure of the porphyry deposits, three distinct end members can be defined:

- **Disseminated style** (Titley, 1982a, 1982b): in this style of porphyry deposits mineralisation occurs predominantly in thin veinlets
- **Lode style** (Einaudi, 1977, 1982): this style is characterised by the presence of major throughgoing Cu-rich veins, minerals that represent a very high sulfidation state, as well as intense sericitic and/or advanced argillic alteration.
- **Breccia style** (Sillitoe, 1985; Skewes & Stern, 1996)

2.6: VARIABLES AFFECTING THE FORMATION OF PORPHYRY SYSTEMS

As demonstrated by the detailed description of the different types of porphyry deposits and their association with different geotectonic settings, the creation of such a system is influenced by a multitude of factors and their relative significance in the genetical sequence. In the following paragraphs, a concise presentation of the importance of temperature, of formation depth and associated pressure and of the geochemical nature of magmatic and hydrothermal fluids, is delineated.

As has been documented by Hemley *et al.* (1992) and Redmont *et al.* (2004) the decline in temperature of hydrothermal fluids results in supersaturation with respect to many ore and alteration minerals. While many researchers (Gustafson & Hunt, 1975; Eastoe, 1978; Carten *et al.*, 1988; Dilles *et al.*, 2000) have determined that hypogene ore deposition takes place at high temperatures, others (Beane & Titley, 1981; Hedenquist *et al.*, 1998; Redmont *et al.*, 2004) have demonstrated that ore deposition can take place at low temperatures too.

In general, most porphyry deposits form under lithostatic pressures, at depths between 2 Km and 5 Km. It has been concluded (Hedenquist & Lowenstern, 1994) that in many deposits, metal grades show a rough correlation with depth. Most strikingly, deep porphyry deposits tend to be Au-poor but Mo-rich. The pressure of the hydrothermal fluids is a key factor in determining the specific characteristics of a porphyry system. Low salinity fluids will undergo brine-vapour phase saturation at a pressure below 1.5 Kbars (Henley & McNabb, 1978) due to fluid immiscibility below a solvus. As Hemley & Hunt (1992), Hemley *et al.* (1992) and Heinrich *et al.* (1999) have demonstrated, this has a pronounced effect on metal partitioning and solubility. It must be mentioned however, that pressure is a function of both depth and hydrologic regime (Seedorff *et al.*, 2005). According to Fournier (1999) while overpressured lithostatic conditions occur near magmas, at temperatures below 375° C, hydrostatic conditions are the main factor determining pressure.

In addition, it is obvious that the composition of the parent magma is a major contributing factor, although it must be stressed that distinct metal endowments do not necessarily correspond to different magmatic sources. There is also the possibility of metal segregation

during progressive fluid separation, from a single, progressively crystallising, magma reservoir (Lodders & Palme, 1991).

The bulk rock chemical composition will naturally be a function of the original chemical composition of the wall rock and that of the hydrothermal fluids. However, there is a third important factor, the **fluid-to-rock ratio**, meaning the proportions of the hydrothermal fluid to wall rock taking part in the studied reactions (Seedorff *et al.*, 2005).

In the case of weak alteration, when the fluid-to-rock ration is low, the chemical composition of the wall rock is the dominant factor determining ore mineral assemblages. Indeed, wall rock composition can buffer pH through reactions with carbonate or feldspar or buffer oxidation state through reaction with Fe-bearing minerals, organic matter or reduced pore fluids, as mentioned by Seedorff *et al.* (2005).

Barton (1970) determined that wall rock alteration may be coupled with ore deposition, since neutralisation and reduction of sulfate to sulfide directly promotes sulfide mineral deposition. In other cases, as mentioned by Carten *et al.* (1988), Seedorff (1988), Zweng & Clark (1995), and Maher (1996). Many types of external fluids can act as significant factors determining the characteristics of porphyry systems. The different kinds of these fluids are:

- Saline formation waters related to coeval or older evaporite basins (Battles & Barton, 1995)
- Dilute meteoric waters (Selby *et al.*, 2000)
- Seawater (Osatenko & Jones, 1976; Chivas *et al.*, 1984)

As described above the sources of components of a porphyry system can be either magmatic or external. From various geological and geochemical evidence, it is apparent that the potassic alteration is the result of a magmatic dominated hydrothermal fluid. Isotopic evidence indicates that a magmatic source gives rise to the fluids responsible for the creation of sericitic and advanced argillic alteration at various depths (Westra, 1982; Zaluski *et al.*, 1994; Watanabe & Hedenquist, 2001). However, hydrothermal fluids creating these hydrolytic and acid alteration types may also include an important external component (Seedorff *et al.*, 2005).

As mentioned by Seedorff & Einaudi (2004b), it is possible for late intermediate argillic alteration and base metal veins to be the product of saline magmatic waters. It has been proposed (Gustafson & Hunt, 1975) that propylitic alteration is the distal equivalent of potassic fluids of magmatic origin, but more recent isotopic data (Bowman *et al.*, 1987; Proffett, 2003a; Seedorff & Einaudi, 2004a) indicate that in some deposits at least, the fluids responsible for the creation of propylitic alteration include both a magmatic and an external fraction. Finally, according to the data of Dilles *et al.* (1992, 1995), sodic-calcic alteration and the associated propylitic alteration is created by non-magmatic brines.

Both the magmatic and the non-magmatic components described above correspond to local scale processes, while the formation of any porphyry deposit is always the result of lithospheric scale processes. The upper mantle, the upper crust, the subducting slab and the

lower crust are all sources of magmatic components. Since, according to the specific geotectonic setting, there are different ratios of different components – different in regard to their origin – there are different types of ore forming magmas (Seedorff *et al.*, 2005). The sources of some components are more or less known – Mo and Pb are contributed by the subducting slab or the crust and PGE are most likely contributed by mantle sources – while the sources of other components, such as sulfur, most likely differ between different deposits¹⁵ (Ohmoto & Rye, 1979).

2.7: GENESIS OF PORPHYRY SYSTEMS

The creation of a porphyry system is linked to the creation of an underlying magma chamber. This whole process begins when the subduction derived fluids or the asthenospheric rise provides the impetus for the generation of a mantle sourced mafic magma.

While this magma intrudes into the crust, it mixes and hybridises with partial crustal melts, undergoing fractional crystallisation (Hildreth, 1981). Hence an intermediate to silicic magma chamber is created, which, in later stages may result in the creation of a porphyry system, provided that it is located in the upper crust. Such magma stages are not constructed until the later stages of a magmatic system, so it can be concluded that porphyry systems are the result of the late stages of magmatic activity (Lang & Titley, 1998). According to Eichelberger *et al.* (2000) magma chambers associated with porphyry deposits behave as open systems¹⁶. Minor magmas are also important in such a genetical process, as they contribute trace elements or volatiles. The addition of volatiles is especially important in that it enables magmatic fluids to rise to the surface (Seedorff *et al.*, 2005).

One most important factor in the creation of a porphyry system is the process of magmatic exsolution, which produces a separate aqueous phase. This phase scavenges metals from a sufficient volume of silicate liquid and magmatic sulfides and then gathers in magmatic cupola, from which it will, in time, ascend to the site of ore deposition, as described by Candela & Piccoli (2005). According to Cline (1995), factors affecting this process are the magma's composition and its water content, as well as depth and pressure. Dilles (1987) and Shinohara & Hedenquist (1997) have also added the parameters of the cupola's geometry and the chamber's homogeneity as contributing factors.

As Seedorff *et al.* (2005) mention, it is essential during the transport of aqueous phases, that there is no eruption, for a porphyry system to be developed. On the other hand, in some cases, the geological structures created by volcanic eruptions are favourable for the later formation of porphyry systems. It is well established that a porphyry mineralisation is the result of multiple magmatic intrusions, over a short time span of not more than $3 \cdot 10^5$ years. The relative positions and volumes of mineralised, intermineral and postmineral intrusions create

¹⁵ Hattori & Keith (2001) mention magma sources while Field *et al.* (2005) mention the possibility of crustal assimilation.

¹⁶ This assertion is evidenced by the nature of the processes associated with magma chambers, namely degassing, erupting, recharging, crystallising, assimilating and commingling with magmas of various compositions (Seedorff *et al.*, 2005).

the geometry of the ore body and affect the distribution of the ore grade within the system (Seedorff *et al.*, 2005).

The spatial and temporal distribution of the various hydrothermal features is dictated by the rate and the mass of the hydrothermal fluids¹⁷, which delineates the thermal evolution of the system – meaning the heating versus cooling rate. Depending upon the thermal «evolutionary path» the ore minerals, the veins and the wallrock alterations are created (Seedorff *et al.*, 2005).

During magma emplacement, the dominance of magmatic hydrothermal fluids is evidenced by the creation of hydraulic fractures, which in turn create a suitable setting for external fluid inflow. These fluids can be earlier magmatic hydrothermal fluids which have in the meantime been depressurised and cooled, altering their composition, dilute meteoric water, seawater, or any combination of these. According to the thermodynamic experiments of Fournier (1999), only dense brines may gain access in the central part of the system, in high temperature conditions – in temperatures higher than 350° C. According to Burnham (1985) and Fournier (1999) the introduction of new magma, which may or may not exsolve hydrothermal fluids, could result in the formation of hydrothermal breccias and hydraulic fractures. Brecciation is a function of the depth of the system, and of the associated pressure conditions.

As can be understood by the above mentioned data, there are many factors which contribute to the creation of porphyry systems and to the differences between them. Although there have been many advances in the processes which give rise to such systems, many particulars regarding the genesis of these systems are still a matter of investigation (Seedorff *et al.*, 2005).

¹⁷ Details on the geochemistry of hydrothermal systems are provided in Appendix V.

CHAPTER 3: THE MAIN CHARACTERISTICS AND THE NATURE OF EPITHERMAL ORE DEPOSITS

Low Sulfidation Epithermal Deposits ~ Intermediate Sulfidation Epithermal Deposits ~ High Sulfidation Epithermal

Deposits ~ Range of Compositions of Hydrothermal Fluids in Active Hydrothermal Systems

Epithermal ore deposits are a specific class of hydrothermal ore deposits which are formed at relatively low temperatures ($< 300^{\circ}\text{C}$) and at shallow depths (ranging from at depth of 2 Km to the surface). According to Simmons *et al.* (2005) and Kesler & Wilkinson (2009) the fluids responsible for the formation of these deposits are both magmatic and meteoric travelling through fractures and permeable rocks. Epithermal deposits represent the most common and widely distributed hydrothermal concentrations of Au¹⁸ (Figure 3.1) and most such deposits are mined for Ag, Hg, Sb and As, as well as Au (Kesler & Wilkinson, 2009).

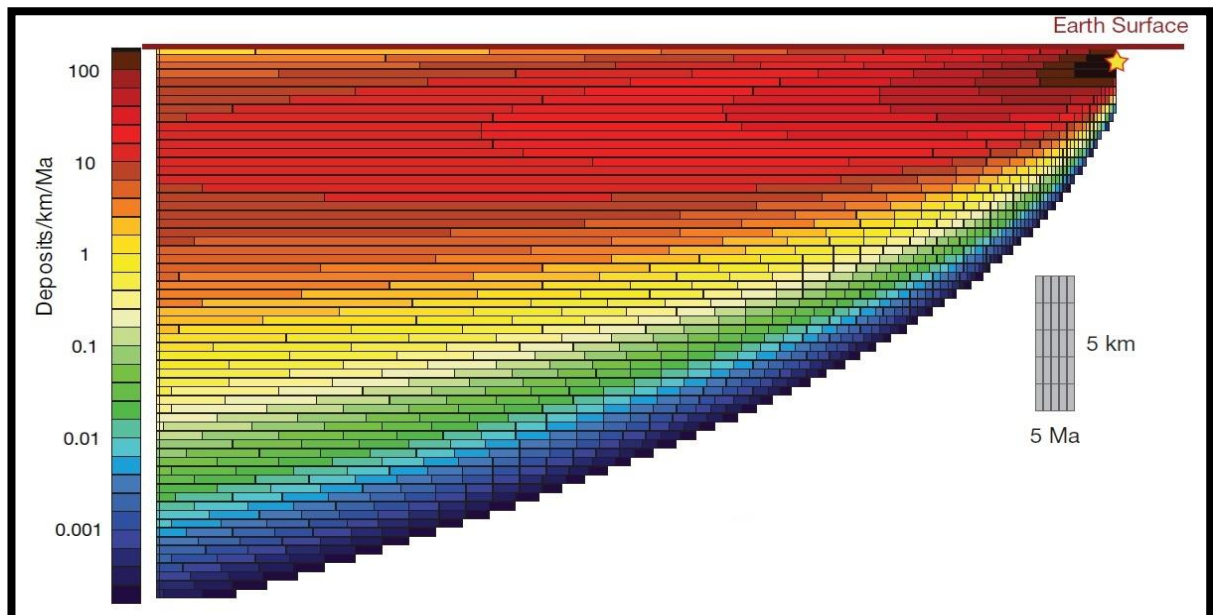


Figure 3.1: Model distribution of epithermal Au deposits in age-depth-space for the last 250 Ma of Earth history (age is shown on the X axis and depth on the Y axis; maximum age is 250 Ma and maximum depth is 20 Km), assuming that the number of the deposits on the current database (1164) represents all such deposits in the current database. Deposits enter the diagram at the upper right source region (star) at the rate of 562 deposits per m.y. and migrate (diffuse) across the diagram through time. Of the ~ 307000 deposits that formed over Phanerozoic time, about 20 % (63000) are preserved in the crust (42700 of those < 250 Ma in age are represented here), while 83 % have been removed by uplift and erosion. The gradual deepening of the maximum number of deposits with increasing time results from the loss of large numbers of deposits to erosion (from Kesler & Wilkinson, 2009).

¹⁸ Candela (2004) estimated that the average Au content of the crust is about 2.21 ppb and as Lodders & Feggly (1998) estimated the mass of the crust to be about $1.52 \cdot 10^{19}$ t, it can be calculated that the crust contains about $3.2 \cdot 10^{18}$ t Au, according to Kesler & Wilkinson (2009). Richards (2009) asserted that at one time around 0.03 % of crustal Au is concentrated in epithermal deposits, while significant amounts of Au pass through these deposits without being trapped (Simmons & Brown, 2007). The fact that epithermal deposits retain only a small fraction of the metal flux that passes through them – and not only Au in particular – underscores the conclusion that they are highly unusual geoclastic features (Kesler & Wilkinson, 2009).

It is most common to find such deposits spatially associated with volcanic rocks or shallow intrusive rocks, in plate convergence geotectonic settings. However, as has been demonstrated by many researchers (Sillitoe, 1993b; Cooke & Simmons, 2000; Hedenquist *et al.*, 2000; Simmons *et al.*, 2005; Kesler & Wilkinson, 2009), and as will be mentioned later in this chapter, epithermal deposits are found in rift and back-arc settings and even in areas exhibiting no magmatism. Since all these geodynamic settings were present throughout the geological history of the Earth, it is to be expected that such deposits are temporally and spatially widespread (Figure 3.2).

The characteristics of each epithermal deposit are controlled mainly by the composition of the ore fluid. This happens because, according to Henley (1990), there are differences in the solubilities of Au, Ag and base metals, depending upon the available chemical complexes. In effect, Au and Ag are transported as sulfide complexes and Ag plus any base metals as chloride complexes, in the temperature range at which epithermal deposits are formed. Moreover, S activity and the fluid's redox state affect the mineralogy as deduced by Barton *et al.* (1977) and Einaudi *et al.* (2003).

The fluid's composition and reactivity can be partly indicated by alteration and gangue mineral assemblages. However, the cardinal indicator of the composition of the ore fluid is the ore mineral assemblage. Indeed, there are many cases where distinctly different fluids are responsible for the mineralisation and the alteration (Sillitoe & Hedenquist, 2003). For example, many lithocaps hosting high sulfidation deposits are barren initially and are mineralised by later fluids. In intermediate sulfidation systems the fluid which creates quartz and carbonate gangue minerals is more often of lower salinity than the mineralising fluid (Simmons, 1991; Albinson *et al.*, 2001). In any case, as asserted by Saunders *et al.* (2008), Deditius *et al.* (2009), and Saunders & Brueseke (2012), the mineral textures indicate that a repetitive process of episodic nature is responsible for the formation of epithermal deposits.

There is considerable uncertainty surrounding the nature of magmatic contributions to epithermal precious metal deposits, although it is now generally accepted that the particular characteristics of an epithermal system are mainly dictated by the nature of the associated magmatism. Indeed, as Sillitoe & Hedenquist (2003) assert, this conclusion is corroborated by the control of metal associations in lithocap hosted deposits by the magma's oxidation state and the geochemical differences between arc hosted and rift hosted epithermal systems, which stem from the association with different magmatic suites (Figure 3.3).

It is difficult to estimate the initial depth at which an epithermal deposit was formed due to erosion. In most cases, the palaeosurface is not preserved; exceptions include some cases where the palaeosurface is preserved in the form of hot spring and/or sinter deposits. As Vikre (1987), Sherlock *et al.* (1995), and Wallace (2003) assert, only in these few cases there can be a direct – and consequently accurate – assessment of the epithermal deposit's formation depth. In other cases, Kesler & Wilkinson (2009) postulate that only fluid inclusion geobarometry can provide an estimation of an epithermal systems formation depth.

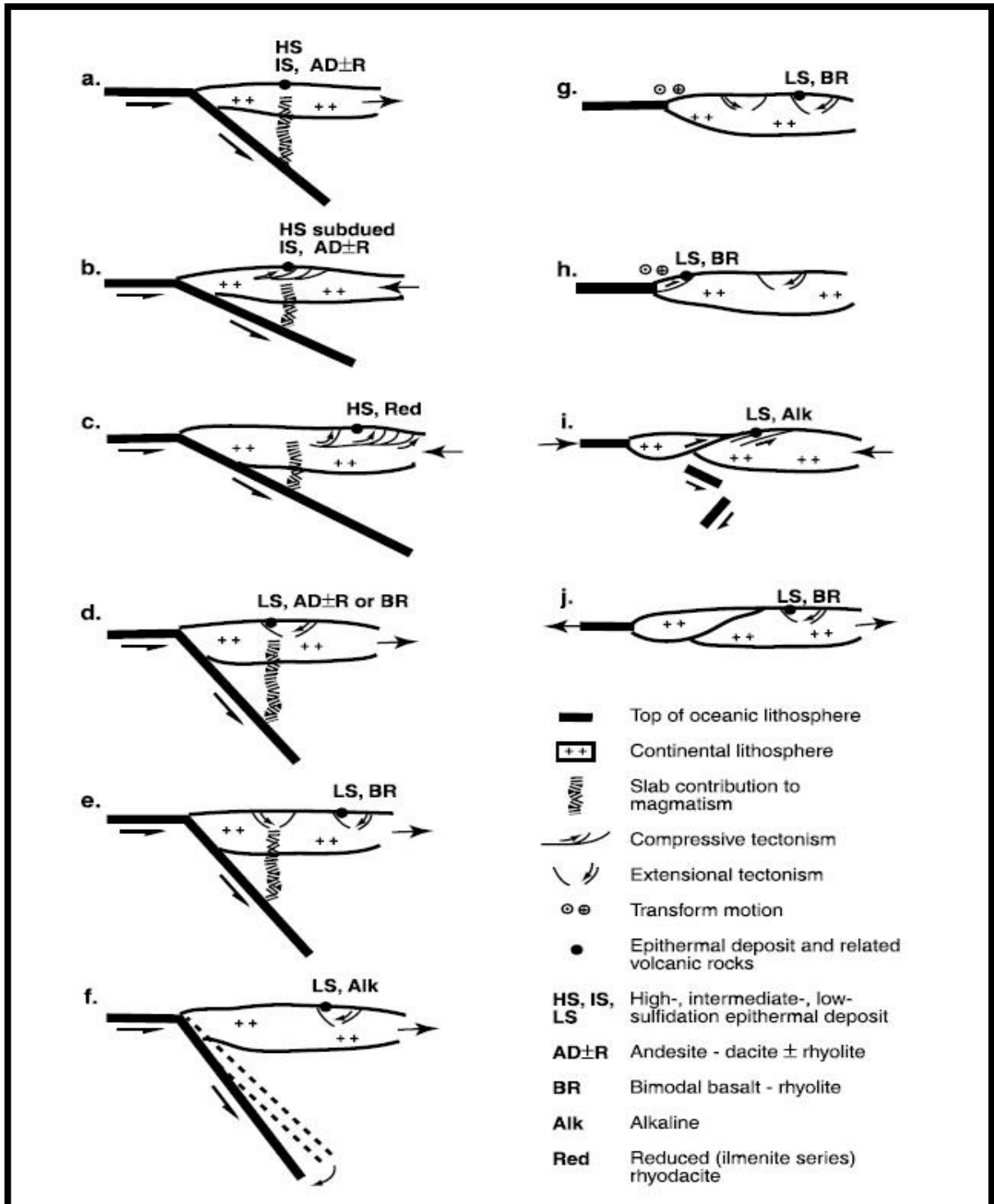


Figure 3.2: Schematic continental margin-scale sections illustrating selected volcanotectonic settings for high sulfidation, intermediate sulfidation, and low sulfidation epithermal deposits. a) Neutral stress to mildly extensional arc (e.g., Yanacocha, Peru). b) Compressive back arc during arc volcanism (e.g., Potosí, Bolivia). c) Compressive arc with subducted volcanism (e.g., El Indio). d) Extensional arc (e.g., Bodie, California or El Peñón, Chile). e) Extensional back arc during arc volcanism (e.g., Cerro Vanguardia, Argentina). f) Extensional back arc during transition from subduction-related to rift-related bimodal magmatism (e.g., Cripple Creek, Colorado). g) Extensional continental margin following cessation of subduction and advent of transform faulting (e.g., Bullfrog, Nevada). h) Compressive tectonism linked to transform fault boundary (e.g., McLaughlin, California). i) Restricted postcollisional magmatism during collision-induced slab breakoff and compressive tectonism (e.g., Porgera, Papua New Guinea). j) Extension due to tectonic collapse following continental collision (e.g., Baley, Russia) (from Sillitoe & Hedenquist, 2003).

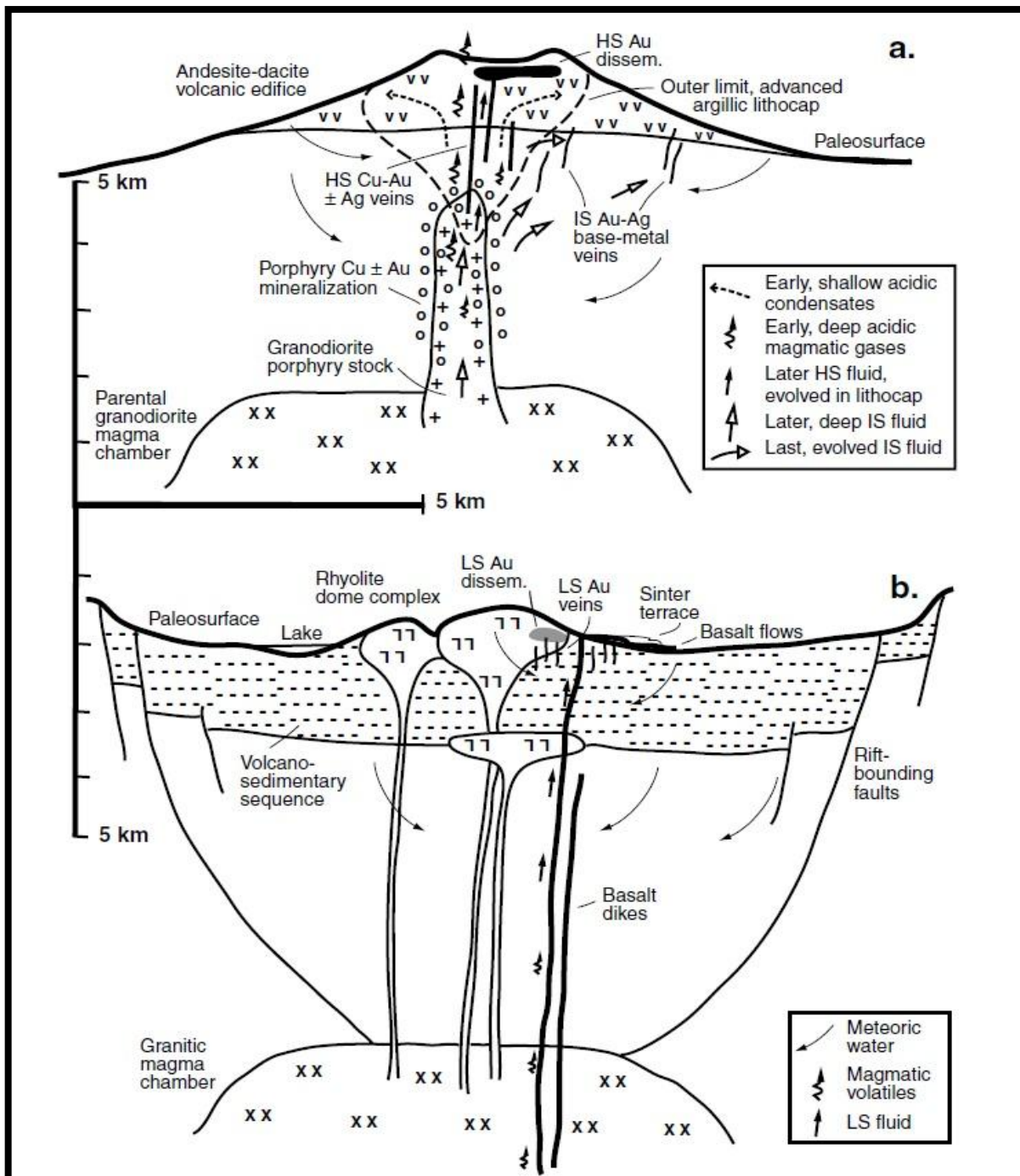


Figure 3.3: Schematic sections of end-member volcanotectonic settings and associated epithermal and related mineralization types. a) Calc-alkaline volcanic arc with neutral to mildly extensional stress state showing relationships between high- and intermediate-sulfidation epithermal and porphyry deposits (note that the complete spectrum need not be present everywhere). Early magmatic volatiles are absorbed into ground water within the volcanic edifice (shown here as a stratovolcano, but it may also be a dome setting) to produce acidic fluid for lithocap generation, over and/or supra-adjacent to the causative intrusion. Later, less acidic intermediate-sulfidation fluid gives rise to intermediate-sulfidation mineralization, both adjacent to and distal from the advanced argillic lithocap. Where the intermediate-sulfidation fluid flows through the leached lithocap environment, it evolves to a high-sulfidation fluid (Einaudi *et al.*, 2003) to produce high-sulfidation veins or disseminated mineralization, depending on the nature of the structural and lithological permeability. The high-sulfidation fluid may evolve back to intermediate-sulfidation stability during late stages, supported by paragenetic relationships and lateral transitions of high- to intermediate-sulfidation mineralogy. b) Rift with bimodal volcanism and low-sulfidation deposits. Deep neutralization of magmatic volatiles, typically reduced, results in a low-sulfidation fluid for shallow low-sulfidation vein and/or disseminated mineralization and related sinter formation (from Sillitoe & Hedenquist, 2003).

A comparison between the main geochemical characteristics and differences of porphyry and epithermal deposits can give an insight to the different formation procedures and the rate of accumulation of metals in the Earth's crust. According to Kesler & Wilkinson (2009) approximately 3.4 times more Cu has been «trapped» in porphyry deposits than Au in epithermal ones. This indicates that the associated geochemical processes are more efficient in extracting Cu rather than Au. In general, epithermal deposits are more numerous, albeit smaller, than porphyry deposits, which can be attributed to the limited thermal potential of short lived geothermal systems in the upper crust. Additionally, porphyry deposits conform more or less to general mineralisation style and form; epithermal deposits are significantly more varied. Finally, the cardinal difference between porphyry deposits and high sulfidation epithermal systems is that the low salinity fluid associated with the high sulfidation ores is separated from the higher salinity fluid at depth, whereas in porphyry systems, hypersaline brine and low salinity vapour coexist¹⁹ (Hedenquist & Lowenstern, 1994).

3.1: LOW SULFIDATION EPITHERMAL DEPOSITS

One significant characteristic of low sulfidation deposits is the absence of ore concentrations of Cu. Most probably this is the result of the neutral low salinity reducing fluids by which they are formed and which are not efficient in the transport of Cu (Hedenquist & Lowenstern, 1994). According to Sillitoe (1989) they form at a distance from the inferred magmatic source, at temperatures between 200° and 300° as mentioned by Heald *et al.* (1987).

There are several classification schemes for epithermal deposits, although the most appropriate one seems to be the classification based on metal content, which reflects intrinsic geochemical differences. Accordingly, low sulfidation epithermal deposits are subdivided in two major classes:

- Au-rich low sulfidation epithermal deposits, associated with low salinity but gas rich fluids, with an Ag/Au ratio between 1/10 and 10 (Hedenquist & Henley, 1985).
- Ag-rich low sulfidation epithermal deposits, associated with more saline liquids (Simons *et al.*, 1988), with an Ag/Au ratio of over 100.

As Seward (1981) has mentioned, the difference in salinity is crucial to the metal transporting capacity of fluids, as Au is transported as a bisulfide complex, while Ag, Zn and perhaps Pb, are transported by chloride complexes in such a reduced environment.

In most of the low sulfidation deposits gangue minerals are dominated by bands of botryoidal chalcedony and cryptocrystalline quartz²⁰ with adularia – and typically late – calcite. Illite and smectite may also be present.

The argillic alteration haloes consist of illite or illite-smectite. In many classic such deposits electrum is associated with pyrite, marcasite, arsenopyrite, pyrargyrite, acanthite and Ag-selenides. There may also be minor chalcopyrite, Fe-sphalerite, pyrrhotite, typically up to 2 vol % of the ore zones (Sillitoe, 1993b; John, 2001).

¹⁹ It is possible that this fact can be attributed to the difficulty of a dense brine to ascend at shallow depths.

²⁰ Quartz textures in epithermal systems are analysed at Appendix VI.

3.1.1: Volcanotectonic Setting of Low Sulfidation Deposits

A significant number of low sulfidation deposits are associated with bimodal volcanism, in a variety of continental and island arc rifts. These rifts may occur in back arc settings, intra-arc settings or near arc settings²¹. Subduction of oceanic crust can be happening concurrently or not. The tectonic cause of the rifting can be one of the following:

- Slab rollback caused by steepening or waning subduction (Sillitoe & Hedenquist, 2003)
- Oblique subduction possibly leading to the creation of slab windows (Sillitoe & Hedenquist, 2003)
- Asthenospheric upwelling caused by slab breakoff (Sillitoe & Hedenquist, 2003)
- Gravitationally controlled lateral expansion of thickened crust due to contractional deformation (Sillitoe & Hedenquist, 2003)
- Hot spot activity (Sonder & Jones, 1999)

In all these cases there is widespread bimodal activity with a combination between basaltic (or basaltic andesite) and rhyolite (or rhyodacite), of calc-alkaline and/or tholeiitic affinities. There is a notable deficiency of andesitic and dacitic rock compositions (Sillitoe & Hedenquist, 2003).

In island arc environments, where there exists intra-arc and back arc rifting, accompanied by bimodal volcanism, the low sulfidation deposits appear to form along strike from marginal ocean basins. This is the case of the low sulfidation deposits in Southern Kyushu and NE Hokkaido in Japan (Watanabe, 1995). Also, Hillemeier *et al.* (1991) report many such deposits from the Gulf of California, which are associated with bimodal magmatism with a pronounced basaltic component.

In some fairly rare cases, low sulfidation deposits can be formed even in andesite-dacite-rhyolite arc terranes. It is hypothesised that extension must be quite advanced, and possibly close to bringing about bimodal magmatism. This is the case of the Round Mountain Au deposit in Nevada, reported by Axen *et al.* (1993).

A common characteristic of the aforementioned settings is the existence of a low topographic relief. Such a relief results in the accumulation of siliciclastic sediments of fluvial and lacustrine origin. Hydrothermal activity and sedimentation are contemporaneous, since there is a spatial association between low sulfidation deposits and sediments – in some cases the deposits themselves are hosted by the sedimentary sequences. It is possible for disseminated low sulfidation mineralisations to form before or after lithification (Sillitoe & Hedenquist, 2003).

According to Fournier (1987) this setting is very favourable for the preservation of hot springs' sinters, which are a feature of many low sulfidation deposits. Such sinters appear

²¹ Although low sulfidation deposits are, as a rule, connected to extensive tectonic settings, there is an exception. The McLaughlin deposit, in the Coast Ranges of California, was formed during a regional transpressive setting, within the San Andreas transform fault (Tosdal *et al.*, 1996).

only rarely in relation to intermediate sulfidation deposits and never in relation to high sulfidation deposits, since the prevailing conditions are highly acidic.

At this point low sulfidation deposits related to alkaline rocks must be mentioned. Although not a typical case, this category involves some giant deposits, along with some smaller ones. Alkaline magmatism occurs within or beyond inactive arcs, and also in back arc settings and near arcs' termini during active subduction (Sillitoe & Hedenquist, 2003). In general, alkaline rocks seem to be generated in response to tectonic readjustments (Richards, 1995). The most prominent examples of these deposits are the Au telluride veins at Cripple Creek, Colorado (Kelley *et al.*, 1998), the Au telluride veins at Emperor, Fiji (Eaton & Setterfield, 1993) and the Au mineralisation at Ladolam, Papua New Guinea (Müller *et al.*, 2002; Carman, 2003).

3.1.2: Chemical Composition of Low Sulfidation Hydrothermal Fluids

The temperature and salinity constraints on low sulfidation fluids remain somewhat ambiguous since there are analytical problems regarding the associated fluid inclusions, which provide much of the necessary information. The difficulty in studying these fluid inclusions stems from the fine crystallinity of their main host, quartz. According to Sander & Black (1988) even some existing results may be false, since some chalcedony bands may have originally precipitated as opal or amorphous gel.

Despite the aforementioned, John (2001) has deduced that the salinity of these fluids is no higher than 2 wt. %. As Hedenquist & Henley (1985) point out, it cannot be precisely estimated how much of this apparent salinity is contributed by CO₂ and H₂S. Etoh *et al.* (2002) indicate similarly low salinities, below 1.5 wt. % NaCl_{equiv.} in average.

The aforementioned fluids correspond to low sulfidation environments linked to tholeiitic and calc-alkaline magmatism, with a usually pronounced bimodal magmatism. In stark contrast, low sulfidation environments linked to alkaline magmatism exhibit salinities between 3 and 9.6 wt. % NaCl_{equiv.}, as attested by Richards (1995). There is still no clear explanation for this difference (Sillitoe & Hedenquist, 2003).

3.1.3: Sources of Low Sulfidation Hydrothermal Fluids

The clear association of low sulfidation deposits, associated with alkaline rocks, to magmatism and, in some cases, porphyry deposits has long been emphasised by Bonham (1988), Richards (1995), and Jensen & Barton (2000). This relationship drove Giggenbach (1997) to suggest that rock buffering in systems hosted by alkaline rocks is much more effective than in systems hosted by calc-alkaline rocks. So, according to Sillitoe (2002) the former can generate low sulfidation and not high sulfidation mineralisations.

Hedenquist & Lowenstern (1994) have concluded that the evidence for meteoric water contribution in these systems is more prominent when the magmatic activity is most voluminous. This can be explained by the heat provided by the magma source, which leads to extensive meteoric water convection – such a convection will obliterate any evidence of early magmatic water contribution.

The magmatic input mentioned may be of a distinctive character. This is inferred by the presence of roscoelite – the vanadian mica – in many low sulfidation systems hosted by alkaline rocks. Characteristic examples are the Cripple Creek deposit, USA, the Emperor deposit, Fiji, and the Porgera zone VII deposit, Papua New Guinea (Sillitoe & Hedenquist, 2003).

Many epithermal deposits, of all sulfidation states, are characterised by the presence of Hg-bearing, Au-bearing, Ag-bearing and Bi-bearing tellurides, albeit in minor amounts. In the special case of alkaline hosted low sulfidation deposits, Te is sometimes sufficiently abundant so as most of hypogene Au occurs as tellurides²² (Sillitoe & Hedenquist, 2003).

Such a close connection to magmatism is the most likely cause of the high salinities measured in low sulfidation hydrothermal fluids. It must be noted however that the Ag/Au ratios of such fluids is extremely low, most often ≤ 1 , a fact most probably indicative of the distinctive character of magmatic input (Sillitoe & Hedenquist, 2003).

All the aforementioned low sulfidation deposits, which are related to alkaline rocks, show clear-cut relations to magmatism. This is not the case for the rest of the low sulfidation deposits as Heald *et al.* (1987), Hedenquist (1987) and Cooke & Simmons (2000) have pointed out. For the source of precious metals in these deposits, Hedenquist & Lowenstern (1994) proposed the concept of wall rock flushing, which seems less likely today. Matsuhisa & Aoki (1994) have instead proposed the possibility of contribution from deep seated magma chambers.

The study of the nature of low sulfidation mineralising fluids is not feasible by means of stable isotope studies, due to the recrystallisation of amorphous silica to quartz (Sillitoe & Hedenquist, 2003). However, Faure *et al.* (2002) have studied stable isotopes from associated clays and have corroborated the existence of a degree of magmatic input.

In the case of rift related low sulfidation deposits there is a deficiency of base metals, Mn-carbonates and Mn-silicates. Such characteristics may be the result of the nature of the magmatic fluid (Sillitoe & Hedenquist, 2003). Many such deposits are related to rhyolitic domes, and the basaltic component of the bimodal magmatic suites may play a fundamental role in the provision of S, chloride and even metals (Noble *et al.*, 1988; Hattori & Keith, 2001).

In general, there are multiple sources of components in low sulfidation fluids, which are attributed to the extensive amount of interaction between thermal waters and host rocks. Any reactive magmatic components will be neutralised and reduced and in turn derive components from the host rocks (Hedenquist & Lowenstern, 1994). Such a process also results in an integrated isotopic signature which «masks» the variety of fluids present at early stages, as mentioned before.

²² The Sacarimb deposit in Romania and the Kochbulak deposit in Uzbekistan are exceptions to this rule. Both are intermediate sulfidation deposits which are however characterised by the fact that most of the hypogene Au is present as tellurides (Kovalenker *et al.*, 1997; Alderton & Fallick, 2000).

3.2: INTERMEDIATE SULFIDATION EPITHERMAL DEPOSITS

Intermediate sulfidation deposits are characterised by a wide range in metal complement and characteristics. With a division at $\text{Ag}/\text{Au} \approx 50$, there are Au-Ag and Ag-Au deposits, and Ag base metal deposits as mentioned by Albinson *et al.* (2001).

The quartz veins associated with such deposits are typically crystalline and include Mn-bearing carbonates and silicates, and up to roughly 10 wt. % sulfides. The minerals characteristic of intermediate sulfidation systems are galena, tetrahedrite-tennantite, chalcopyrite and low Fe-sphalerite (Sillitoe & Hedenquist, 2003).

Base metal rich intermediate sulfidation deposits typically contain sericite instead of adularia and as such they are believed to have formed at higher temperatures and with limited boiling – most probably this is the result of greater formation depths. Such deposits are found in Northern Peru (Kamilli & Ohmoto, 1977) and in Philippines and in Papua New Guinea (Sillitoe, 1989).

3.2.1: Volcanotectonic Setting of Intermediate Sulfidation Deposits

These deposits are mostly found in calc-alkaline dacitic-andesitic arcs, much like high sulfidation deposits, but they are hosted by more felsic rocks (Sillitoe & Hedenquist, 2003). Small such deposits adjoin advanced argillic lithocaps which sometimes host high sulfidation deposits (Sillitoe, 1999). Claveria (2001) has reported the largest such example, the Victoria deposit, alongside the Lepanto high sulfidation deposit in Philippines.

It is possible for an intermediate sulfidation deposit to be spatially associated with a porphyry deposit, or be entirely unrelated. Examples of the first category are the Baguio district (Sillitoe, 1989) and the deposits in the South Apuseni Mountains of Romania, the Valea Morii and Rosia Poeni deposits (Ivascanu *et al.*, 2002). In the second category the most characteristic examples are those of the epithermal Ag belt of Mexico (Albinson *et al.*, 2001).

The most important examples of intermediate sulfidations deposits – especially Au-Ag intermediate sulfidation deposits – have formed in neutral to mildly extensional geodynamic settings (Sillitoe & Hedenquist, 2003). Such is the case of the intermediate sulfidation deposits of the Great Basin in Nevada, first reported by Bonham (1969). Other examples include the Kelian deposit in Indonesia (van Leeuwen *et al.*, 1990) and the Toyoha deposit in Japan (Watanabe, 2003). Sometimes, it is also possible to find intermediate sulfidation deposits in compressive arcs, such as the Victoria deposit in Philippines (Sillitoe & Hedenquist, 2003).

3.2.2: Chemical Composition of Intermediate Sulfidation Hydrothermal Fluids

As mentioned by Simmons (1991) and verified by Albinson *et al.* (2001), in most intermediate sulfidation deposits there is evidence for a high degree of mixing of end member fluids, which most likely correspond to different stages. For Zn-Pb-Ag deposits salinities range between 12 and 23 wt. % NaCl_{equiv.} and for Ag-Zn-Pb deposits between 7.5 and 12

wt. % NaCl equiv. Ag-rich precious metal deposits are characterised by salinities < 3.5 wt % NaClequiv. – Albinson *et al.* (2001) mention the likelihood that a portion of the apparent salinity is caused by dissolved gas. Sillitoe & Hedenquist (2003) have reported that Ag-Au deposits exhibit lower salinities (2-4 wt. % NaClequiv.) at a late Au rich stage.

So, it can be concluded that there is a regular increase in salinity, and most strikingly in the maximum salinity, with increasing base metal content and Ag/Au ration. The majority of intermediate sulfidation deposits bear evidence of low salinities (with a minimum of 2 wt. % NaClequiv.) although careful examination reveals sharp fluctuations in salinity depending on the genetic stage of the system (Albinson *et al.*, 2001).

3.2.3: Sources of Intermediate Sulfidation Hydrothermal Fluids

It seems that in the case of intermediate sulfidation deposits there is a close magmatic association, which is however not as strong as in the case of high sulfidation deposits (Albinson *et al.*, 2001). Margolis *et al.* (1991) and Sillitoe (1989, 1999) have reported that it is common for intermediate sulfidation deposit to be temporally and spatially linked to high sulfidation deposits and volcanic centres. Such a connection between high and intermediate sulfidation systems has two possible explanations:

- The deep fluid completely bypasses the lithocap thus generating intermediate sulfidation veins in various distal positions (Sillitoe & Hedenquist, 2003).
- A deep intermediate sulfidation fluid evolves to a high sulfidation one upon entering the unbuffered lithocap. Then neutralisation and reduction follow, which revert the fluid back to intermediate sulfidation, as a result of the fluid-rock interaction (Margolis *et al.*, 1991; Sillitoe, 1999; Einaudi *et al.*, 2003).

In general, it seems that the second option is more viable, since it is supported by field observations and relevant data from the Julcani and Colquijirca districts of Peru and from the Pyramid district of Nevada (Deen *et al.*, 1994).

Base metal rich Ag intermediate sulfidation deposits are formed by saline fluids, with salinities ranging between 5 and 20 wt. % NaClequiv. Despite the fact that their existence is known in epithermal systems they have not been observed in active volcanic hosted systems. Simmons (1991) has reported that it is possible for brines to be injected into otherwise low salinity systems, so this may be a viable explanation to the aforementioned enigma.

Additionally, it is yet not possible to explain the reason why saline fluids give rise to Zn-Pb dominated mineralisation and not Cu dominated mineralisation. Einaudi *et al.* (2003) have speculated that Zn-Pb mineralisations are zoned from deeper Cu mineralisation due to the existence of the thermal gradient. There is also the possibility that the magmatic metal inventory is radically different (Sillitoe & Hedenquist, 2003).

3.3: HIGH SULFIDATION EPITHERMAL DEPOSITS

Most high sulfidation deposits are hosted by lithocaps but not all lithocaps are mineralised on initial formation. High sulfidation deposits are typically formed at shallow depths, and bear evidence of magmatic involvement in their formation (Rye, 1993). It must be noted that high sulfidation epithermal systems share many mineralogical and stable isotope characteristics with the advanced alteration zone capping porphyry Cu deposits (Hemley & Hunt, 1992; Rye, 1993).

3.3.1: Volcanotectonic Setting of High Sulfidation Deposits

It is most common to find the typical Au-Cu bearing high sulfidation epithermal deposits in calc-alkaline andesitic-dacitic arc terranes (Sillitoe & Hedenquist, 2003). However, even felsic rocks, such as quartz latites can exhibit a genetic link to such mineralisations. This is the example of the Summitville HS hydrothermal deposit in Colorado, which was reported by Steven & Ratté (1960). According to Sillitoe (1993a) rhyolitic rocks lack HS mineralisations in general and it is evident that the majority of such deposits are found in neutral stress or mild extension tectonic settings. The most characteristic such example is the giant low grade high sulfidation Au deposit – along with the underlying porphyry Cu deposit – at Yanacocha, which lies in the extensional Calipuy arc, in Peru (Petford & Atherton, 1994).

Other examples of high sulfidation deposits are Bor and Chelopech in the Srednogie belt (Ciobanu *et al.*, 2002), which were formed in an extensional tectonic setting controlling the manifestation of intermediate to high K calc-alkaline volcanism.

The development of a bimodal (basaltic-rhyolitic) magmatic character is evidence of advanced extension in arc environments, which is not associated with high sulfidation deposits and their precursor lithocaps (Sillitoe & Hedenquist, 2003). Franco *et al.* (1999) have reported one of the few exceptions to this general rule, the high sulfidation Au occurrences in the Los Menucos district in the Patagonian Andes in Argentina, where there is a spatial association with rhyolitic domes.

Likewise, according to Sillitoe (2002) alkaline volcanic and associated subvolcanic rocks are not correlated with either high sulfidation mineralisations or at least barren lithocaps, whatever the tectonic setting. However, there are once more exceptions to this deduction, like the Navisi III prospect in Fiji, reported by Eaton & Setterfield (1993).

Additionally, in compressive arc settings, both low grade and high grade HS Au-Ag deposits can be found. The most characteristic example is that of the El Indio belt in Chile (Bissig *et al.*, 2002). In this locality, the intense compression acted against eruptive activity (Takada, 1994), so there are no large volumes of coeval volcanic and subvolcanic rocks associated with such deposits (Sillitoe & Hedenquist, 2003). Another example is found in the Luzon Central Cordillera, North Philippines, where there exists an advanced argillic lithocap hosting a HS mineralisation, in spatial association with numerous Cu-Au porphyry deposits.

It must be noted that, as Sillitoe (1998) asserts, the most important Cu porphyry deposits have formed in compressive tectonic regimes, most commonly during periods of stress relaxation (Tosdal & Richards, 2001). It is remarkable that, despite the presence of advanced argillic lithocaps, there are no contemporary associated high sulfidation epithermal mineralisations. Such is the example of the porphyry Cu belt of Northern Chile (Sillitoe & Hedenquist, 2003).

A special case is that of Ag ± Sn ± Sb high sulfidation deposits, lacking appreciable Cu, Au and As, found in back-arc settings. These deposits are associated with reduced rhyodacites of mostly peraluminous nature (Sillitoe *et al.*, 1998). Such is the example of the Cordillera Oriental in Bolivia (Lamb *et al.*, 1997).

3.3.2: Chemical Composition of High Sulfidation Hydrothermal Fluids

The hydrothermal fluids which form high sulfidation ore deposits are of strongly acidic nature, since a pH lower than 2 is required for the leaching necessary to create the lithocap, as well as for the creation of quartz-alunite alteration. According to Stoffregen (1987), a pH lower than 2 is necessary for the mobilisation of alumina, and in addition to this alunite is formed at pH values between 2 and 3. The hosting of ore minerals by the vuggy quartz zone means that there seldom are any minerals indicative of pH (Sillitoe & Hedenquist, 2003).

Studies by Arribas (1995) and Hedenquist *et al.* (1998) indicate that the early leaching fluid, preceding high sulfidation mineralisation is a condensate of magmatic vapour, with a relatively low salinity (< 1 wt. % NaCl equiv.). Fluid inclusion studies by Arribas (1995) were indicative of the presence of many hydrothermal fluids during the life of a hydrothermal system, with salinities ranging between 1 wt. % and 45 wt. %. According to Rye (1993) and Arribas *et al.* (1995) the hypersaline fluids are either present early in the paragenesis or in sericitic and K silicate alteration related to deeper intrusions.

It is believed that Ag/Au ratios are possibly controlled by the metal endowment of the associated magmas – this is the case of the lithocap hosted deposits of the Bolivian Sn-Ag belt reported by Sillitoe *et al.* (1998). In effect, the chloride contents of the early sulfide precipitating fluids do not totally control the Ag content of high sulfidation deposits. Hedenquist *et al.* (1998) mention also that the high sulfidation ore fluids are affiliated with the sericitic stage of underlying porphyry deposits.

3.3.3: Sources of High Sulfidation Hydrothermal Fluids

It is generally believed that the early hydrothermal fluids responsible for the advanced argillic alteration are generated by absorption of magmatic volatiles – most notably HCl and SO₂ – into meteoric water aquifers (Sillitoe & Hedenquist, 2003). There is as yet no consensus as to the origin of the mineralising fluid. Sillitoe (1983) and Heinrich *et al.* (1999) have proposed the possibility of magmatic vapour, while White (1991) supports the idea of magmatic brines, and Hedenquist *et al.* (1998) the existence of unseparated magmatic fluid. Sulfur isotope data are indicative of magmatic fluids according to Rye (1993, 2005). In any case as thermal

activity wanes the involvement of groundwater and/or seawater becomes more evident (Figure 3.4).

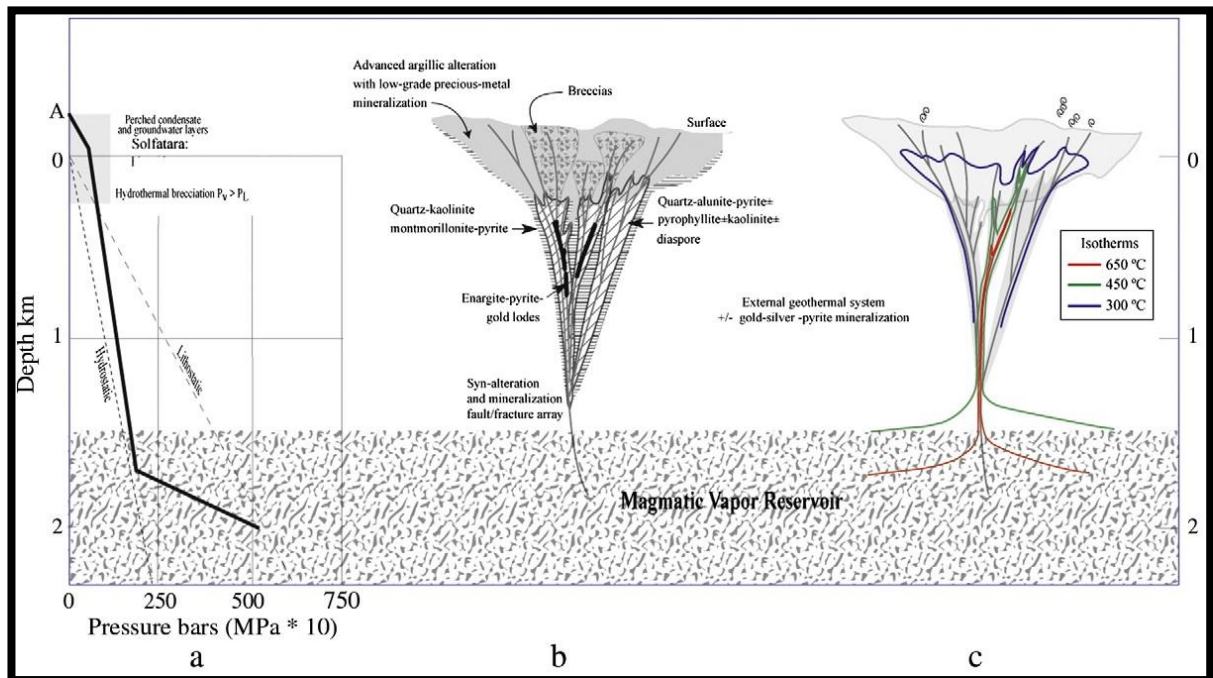


Figure 3.4: The relationship between pressure, temperature and depth for a magmatic vapour expanding to the surface through a fracture array, in relation to the scale and geologic elements of a typical high sulfidation deposit. At the surface, rapid open system cooling occurs due to atmospheric intrusions and mixing with shallow groundwater or perched layers of condensate to produce a solfataric environment (from Henley & Burger, 2011).

According to Hedenquist *et al.* (1998), and Sillitoe (1999) Au precipitates later in the paragenetic sequence and is associated with intermediate sulfidation minerals like chalcopyrite and tennantite. On the other hand, Cu deposition precedes this stage and happens by intermediate salinity – between 4 and 20 wt. % NaCl equiv. – high sulfidation fluids, as evidenced by the presence of enargite. It is even possible for this high sulfidation fluid to become locally neutralised which results in the deposition of carbonate minerals (Sillitoe & Hedenquist, 2003).

Most rhyolitic magmatic volcanic sequences are characterised by deep magma chambers which results in a frequent absence of lithocaps. The deeper the magma chamber the lower the amount of volatiles that will be exsolved. Those volatiles that are exsolved will react with the rocks while they ascend and will more or less be neutralised. This process was termed «**primary neutralisation process**» by Giggenbach (1992).

Conversely, high sulfidation epithermal deposits linked to alkaline magmatism most often lack lithocaps but the magma chambers of alkaline suites are placed close to the surface. Moreover, according to Bailey & Hampton (1990), Hedenquist (1995) and Hattori & Keith (2001) alkaline magmas exsolve vapours richer in SO₂ – compared to calc-alkaline ones – and exhibit increased Cl solubilities, being alkali rich and silica poor (Signorelli & Carroll, 2000). Taking these into account, Sillitoe (2002) asserted that the creation of advanced argillic alteration can be explained by the high acid-buffering capacity of alkaline rocks when subjected to intense alkali and carbonate alteration. On the other hand, lithocaps have no

buffering capacity and as such no high sulfidation state minerals can be developed (Jensen & Barton, 2000; Einaudi *et al.*, 2003; Sillitoe & Hedenquist, 2003).

3.4: RANGE OF COMPOSITIONS OF HYDROTHERMAL FLUIDS IN ACTIVE HYDROTHERMAL SYSTEMS

Active hydrothermal systems have been studied extensively (Henley & Ellis, 1983; Giggenbach, 1992, 1997), both in the magmatic-hydrothermal and in the geothermal environment, which are the two extremes regarding fluid composition. The most important characteristics in determining the volcanotectonic setting are salinity and gas content.

Geothermal systems are characterised by an almost neutral pH and are quite reduced in nature. The ascent of fluids in geothermal systems is relatively slow and, as deduced by Giggenbach (1992), it results in them being in equilibrium – or at least close to equilibrium – with the altered host rocks (this is termed a «**rock dominated environment**»). Salinity values range between < 1 and 2 wt. % NaClequiv. and the fluids are relatively gas rich, dominated by CO₂ with subordinate H₂S and N₂ (Sillitoe & Hedenquist, 2003). There are geothermal systems with relatively saline waters but they are not frequently observed. Those that do exist are found inside closed sedimentary basins, the high density of liquid preventing discharge to the surface.

There are many different volcanotectonic settings but as various studies have demonstrated (Hedenquist & Henley, 1985; Giggenbach, 1995) the salinity of hydrothermal fluids is limited to ≤ 2 wt. % NaClequiv., even at drilled depths of 2 or 3 Km. So this is a low salinity range, within which there are two end members which can be distinguished (Sillitoe & Hedenquist, 2003):

- Andesite arc hosted systems like those in Philippines and Japan, which have actual salinities up to 1 to 2 wt. % NaCl equiv.
- Felsic rock hosted systems like those in the Taupo Volcanic Zone, North Island, New Zealand and basalt systems in Iceland, which have maximum salinities between 0.3 and 0.5 wt. % NaCl equiv.

Magmatic-hydrothermal systems occur proximal to volcanic vents, which focus the discharge of magmatic vapours to the surface. Their surface manifestation is in the form of fumaroles and condensates of highly acidic water (with a pH value of about 1). According to Giggenbach (1997) the acidic fluid is not at equilibrium with the host rocks, owing to its magmatic origin (this is termed a «**fluid dominated environment**»). In these systems, the fluids leach the host rocks and so create distinctive lithocaps – these may later host high sulfidation deposits. However, according to Einaudi *et al.* (2003) the mineralising fluids are more oxidised and less acidic, similar to those in intermediate sulfidation deposits. In any case, as Einaudi *et al.* (2003) have indicated, the evolutionary paths of low sulfidation fluids and high sulfidation fluids are distinctly different. Volcanic hosted systems worldwide have salinities lower than those of seawater – typically less than 2 wt. % NaClequiv. – with the exception of the apparently amagmatic closed basin systems (Sillitoe & Hedenquist, 2003).

CHAPTER 4: CRYSTALLOGRAPHY AND MINERAL CHEMISTRY OF MOLYBDENITE

Occurrence and Geochemistry of Molybdenite ~ Trace Elements in Molybdenite

Despite many decades of research, there is not yet any consensus on the source of molybdenum in mineralised magmatic suites. Earlier researchers (Westra & Keith, 1981; Carten *et al.*, 1993) have proposed that molybdenum has a mantle origin, since there is a strong link between molybdenum and within-plate basalts. On the other hand, based mainly on the example of the Colorado Mineral Belt, Sinclair (2007) proposed that molybdenum may originate from the upper mantle.

Data from relative literature (Shirey & Richardson, 2011; van Kranendonk, 2011; Golden *et al.*, 2013) suggest that there were episodic pulses of molybdenum mineralisation, dating back to almost 3 Ga. It must be borne in mind that molybdenum is a trace element in Earth's crust, with an average concentration of 1 ppm. So, it is a logical assumption that molybdenum was cycled repeatedly through geological processes, since the beginning of modern plate tectonics²³. Mo exhibits the greatest enrichment in reducing sediments (Miller *et al.*, 2011), and is also present in modern seawater²⁴ as the oxyanion molybdate (MoO_4^{2-}), as documented by Letowski *et al.* (1966).

The crystal structure of molybdenite comprises S-Mo-S layers, characterised by dense packing. Theoretically, there could be many different ways for the spatial arrangement of such layers. However, studies in both natural and synthetic molybdenites indicate that there only two possible arrangements – in crystallographical terms different arrangements are called «**stacking sequences**».

In both stacking sequences the S-Mo-S layers are identical and the only difference is the length of *c*. Hence, molybdenite has two **polytypes** (Newberry, 1979a). The most common polytype in nature, 2H, is characterised by two layers per unit cell and the less common, 3R, is characterised by three layers per unit cell. The first polytype is hexagonal and the second is rhombohedral²⁵ (Newberry, 1979a).

²³ In fact molybdenums' and molybdenites' fluctuations can be correlated with supercontinent stability and breakup phases, as demonstrated by Golden *et al.* (2013).

²⁴ There are also other examples of the presence of Mo and Re in the biosphere. Most notably, Mo is incorporated into the enzyme nitrogenase (Einsle *et al.*, 2002), and Re is bioaccumulated into certain seaweeds (Yang, 1991; Miller *et al.*, 2011).

²⁵ More details on the determination of molybdenite's crystal structure and on the polytypism phenomena are referred in Appendix VII.

4.1: OCCURENCE AND GEOCHEMISTRY OF MOLYBDENITE

Molybdenite (MoS_2) is a relatively common accessory mineral in silicic magmas and according to Herd (2008) can be found more often in within-plate rhyolitic magmas. This is most probably due to their relatively reduced state. Yet, molybdenite is considered by Audétat *et al.* (2011) to be a very uncommon magmatic phase, with the only such case reported being in peralkaline rhyolites from Pantelleria, Italy (Lowenstern *et al.*, 1993).

Molybdenite contains about 60 wt. % Mo, which is 10^4 times more than the Mo contained in the coexisting melt. Consequently, once Mo saturation has been attained, then the concentration of Mo in the melt (symbolised as [Mo]) cannot be increased further, unless, as Audétat *et al.* (2011) postulate, changes in $f\text{O}_2$, $f\text{S}_2$ and temperature increase the maximum Mo saturation.

Pearce *et al.* (1984) have studied melt inclusions from molybdenite-saturated samples, which indicate a clear affinity to within-plate granites and thus to an enriched mantle source. Conversely, melt inclusions from molybdenite-undersaturated samples are more diverse, and cover the fields of within-plate, volcanic-arc and syn-collisional granites, as mentioned by Audétat *et al.* (2011).

As Zajacz *et al.* (2008) have noted, silicate melts, even those characterised by a high degree of fractionation, do not contain more than 20 ppm of molybdenum. This can be explained by the above-mentioned constraints on molybdenum's magmatic saturation. Mo can be removed by exsolving fluids, as Candela & Holland (1984) and Keppler & Wyllie (1991) have ascertained. It can also be incorporated into crystallising minerals, like magnetite, pyrrhotite or ilmenite. However, Audétat *et al.* (2011) do not believe that this would have any meaningful impact due to the fairly low relevant crystal/melt partition coefficients. So, it can be concluded that the main process by which molybdenum's concentration in the melt can be lowered is its removal by exsolving fluids.

Audétat *et al.* (2011) report that it is possible for Mo to be fractionated by physical processes. For example, gravitational settling could be an important mechanism, which however is not considered to be efficient in this particular case, owing to the small size of molybdenites' grains. Moreover, the grains of molybdenite tend to adhere to quartz phenocrysts.

Geochemical experiments by Shinohara *et al.* (1995) and Audétat *et al.* (2011) have come to the conclusion that it is feasible for molybdenite platelets to be transported upward attached to rising fluid bubbles. This fact coupled with molybdenum's hydrophobic nature – which creates its tendency to float on a fluid's surface – has led the aforementioned researchers to conclude that the transport of molybdenum through magmatic fluids could be very effective.

Molybdenite can be found in porphyry and epithermal deposits, in sulfide veinlets, or as disseminations in the matrix and the wallrocks. A special case is that of the Escondida Norte porphyry deposit in Chile, where Romero *et al.* (2010) documented the existence of

monomineralic molybdenite veinlets. Molybdenite mineralisation is thought to have been triggered by the advanced argillic alteration.

In porphyry Cu-Au deposits, molybdenite commonly occurs in low-grade peripheral zones, outside the copper ore body, while in porphyry Cu-Mo deposits, it may be deposited within both copper ore bodies and peripheral pyrite zones. It must be noted that while molybdenite is the predominant carrier of molybdenum, this element can be found in the oxomolybdate species powellite (CaMoO_4) and sheelite (CaWO_4). In this last mineral phase it is ubiquitous as noted by Minubayeva & Seward (2010). Molybdenum also exhibits high concentrations in common accessory minerals such as magnetite and titanite (Miller *et al.*, 2011).

Finally, molybdenum can precipitate from volcanic gas fumaroles, hot springs and geothermal waters, as noted by Williams-Jones & Heinrich (2005); Seward & Sheppard (1986) and Arnorsson & Oskarsson (2007).

4.2: TRACE ELEMENTS IN MOLYBDENITE

Molybdenite, while being the primary source of Mo, is also an important carrier of many trace elements. It commonly incorporates Re and other redox-sensitive transition elements as trace constituents, and thus is likely to reflect changing geochemical environments through time (Golden *et al.*, 2013). Additionally, the type and amount of trace elements affects the crystal structure of molybdenite.

The most frequent such elements in molybdenite are Sn, Ti, Bi, Re, Te, W and Nb. These elements all form MS_n layer sulfides, and as such are of approximately the correct size to fit into the molybdenite's crystal lattice (Newberry, 1979a).

4.2.1: Rhenium Enrichment in Molybdenite

Rhenium is one of the scarcest elements in Earth's crust, with an average abundance of 0.5 ppb as estimated by Taylor & McLennan (1985). A more recent estimation by McLennan (2001) is 0.4 ngr/gr. Rhenium is also present in seawater as the oxyanion perrhenate (ReO_4^-) as documented by Brookins (1986). The solubility of the oxidated species of Re as well as Mo (ReO_4^- and MoO_4^{2-} respectively) is high, and the association of S, Mo and Re in the crust implies the effective mobilisation of these elements by oxidative weathering and suggests an association with a dissolved phase (Miller *et al.*, 2011).

According to Li (2014) rhenium behaves incompatibly, entering preferentially fluid phases, so it can be found in higher concentrations in hydrothermal systems. Also, in the same research, it was mentioned that, while Re is considered a chalcophile element when sulfide is present, the partitioning of Re between sulfide phases and silicate melt could not be accurately determined, despite extensive experiments. Re is associated exclusively with sulfide minerals, like pyrite (FeS_2), chalcopyrite (CuFeS_2), arsenopyrite (FeAsS) and molybdenite (MoS_2), according to Fleischer (1959), and Morelli *et al.* (2005). Very rarely, Re can be found as an actual Re mineral (Capitant *et al.*, 1963; Power *et al.*, 2004). Rhenium

can be obtained as a byproduct during molybdenum and copper refinement, from Cu-Mo deposits, as well as from sediment-hosted deposits (Melfos *et al.*, 2001; Sinclair *et al.*, 2009).

The existence of rhenium as a trace element in molybdenite has been studied by many researchers. Of course, not all molybdenite grains exhibit the same levels of enrichment, and according to Berzina *et al.* (2005) and Sinclair (2007), Re concentrations in molybdenite vary by 7 to 8 orders of magnitude.

I. Sources and controls of Re enrichment in molybdenite

It has been suggested that primary magmatic compositional controls, such as those who influence the ore element ratios, including the Cu:Mo ratio, may be an important controlling factor on the Re content of molybdenite. The atomic Re:Mo ratios of molybdenite and the degree of fractionation of the related granites have a strongly negative correlation, as shown by Blevin (2009). According to Berzina *et al.* (2005), the factors controlling Re enrichment in molybdenite are the following:

- 1) Composition of ore-forming solutions
- 2) Nature and source of the host rock
- 3) Total amount of molybdenite in a given deposit
- 4) Physicochemical conditions of ore formation

Xiong & Wood (2002) have suggested that, since reducing mineralising fluids cannot transport high amounts of Re, they form, as a result, Re-enriched sulfide deposits. Additionally, Voudouris *et al.* (2013a) have proven that, for Re-enriched deposits to form there must exist, at least at some stage of ore formation, oxidising fluids.

Christofides *et al.* (1998) and Pe-Piper & Piper (2002) have conducted extensive research in the genesis and evolution of porphyry intrusions, which give rise to porphyry mineralisations. The geochemical and stable isotope data they have provided corroborate the conclusions of Xiong & Wood (2002) and Voudouris *et al.* (2013a).

As Shirey & Walker (1998) have ascertained, during mantle melting rhenium behaves moderately incompatibly, so there is significant enrichment of Re in mantle derived melts. According to data from Berzina *et al.* (2005) and Voudouris *et al.* (2009, 2013a), there is a progressive decrease of Re from > 100 ppm in molybdenite derived from mantle sources through tens of ppm for mixed mantle/crust source, to 10 ppm < for crustal sources.

Stein *et al.* (2001) have proposed that the melting of mafic or ultramafic rocks, as well as involvement of mantle underplating or metasomatism in the source rocks, could also contribute to Re-enrichment²⁶. According to Li (2014), in oxidised arc magmas, the crystallised silicate minerals – olivine, clinopyroxene, plagioclase – do not sequester considerable amounts of Re. In the following table (Table 4.1) the correlation between molybdenites' Re contents and the origin of these contents is presented.

²⁶ A host of other fluid-mobile elements, such as Te, Pb, As, Sb, Cu, Au and PGE, can be released from the subducted slab and associated sediments (Stein *et al.*, 2001).

Table 4.1: Correlation between Molybdenites' Re Contents and Origin		
% Re Contents in Molybdenite	Origin	Reference
High Re contents	Melting of ultramafic rocks and/or rocks involving mantle underplating or metasomatism	Stein <i>et al.</i> (2001)
Intermediate Re contents	Intermediate crustal rocks and general metamorphic derivation	Stein <i>et al.</i> (2001)
Low Re contents	Intrusion-related systems and highly evolved granite systems	Stein (2006)

Mo-dominant mineralising systems, which are genetically related to more evolved granites, are associated with low Re:Mo ratios. On the other hand, the highest atomic Re:Mo ratios are observed in Cu-Au deposits. Low ppb Re in molybdenites is commonly found in reduced intrusion related systems. Stein *et al.* (2003) have proposed that maybe the distribution of Re in molybdenite is influenced by mass considerations. In effect, this means that when the molybdenite quantity is lower, then the available Re will be in a higher percentage, between two systems containing the same net amount of Re. However, Voudouris *et al.* (2010) mention that there is no clear correlation between molybdenite abundance and Re percentage.

So, from the aforementioned data, it becomes evident that Re-poor molybdenite should be an indication of a crustal source. However, data from numerous systems in Greece remain controversial. For example, Re-poor molybdenites are associated with the Xanthi granodiorite, for whose origin there are two conflicting theories: either a dehydration melting of lower crust without any contribution from mantle components, or a mantle origin with a more important felsic component (Jones *et al.*, 1992; Christofides *et al.*, 1998).

Voudouris *et al.* (2013a) have studied telescoped ore deposits in NE Greece, where molybdenite remains Re-enriched in all mineralising stages. In the Myli and Fakos prospects, the Re content of molybdenite is slightly reduced which may be an indication that the corresponding mineralising fluids were also of a slightly reduced nature.

Also, Voudouris *et al.* (2013a) have postulated that there is no correlation between the Re-content of molybdenite and its abundance in a given system. They characteristically report that at the Maronia and Melitena ore deposits molybdenite is both abundant and Re-enriched. In such settings, the Re enrichment could be explained by a release of Re from the asthenospheric mantle wedge by subduction-related fluids²⁷, according to Voudouris *et al.* (2010).

Both Re and Mo are insoluble in their more reduced tetravalent forms, whereas Mo⁶⁺ and Re⁷⁺ are more soluble in aqueous fluids and are thus mobilised under more oxidising conditions²⁸ (Crusius *et al.*, 1996; Algeo & Lyons, 2006; Miller *et al.*, 2011). Inside a mineralised zone, the fluctuations of Re, might, at least partly, reflect systematic variations in

²⁷ Such fluids could be similar to those reported by Tessalina *et al.* (2008) at the Kudryany volcano, Kurile Islands.

²⁸ The element Mo exemplifies mineral coevolution with biology, for example in its role in the nitrogen fixation enzyme nitrogenase (Schwartz *et al.*, 2009; Zehr & Ward, 2002; Rees *et al.*, 2005). Variations of Mo mineral distribution may thus shed light on the biological Mo cycle (Golden *et al.*, 2013).

the temperature, depth, magmatic composition and host lithology of the mineralised zone (Golden *et al.*, 2013). Rhenium is concentrated commonly in sulfides and tends to be much more abundant in molybdenite than in coexisting sulfides (Pašava *et al.*, 2016).

It has been proposed that magnetite crystallisation may control the geochemical behaviour of Re (Li, 2014). Mallmann & O'Neill (2007) showed that Re^{4+} substitutes readily for Ti^{4+} in silicate minerals. So, it seems plausible that Re may substitute for Ti in magnetite under favourable conditions. However, following magnetite stabilisation and fractionation, Re concentration in magnetite starts to drop (Righter *et al.*, 1998), instead of following the FeO and TiO_2 enrichment trend as happens during crystallisation of olivine, augite and plagioclase.

II. Rhenium heterogeneity in molybdenite and polytypism

As mentioned before, the heterogeneity of Re in molybdenite grains is indicative of different geological settings (Aleinikoff *et al.*, 2012; Ciobanu *et al.*, 2013). Microchemical studies by Kosler *et al.* (2003) and Selby & Creaser (2004) have deduced that the distribution of Re within individual molybdenite grains is highly heterogeneous as well, with variations approaching up to three orders of magnitude (Rathkopf *et al.*, 2017). Apart from the general variation between Re percentage in molybdenite grains from different deposits, there are quite significant differences between Re enrichment in grains from the same deposit. This heterogeneity may be attributed to some or all of the following causes:

- 1) Different Re concentrations in the magma or devolatilising slab that produced the magma (Sun *et al.*, 2004)
- 2) Different amounts of boiling in the porphyry system (Candela & Holland, 1986)
- 3) Different oxidation states of the magmas (Berzina *et al.*, 2005)
- 4) Variable rates and temperatures of degassing in magmas (Gannoun *et al.*, 2015)

There are many cases documented in literature, where different Re contents in molybdenite can be linked to different mineralising events²⁹. However, there are instances where the same deduction cannot be made. One example is the Bagdad Cu-Mo porphyry deposit in Arizona (Rathkopf *et al.*, 2017), where Re variations in molybdenite grains cannot be linked to any variation in lithology, alteration type or any other feature. There is also the possibility that Re in molybdenite is redistributed by post-formation processes, such as alteration processes (McCandless *et al.*, 1993) and metamorphism (Stein, 2006). Regardless of all the

²⁹ One example is the Salobo iron-oxide-copper-gold deposit in the Carajas belt of Brazil, where multiple episodes of mineralisation produced molybdenite with disparate Re contents (Requia *et al.*, 2003). Also, at the Boddington Cu-Au deposit, in New South Wales, Australia, different Re concentrations in molybdenite are associated clearly with two different mineralising events (Stein *et al.*, 2001). At the Cadia Quarry deposit, also in New South Wales, rhenium concentration in molybdenite follows a similar temporal pattern, where older generation molybdenites are characterised by higher Re contents. Moreover, at the Pagoni Rachi deposit, the highest Re values are found in molybdenites associated with the late stage porphyry-to-epithermal transition (Voudouris *et al.*, 2009, 2013a). At the Hilltop deposit, in Nevada, USA, Re contents are highest in molybdenites associated with a late stage hydrothermal episode (Ciobanu *et al.*, 2013). Finally, at the Sar Cesmeh deposit, in Iran, the oldest generation quartz-molybdenite veinlets contain the least Re, and Re contents increase over time (Aminzadeh *et al.*, 2011).

aforementioned, it must be noted that molybdenite is heterogenous in the sub-grain scale, regarding Re content (Stein *et al.*, 2003; Selby & Creaser, 2004; Rathkopf *et al.*, 2017).

Of principal importance is the association between Re enrichment and molybdenite polytypism. There are only two molybdenite polytypes, the hexagonal (termed the 2H polytype) and the rhombohedral (termed the 3R polytype), which is much rarer. Frondel & Wickman (1970) have postulated that the mechanism explaining Re enrichment in molybdenite is the expansion of the crystal lattice via polytypism. Mo^{4+} and Re^{4+} have similar ionic radii (0.65 Å and 0.68 Å respectively), so Re can be quite easily incorporated into the molybdenite lattice (Ciobanu *et al.*, 2013). McCandless *et al.* (1993) have confirmed that the 3R polytype is commonly richer in Re and reported up to 0.42 wt. % Re in molybdenite from the Copper Creek porphyry base metal deposit in Arizona, USA.

Cell expansion by polytypism is not sensitive to order-of-magnitude differences in trace element concentrations, even if there is a stacking disorder, which can be related to lattice-scale defects initiating 2H → 3R transformation (Ciobanu *et al.*, 2013). Crystal-structural defects and porosity enhance fluid infiltration and promote incorporation, nucleation and coarsening of impurities (Stein *et al.*, 2003; Ciobanu *et al.*, 2013).

It had been hypothesised (Newberry, 1979a, 1979b) that the Re-rich molybdenite from Pagoni Rachi belonged to the 3R polytype. Voudouris *et al.* (2009) concluded that this was not the case. In fact, they determined that this particular Re-rich molybdenite belongs to the 2H polytype. This suggests that particular values of Re do not correlate with specific polytypes (Voudouris *et al.*, 2013a). It is far more probable that Re substitutes for Mo in the structure of molybdenite (Voudouris *et al.*, 2009; Fleisher, 1959, Stein *et al.*, 2001). This conclusion is supported by the almost perfect linear correlation between Re and Mo contents in molybdenite crystals. Also, the Re distribution is homogenous within molybdenite.

III. Rhenium content relative to the mineralisation stage of porphyry deposits

Existing geochemical data indicate that Re oxides are more volatile than the corresponding Mo oxides (Morris & Short, 1969). Morachevskii & Nechaeva (1960) have also proven that Re can be preferentially reached from molybdenites at moderate temperatures.

If molybdenum grades and average rhenium contents from most large porphyry are plotted into a binary diagram it is evident that the actual grade of rhenium does not fluctuate significantly, despite the large variation in molybdenum grades (Newberry, 1979b). However, there is a correlation with the type of porphyry veins. A-type veins are associated frequently with high Mo grades and low Re contents, whereas the opposite is true for B-type veins (Newberry, 1979b). This conclusion is supported by the study of Giles & Schilling (1972) in Bingham ore deposit in Utah, Questa ore deposit in New Mexico and Lime Creek ore deposit, in British Columbia. So, it can be concluded that, in general, deposits characterised mostly by A type veinlet deposition are low in Re, and deposits characterised mostly by B-type veinlet deposition exhibit Re enrichment. The Re contents of D-type veins are generally low (Newberry, 1979b).

IV. Rhenium content and alteration style in porphyry deposits

Rhenium contents in molybdenite have been found to differ depending upon the alteration style inside the same deposit (Figure 4.1). A-type porphyry veins are mostly associated with potassic alteration (Gustafson & Hunt, 1975; Seedorff *et al.*, 2005). As the feldspars are altered to plagioclase and hornblende to biotite, the local $K^+ : Na^+$ ratio of the mineralising fluid decreases. This in turn causes a deposition of Mo (Newberry, 1979b) due to the increase in MoS_2 solubility (Isuk, 1976). However, this decrease does not bring about a similar decrease in Re solubility. Thus, molybdenites associated with A-type veins are low in Re, and their structure is that of the 2H polytype (Newberry, 1979b).

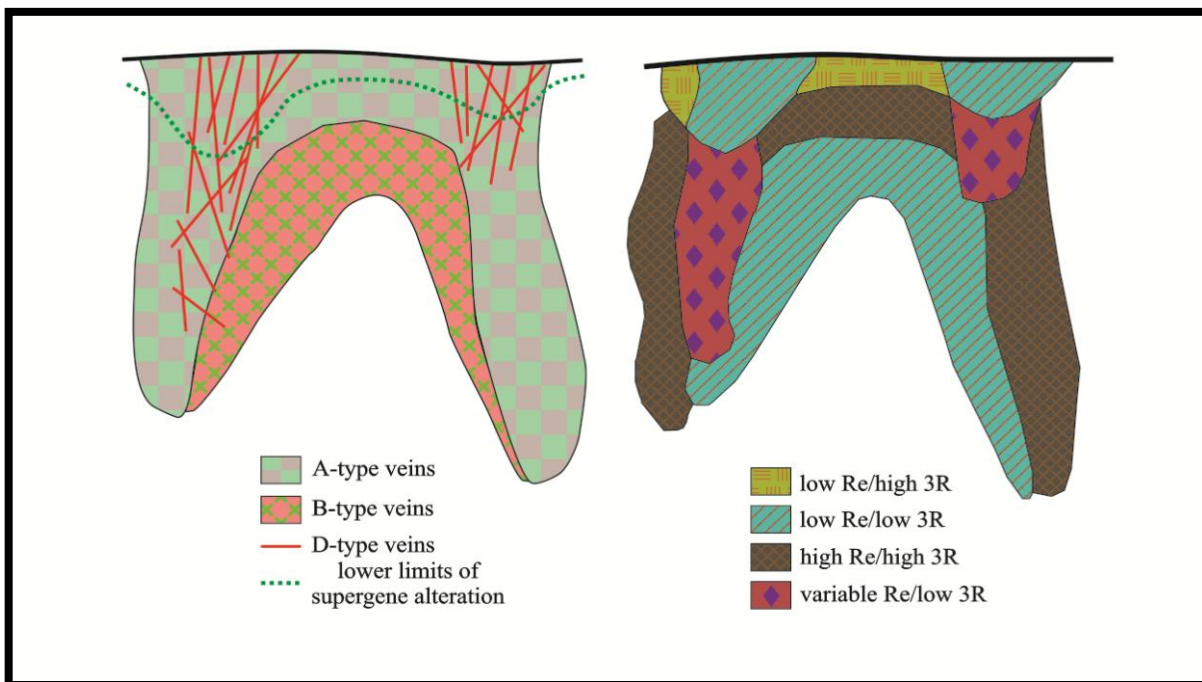


Figure 4.1: Spatial distributions of 3R/Re relationships for a hypothetical porphyry Cu deposit in cross section. To the left there is the hypothetical configuration of vein types and to the right the corresponding 3R and Re contents analogies (after Newberry, 1979b).

B-type veins are not associated with any specific alteration and it is believed the Mo precipitation occurs as a result of a decrease in temperature. The Re:Mo ratio within the mineralising fluids must be now higher, since a significant amount of Re has been deposited in the previous stage. Alternatively, in Mo-poor systems, there is not enough molybdenum to be deposited. Molybdenites deposited in this stage will be Re-rich and their structure is that of the 3R polytype (Newberry, 1979b). D-type veins are associated with hypogene hydrolytic alteration and thus indicate the presence of low pH fluids. According to Vlasov (1966), such fluids are able to leach rhenium from molybdenite (Newberry, 1979b). Supergene alteration processes are unable to induce recrystallisation between the two polytypes since the kinetic energy available in such low temperatures is insufficient. Thus, weathered 3R molybdenites may or may not be Re-rich, depending upon the effectiveness of Re leaching (Figure 4.2).

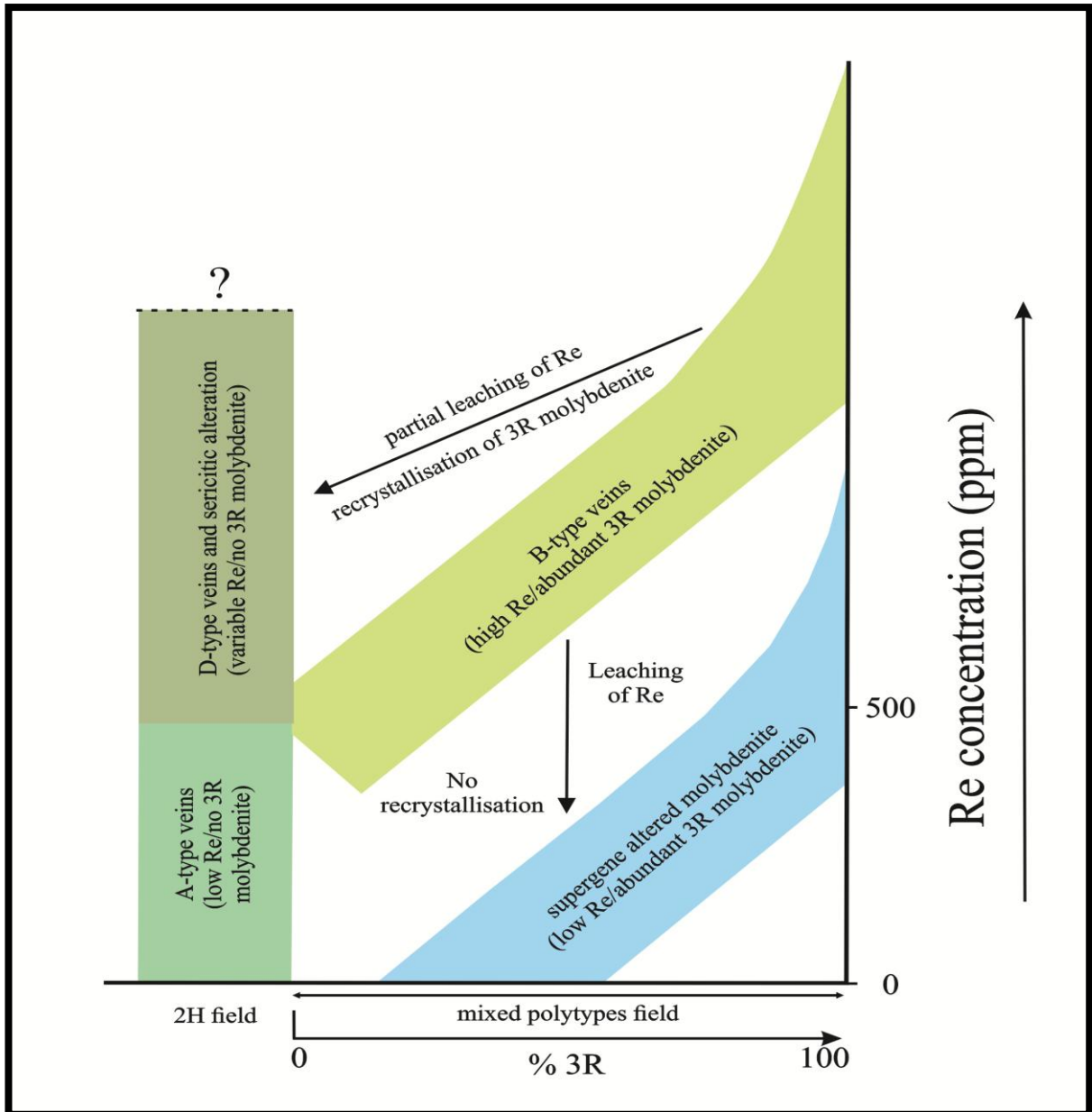


Figure 4.2: A diagrammatic representation of 3R/Re relations in porphyry deposits during the various stages of molybdenite deposition and alteration (after Newberry, 1979b).

4.2.2: Other Trace Elements in Molybdenite

The relative amounts of different trace elements in molybdenite affect its crystal lattice and provide valuable insights into the timing and ways of molybdenite crystallisation. Molybdenite cores and rims cannot be dated separately, but they can be investigated by spot trace element analysis, under the assumption that different trace elements could lead to the identification of multiple growth zones of a single molybdenite crystal (Aleinikoff *et al.*, 2012), thereby giving a relative timing to its creation, in comparison to other minerals and mineralising events. The indicated method should be EPMA line scan data and LA-ICP-MS spot analyses (Aleinikoff *et al.*, 2012). An example of trace element zonation in molybdenites comes from samples of molybdenites from the world class Bodington Cu-Au-(Mo) deposit. Ciobanu *et al.* (2013) have detected a high variability in trace element concentrations, ranging

from tens to $> 10^3$ ppm. More specifically, Re displays oscillatory zonation in a depleted inner-core, and no marked boundary between the outer core and the halo, whereas W shows an inverse pattern to Re in the core. Intensely deformed grains show enrichment in W, but Re remains unaffected. In the following paragraphs, the most frequent trace elements in molybdenite, other than Re, are presented.

I. Tungsten in molybdenite

It has been suggested by Frondel & Wickman (1970) that W, similarly to Re, is incorporated homogeneously into the molybdenite lattice. There are some crystallochemical similarities between Re and W, which are supported by a significant positive correlation in a group of greisen-related molybdenites, but other data remain inconclusive, as mentioned by Pašava *et al.* (2016). In the same research it was mentioned that W content in molybdenite is an indication of its abundance, and of the ratio of S/O activity.

II. Niobium and selenium in molybdenite

According to Newberry (1979a) there is a correlation between the crystal structure and the chemistry of molybdenite, noting that elements like W, Nb, V, Fe and Ti are incorporated into the 3R polytype. Pašava *et al.* (2016) state that as MoSe_2 ³⁰ is isostructural with MoS_2 , there is a theoretical possibility for ionic substitution between Se^{2+} and S^{2-} in the structure of molybdenite, which has been experimentally confirmed by Drábek (1995). In addition, molybdenite can accommodate up to 25 % Se as an isomorphous constituent.

III. Tellurium in molybdenite

MoTe_2 is isostructural with MoS_2 , and there is consequently the theoretical possibility for ionic substitution of Te^{2-} for S^{2-} , with the structure of molybdenite (Pašava *et al.*, 2016). The phase MoTe_2 has only been synthesised *in vitro* (Morette, 1942), and not reported as a naturally occurring mineral. However, experiments between 600° and 800° C, have proven the existence of a solid solution between MoTe_2 and MoS_2 , which may extend down to 400° C (Drábek, 1995).

IV. Other trace elements in molybdenite

Gold related molybdenite typically has the highest mean and median values of Au (average 24 ppm, median 4 ppm), Ag, Bi, Sb, Se and Te. Gold mostly occurs as inclusions of native Au or in association with Bi in maldonite, and/or as a Bi-Au-Te phase (Pašava *et al.*, 2016).

Base metal related molybdenite is characterised by the highest mean and median values of Pb (average 1800 ppm, median 1420 ppm), and the highest Ag median value (15 ppm). Both metals occur as impurities with abundant galena locally accompanied by an Ag-S and anglesite (Pašava *et al.*, 2016).

³⁰ In fact, MoSe_2 has been described as the mineral drysdallite, by Čech *et al.* (1973).

Granite related molybdenite shows the highest median Ni value (16 ppm). They are either inclusion-free, or contain micro-inclusions and also indications of sub-nano-impurities depending on the deposit's locality and the type of mineralisation processes, reported from the region of the Bohemian Massif (Pašava et *al.*, 2016).

CHAPTER 5: TECTONIC ACTIVITY IN THE AEGEAN SEA

The Geological History of the Hellenides ~ The Terranes and the Ophiolite Belts of the Hellenides

The formation of the Aegean Sea is believed to have started during the Oligocene³¹, above the retreating African slab, which is sinking currently below Crete and the Mediterranean (Le Pichon & Angelier, 1981; Jolivet & Faccenna, 2000). Brun & Sokoutis (2007) recognised marine phases in the Rhodope Massif, which may indicate an earlier extension, since the Eocene. The Rhodope and the Hellenides are in effect an Early Cenozoic collapsed mountain belt. Of particular note are the variations of crustal thickness in the Aegean (Jolivet & Brun, 2010).

On one extreme, with a crustal thickness of about 15 Km, the North Aegean Trough and the Cretan Sea are characterised by a significantly thinned crust. The Island of Crete, continental Greece and Asia Minor are all characterised by a crustal thickness of about 30 Km, as Bohnhoff *et al.* (2001a) have reported. On the other extreme, Makris *et al.* (2001) note that the Rhodope Massif is characterised by a crustal thickness of about 45 Km, and this happens despite its association with large scale extensional structures, as mentioned by Sokoutis *et al.* (1993).

All these crustal thickness variations and a plethora of other geological structures are explained by the **Model of a Single Subduction**, proposed by van Hinsbergen *et al.* (2005a). This means that the different palaeogeographic domains of the Hellenides³² belong to the same plate, and follow a course of successive subductions and partial accretions to the margin of Eurasia. The tomographic models by Piromallo & Morelli (2003) have proven that it is possible to «follow» the Aegean slab down to the lower mantle. Moreover, it is in reality a single slab with a length of more than 1500 Km.

5.1: THE GEOLOGICAL HISTORY OF THE HELLENIDES

The Hellenides represent a characteristic segment of Tethyan palaeogeography, with their palaeogeographic organisation being a somewhat complex alteration of ridges, with shallow water carbonate platforms, interspersed with furrows with pelagic sediments, and volcanosedimentary rocks (Papanikolaou, 2009). The Aegean region can be considered as one of the Mediterranean Cenozoic basins (Jolivet *et al.*, 2013).

Smith (1971) and Dewey *et al.* (1973) interpreted ophiolites as ancient oceanic crust, in the wake of the development of the Theory of Plate Tectonics. Accordingly, the ophiolites of the Hellenides were recognised as major palaeogeographic elements, dividing the ocean basins

³¹ For a complete understanding of the tectonics of the Aegean Sea, within the framework of Plate Tectonics and Alpine orogeny, the reader is referred to Appendixes IX and X.

³² The main palaeogeographic domains of the Hellenides are the Vardar-Axios Ocean, the Pelagonian microcontinent, the Pindos Ocean and the Eastern Mediterranean Oceanic Domain, according to Jolivet & Brun (2010).

within the Tethys. According to Papanikolaou (2009) the simple Atlantic type model³³ cannot be applied in the case of the Hellenides, which are characterised by many ophiolite belts. As Jolivet & Brun (2010) have asserted, within the relatively restricted region of the Aegean, many features characteristic of subduction zone tectonics coexist. Those major elements are:

- Exhumation of HP-LT metamorphic rocks within the subduction channel.
- Formation of metamorphic core complexes in a backarc environment.
- Interaction between intracontinental large scale strike-slip faults, like the North Anatolia Fault, and active rifting in the backarc region, as is happening currently in the Corinth Rift.

In the Eastern Mediterranean, the concept of tectonostratigraphic terranes was applied by Papanikolaou (1997, 2009), with the aim to locate the microcontinents existing within the Tethyan belt and to elucidate their geological history. In each oceanic basin, the timing of tectonic emplacement of the ophiolites is a characteristic feature, related to the closure of the basin. Jolivet & Brun (2010), Ring *et al.* (2010), and Jolivet *et al.* (2013), have summarised the geotectonic development of the Hellenides, as the product of the off-scraping of crustal units from the Pelagonian microcontinent in the North and then the Pindos Ocean, above the Hellenic subduction, from Late Jurassic to the present day.

That there was a degree of extension in the Aegean Sea was recognised at first by Aubouin (1959). This extension, which is linked to the North Anatolia Fault, postdates the formation of both the Hellenic and the Dinaric Mountain Ranges. According to Papanikolaou *et al.* (2004), the pre-extensional structure is partially preserved in continental Greece, where there exists a complete stack of nappes. All the other regions of Greece were affected by extensional tectonics, especially the Islands of the Cyclades. In some places, the extension is so pronounced, that HP-LT metamorphic rocks crop out on the surface. Jolivet *et al.* (2004) have deduced that the aforementioned extension is characterised by the following distinct phases:

- Syn-orogenic extension during the formation of the Hellenides, which was the first step of the exhumation process.
- Post-orogenic extension concurrently with the general Aegean extension, which was the second and final step of the exhumation process.

As Duermeijer *et al.* (2000) have recorded, in the whole of the Aegean region there are palaeomagnetic rotations, of mostly clockwise nature in the Hellenides and in the Rhodope Massif. In the Cyclades Islands, a more complex pattern can be observed. A more recent investigation by van Hinsbergen *et al.* (2005b) indicates that the whole of Western Greece has rotated clockwise by some 50° - 40° between 15 and 8 my ago and the last 10° after 4 my.

To be able to accommodate such a rotation, there must have been a fault zone with a partly strike-slip and partly extensional character. Walcott & White (1998) proposed such a fault zone in the Aegean, which they called the Mid-Cycladic lineament. However, as Jolivet &

³³ The classic Atlantic type model comprises two passive continental margins with a central mid-ocean ridge.

Brun (2010) have noted, due to the incoherence of block rotations on either side, the existence of such a zone can only be inferred but not confirmed.

5.2 THE TERRANES AND THE OPHIOLITE BELTS OF THE HELLENIDES

According to Papanikolaou (1989, 1997) and Papanikolaou *et al.* (2004) the palaeogeographic organisation of the Hellenides comprises four oceanic and five continental tectonostratigraphic terranes. Each terrane³⁴ is symbolised by the symbol H and a corresponding number. Continental terranes are characterised by odd numbers and oceanic terranes are characterised by even numbers³⁵. The tectonic events of the inner parts of the Hellenides are older, compared to those on the outer parts. This means that all tectonostratigraphic formations and geodynamic events of the external arc are younger, and become progressively older, towards the Rhodope Massif, which represents the central «core» of the system (Papanikolaou, 2009). Deformation, metamorphism and magmatic/volcanic arc activity events correlate directly with the orogenic migration (Figure 5.1), as is described bellow (Papanikolaou, 1984, 1997; Papanikolaou *et al.*, 2004):

- Late Tertiary events correspond to the external tectonometamorphic belt, which comprises the terranes H₁ and H₂.
- Early Tertiary events correspond to the medial tectonometamorphic belt, which comprises the terranes H₁, H₂, H₃ and H₄.
- Late Mesozoic events correspond to the internal tectonometamorphic belt, which comprises the terranes H₆, H₇, H₈ and H₉.

Papanikolaou (1989, 1993, 1997) has asserted that the overall tectonic polarity of the Hellenides involved constant northward subduction of the Tethyan palaeogeographic elements since the Jurassic, which resulted in the closure of the Tethyan oceanic basins and the accretion of the intermediate continental blocks (Figure 5.1).

According to the aforementioned assertions, it is logical that the tectonic emplacement of the ophiolites over the adjacent terranes, had a general South direction, and occurred during the final stages of closure of each oceanic basin. So there are successive phases of ophiolite obduction (Papanikolaou, 2009).

This general concept of westward migration however does not imply that the direction of tectonic emplacement of ophiolites was always towards the east following the present day orientation of the arc in continental Greece. Based on Papanikolaou (2009) the criteria regarding the timing of tectonic emplacement of ophiolites in the Hellenides are:

- Dating the post-emplacement sedimentary cover sealing the tectonic contacts between the ophiolites and the underlying geological formations. It is to be expected that, in most cases, each tectonic event is characterised by stratigraphic unconformities.

³⁴ The particular criteria according to which each terrane was recognised and classified were analysed by Papanikolaou (1989, 1997) and Papanikolaou *et al.* (2004). Their detailed presentation is beyond the scope of this research.

³⁵ So, the continental terranes are H₁, H₃, H₅, H₇, H₉, and the oceanic terranes are H₂, H₄, H₆, H₈.

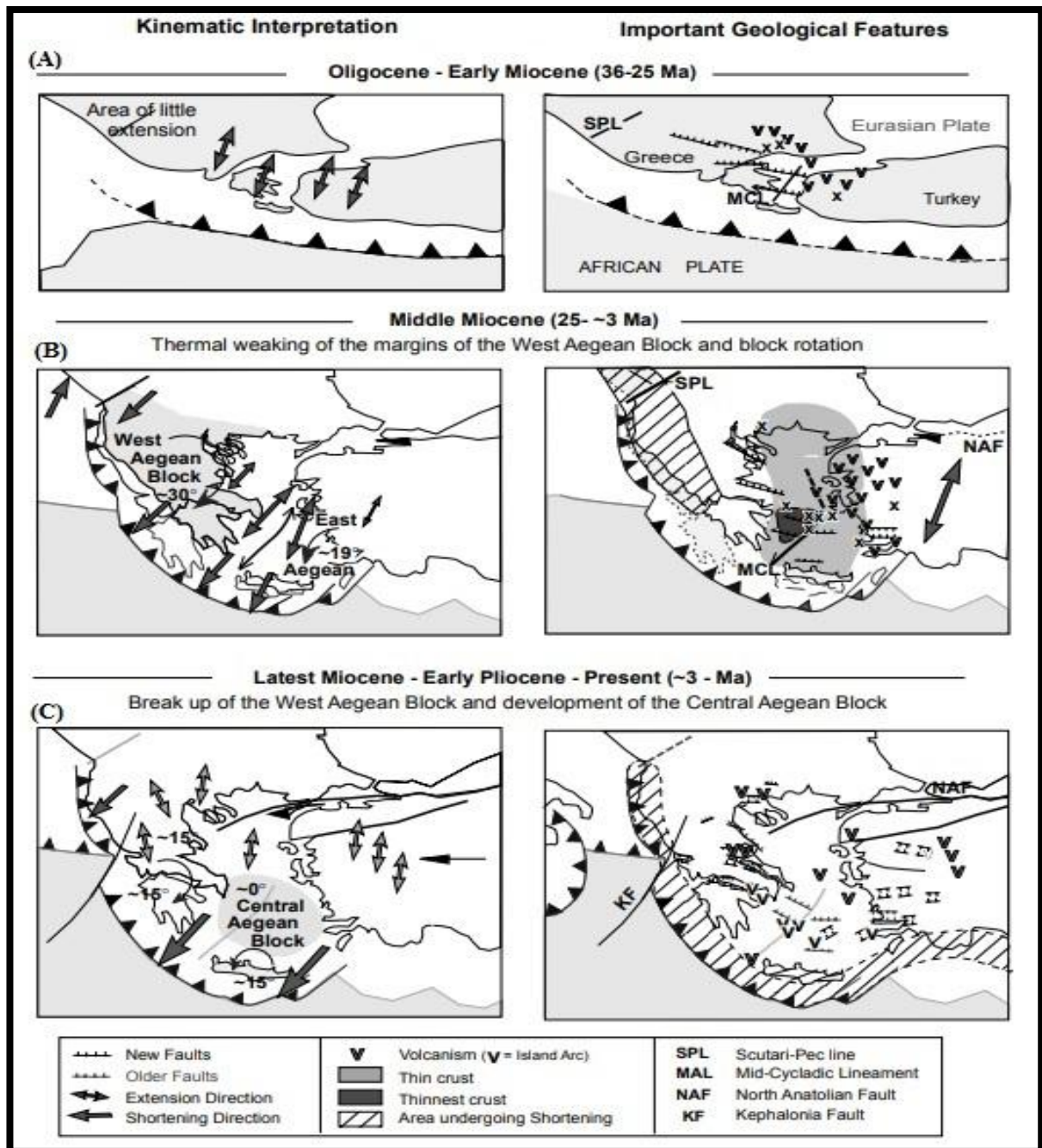


Figure 5.1: A schematic scenario for regional extension within the Aegean. a) Regional extension initiated in the Oligocene-Miocene (~ 35 - 22 my ago) in a ~ 023° trend. b) Extension taking place in the Central Aegean while the NW Aegean undergoes shortening. The resultant couple forced the west Aegean to rotate 30° clockwise. This semi-coherent block rotation was aided by thermal weakening of the inner margins and the pre-existing zones of weakness near the Mid-Cycladic and Scutari-Pec Lineaments. The Mid-Cycladi lineament acted as a continental fracture zone, which extended in length as it accommodated the rotation of the West Aegean block. The East Aegean block rotated about 19° counterclockwise during this period, although in a less coherent way than the West Aegean. c) At about 3 my ago, the West Aegean block rotated to such a position that it was more mechanically favourable to form new grabens trending WNW-ESE, than to continue reactivating pre-existing structures. These grabens caused the cessation of the Mid-Cycladic Lineament's activity and the splitting of the West Aegean block into two portions. The SE portion was coupled with a SW portion of the East Aegean block to form the Central Aegean block (from Walcott & White, 1998).

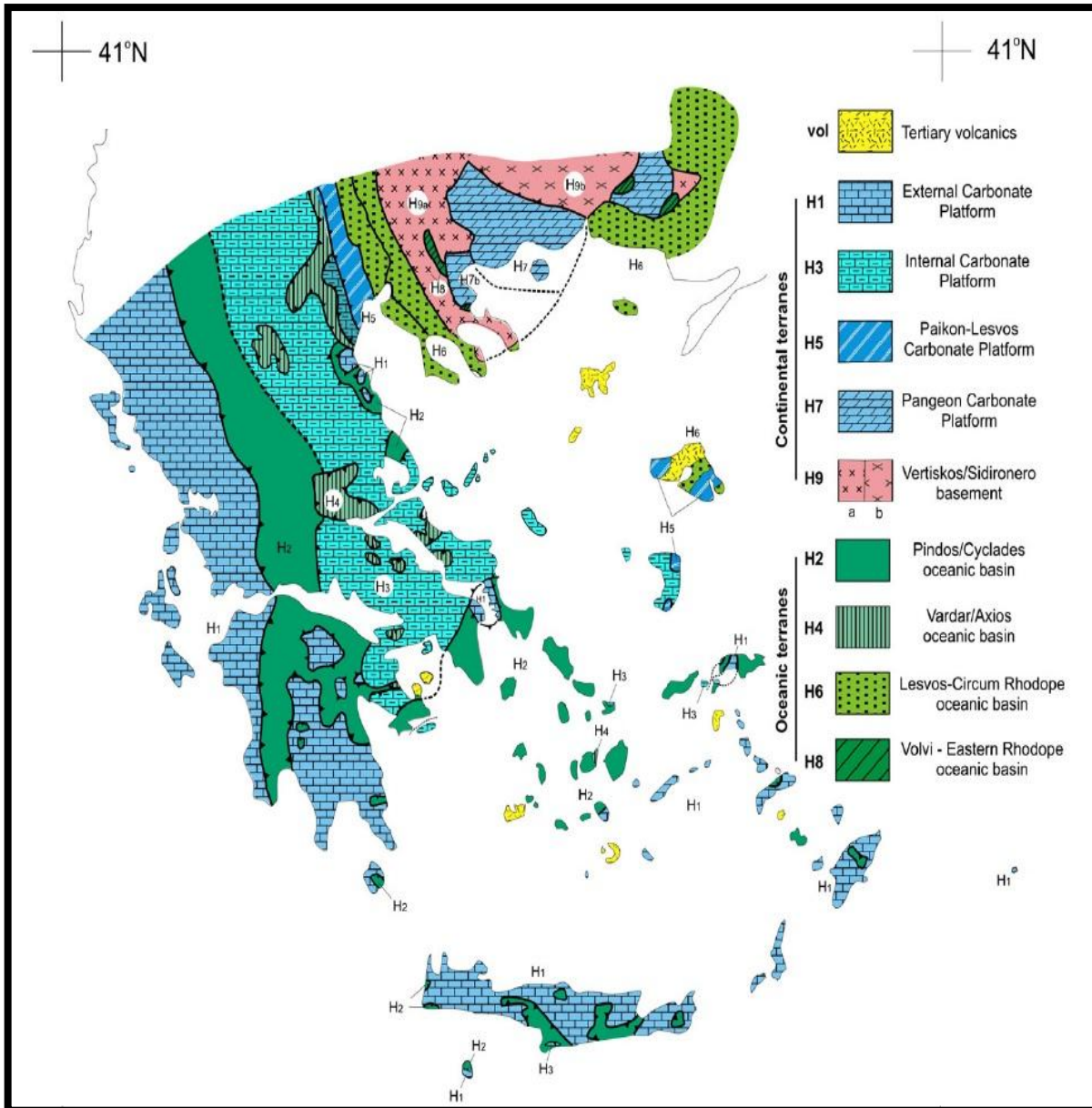


Figure 5.2: The terranes of the Hellenides, from H₁ to H₉ as described by Papanikolaou (1989, 1997). The oceanic terranes are characterised by even numbers and the continental terranes by odd numbers (from Papanikolaou, 2009).

- Dating of post-emplacement intrusive rocks with the aim of providing temporal constraints regarding upper crust deformation.
- Dating of syn-emplacement tectonostratigraphic formations, which have developed along the front of the advancing ophiolite nappes. These are flysch-type deposits consisting of ophiolite detritus and mélanges.
- Dating of the youngest geological formations involved in the structure of the allochthon and autochthon units.

It must be stressed that the age of tectonic emplacement of an ophiolite is different from its actual age, and this has given rise to significant confusion amongst researchers. Additionally, the fact that the age of an ophiolite is determined indirectly, through dating of its amphibolitic metamorphic sole, leads to the dating of the whole oceanic crust, rather than one particular segment. The ophiolite belts of the Hellenides, as determined by Papanikolaou (2009) are:

- **External ophiolite belt of the Pindos-Cyclades tectonostratigraphic terrane (H₂ terrane):** the ophiolites of this terrane were emplaced during the Early Cenozoic, according to Papanikolaou (1989). In Pindos Mountain this emplacement took place in Middle to Late Eocene, and in Crete between Late Eocene and Late Oligocene. The ophiolites of H₂ terrane were obducted over different parts of the external carbonate platform of the H₁ terrane, between Late Eocene and Early Oligocene.
- **Internal ophiolite belt of the Vardar/Axios tectonostratigraphic terrane (H₄ terrane):** the ophiolites of this unit were tectonically emplaced over the H₃ terrane, between Late Jurassic and Early Cretaceous. The emplacement process of these ophiolites is thought to have lasted 40 my (Papanikolaou, 1989, 1997).
- **Ophiolites of the Lesvos/Circum Rhodope belt (H₆ terrane):** the ophiolites of this terrane are found in many different outcrops, in Central Macedonia, Western Thrace and the North Aegean Islands. However, their tectonic emplacement is poorly dated due to the absence of transgression sediments post-dating their tectonic emplacement. It is also difficult to determine the age of their underlying metamorphosed sediments. In the particular case of the Lesvos Island, the ophiolites of H₆ are found tectonically emplaced over H₅, which comprises a shallow-water carbonate platform of Upper Palaeozoic-Upper Triassic age (Papanikolaou, 1999). This is the Lesvos allochthon, which comprises two different lithologies, the ophiolite complex and a volcano-sedimentary pelagic sequence. In SE Lesvos, in the area of the Amali peninsula the sediments can be observed in stratigraphic succession, overlying the ophiolite complex and the basaltic metalavas (Papanikolaou, 2009).
- **Ophiolites of the Volvi-Eastern Rhodope (H₈ terrane):** the ophiolites of this terrane can be observed in the Serbo-Macedonian Massif and the East Rhodope Massif, around Komotini. Both ophiolites lie within the internal tectonometamorphic belt of the Hellenides and it is impossible to discern their protoliths (Papanikolaou, 1989, 1997). The age of their emplacement remains uncertain but is believed to have occurred before the Late Jurassic (Papanikolaou, 2009).

From all the aforementioned it can be concluded that the palaeogeography of the Hellenides within the Tethys Ocean is controlled by the dimensions of the continental terranes, upon which the shallow water carbonate platforms are found. As can be seen in the terrane map of the Hellenides (Figure 5.2) if one were to draw parallel lines, then the number of oceanic basins would sometimes be different, across two parallel segments, since continental terranes wedge out in many cases. So possible connections between terranes H₂ and H₄ on both sides of H₃, terranes H₄ and H₆ on both sides of H₅ and terranes H₆ and H₈ on both sides of H₇, can be inferred (Papanikolaou, 2009).

In other words, the Hellenides can be thought of as representing a number of sub-basins which developed in between continental terranes, drifting northwards, since Late Palaeozoic-Triassic. In fact, the very nature of palaeogeographic development of the Hellenides explains the existence of different type of ophiolitic environments (Figure 5.3). It can be concluded then, that the general tectonic setting of the Hellenides, is that of an obduction of the oceanic

areas, over the more external continental ones, which are covered by shallow water carbonate platforms (Papanikolaou, 2009).

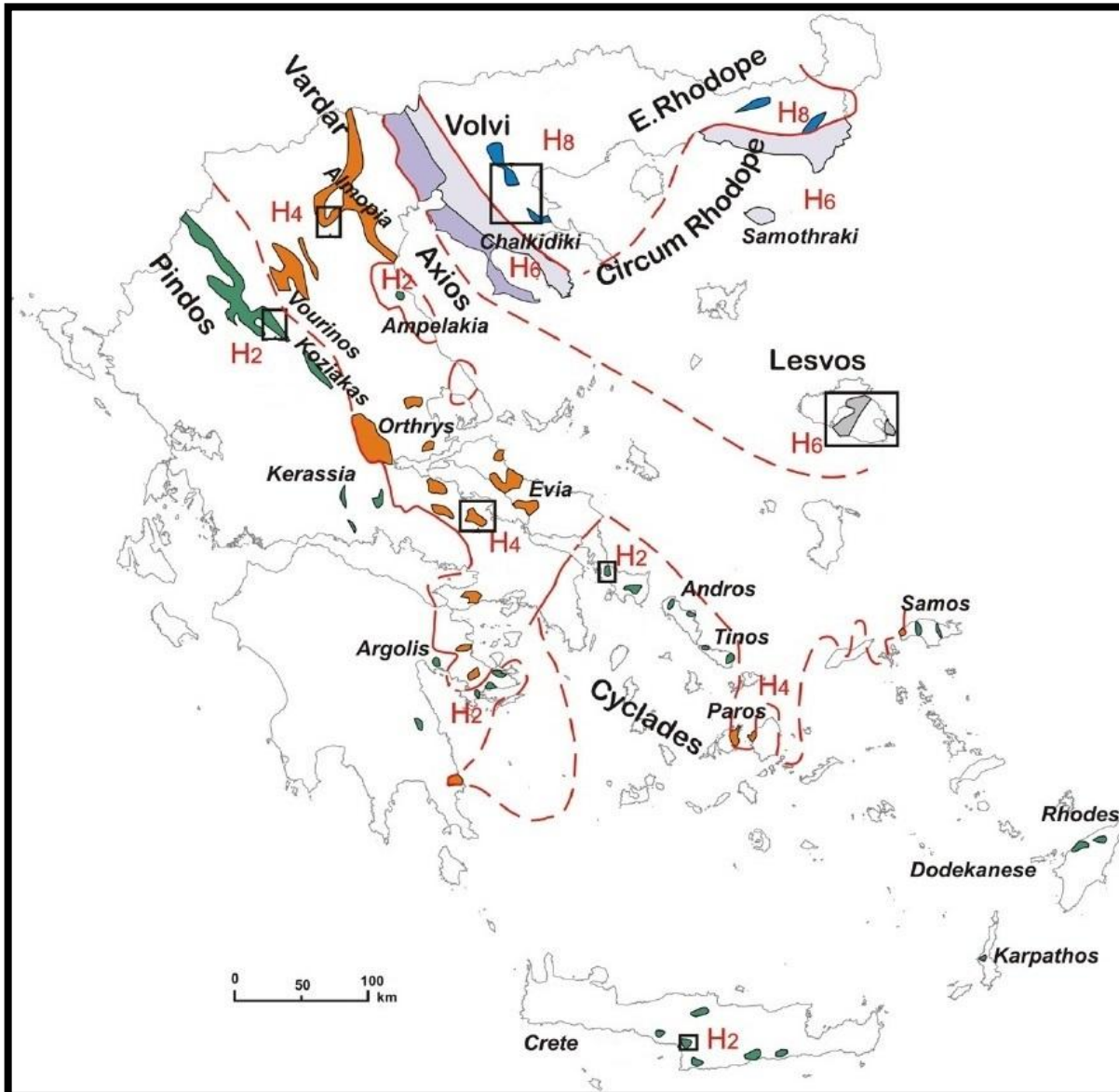


Figure 5.3: The main ophiolite outcrops of the Hellenides are distinguished in four different groups, the oceanic terranes H₂, H₄, H₆ and H₈. The quadrangles represent locations with characteristic transsects for each terrane (from Papanikolaou, 2009).

As Papanikolaou (2009) has deduced, the general geodynamic process of the formation of the Hellenides implies a relatively short duration of opening for each oceanic basin followed by a northward subduction and the final obduction of ophiolites during its closure. It is possible that the intra-Tethyan plate tectonics may result in the coexistence of MORB and SSZ ophiolites in the oceanic terranes of the Hellenides. There are of course, differences in the timing of closure and suturing between different oceanic basins, caused by the continental terranes' geometry (Figure 5.4). Were a continental terrane «dies out» two adjacent continental basins merge into a larger one (Papanikolaou, 2009).

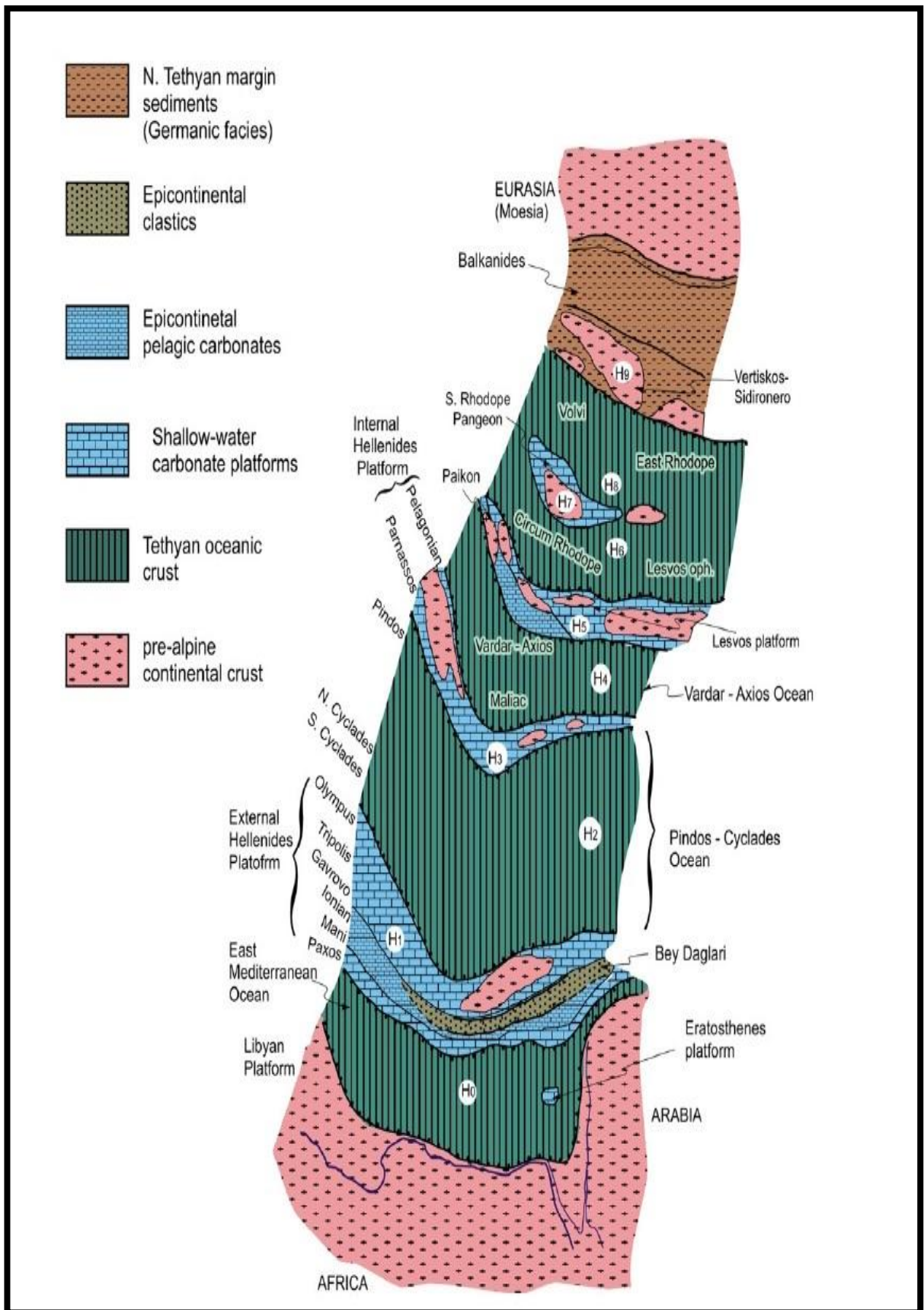


Figure 5.4: A schematic representation of the palaeogeographic organisation of the terranes in the Hellenides, with a reference to the location of the main tectonic units of the Hellenides belonging to each terrane (from Papanikolaou, 2009).

Regarding the Rhodope Massif, Bonev *et al.* (2006a, 2006b) mention that it is a segment of the Alpine orogenic belt, and is characterised by two major phases of deformation:

- A compressional stage with south-verging thrusting and amphibolite facies metamorphism which probably culminated during the Middle Cretaceous.
- A stage of syn-orogenic and post-orogenic extension which began in Early Cretaceous and continued until the Tertiary in a back-arc setting.

The geodynamic evolution of the Rhodope Massif is a complex one, characterised by both nappe stacking and crustal thickening. The Massif itself consists of two tectonic units, the Vertiskos and the Kimi complexes, which comprise meta-sedimentary and meta-igneous rocks (Zagorchev, 1998; Krohe & Boskos, 2002; Brun & Sokoutis, 2007).

As has been mentioned above, there is no slab-break off (Figure 5.5), which deviates from the norm, for in other cases of continental subduction, gravitational forces stretch the oceanic slab, separating it from the continental lithosphere which resists subduction (Davies & von Blackenburg, 1995).

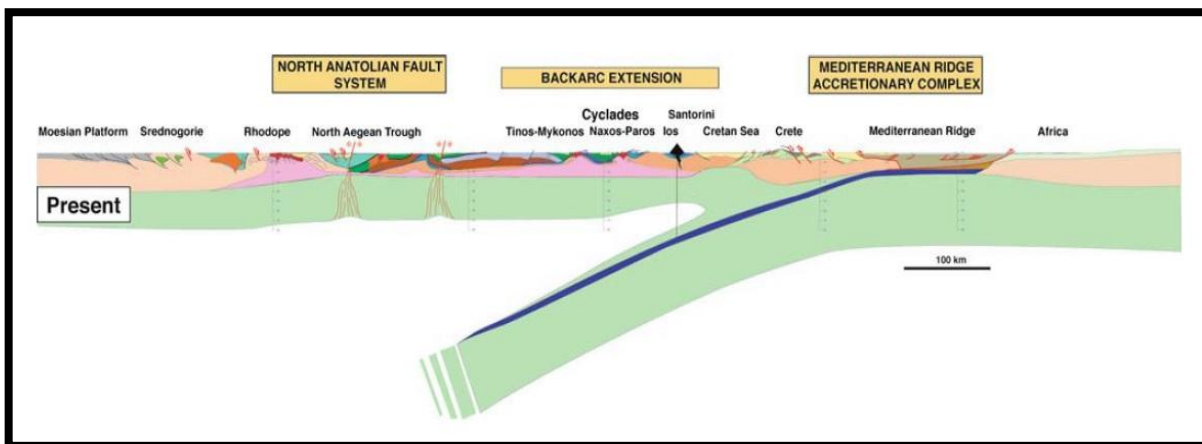


Figure 5.5: Compiled lithospheric-scale cross-section of the Aegean region from the Balkan foreland to the African passive margin. This section is based upon surface geological observations as well as geophysical data. The Moho depth is taken from Bohnhoff *et al.* (2001), Papanikolaou *et al.* (2004), Kuhlemann *et al.* (2004) and Tirel *et al.* (2004). The geometry of the contact between the upper and the lower plate in the subduction zone is taken from the research of Li *et al.* (2003). The base of the lithosphere has been set at approximately 100 Km. For the part of the Moesian Platform and Srednogorie, this cross-section is based on that published by the TRANSMED team (Papanikolaou *et al.*, 2004). In the rest of the cross-section, new data have been used from Gautier & Brun (1994a, 1994b), Burg *et al.* (1995), Ricou *et al.* (1998), and Jolivet & Patriat (1999), Chamot-Rooke *et al.* (2005), Bonev *et al.* (2006b), and Brun & Sokoutis (2007). The principal difference between the cross-section presented here and the cross-section presented by the TRANSMED team, is the emphasis on crustal extension given here, during the formation of the Aegean Sea in the Oligocene and Miocene (from Jolivet & Brun, 2010).

CHAPTER 6: GEOLOGY OF LESVOS ISLAND

Autochthonous Basement Unit ~ Allochthonous Ophiolites ~ Tertiary Volcanic Sequence ~ Post-Miocene Sediments

Lesvos Island is located in the Northeastern part of the Aegean Sea, close to Asia Minor – which is nowadays a part of Turkey (Figure 6.1). It is the third largest Island of Greece³⁶, occupying some 1630 Km². The larger part of the Island, around 66 % of its surface, is occupied by volcanic rocks and structures (Vamvoukakis *et al.*, 2005; Vamvoukakis, 2009). The Island of Lesvos is characterised by intense geothermal activity due to the recent volcanism which is the cause of the extensive kaolinisation and betonisation of the volcanic rocks and the formation of hydrothermal mineral deposits (Kelepertsis & Esson, 1987).

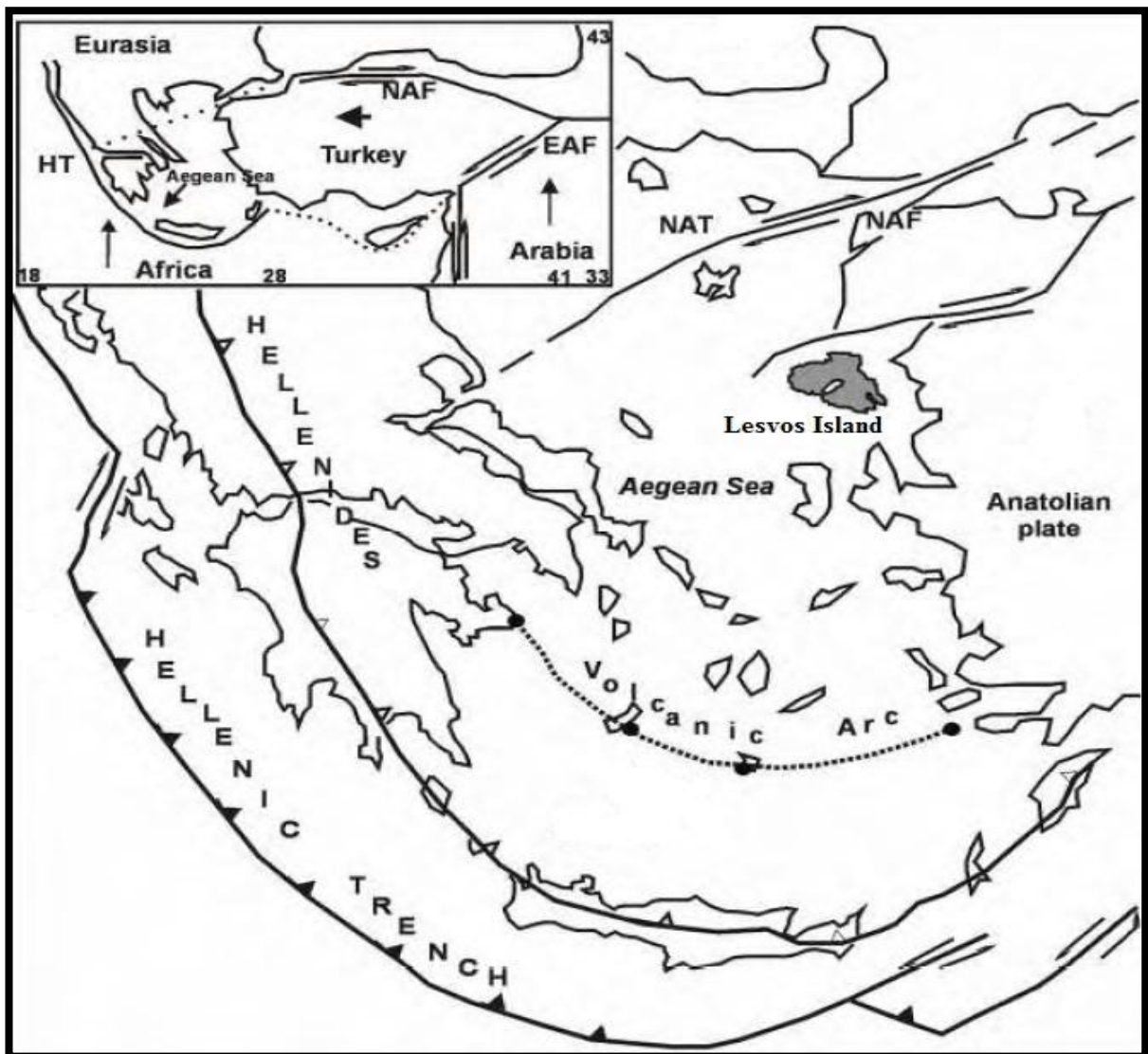


Figure 6.1: The location of Lesvos Island in the NE Aegean Sea, in relation to the Hellenic trench, the modern volcanic arc of the Aegean and the North Anatolia fault (from Vamvoukakis, 2009).

³⁶ Crete and Evvia are the only larger ones.

The earliest geological work on Lesvos Island was carried out by de Launay (1898) and later Georgalas (1949) studied the chemical composition of its volcanic rocks. Hecht (1970, 1972a) carried out detailed investigations of the SE part of Lesvos, and also produced the first detailed geological maps of the Island in a 1:50000 scale (Hecht, 1972b, 1973, 1974a, 1974b, 1975). Pe-Piper (1978, 1980a, 1980b) studied extensively the volcanic rocks of the whole island. As Barr *et al.* (1999), Robertson (2002) and Okay & Göncüoğlu (2004) have asserted the rocks on Lesvos Island are divided into four major groups: shist-marble unit, volcanosedimentary unit, ultramafic unit and Cenozoic cover unit.

In reality, the geological structure of the Island of Lesvos is rather more complex. Using the data of Hecht (1970, 1972a, 1972b, 1973, 1974a, 1974b, 1975), in conjunction with the petrographic data provided by Pe-Piper (1978, 1980a, 1980b), Pe-Piper & Piper (1992, 2002) and Pe-Piper *et al.* (2001) and the palaeomagnetic data of Pe-Piper & Piper (1993) it is possible to divide the Island of Lesvos in seven tectonic units. These are (mentioned from oldest to youngest): Autochthonous Metamorphic Basement Unit, Allochthonous Unit, Skoutaros Unit, Acid Volcanics Unit, Sikaminea Unit, Mytilene Unit, and Hypabyssal Intrusions. They are covered in places by sediments of Pleiocene and Quaternary age.

The simplified geological map of Lesvos according to the synthesis, in this Thesis, of existing data is presented in Figure 6.2³⁷. In the following paragraphs, each tectonic unit is presented in detail, regarding its petrography, and any particular characteristics worthy of mention.

6.1: AUTOCHTHONOUS BASEMENT UNIT

This Unit comprises all the Palaeozoic sedimentary rocks which have undergone low grade metamorphism (Hecht, 1970, 1972a; Pe-Piper, 1992, 1993; Papanikolaou, 1999). This is the «autochthonous unit», a conclusion corroborated by Papanikolaou (1999) who, in addition, proposed that this Unit is part of the H₅ Oceanic Terrane.

At the base of this Unit, there are Permian schists and marbles of varying degrees of metamorphism. The petrographic study of these rocks reveals a series consisting of meta-arcozes, meta-sandstones and meta-conglomerates, which are interlaminated with white to bluish marbles. Some parts of this formation exhibit characteristics of greenschist facies metamorphism (Hecht, 1972a, 1972b). Permian to Carboniferous greenschist facies marbles and schists are superimposed upon the former formation. They are characterised by intercalations of bituminous marbles, massive marbles and dolomites with phyllites – these phyllites are meta-arcozes, meta-argillaceous shales and meta-conglomerates (Hecht, 1972a, 1972b). In stratigraphic succession follow Permian to Triassic intercalated marbles and schists in the greenschist facies. They consist of massive blue and greyish marbles, dolomites and phyllites. These phyllites are similar to the earlier ones in petrographic constitution. Above these rocks follow Triassic fine to massive coarse grained marbles intercalated with anchimetamorphic to epimetamorphic phyllites (Hecht, 1972a, 1972b).

³⁷ A more detailed geological map is provided in the backleaf of this Thesis.

It must be stressed that the full stratigraphic succession of this Unit is not encountered. The lowest rocks, i.e. those of Carboniferous age, are encountered to the NW coast of the Island, around Palaeochorion and to the North of Plomarion, reaching up to the mouth of the Gulf of Geras. The Permian to Carboniferous greenschists and marbles are found to the South side of the Gulf of Geras from the village of Ippion to the North, to Plakados and Pappados to the East and Megalochorion to the West. They are delineated by a circular normal fault from the West to the South to the East, which divides them from the underlying Carboniferous schists and marbles. To the NW they are found under the ophiolites which have been thrust upon them. A relatively small semicircular outcrop of these rocks is found on the East side of the Gulf of Geras, roughly following a curve from the Skala Louton village, to Akrochorion to Ano Chalikas. The Permian to Triassic marbles and schists are found in the Eastern coast of the Island, to the NW of the City of Mytilene. The Triassic marbles and schists are found in the NE coast of the Gulf of Geras in an elongated outcrop between the City of Mytilene and the village of Moria.

Carboniferous to Permian schists and marbles are also observed to the North of Antissa (Hecht, 1972a, 1975). Triassic plated, black to bluish to grey limestones are intercalated with psammitic schists and schistose conglomerates and minor phyllites (Hecht, 1972a, 1975). These are found only in the the NW coast of the Island to the North of Sigrion.

6.2: ALLOCHTHONOUS OPHIOLITES

This unit is found only in two locations in Lesvos Island, thrust over the Autochthonous Basement Unit and underlain by the Polychnitos Ignimbrites (Koglin *et al.*, 2009). Thus there are only two extensive ophiolite bodies. The first, and largest, is observed along a series of relatively low ridges – Koutsouk Toumba (554 m), Apidovouno (507 m), Peukovouno (401 m), Apostoleli (289 m) and Dendreli (412 m) – which form a concave line trending SW to NE. The other small outcrop is on the Amali Peninsula, on the Eastern part of the Gulf of Geras between Agia Marina village and Cape Agrilia. These ophiolites are variably serpentinitised and the most abundant minerals are olivine and pyroxene (Hecht, 1970, 1972a, 1972b). According to Hatzipanagiotou & Pe-Piper (1995) and Pe-Piper *et al.* (2001), the dominant rock type is lherzolite with minor harzburgite and dunite. Pe-Piper *et al.* (2001) have reported the presence of an amphibolitic sole, which is made up from amphibolites and amphibolitic schists, with N-MORB and WPB affinities. The obduction age of the ultramafic unit was inferred by K/Ar dating in hornblende from the amphibolitic sole, as being between 153 and 158 (± 5) my ago (Hatzipanagiotou & Pe-Piper, 1995).

In this tectonic unit, outcrops of metamorphosed basalts and hornblendites must be subsumed (Hecht, 1970, 1972a, 1972b). These rocks exhibit greenschist facies metamorphic indications and are intercalated in places with the rocks of the underlying Unit. The ophiolites are thrust over their metamorphic basement or the underlying Unit, and are overlain by rocks of the Acid Volcanics Unit.

The Lesvos mélangé and the ultramafic unit are believed to represent an incipient continental rift setting, which subsequently lead to the formation of a branch of the Neotethys Ocean.

This model also supports the low degree of melting calculated and the occurrence of N-MORB and WPB characteristics in basalts (Koglin *et al.*, 2009). In general, the geochemistry of mafic-ultramafic complex of Lesvos Island has been studied extensively by Tsikouras *et al.* (1994), Migiros *et al.* (2000) and Pe-Piper *et al.* (2001).

6.3: TERTIARY VOLCANIC SEQUENCE

The rocks comprising the Tertiary Volcanic Sequence were extruded during the Pleiocene, and are the direct result of the Southward migration of the volcanic arc during the subduction of the African plate beneath the Eurasian one. All the volcanic rocks are intermediate to acidic and they belong to a calc alkaline to shoshonitic series. The volcanism in Lesvos was relatively short lived not exceeding one million years (Pe-Piper & Piper, 1992, 1993). This is in stark contrast to the inferred long periods of subduction (Spakman *et al.*, 1990). Although the tectonic units of the tertiary volcanic sequence comprise roughly synchronous rocks, they are presented below, from older to younger, on the basis of their relative tectonic positions.

6.3.1: Skoutaros Unit

The Skoutaros Unit comprises all the volcanic rocks termed as Lower Lavas by Hecht (1970, 1972a, 1972b, 1973, 1974a, 1974b). The lowermost layer of the Lower Lavas consists of latitiandesitic to latitic lavas and is the oldest Neogene extrusive layer on the Island. In places there are minor lapilli tuff and tuff breccia. This layer is found to the Northern tip of Lesvos, North of Vafios and Argennos and West of Skala Sikamineas, up to the coastline. One fairly elongated and extensive outcrop is also observed to the South of Petri, Stypsi and Ipsilometopon villages, up to the North of the area of Petsofas and the village of Lafionas. Finally, one semicircular outcrop is observed around Vatoussa and Revma villages and to the NE of Pterounta.

The intermediate layer of Lower Lavas comprises latitiandesitic to dacitic rocks, lapilli tuff, magmatic breccia and agglomerates. The lava outflows are sometimes cut by lava domes. This particular type of Lower Lavas is found around Eressos and Mantamados and a «two pronged wedge» is observed between Agia Paraskevi and Napi. The uppermost layer of the Lower Lavas consists of latitic, latitiandesitic and dacitic lavas. It is found to the West of the Gulf of Kalloni, around Parakila, Chidira and Anemotia.

6.3.2: Acid Volcanics Unit

On the basis of this Unit, there is a pyroclastic formation, consisting of lapilli tuff and tuff breccia, agglomerates and volcanic bombs. This layer underlies the Sikaminea Unit and is intercalated with its lowest layers for the most part. It also partly underlies or overlies the Polichnitos Ignimbrites (Hecht, 1970, 1972a, 1972b, 1973, 1974a, 1974b). This pyroclastic formation can readily be observed around Agia Paraskevi, Napi, Dafia, Filia and Mantamados amongst other occurrences of smaller size.

The Kapi Rhyolite Formation (Pe-Piper & Piper, 1993) postdates this pyroclastic formation. It is a rhyolitic vitrophyric lava containing perlitites towards its lowest parts. These rhyolites are observed near Kapi and Klio, to the North of Kalloni and to the North of Skoutaros.

The Ignimbrites of Polichnitos (Pe-Piper & Piper, 1993) are roughly synchronous with the Kapi Rhyolite Formation. They are rhyolitic to rhyodacitic ignimbritic layer, more vitrophyric in their upper parts and more tuffitic in their lower parts, with a lower degree of welding. In parts there are lenses of black obsidian (Hecht, 1970, 1972a, 1972b, 1973, 1974a). Layers of tephra – rhyolitic sinders, lapilli, pumice, volcanic bombs, blocks and obsidian – are embedded inside the Ignimbrites near Akrasion and to the East of Kato Stavros (Hecht, 1972b). The Polichnitos Ignimbrites form a more or less continuous body from the NE coast of Lesvos Island – Cape Takmaki – along the NE coast of the Gulf of Kalloni, to Polichnitos and Akrasion. The Ignimbrites along with the pyroclastic formation cover Barbalias Islet to the SE of Cape Takmaki.

The Acid Volcanics Unit is capped by another layer of pyroclastics, termed the Sigrion Pyroclastic Formation (Pe-Piper & Piper, 1993). This layer consists of mainly stratified tuff breccia, volcanic breccia and minor white lapilli tuff. There are extensive lava domes at whose rimes there are dykes and necks, and more commonly lava breccia and agglomerates. Inside the tephra layers, there are fluvial conglomerates and kaolinised tuff. The pyroclastic layer overlies the ignimbrites and underlies the Sikaminea Unit (Hecht, 1970, 1972a, 1974a, 1975). Within these pyroclastic rocks, mainly at their base, there are numerous silicified trunks, roots and seldom fruits of trees, in a remarkable state of preservation. Most silicified samples belong to conifer trees, namely *Cedroxylon*, *Pytioxylon*, *Araucarioxylon* and *Ebenaceae* (Hecht, 1975). The Sigrion Pyroclastic Formation covers the SW of the Island, along with Megalonision, Kavalouris and Sarmosak Islets, to the West of Sigrion.

6.3.3: Sikaminea Unit

The Sikaminea Unit comprises all the volcanic rocks termed as Upper Lavas by Hecht (1970, 1972a, 1972b, 1973, 1974a, 1974b). The main body of the Upper Lavas covers extensive areas of central and Western Lesvos. Their petrology is variable and dacitic, latitic, latitiandesitic, quartz andesitic and rhyolitic lavas can be discerned. Characteristically, there are extended lava flows and in places magmatic agglomerates, conglomerates and minor lapilli tuff. To the East of Mesotopos and Skala Mesotopou, the lower part of these lavas, phanerodacitic and phaneroandesitic, can be observed. The lowermost parts of the Upper Lavas are mostly latitic and latitiandesitic and can be observed around Skalochorion and Skoutaros. The Islet of Saint Georgios Petras, to the NE of Petra, is also covered by these lavas. Finally, two phanerodacitic bodies are observed North and South of Skalochorion.

6.3.4: Mytilene Unit

This term was used by Pe-Piper & Piper (1993) to describe the intermediate and basaltic lavas, forming cones and summits, observed mostly around the City of Mytilene, originally mapped by Hecht (1970, 1972a, 1972b). The lavas appear massive, dark and non-

scouracious. It belongs to the main volcanic sequence of Lesvos according to palaeomagnetic data (Pe-Piper & Piper, 1993). Most probably, such rocks represent the final stages of the magmatic activity, and are thus slightly older than the rocks of the Sikaminea formation.

6.3.5: Hypabyssal Intrusions

These intrusions are naturally slightly older than the other volcanic rocks which they intrude. Rhyodacitic or dacitic dykes of variable geometry are found scattered in the central and Southern parts of the Island. In general their lithology is similar to the rocks which they cut (Hecht, 1970, 1972a, 1973, 1974b, 1975). Notable intrusions appear to the North of Stypsi and Ipsilometopon, North of Argennos and East of Mythimna, South and SE of Filia, NW of Petra, NE of Skoutaros and South of Chidira.

Similar veins occur around Eresos and to the NW of Mesotopos. These were termed «Mesotopos Dykes» by Pe-Piper & Piper (1993). These are of similar geochemical character to the former dykes, but also contain pyroxene in addition to hornblende and biotite (Pe-Piper & Piper, 1993).

An intrusive acidic body, termed «microgranite porphyry» (Periferakis *et al.*, 2017, 2018) was mapped firstly by Voudouris & Alfieris (2005). It intrudes the lavas of the Skoutaros Unit and is thus younger. Finally, a mass of intensely silicified rock (Hecht, 1975), around and NE of Pterounta is included in this Unit, as the silicification must be attributed to hydrothermal activity resulting from an intrusive body.

6.4: POST-MEIOCENE SEDIMENTS

The oldest post-Meiocene sediments are basaltic agglomerates of Pleiocene age. These are agglomerates of phanerobasalts and they lie just below the pyroclastic layer (Hecht, 1970, 1972a, 1973). These sediments are considered to be the product of erosion of ophiolites and predictably they are found near them. More specifically, they are observed to the West and Southwest of Polichnitos. In places they overlie the Ignimbrites of Polichnitos. In addition, Garbias Islet, to the West of Cape Kalloni is covered by these rocks.

Chiefly marly freshwater limestones of Pleiocene age are observed at different locations on the Island. They are of white to grey colour, partly concretionary and partly oolitic. In the lower parts, sandstones and conglomerates are present. In places, there are oligohaline deposits with marls, clays and sandstones and contain several shell beds (Hecht, 1970, 1972a, 1972b, 1973, 1974a, 1974b, 1975). They can be observed on the Eastern side of the Amali Peninsula, to the West and South of Polichnitos, around Lisvorion, West of Panagiouda, at the shores of Cape Machera, and around the City of Mytilene.

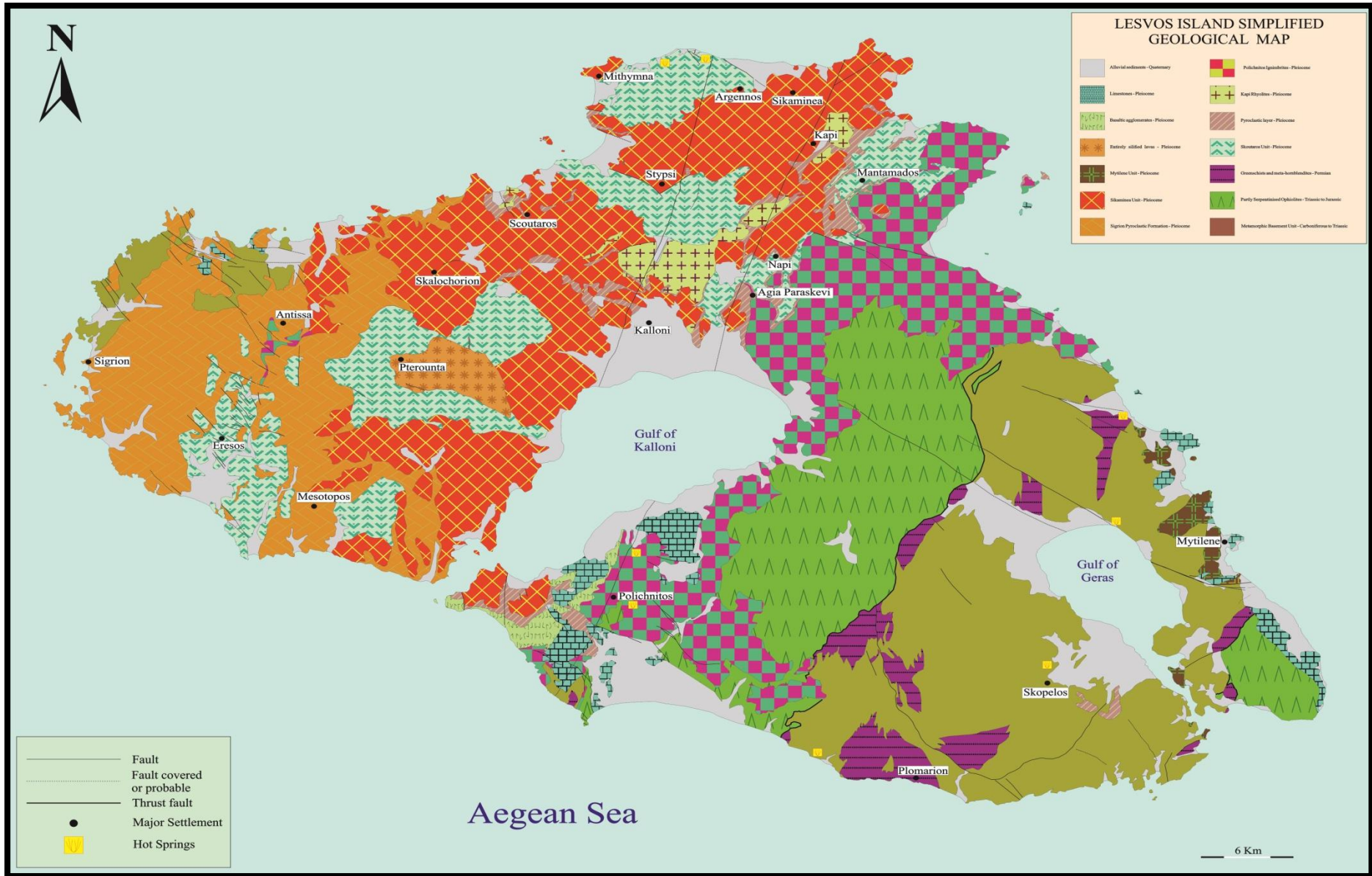


Figure 6.2: The geological structure of Lesvos Island according to the synthesis of existing data, as presented in this Thesis. The geological boundaries are those of Hecht (1970, 1972a, 1972b, 1973, 1974a, 1974b, 1975). The grouping of lithologies into tectonic units is modified after Pe-Piper (1978, 1980a, 1980b) and Pe-Piper & Piper (1992, 1993). The faults and their orientations are based on Hecht (1970, 1972a, 1972b, 1973, 1974a, 1974b, 1975), Voudouris & Alfieris (2005) and Chatzipetros *et al.* (2013).

To the North of Antissa, there are some relatively thin limestone beds. To the East of Lesvos, Venizelos, Tsoukalas and Aspronisos Islets are completely covered by these limestones. In many places, mainly along the coast there are Quaternary alluvial sediments, consisting of mud, sand and clays of grey to red colour (Hecht, 1970, 1972a, 1972b, 1973, 1974a, 1974b, 1975). They cover the Palaeozoic basement around Keramia, Ippion, Paleokipos, Plakados, Pappados and Perama, around the Gulf of Geras. Moreover, the SW coast of the Amali Peninsula is covered by such sediments, as well the areas around Panagiouda and Loutropolis Thermis. Extensive alluvial sediments also cover the igneous rocks around the North, Northeast and Southeast shores of the Gulf of Kalloni. Other such alluvial deposits are found around Skala Eresou, South of Mithimna by the coast, around Skala Sikamineas and Vatera. Smaller alluvial covers are found elsewhere on the island, covering the rocks of the Tertiary Volcanic Sequence and the ophiolites.

Conglomerates with varying degrees of sedimentation, containing fragments of igneous rocks, are observed mostly around the Vriza and near Kato Tritos villages, NW of Loutropolis Thermis, SE of the City of Mytilene on the Amali Peninsula, to the East of Pamfilla and to the North of Skala Loutron. Where the slopes are too steep there are sliding screes (Hecht, 1970, 1972a, 1972b, 1973, 1974a, 1974b, 1975).

CHAPTER 7: FIELD OBSERVATIONS AND GEOLOGY OF THE STUDY AREA

Geology of the Study Area ~ Veins and Alterations of the Stypsi Area

The study area, adjacent to the village of Stypsi, is located in Central Lesvos, to the SW of Lepetimnos Mountain, roughly 10 Km North of Kalloni (Figure 7.1). Topographically, the village of Stypsi is perched up on the SW slope of the Mountain of Lepetimnos. The study area extends below and to the East of village, covering the adjacent hill and the undulating slope in front of it, which is crosscut by numerous streams.

7.1: GEOLOGY OF THE STUDY AREA

The study area, to the South and Southeast of Stypsi, is to the North of the Island, in an area characterised by Tertiary volcanic rocks. The village of Stypsi is situated on the contact of the Sikaminea and the Skoutaros Units. The village itself rests upon the Upper Lavas of the Sikaminea Formation while to the South the underlying lower lavas of the Skoutaros Formation are exposed. To the East of the village, roughly 100-150 m along the regional road, an outcrop of the pyroclastic layer belonging to the Acid Volcanics Unit can be observed. Further to the NNE of Stypsi dykes also belonging to the Acid Volcanics Unit can be seen.

The study area is characterised by a NNE trending fault (Figure 7.2), which continues all the way to Megala Therma. The Lower Lavas of the Skoutaros Unit appear black to greyish black when fresh and they occupy the greatest part of the caldera. Macroscopically the dominant minerals are pyroxene and plagioclase, while in some cases hornblende crystals can be distinguished. The ground mass is very fine grained. These rocks are classified as basaltic andesites to trachyandesites.

The Upper Lavas of the Sikaminea Unit appear red when fresh (Figure 7.7c), and they are characterised by biotite and pyroxene phenocrysts, which are embedded in a fine grained matrix of quartz and plagioclase. To the NE of the village, along the road, an elongated body of the pyroclastic formation at the base of the Acid Volcanics Units is observed. Roughly in the centre of the caldera, an igneous intrusive body, classified as a microgranite porphyry – all classifications are demonstrated in the relevant plots in the next chapter – pierces the lavas of the Skoutaros Unit. The dominant mineral is K-feldspar, whose phenocrysts are found inside a biotite and hornblende very fine grained groundmass. This igneous intrusion is considered to be in direct correlation to the formation of the fault system in the Stypsi area.

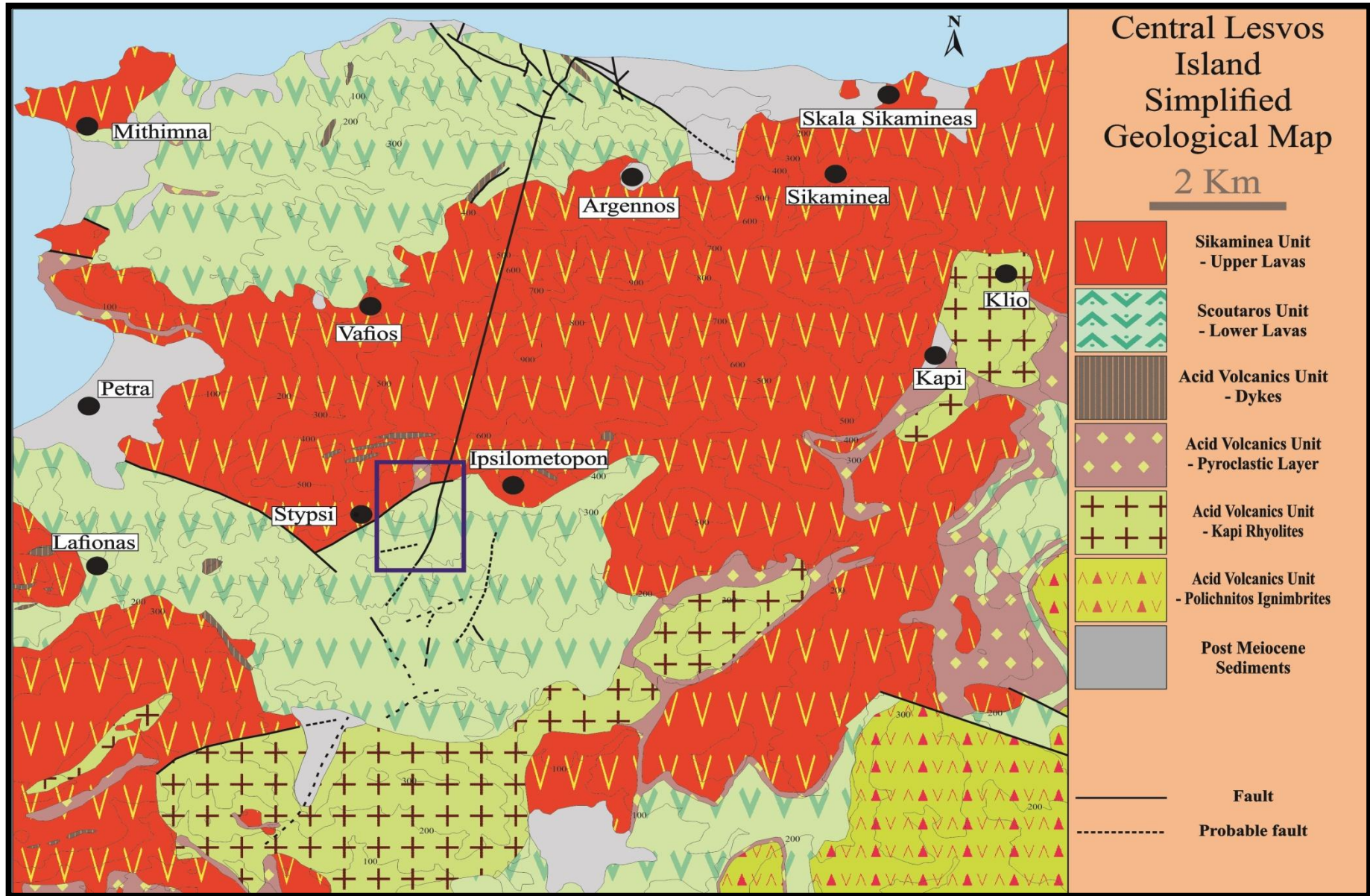
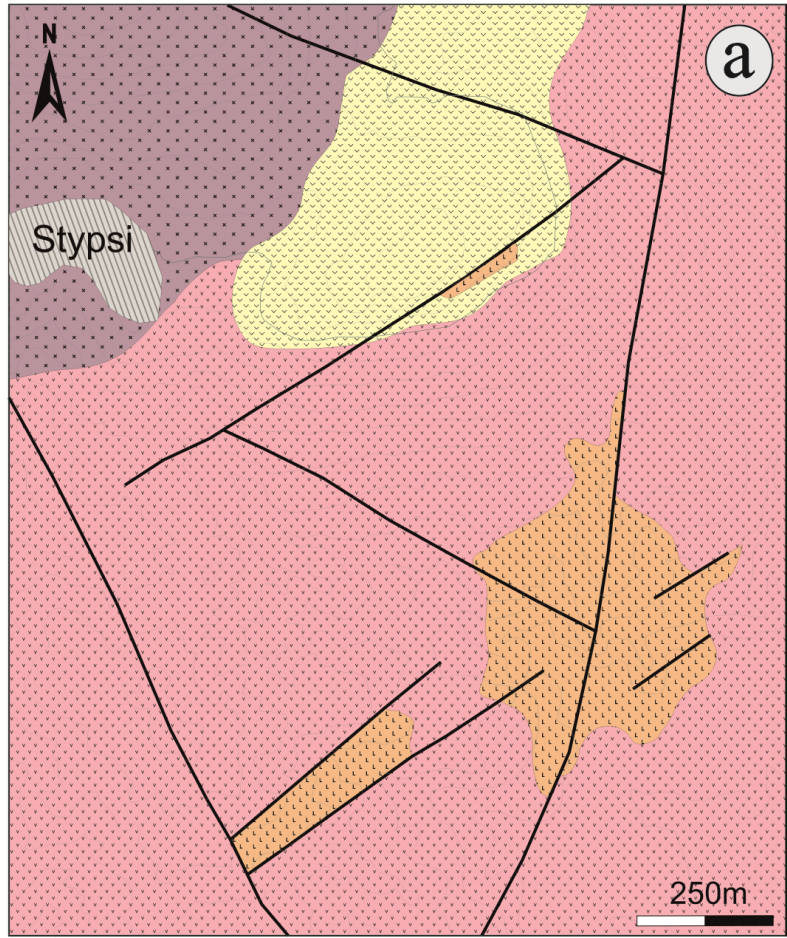


Figure 7.1 (previous page): Simplified geological map of central Lesvos Island. The study area of Stypsi Therma is indicated by the blue rectangle. The large fault running from Stypsi all the way to Megala Therma, trending NNE, is clearly visible. The geological boundaries are those of Hecht (1970, 1972a, 1973, 1974b) and the grouping of lithologies into units is modified after Pe-Piper & Piper (1992, 1993). The faults and their orientations are taken from Hecht (1973, 1974b) and Voudouris & Alfieris (2005).

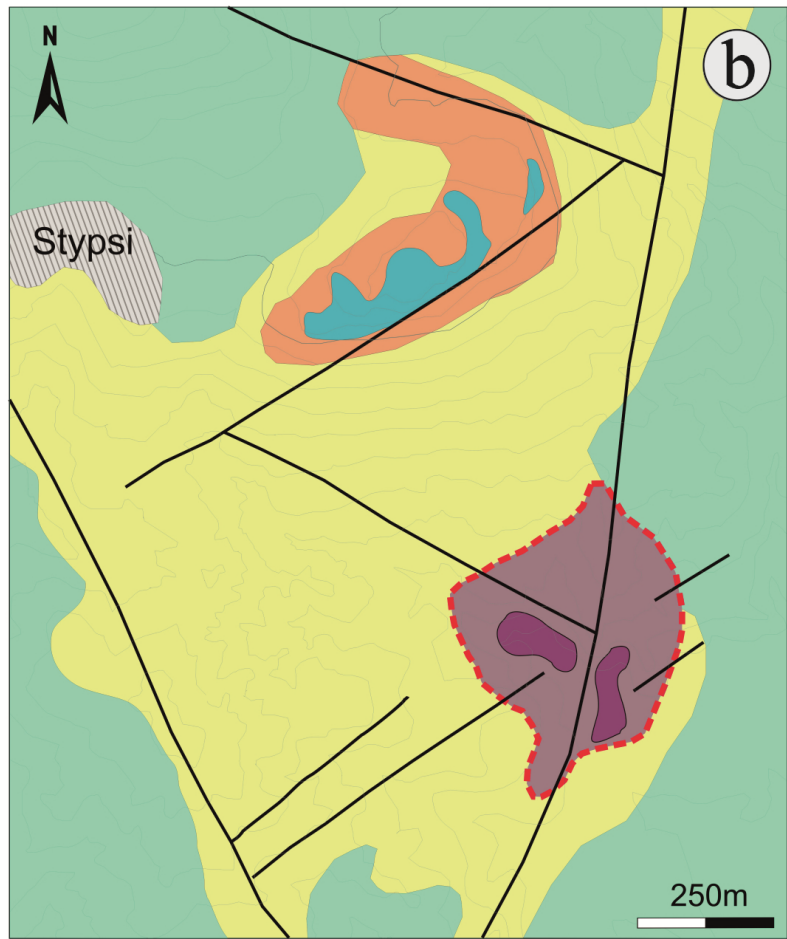
The NNE trending fault is roughly parallel to another extensive fault structure, running from Polichnitos to the South to the village of Skala Sikamineas to the North. All other rocks and structures of the area are cut by the NNE trending fault and this must indicate that not only the fault was synchronous with the intrusion but that it was also active after it. In each and every case where the fault cuts the microgranite the rocks' boundaries are transposed. As expected, the igneous intrusions form the focal point of the mineralising system while mineralisation is hosted, partly, in the lavas of the Skoutaros Unit.

7.2: VEINS AND ALTERATIONS OF THE STYPSI AREA

The rocks around the igneous intrusions are altered to various degrees, according to their distance from the mineralising intrusion. The alterations in the areas within the caldera of Stypsi have been the focus of previous studies (Kelepertsis & Esson, 1987; Voudouris & Alfieris, 2005; Vamvoukakis, 2009). According to these studies, the alterations of the igneous rocks range from propylitic to argillic (Figure 7.7d) and silicic in some areas, while there is also sericite-carbonate, K-Na-silicate and advanced argillic alteration zones reported by Voudouris & Alfieris (2005). To the West of Stypsi there are extensive areas of kaolinitisations, as reported by Hecht (1970, 1972a, 1974b). An advanced argillic lithocap to the East of Stypsi was reported by Vamvoukakis (2009) who also noted the presence of alunite, montmorillonite, illite and pyrophyllite. The porphyry mineralisation consists essentially of a stockwork of quartz veinlets, which is hosted mainly by the microgranite, and by the Skoutaros lavas in some places (Figure 7.2). There are more than one stages of hydrothermal activity, as has been mentioned by Voudouris & Alfieris (2005). The banded quartz veins constitute the early stage (Figures 7.3a, 7.3b, 7.3c, 7.5c) and the pyrite-molybdenite veins constitute the late stage of the mineralisation. The banded quartz veins are associated with Na-Ca alteration and propylitic alteration and the pyrite-molybdenite veins are associated with phyllic alteration (Voudouris *et al.*, 2019). The microgranite porphyry is regarded as the core of the porphyry system and is affected by Na-Ca alteration. Mineralogically, samples from the altered microgranite are characterised by albite and chlorite and actinolite which are the cause for the greenish colour of the rocks (Figure 7.5d). In addition, orthoclase, plagioclase (mostly albite) and calcite are observed. In places, the alteration is so intense that the primary textural features of the rock have been obliterated. This alteration assemblage correlates spatially with banded quartz veins and stockwork (Figure 7.3a, 7.3b, 7.3c, 7.4d). The width of the quartz veins ranges between roughly 0.5 cm and 11 cm. The colour of the veins is alternating between dark grey and black. Abundant vapour-rich fluid inclusions inside quartz crystals are responsible for the dark coloured bands (Voudouris *et al.*, 2019). The quartz crystals of the veins appear granular anhedral or euhedral, under the microscope. The texture of the veins is mostly botryoidal, which is indicative of quartz recrystallisation from a silica gel (Muntean & Einaudi, 2001, 2002).



- Basaltic trachyandesitic lavas (Skoutaros Unit)
- Pyroclastic rocks (tuffs, tuff breccia; Acid volcanic Unit)
- Trachydacitic lavas (Sykaminea Unit)
- Microgranite porphyry
- Fault



- Silicic alteration
- Advanced argillic alteration
- Sericitic alteration
- Sodic/potassic-calcic alteration with sericitic alteration overprint
- Sodic/potassic-calcic alteration
- Propylitic alteration to fresh rock
- Surface outcrop of quartz stockwork
- Fault

Figure 7.2 (previous page): (a) Simplified geological map of the Stypsi area (after Voudouris *et al.*, 2019). (b) Simplified alteration map of the Stypsi area, demonstrating the surface distribution of hydrothermal alteration zones and the location of the porphyry-epithermal prospect (after Voudouris *et al.*, 2019).

The ore mineral assemblage in these veins consists of pyrite, bornite, galena, sphalerite and molybdenite. There is also minor magnetite and hematite. Some grains of the sulfide minerals are visible as disseminations in the matrix, however their majority appears inside the quartz matrix of the veins. It is obvious from the textural relationships between the mineral grains, that the ore minerals were deposited after the quartz crystallisation, probably concurrently with the alteration minerals.

The Na-Ca alteration peters out abruptly to propylitic alteration which surrounds the South, West and East sides of the system (Figure 7.7b). The propylitic alteration is characterised by calcite, quartz, sericite, epidote and hematite in varying amounts. Lower Lavas affected by propylitic alteration are slightly darker in colour than the fresh rocks. Both types of alterations are most probably synchronous (Voudouris *et al.*, 2019).

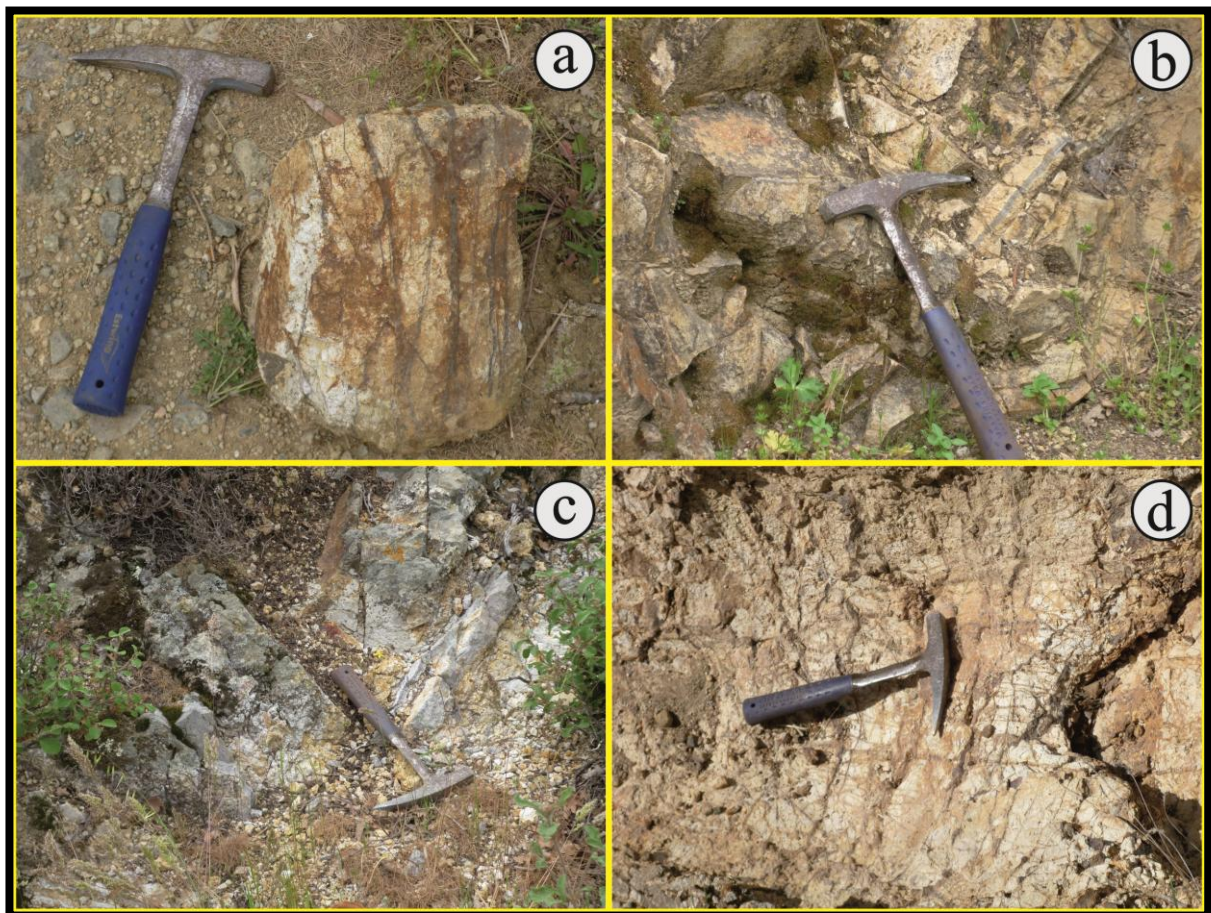


Figure 7.3: (a) Loose stockwork of black banded quartz veins crosscutting the microgranite porphyry. (b) Linear black quartz veins stockwork inside sericitically altered microgranite porphyry. (c) Black quartz veins inside the microgranite porphyry, which has been affected by Na-Ca alteration. (d) D veins inside sericitically altered Lower Lavas.

D-type veins are traditionally associated with phyllic/sericitic alteration (Figures 7.6c, 7.7d) in porphyry systems. Notable examples include El Salvador (Gustafson & Hunt, 1975), Bingham (Parry *et al.*, 2002) and Henderson (Seedorff & Einaudi, 2004a). The pyrite +

molybdenite veins associated with sericitic alteration in Stypsi, are termed D veins (Figure 8.3d), according to the terminology of Gustafson & Hunt (1975).



Figure 7.4: (a, b, c) D vein stockwork inside Lower Lavas affected by sericitic alteration, on the banks of the numerous streams to the South of Stypsi. (d) Black banded quartz veins in clasts inside a stream, with visible signs of Na-Ca alteration, as evidenced by the greenish colour of the rock.

The sericitic alteration at Stypsi has erased any previous textural and mineralogical elements. Sericite, quartz and calcite can be observed replacing feldspars. Most D veins are continuous and more or less on the same plane, while some exhibit signs of intense tectonic stress (Figures 7.4a, 7.4b, 7.4c, 7.5a, 7.5b, 7.7a). Their width varies between 1.5 mm and 18 cm and their general direction is parallel to the main fault discussed above. These veins contain pyrite, bismuthinite, molybdenite and sericite, quartz and calcite. Molybdenite is judged to be older than pyrite based on textural relationships (Voudouris *et al.*, 2019).

The epithermal veins are termed E-type veins, and belong to the latest stage of the porphyry-epithermal system. They cut the porphyry quartz veinlets and all alteration types. The epithermal veins reach up to higher topographic levels, almost to the top of the advanced argillic lithocap to the East of Stypsi (Figure 7.6a, 7.6b, 7.6d). Most E-type veins are milky quartz and platy calcite veins, having a median diameter of 16 cm. The E-type veins are on a parallel direction to the main fault and are associated with argillic alteration, consisting of quartz, sericite and kaolinite. Kontis *et al.* (1994) and Kontis (1997) reported veins of similar mineralogy outside of the Stypsi caldera, which host Ag + Au mineralisation. In contrast, the E-type veins of the study area are completely barren (Voudouris *et al.*, 2019).

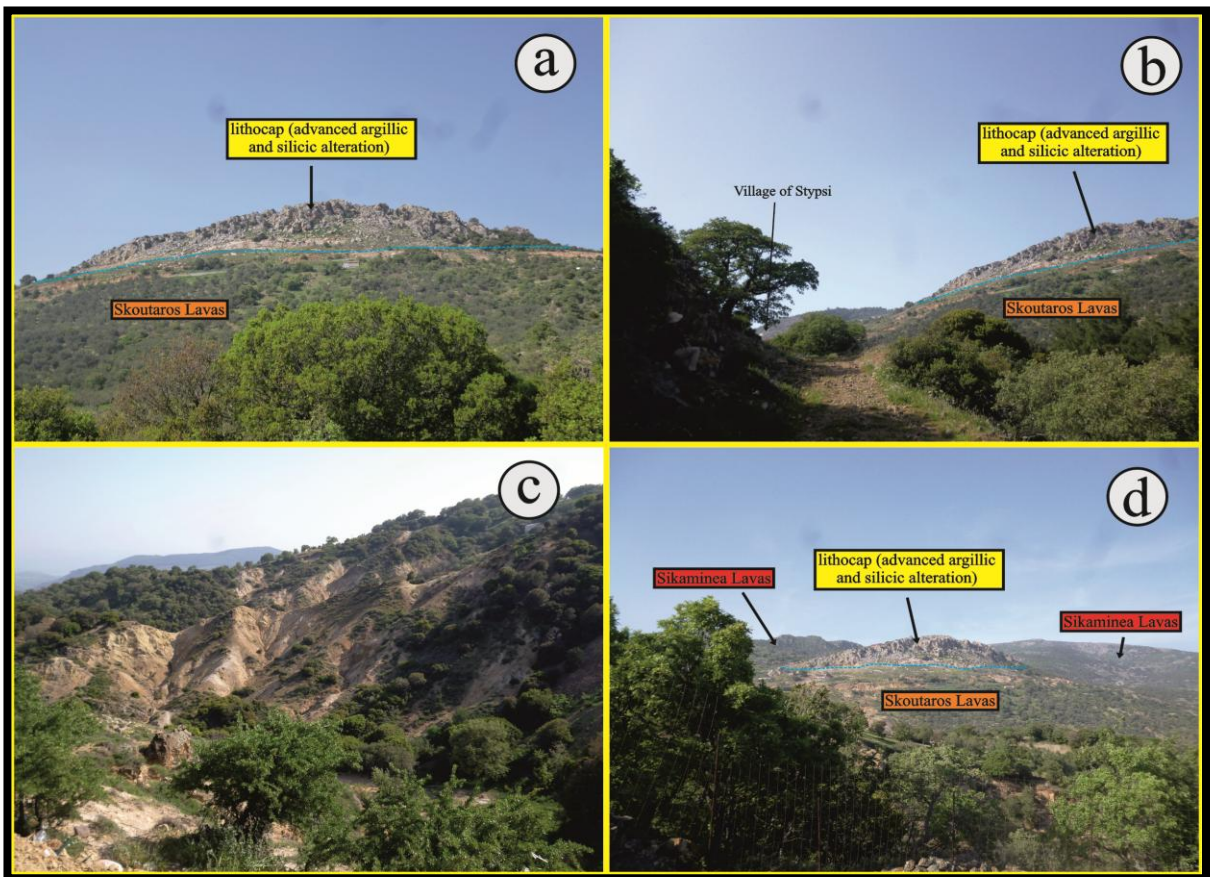
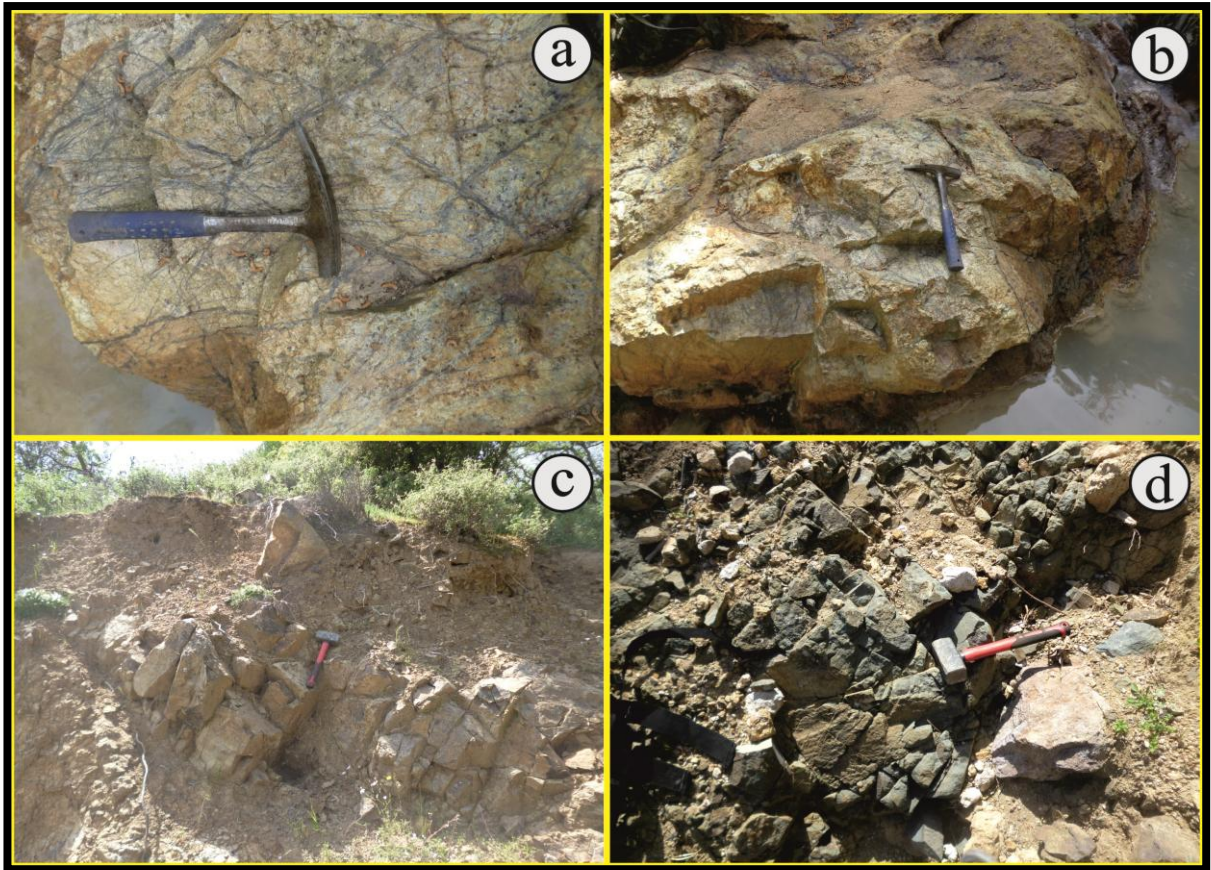




Figure 7.5 (page 85-top): (a, b) D veins quartz stockwork in situ on the bank of one of the numerous streams crosscutting the area. (c) Black banded quartz veins inside the microgranite porphyry, which is affected by Na-Ca alteration. (d) Relatively fresh subvolcanite to the SE of Stypsi.

Figure 7.6 (page 85-bottom): (a) Panoramic view of the silica cup which is to the East of Stypsi. The photo has been taken 400 m directly South of the silica cup. (b) View of the silica cup with the village of Stypsi to the West. The photo is taken roughly 150 m to the West of the aforementioned location. (c) Panoramic view of the sericitic alteration of the Skoutaros Lavas, below the silica cup. This photo is taken 70 m to the West of the silica cup, facing towards SW. (d). Panoramic view of the silica cup and the surrounding area, illustrating the transition between the lithocap and the underlying sericitic alteration. This photo is taken roughly 250 m West of Stypsi.

Figure 7.7 (previous page): (a) Weak D veins stockwork inside sericitically altered Lower Lavas, about 400 m SSE of the village of Stypsi. (b) Weathered propylitic alteration roughly 600 m SSE of Stypsi. (c) Relatively fresh Upper Lavas, about 100 m to the NE of the silica cup, by the road. (d) The transition between sericitic and phyllic alteration, inside the Skoutaros Lavas, 200 m SSW of Stypsi.

CHAPTER 8: WHOLE ROCK AND BULK ROCK GEOCHEMISTRY

Interpretation of Geochemical Data ~ Bulk Ore Geochemistry

In this chapter all the results from the various types of analyses are presented (Tables 8.1 & 8.2), along with their interpretation. The first part of this chapter deals with the presentation of the fresh rock analyses' results. Then, alteration geochemistry plots and the bulk ore analyses results are presented and evaluated.

8.1: INTERPRETATION OF GEOCHEMICAL DATA

8.1.1: Geochemical Classification Plots

In the TAS geochemical classification plots (Figure 8.1a & 8.1b, 8.1c) the samples from the Skoutaros Unit (represented by blue circles) plot into the trachyandesite, basaltic andesite, basaltic trachyandesite fields. The samples from the Sikaminea Unit (represented by purple rectangles) are classified as dacites, trachydacites and rhyolites. The samples from the microgranite porphyry (represented by green triangles) invariably plot into the microgranite field. Overall, it can be observed that there is a slight discrepancy between the geochemical classifications of the samples from the Sikaminea Unit in the three different TAS plots. This must be attributed to the slight differences between the limits of each field of different TAS plots, as both the x and y coordinate axes are the same in all three plots. Using the Jensen Cation Plot (Figure 8.1d) it can be observed that the samples from the Skoutaros Unit plot into the basalt and andesite field, which is consistent with their geochemical classification by previous studies. The two samples from the Sikaminea Unit plot into the dacite field, again in accordance to previous geochemical classifications. Finally, the samples from the microgranite porphyry are classified as rhyolite, something consistent with their geochemical nature. This classification plot is believed to be more accurate, since the cations of Al_2O_3 , Fe_2O_3 , TiO_2 and MgO , which form the apices of the ternary plot are less susceptible to chemical migration and therefore are less affected by weathering and alteration.

In the A/CNK versus A/NK geochemical classification plot (Figure 8.2a) most samples plot into the metaluminous field, while one sample from the Sikaminea Unit, two samples from the Skoutaros Unit and both samples from the microgranite porphyry plot into the peraluminous field³⁸. In the R1-R2 Plot (Figure 8.2b), the samples from the Skoutaros Unit plot into the andesite and andesite-basalt field. The samples from the Sikaminea Unit plot into the dacite and rhyodacite fields. The samples from the microgranite porphyry plot into the rhyodacite field. It is observed that there are slight differences when comparing this

³⁸ The term «**metaluminous**» means that the rock is characterised by the following molecular relationship: $\text{Al}_2\text{O}_3 < (\text{CaO} + \text{Na}_2\text{O} + \text{K}_2\text{O})$. The term «**peraluminous**» corresponds to the opposite molecular relationship, i.e. $\text{Al}_2\text{O}_3 > (\text{CaO} + \text{Na}_2\text{O} + \text{K}_2\text{O})$.

geochemical classification to the previous ones. This is probably due to the fact that the axes of this plot are constructed based on many variants $[R1 = 4 \cdot Si - 11 \cdot (Na + K) - 2 \cdot (Fe + Ti)]$ and $R2 = 6 \cdot Ca + 2 \cdot (Mg + Al)$, consequently being more complex than those of the previous plots, and that the limits of different fields are somewhat different, to conform to the majority of the igneous rocks worldwide used in constructing the plot.

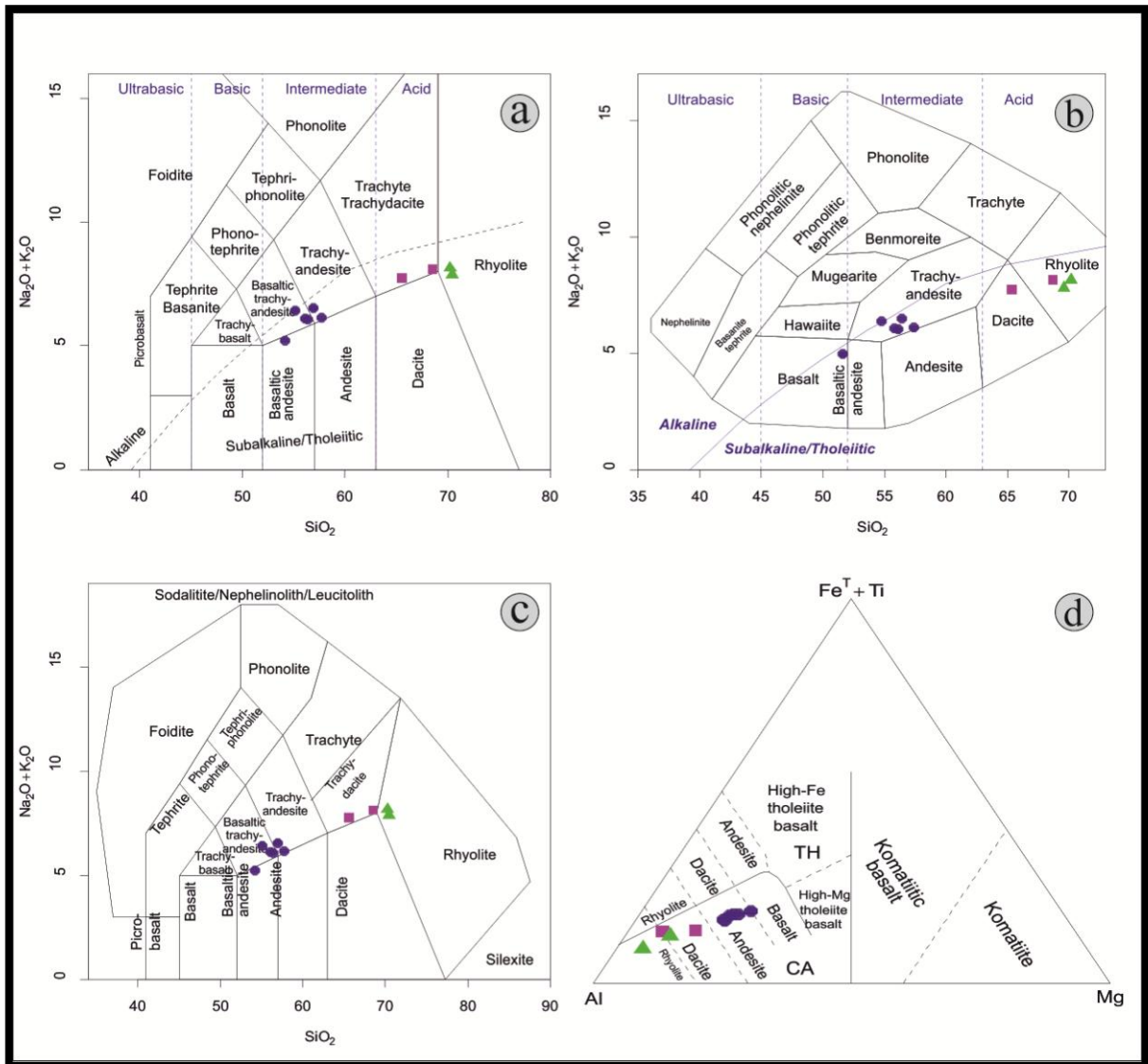


Figure 8.1: Geochemical classification plots. (a) TAS geochemical classification plot, where the samples from the Skoutaros Unit plot into the basaltic andesite, basaltic trachyandeiste and trachyandesite fields, the samples from the Sikaminea Unit plot into the trachyte-trachydacite field, and the samples from the microgranite porphyry plot into the rhyolite field (after le Bas *et al.*, 1986). (b) TAS geochemical classification plot, where it can be observed that the samples from the Skoutaros Unit (blue circles) plot into the basaltic andesite and trachyandesite fields, the samples from the Sikaminea Unit (purple rectangles) plot into the dacite and rhyolite fields, and the samples from the microgranite porphyry (green triangles) plot into the rhyolite field (after Cox *et al.*, 1979). (c) TAS geochemical classification plot, where it can be observed that the samples from the Skoutaros Unit (blue circles) are classified as basaltic trachyandesites, trachyandesites and andesites. The samples from the Sikaminea Unit (purple rectangles) are classified as trachydacite, and the samples of the microgranite porphyry (green triangles) are plotted as rhyolites (after Middlemost, 1994). (d) Jensen Cation Plot, where the samples from the Skoutaros Unit plot into the basalt and andesite fields, those from the Sikaminea Unit plot into the dacite field, and the samples from the microgranite porphyry plots into the rhyolite field (after Jensen, 1976).

In the Co versus Th plot (Figure 8.2c), which acts as a proxy for a SiO₂ versus K₂O plot (Hastie *et al.*, 2007), all the samples plot into the high-K calc-alkaline and shoshonite series. This is in stark contrast to all the previous plots, and it is probable that the Th and Co values of the analyses are not very precise, owing to analytical constraints. In the AFM geochemical classification plot (Figure 8.2d), the entirety of the samples plot into the calc-alkaline series.

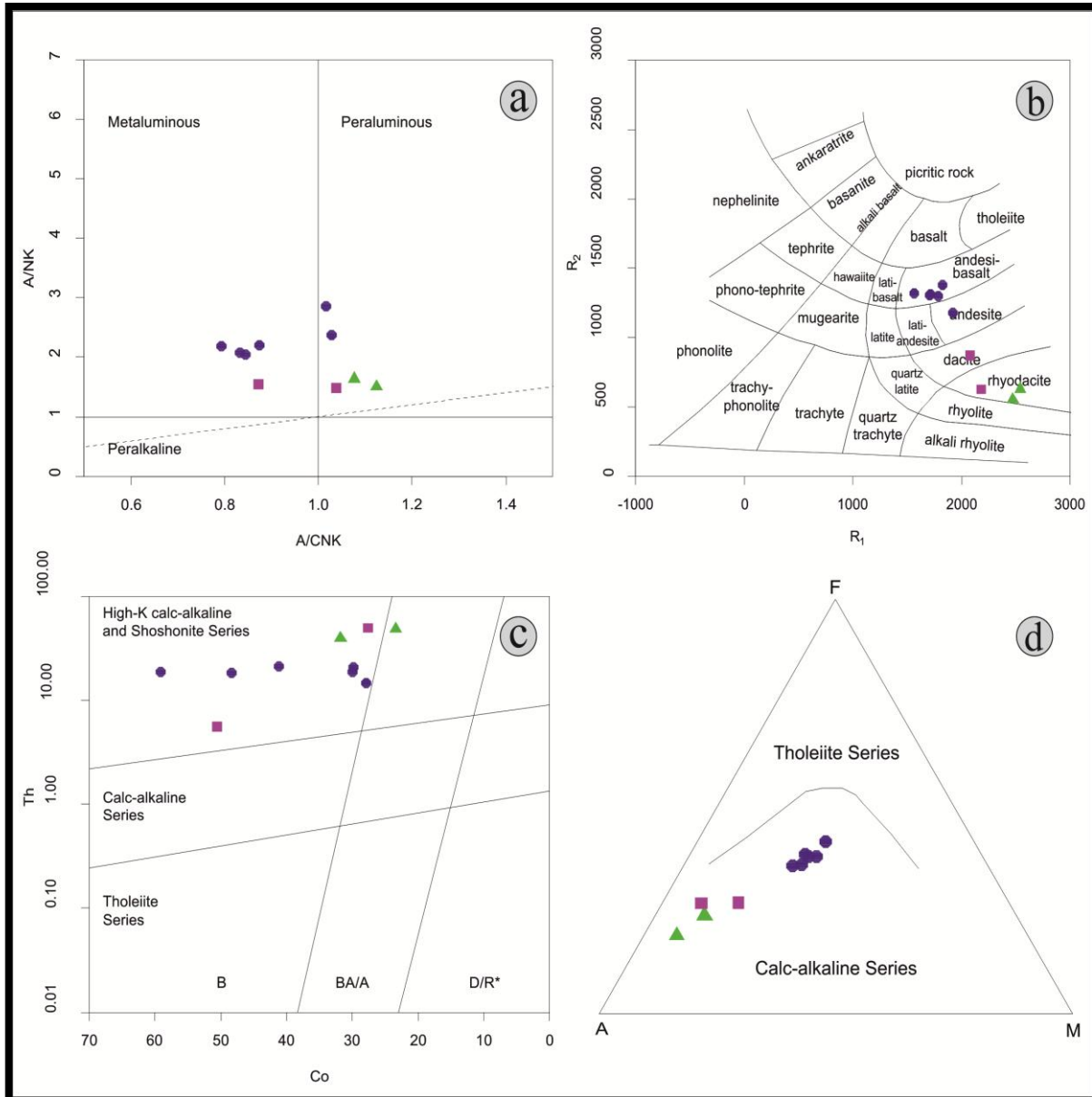


Figure 8.2: Geochemical Classification Plots. (a) A/CNK versus A/NK geochemical classification plot, where the samples from the Skoutaros Unit (blue circles) and the Sikaminea Unit (purple rectangles) are classified as either metaluminous or peraluminous, and the samples from the microgranite porphyry (green triangles) plot into the peraluminous field (after Shand, 1943). (b) R₁-R₂ geochemical classification plot, where the samples from the Skoutaros Unit are classified as andesite-basalts and andesites, those from the Sikaminea Unit as dacite and rhyodacite and those from the microgranite porphyry as rhyodacites (after de la Roche *et al.*, 1980). (c) Co versus Th geochemical classification plot where all the samples plot into the high-K calc-alkaline and shoshonite series field, exhibiting a basaltic to andesitic affinity (after Hastie *et al.*, 2007). (d) AFM geochemical classification plot where all the samples plot into the calc-alkaline series field (after Irvine & Baragar, 1971).

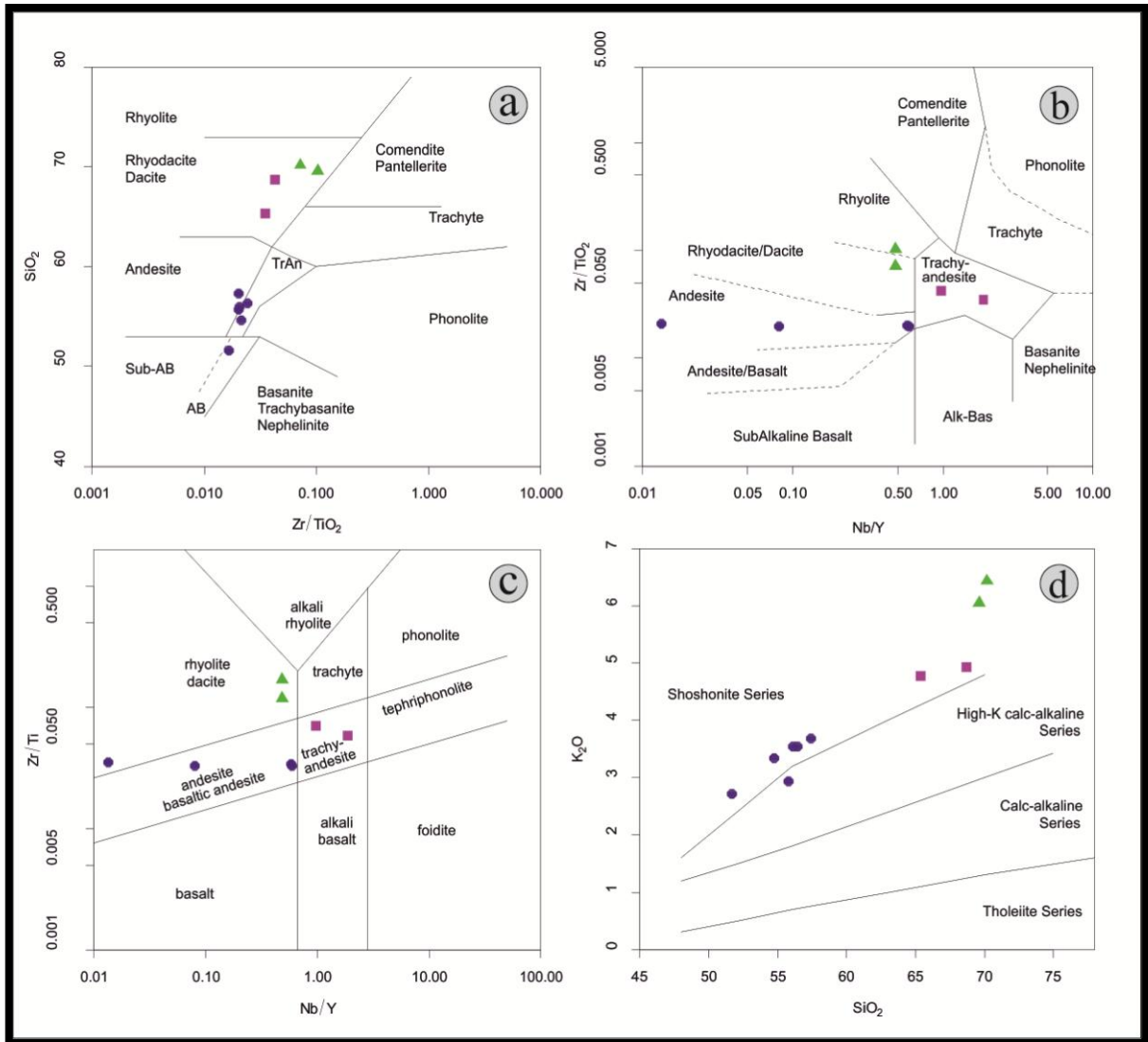


Figure 8.3: Geochemical classification plots. (a) (Zr/TiO_2) versus SiO_2 geochemical classification plot, where the samples from the Skoutaros Unit (blue circles) plot into the trachyandesite and andesite fields, those from the Sikaminea Units (purple rectangles) plot into the rhyodacite/dacite field as well as those from the microgranite porphyry (green triangles), which are however more acidic and as such are plotted closer to the rhyolite field (after Floyd & Winchester, 1978). (b) (Nb/Y) versus (Zr/TiO_2) geochemical classification plot, where the samples from the Skoutaros Unit are plotted as andesites and the samples from the Sikaminea Unit are plotted as trachyandesites. The samples from the microgranite porphyry are plotted as rhyodacite and rhyolite (after Floyd & Winchester, 1978). (c) Nb/Y versus Zr/Ti geochemical classification plot, where the samples from the Skoutaros Unit are plotted as dacites, andesites and basaltic andesites. The samples from the Sikaminea Unit are plotted as trachyandesites, and those from the microgranite porphyry plot into the rhyolite/dacite field (modified by Pearce, 1996). (d) SiO_2 versus K_2O geochemical classification plot, where all the samples plot into the shoshonite series, with the exception of one sample from the Skoutaros Unit, which plots into the high-K calc-alkaline series field (after Peccerillo & Taylor, 1976).

In the (Zr/TiO_2) versus SiO_2 geochemical classification plot (Figure 8.3a) the samples from the microgranite porphyry and the Sikaminea Units plot into the rhyodacite/dacite field, while the samples from the Skoutaros Unit plot as andesites and trachyandesites. In the Nb/Y versus (Zr/TiO_2) geochemical classification plot (Figure 8.3b) the samples from the microgranite porphyry are plotted as rhyodacite and rhyolite. The samples from the Sikaminea Unit plot into the trachyandesite field and those from the Skoutaros Unit are plotted as andesites. These classifications are considered more accurate compared to those obtained from the TAS plots, since Nb, Ti and Zr are more immobile during alteration and

metamorphic events (Floyd & Winchester, 1978). In the (Nb/Y) versus (Zr/Ti) plot (Figure 8.3c), the samples from the Sikaminea Unit plot into the trachyandesite field. The samples from the Skoutaros Unit plot into the dacite and andesite/basaltic andesite field. The samples from the microgranite porphyry plot into the rhyolite/dacite field. In the SiO₂ versus K₂O plot (Figure 8.3d) all the samples, with the exception of one sample from the Skoutaros Unit, plot into the shoshonite series field.

So, to summarise, all the samples from the igneous rocks belong to a calc alkaline to shoshonite series, being metaluminous to peraluminous. This is consistent with previous geochemical classification of Pe-Piper & Piper (1992), and the general geochemical character of Tertiary magmatism in the NE Aegean Sea area (Pe-Piper & Piper, 2002). The samples from the Skoutaros Unit are classified as basaltic andesites, andesites, and trachyandesites. The samples from the Sikaminea Unit are classified as rhyodacites to dacites and the samples from the microgranite porphyry as being of rhyolitic geochemical composition. For the samples from the Skoutaros and the Sikaminea Units, the results hereto presented are in accordance with existing data (Hecht, 1970, 1972a, 1972b, 1973, 1974a, 1974b, 1975; Pe-Piper, 1978, 1980a, 1980b; Pe-Piper *et al.*, 1993).

Table 8.1: Geochemical Analyses Results of Fresh Samples

Sample Element		ST 20	ST 21	ST 25	ST 28	ST 32	ST 34	ST 35	Ar 100b	LS 1	LS 2
SiO ₂	%	66.81	52.81	54.15	66.52	49.53	66.54	53.55	57.38	65.36	65.42
Al ₂ O ₃	%	14.81	17.11	17.98	13.99	18.37	15.33	16.71	18.98	15.55	18.19
Fe ₂ O ₃	%	2.11	7.45	6.83	3.09	8.05	3.62	6.65	6.28	4.03	6.28
MnO	%	0.04	0.17	0.12	0.08	0.13	0.03	0.09	0.12	0.08	0.11
MgO	%	0.71	4.72	3.82	1.23	4.13	1.02	3.96	3.88	2.18	3.63
CaO	%	2.59	6.57	6.87	1.75	6.42	2.43	7.44	5.76	4.29	7.23
Na ₂ O	%	1.67	2.94	3.05	1.62	2.17	3.12	2.38	2.43	2.95	2.95
K ₂ O	%	5.82	3.23	2.86	6.10	2.62	4.82	3.40	3.69	4.78	3.56
TiO ₂	%	0.30	0.98	0.94	0.33	1.06	0.44	0.89	1.01	0.51	0.86
P ₂ O ₅	%	0.08	0.47	0.45	0.11	0.53	0.18	0.44	0.48	0.26	0.42
SO ₃	%	0.15	0.05	0.03	0.04	0.78	0.00	0.00	0.00	0.00	0.00
H ₂ O	%	4.28	2.81	2.22	4.13	5.81	1.89	2.94	2.10	4.63	8.13
Total	%	99.37	99.31	99.32	98.99	99.60	99.42	98.45	98.89	99.24	99.84
Ag	ppb	105.00	105.00	32.00	426.00	92.00	28.00	51.00	52.00	-	-
As	ppm	4.30	40.10	6.00	3.70	37.10	2.80	7.20	1.00	-	-
Au	ppb	2.00	2.40	2.00	97.70	2.40	1.50	2.80	1.20	-	-
B	ppm	2.00	1.00	2.00	2.00	2.00	2.00	2.00	1.00	-	-
Ba	ppm	1131.0	1692.0	1681.0	1435.0	2292.0	1606.0	1531.0	1506.0	1466	1077
Be	ppm	1.50	0.60	1.00	1.80	1.80	0.80	1.30	0.10	-	-
Bi	ppm	0.13	0.21	0.03	0.08	1.28	0.10	0.12	0.19	-	-
Cd	ppm	0.57	0.22	0.07	2.14	0.18	0.03	0.07	0.02	-	-
Ce	ppm	173.90	97.70	107.40	125.70	120.20	101.80	99.00	29.10	139.00	120.00
Co	ppm	19.00	40.30	29.90	31.80	59.30	27.60	41.30	50.60	28.00	30.00
Cr	ppm	2.00	21.00	14.00	5.00	5.00	15.00	19.00	21.00	16.00	34.00
Cs	ppm	1.46	2.00	1.60	1.01	2.10	0.52	0.28	0.76	-	-
Cu	ppm	13.41	66.06	37.99	339.1	117.61	26.92	73.23	32.00	60.00	48.00
Dy	ppm	5.85	4.17	3.89	3.54	4.44	3.62	3.87	0.81	-	-
Er	ppm	2.80	2.05	1.96	2.00	2.09	1.99	2.01	0.37	-	-

Eu	ppm	2.35	1.87	1.79	1.34	1.97	1.13	1.72	0.20	-	-
Ga	ppm	14.60	18.30	17.50	4.50	17.20	15.20	17.30	3.20	22.00	21.00
Gd	ppm	9.38	6.35	5.74	4.88	6.57	4.36	5.70	1.39	-	-
Ge	ppm	< 0.10	< 0.10	< 0.10	< 0.10	0.10	< 0.10	< 0.10	0.10	-	-
Hf	ppm	9.10	6.00	5.10	7.10	5.00	5.40	5.40	0.10	-	-
Hg	ppb	< 5.00	< 5.00	< 5.00	< 5.00	< 5.00	< 5.00	< 5.00	< 5.00	-	-
Ho	ppm	1.04	0.76	0.70	0.69	0.78	0.66	0.70	0.17	-	-
In	ppm	< 0.02	0.03	< 0.02	0.18	0.05	< 0.02	0.02	< 0.02	-	-
La	ppm	114.20	49.20	56.10	67.60	62.10	60.40	51.40	15.20	88.00	57.00
Li	ppm	1.80	4.70	4.30	2.70	15.60	3.60	2.70	1.20	-	-
Lu	ppm	0.42	0.27	0.26	0.33	0.28	0.34	0.28	0.06	-	-
Mo	ppm	2.70	2.00	1.27	34.87	1.78	0.51	1.61	0.45	-	-
Nb	ppm	23.30	14.90	11.90	16.80	10.30	18.00	11.70	0.52	0.00	2.00
Nd	ppm	76.20	44.80	45.00	43.90	53.10	35.00	42.40	10.65	55.00	50.00
Ni	ppm	5.30	14.30	11.70	4.80	13.70	9.50	15.70	8.90	17.00	23.00
Pb	ppm	35.44	72.40	27.00	207.24	44.99	11.92	16.53	3.70	28.00	34.00
Pd	ppb	< 10.0	10.00	< 10.0	< 10.0	< 10.0	< 10.0	< 10.0	< 10.0	-	-
Pr	ppm	21.60	11.53	12.05	13.03	13.94	10.66	11.62	3.25	-	-
Pt	ppb	< 2.00	< 2.00	3.00	< 2.00	< 2.00	< 2.00	2.00	< 2.00	-	-
Rb	ppm	177.00	90.20	83.20	201.40	35.60	180.30	109.90	27.30	131.00	132.00
Re	ppb	< 1.00	< 1.00	< 1.00	20.00	1.00	< 1.00	2.00	4.00	-	-
Sb	ppm	0.03	0.64	0.09	0.06	0.68	0.36	0.09	0.12	-	-
Sc	ppm	1.10	2.10	5.20	1.40	13.00	6.60	5.20	1.70	16.00	24.00
Se	ppm	< 0.10	< 0.10	< 0.10	< 0.10	1.70	< 0.10	< 0.10	< 0.10	-	-
Sm	ppm	11.82	7.75	7.38	6.53	8.60	5.54	7.31	1.79	-	-
Sn	ppm	0.20	0.30	0.60	1.10	1.00	0.90	1.00	0.70	-	-
Sr	ppm	499.50	1030.50	1144.60	453.20	555.00	607.30	1069.20	73.70	942.00	748.00
Ta	ppm	1.70	0.90	0.80	1.30	0.50	1.50	0.80	< 0.05	-	-
Tb	ppm	1.17	0.79	0.74	0.66	0.85	0.61	0.74	0.14	-	-
Te	ppm	0.09	0.12	0.03	0.03	0.20	< 0.02	0.03	< 0.02	-	-
Th	ppm	49.00	18.60	20.90	39.90	19.10	49.90	21.60	5.60	15.00	19.00

Tl	ppm	0.18	0.05	< 0.02	0.10	0.13	0.11	0.06	0.17	-	-
Tm	ppm	0.42	0.28	0.30	0.31	0.30	0.32	0.29	0.06	-	-
U	ppm	10.10	5.00	4.40	8.10	3.70	8.20	5.00	0.60	1.00	8.00
V	ppm	30.00	213.00	190.00	55.00	215.00	74.00	139.00	70	160.00	179.00
W	ppm	> 100	> 100	57.90	181.40	87.50	> 100	76.70	> 100	-	-
Y	ppm	30.80	20.30	20.20	19.00	22.00	18.50	20.40	4.79	24.00	25.00
Yb	ppm	2.61	1.83	1.82	2.00	1.82	2.16	1.82	0.40	-	-
Zn	ppm	37.40	64.40	32.40	390.50	66.30	29.10	48.20	26.90	55.00	57.00
Zr	ppm	317.50	215.90	193.20	251.10	180.50	191.20	190.20	3.00	208.00	202.00

Table 8.2: Geochemical Analyses Results of Altered Samples

Type of Alteration		Na-Ca alteration	Sericitic alteration								
		ST 10	ST 11	ST 12	ST 12a	ST 12b	ST 12c	ST 12d	ST 14	ST 15	ST 16
SiO₂	%	-	-	-	70.21	78.44	66.48	74.76	-	53.02	-
Al₂O₃	%	-	-	-	10.53	12.06	12.49	13.56	-	15.75	-
Fe₂O₃	%	-	-	-	3.25	2.17	3.38	2.88	-	5.71	-
MnO	%	-	-	-	0.05	0.01	0.04	0.01	-	0.20	-
MgO	%	-	-	-	0.84	0.29	0.43	0.43	-	6.00	-
CaO	%	-	-	-	3.13	0.00	4.99	0.01	-	5.34	-
Na₂O	%	-	-	-	0.01	0.00	0.00	0.00	-	4.63	-
K₂O	%	-	-	-	3.85	2.29	1.50	1.73	-	2.04	-
TiO₂	%	-	-	-	0.20	0.24	0.27	0.29	-	0.84	-
P₂O₅	%	-	-	-	0.05	0.03	0.08	0.02	-	0.42	-
SO₃	%	-	-	-	0.52	0.45	1.54	1.14	-	0.39	-
H₂O	%	-	-	-	6.22	4.19	8.35	5.73	-	4.80	-
Total	%	-	-	-	98.86	100.17	99.55	5.73	-	99.14	-
Ag	ppb	-	-	-	1406.00	1325.00	372.00	969.00	-	325.00	-
As	ppm	-	-	-	5.80	5.30	5.50	6.30	-	22.40	-
Au	ppb	-	-	-	118.10	50.60	41.10	35.30	-	32.20	-
B	ppm	-	-	-	2.00	2.00	< 1.00	< 1.00	-	2.00	-
Ba	ppm	292.00	536.00	453.00	217.40	700.00	975.00	1250.0	548.00	704.00	20.00
Be	ppm	2.00	3.00	2.00	0.80	0.30	1.10	0.40	4.00	0.90	3.00
Bi	ppm	-	-	-	0.76	3.48	0.57	2.38	-	0.87	-
Cd	ppm	-	-	-	3.48	0.12	3.97	6.34	-	7.07	-
Ce	ppm	34.70	74.00	53.40	84.40	94.00	81.70	86.80	71.20	100.10	4.30
Co	ppm	23.30	26.20	26.20	37.20	26.20	23.50	19.60	29.20	40.80	-
Cr	ppm	-	-	-	0.00	5.00	4.00	3.00	-	45.00	-
Cs	ppm	0.70	1.40	2.00	0.55	0.76	0.56	0.58	10.90	0.51	0.70
Cu	ppm	-	-	-	842.64	85.44	207.87	505.17	-	109.75	-
Dy	ppm	0.54	1.76	1.54	2.53	0.83	3.52	2.50	3.11	4.63	0.06

Er	ppm	0.43	0.96	0.88	1.33	0.26	1.76	1.42	1.60	2.28	< 0.03
Eu	ppm	0.17	0.74	0.59	0.86	0.57	1.72	0.76	1.51	1.83	< 0.02
Ga	ppm	10.00	9.30	10.70	9.00	0.60	14.40	13.00	12.50	16.50	1.70
Gd	ppm	0.67	3.02	2.26	3.56	1.53	5.48	3.19	4.33	6.47	0.08
Ge	ppm	-	-	-	< 0.10	< 0.10	< 0.10	< 0.10	-	0.60	-
Hf	ppm	3.40	7.60	5.30	5.20	< 0.02	4.20	8.20	3.80	4.80	0.10
Hg	ppb	-	-	-	-	< 5.00	10.00	12.00	-	< 5.00	-
Ho	ppm	0.12	0.33	0.29	0.53	0.11	0.61	0.42	0.55	0.85	< 0.02
In	ppm	-	-	-	0.28	0.04	0.10	0.38	-	0.58	-
La	ppm	25.70	39.80	28.20	44.80	25.30	42.00	39.20	37.40	51.90	3.00
Li	ppm	-	-	-	0.40	0.30	0.80	0.70	-	13.80	-
Lu	ppm	0.09	0.17	0.16	0.22	< 0.02	0.21	0.29	0.21	0.30	< 0.01
Mo	ppm	-	-	-	76.19	64.69	39.42	29.42	-	17.40	-
Nb	ppm	9.80	10.90	15.80	15.40	0.07	9.90	25.60	7.00	9.30	0.80
Nd	ppm	7.80	31.90	20.20	29.80	19.08	38.30	32.30	31.00	45.20	1.00
Ni	ppm	-	-	-	2.30	1.40	4.50	3.90	-	24.60	-
Pb	ppm	-	-	-	166.29	288.02	339.02	35.16	-	218.39	-
Pd	ppb	-	-	-	< 10.0	< 10.0	< 10.0	< 10.0	-	< 10.0	-
Pr	ppm	2.96	2.96	5.92	8.76	6.70	10.10	9.45	8.10	11.72	0.38
Pt	ppb	-	-	-	< 2.00	3.00	< 2.00	3.00	-	< 2.00	-
Rb	ppm	31.50	79.10	100.50	96.60	101.00	87.30	98.60	132.80	98.20	2.50
Re	ppb	-	-	-	54.00	50.00	24.00	20.00	-	31.00	-
Sb	ppm	-	-	-	0.94	1.49	0.46	0.21	-	0.36	-
Sc	ppm	-	-	-	0.70	0.20	0.50	0.50	-	10.10	-
Se	ppm	-	-	-	0.30	1.90	1.60	2.30	-	0.40	-
Sm	ppm	1.05	4.20	3.10	4.55	3.00	6.82	4.65	5.30	7.85	0.12
Sn	ppm	11.00	11.00	10.00	1.10	0.80	1.30	2.00	15.00	10.30	< 0.10
Sr	ppm	32.20	44.50	75.70	80.50	12.50	808.90	53.50	78.80	835.90	25.60
Ta	ppm	0.80	1.10	1.20	1.20	< 0.05	0.70	1.50	0.60	0.60	1.10
Tb	ppm	0.10	0.38	0.28	0.47	0.18	0.68	0.44	0.59	0.85	< 0.01
Te	ppm	-	-	-	0.49	0.24	0.44	0.34	-	0.04	-

Th	ppm	18.00	17.10	29.60	28.00	30.00	13.60	50.60	12.20	15.20	2.40
Tl	ppm	-	-	-	0.17	0.20	0.15	0.32	-	0.05	-
Tm	ppm	0.08	0.15	0.14	0.22	0.05	0.24	0.23	0.22	0.32	< 0.01
U	ppm	4.20	3.60	6.00	7.10	2.40	2.90	7.90	2.70	2.90	< 0.10
V	ppm	71.00	52.00	37.00	35.00	29.00	160.00	38.00	127.00	184.00	< 8.00
W	ppm	372.80	198.30	225.60	210.80	> 100	245.20	> 100	157.90	> 100	> 100
Y	ppm	3.50	10.10	8.20	15.00	15.00	18.70	12.10	16.90	24.00	0.30
Yb	ppm	0.54	1.05	0.98	1.37	0.24	1.45	1.69	1.35	1.97	< 0.05
Zn	ppm	-	-	-	479.20	20.80	410.30	795.40	-	659.20	-
Zr	ppm	118.10	267.10	187.10	178.90	230.00	154.40	276.20	138.80	176.20	3.90

Table 8.2 (cont.): Geochemical Analyses Results of Altered Samples

Type of Alteration		Sericitic alteration	Sericitic alteration	Sericitic alteration	Advanced Argillic Alteration	Advanced Argillic Alteration	Advanced Argillic Alteration	Na-Ca alteration	Sericitic alteration	Na-Ca alteration	Sericitic alteration	Sericitic alteration	Sericitic alteration
		ST 17	ST 18	ST 19	ST 22	ST 23	ST 24	ST 26	ST 27	ST 29	ST 31	ST 33	ST 33b
Sample Element													
SiO ₂	%	53.93	62.19	66.34	80.50	74.25	69.41	53.05	74.31	55.13	52.22	-	43.68
Al ₂ O ₃	%	17.21	17.28	14.39	11.85	16.31	17.10	17.22	15.81	15.12	19.80	-	17.26
Fe ₂ O ₃	%	6.65	6.04	1.98	1.37	1.23	1.66	6.38	0.53	6.98	9.42	-	7.82
MnO	%	0.13	0.01	0.03	0.00	0.02	0.01	0.08	0.01	0.18	0.00	-	0.23
MgO	%	4.16	0.86	2.16	0.00	0.06	0.08	4.46	0.57	4.83	0.00	-	5.64
CaO	%	7.23	0.02	3.10	0.04	0.09	0.22	4.92	0.01	5.42	0.15	-	4.79
Na ₂ O	%	3.26	0.11	0.00	0.00	0.41	1.61	2.11	0.00	3.18	0.00	-	0.06
K ₂ O	%	2.85	3.48	2.66	0.04	0.99	4.96	4.19	3.14	3.16	0.09	-	4.26
TiO ₂	%	0.86	0.97	0.30	0.41	0.34	0.41	0.86	0.34	0.81	1.06	-	0.95
P ₂ O ₅	%	0.35	0.20	0.08	0.19	0.11	0.13	0.42	0.03	0.41	0.62	-	0.43
SO ₃	%	0.00	1.49	0.40	0.10	0.01	0.02	0.00	0.05	0.54	3.37	-	1.76
H ₂ O	%	2.07	8.05	8.41	5.24	6.18	4.23	5.75	4.55	3.54	14.38	-	12.78
Total	%	98.70	100.70	99.85	99.74	100.00	99.84	99.44	99.35	98.99	101.11	-	98.99
Ag	ppb	79.00	53.00	127.00	43.00	5.00	13.00	74.00	34.00	395.00	26.00	10.00	74.00
As	ppm	9.90	8.10	14.40	9.80	0.70	7.80	2.60	8.50	18.90	41.10	1.30	39.70
Au	ppb	< 0.20	< 0.20	4.40	3.90	< 0.20	< 0.20	2.70	1.80	63.20	7.80	< 0.20	1.70
B	ppm	4.00	3.00	2.00	< 1.00	< 1.00	2.00	2.00	< 1.00	< 1.00	< 1.00	< 1.00	< 1.00
Ba	ppm	1412.0	1069.00	1062.0	2620.0	514.00	887.00	1618.0	2761.0	1559.0	881.00	2137.0	2591.0
Be	ppm	0.70	0.40	0.90	0.20	0.10	0.50	0.90	0.10	0.80	0.10	< 0.10	1.60
Bi	ppm	0.21	0.91	0.42	< 0.02	0.10	0.27	< 0.02	0.22	0.14	4.28	0.11	0.78
Cd	ppm	0.07	0.67	0.58	< 0.01	< 0.01	0.02	0.03	< 0.01	3.66	0.02	0.03	1.42
Ce	ppm	91.50	85.80	138.40	164.60	30.60	135.40	103.50	34.90	100.90	120.20	96.70	38.10
Co	ppm	46.30	33.40	11.00	20.20	6.20	18.40	33.20	18.40	31.80	37.80	8.50	28.20
Cr	ppm	23.00	21.00	8.00	0.70	2.00	11.00	12.00	5.00	51.00	1.60	< 0.50	13.00
Cs	ppm	0.26	0.83	1.59	< 0.02	0.20	3.50	3.20	0.49	1.73	0.02	2.40	2.20
Cu	ppm	71.32	135.97	9.97	7.26	3.14	6.54	71.85	23.10	216.28	108.73	3.71	82.95

Dy	ppm	3.74	2.69	3.96	9.80	0.68	3.44	3.88	2.80	4.82	2.17	3.76	0.93
Er	ppm	1.89	1.46	2.17	5.34	0.39	1.73	1.89	1.99	2.16	0.95	1.92	0.38
Eu	ppm	1.66	5.87	1.37	3.06	0.10	1.51	1.61	0.31	1.98	2.19	1.83	0.61
Ga	ppm	18.00	21.20	13.00	12.10	1.50	15.80	16.50	0.60	9.50	3.30	17.00	2.90
Gd	ppm	5.55	4.10	5.52	12.39	0.77	5.72	5.30	2.01	6.81	4.99	5.57	1.87
Ge	ppm	0.30	0.10	< 0.10	< 0.10	< 0.10	< 0.10	0.20	< 0.10	0.10	< 0.10	< 0.10	< 0.10
Hf	ppm	5.10	5.50	8.50	6.50	1.40	9.30	5.20	9.90	4.40	5.50	4.40	1.70
Hg	ppb	< 5.00	59.00	< 5.00	-	17.00	58.00	< 5.00	< 5.00	< 5.00	18.00	18.00	10.00
Ho	ppm	0.68	0.53	0.74	1.93	0.15	0.60	0.68	0.61	0.83	0.33	0.71	0.13
In	ppm	< 0.02	0.06	< 0.02	< 0.02	< 0.02	0.02	< 0.02	< 0.02	0.28	< 0.02	< 0.02	0.13
La	ppm	46.80	45.20	80.50	83.60	14.20	73.70	51.90	18.40	51.00	60.80	50.90	19.80
Li	ppm	4.80	1.10	0.90	0.30	2.70	3.40	9.50	0.30	14.20	10.50	0.10	13.50
Lu	ppm	0.28	0.22	0.35	0.75	0.06	0.28	0.28	0.36	0.28	0.18	0.26	0.06
Mo	ppm	1.52	1.88	3.55	2.26	0.22	0.83	0.23	2.23	16.61	2.27	0.12	0.99
Nb	ppm	10.80	13.40	21.40	16.80	3.60	24.90	10.90	25.10	9.20	12.10	9.20	3.40
Nd	ppm	39.60	36.80	48.80	73.00	10.10	51.10	43.10	11.30	47.00	55.70	43.30	16.90
Ni	ppm	19.90	21.30	3.00	1.20	1.00	0.90	13.60	0.90	25.30	22.40	0.40	18.40
Pb	ppm	21.21	26.90	133.67	12.73	8.18	22.18	14.43	113.24	189.92	< 10.0	5.79	81.85
Pd	ppb	< 10.0	< 10.0	< 10.0	< 10.0	< 10.0	< 10.0	< 10.0	< 10.0	< 10.0	10.00	10.00	< 10.0
Pr	ppm	10.55	9.79	14.60	18.98	3.23	14.76	11.65	3.45	12.08	14.22	11.23	4.41
Pt	ppb	< 2.00	3.00	< 2.00	< 2.00	< 2.00	< 2.00	< 2.00	< 2.00	< 2.00	3.00	< 2.00	7.00
Rb	ppm	88.30	160.30	107.50	2.90	2.40	162.60	134.70	115.70	106.70	1.90	118.80	53.20
Re	ppb	1.00	2.00	1.00	3.00	< 1.00	< 1.00	< 1.00	1.00	32.00	2.00	8.00	15.00
Sb	ppm	0.98	0.39	0.03	0.71	0.16	0.80	0.13	0.02	0.31	0.46	0.09	0.28
Sc	ppm	4.00	1.30	0.80	0.80	1.10	1.70	7.50	0.50	6.60	1.00	0.30	9.20
Se	ppm	< 0.10	2.20	0.70	0.20	< 0.10	< 0.10	< 0.10	0.30	< 0.10	10.30	< 0.10	2.10
Sm	ppm	6.71	5.87	7.24	15.56	1.11	8.27	7.08	1.91	8.22	8.86	7.01	2.59
Sn	ppm	2.00	0.01	0.30	0.40	0.80	2.10	0.70	0.20	5.50	4.00	< 0.10	1.30
Sr	ppm	1175.40	32.90	66.00	733.70	67.10	633.20	707.30	78.50	830.90	1765.9	308.70	198.00
Ta	ppm	0.70	0.70	1.40	1.30	0.60	1.70	0.60	1.60	0.60	0.70	0.50	0.20
Tb	ppm	0.72	0.51	0.37	1.70	0.11	0.69	0.71	0.40	0.88	0.51	0.71	0.20

Te	ppm	< 0.02	0.78	0.47	0.04	< 0.02	0.09	< 0.02	0.13	0.03	3.46	0.08	1.57
Th	ppm	16.90	17.70	45.70	34.50	7.50	52.70	20.60	48.30	14.70	21.50	15.70	6.00
Tl	ppm	< 0.02	0.34	0.20	< 0.02	0.05	0.24	0.04	0.17	0.06	0.06	< 0.02	0.09
Tm	ppm	0.29	0.21	0.32	0.77	0.06	0.25	0.27	0.33	0.29	0.15	0.26	0.05
U	ppm	3.80	4.40	10.30	7.20	5.50	9.60	4.20	9.90	2.90	3.50	3.20	1.10
V	ppm	187.00	227.00	29.00	61.00	< 8.00	31.00	164.00	30.00	164.00	154.00	196.00	75.00
W	ppm	> 100	47.50	> 100	> 100	38.70	51.40	40.60	67.10	162.50	55.00	15.50	6.80
Y	ppm	19.50	13.50	23.20	52.30	4.80	15.80	18.60	17.70	23.80	7.80	17.90	4.00
Yb	ppm	1.73	1.32	2.17	4.84	0.40	1.75	1.74	2.28	1.83	1.11	1.72	0.36
Zn	ppm	65.00	141.60	24.30	3.20	9.60	4.90	57.70	3.10	815.90	2.80	4.60	171.00
Zr	ppm	188.70	204.20	287.20	230.40	47.90	307.00	188.50	332.00	164.30	207.50	158.10	62.50

8.1.2: Harker Variation Plots

From the SiO_2 versus Al_2O_3 plot (Figure 8.4a) it can be seen that the samples from the Scoutaros Unit (represented by blue circles) plot into the upper left corner, in a coarse convex line. This is consistent with the geochemical classification of these rocks as trachyandesites and basaltic trachyandesites (Hecht, 1970, 1972a, 1972b, 1973, 1974a, 1974b, 1975; Pe-Piper, 1978, 1980a, 1980b; Pe-Piper *et al.*, 1993; this study). Indeed, in most series of igneous rocks, alumina is contained principally in feldspars, and in the corresponding plot the alumina curve rises sharply from the left – where most basic rocks are plotted – as the feldspars are rich in anorthite³⁹ and then falls, as the more acidic the rocks become the more orthoclase crystallises⁴⁰, and also the presence of quartz reduces the total feldspar percentage of the rock. Indeed, the samples from the Sikaminea Unit (represented by purple rectangles) plot into the bottom right corner, which is consistent with their geochemical classification – they are classified as trachydacitic to dacitic lavas, i.e. intermediate to acidic extrusives (Hecht, 1970, 1972a, 1972b, 1973, 1974a, 1974b, 1975; Pe-Piper, 1978, 1980a, 1980b; Pe-Piper *et al.*, 1993; this study). Finally, the samples from the igneous intrusion South of Stypsi, which are represented by green triangles, are plotted to the right, and slightly lower, of those of the Sikaminea Unit, as they are even more acidic.

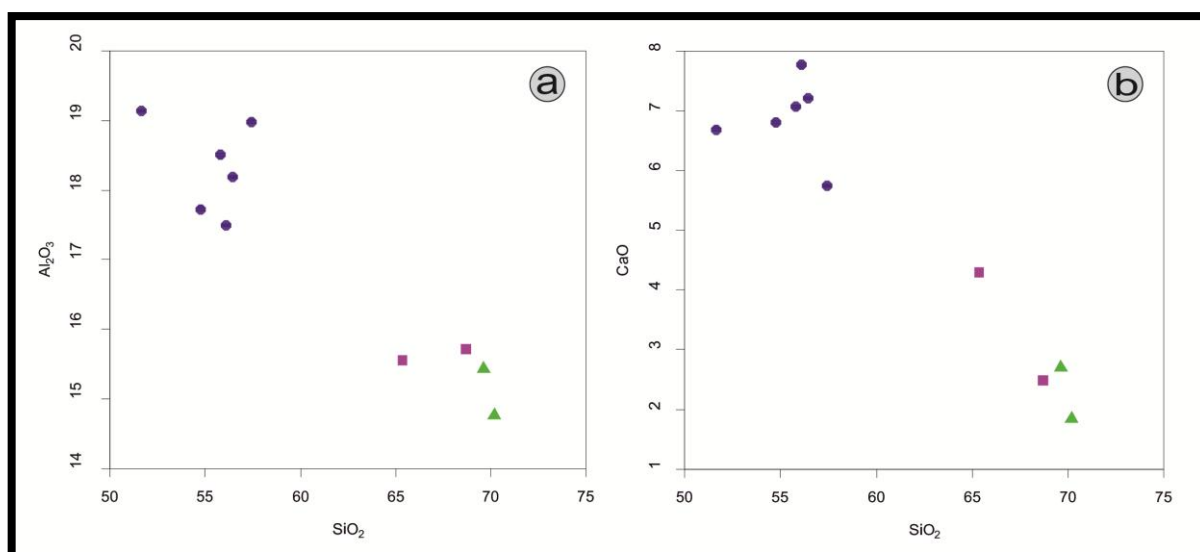


Figure 8.4: Harker binary plots of SiO_2 versus main elements. (a) Binary plot of SiO_2 versus Al_2O_3 (after Harker, 1909). (b) Binary plot of SiO_2 versus CaO (after Harker, 1909). In both plots there is a distinct negative trend, which is expected in this case, where all the igneous rocks occur, following the fractional crystallisation of a common magma source.

In the SiO_2 versus CaO plot (Figure 8.4b) the trend is again negative with increasing SiO_2 content. This is consistent with the fractional crystallisation trend, as with increasing SiO_2 content, the plagioclase becomes richer in Na rather than in Ca. In the SiO_2 versus FeO plot (Figure 8.5a) the trend is negative with increasing SiO_2 content, albeit with a more gentle gradient, which is consistent with the gradual decrease in the crystallisation of Fe-bearing

³⁹ Anorthite, with the chemical formula $\text{CaAl}_2\text{Si}_2\text{O}_8$, has a median percentage of alumina of about 35 % , which corresponds to around 19 % Al (Goldsmith, 1980).

⁴⁰ Orthoclase, with the chemical formula KAlSi_3O_8 contains about 18.5 % Al (Harker, 1909).

minerals (pyroxenes, amphiboles and biotite). On the SiO_2 versus K_2O plot (Figure 8.5b) the trend is positive, which is consistent with the gradual crystallisation of orthoclase and muscovite with increasing SiO_2 content.

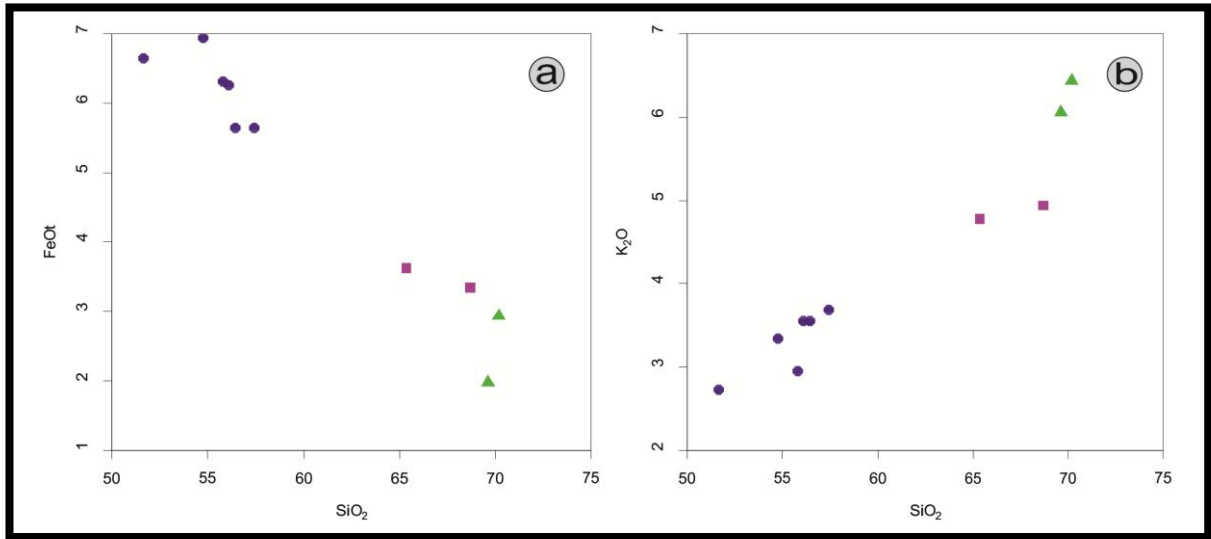


Figure 8.5: Harker binary plots of SiO_2 versus main elements. (a) Binary plot of SiO_2 versus FeOt. In this plot, the trend is negative, an expected result in this case, as mentioned above (after Harker, 1909). (b) Binary plot of SiO_2 versus K_2O , where the distinct positive trend corroborates the aforementioned conclusions for a common magmatic source (after Harker, 1909).

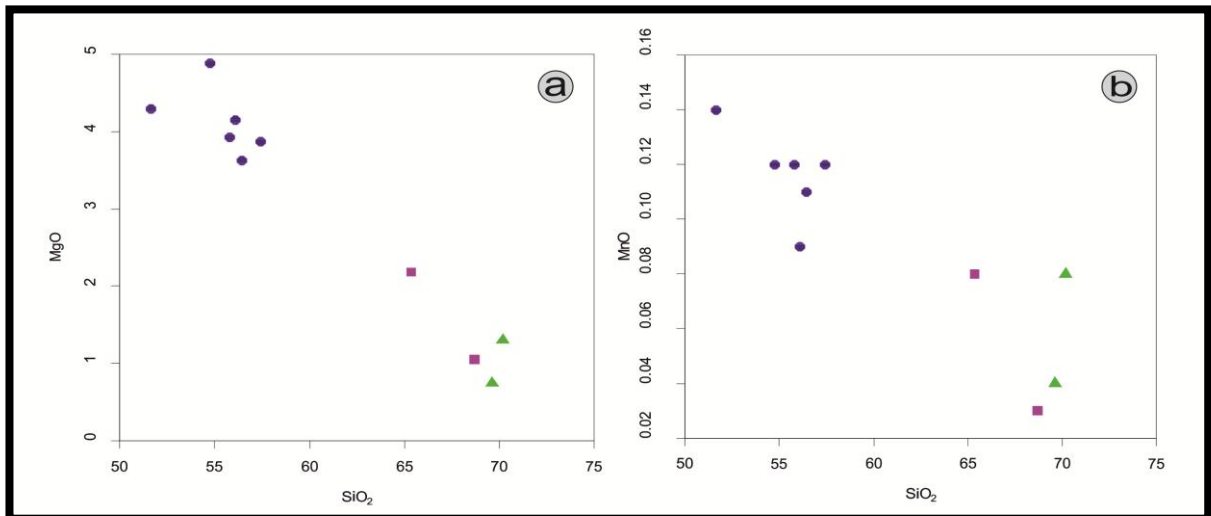


Figure 8.6: Harker binary plots of SiO_2 versus main elements. (a) Binary plot of SiO_2 versus MgO (after Harker, 1909). (b) Binary plot of SiO_2 versus MnO (after Harker, 1909). In both plots the trend is negative, which is explained by the fractional crystallisation of a common magma source.

In the SiO_2 versus MgO plot (Figure 8.6a), the curve starts from the top left corner, with the more basic rocks of the Skoutaros Unit declining sharply to the intermediate rocks of the Sikaminea Unit and the samples from the microgranite porphyry. The curve here is of a concave shape, corresponding to the rapid initial decrease of magnesian minerals with increasing acidity followed by a slower decrease. In the SiO_2 versus MnO plot (Figure 8.6b), the trend is negative, roughly mimicking the shape of the trend of the SiO_2 versus MgO plot. This is explained by the gradual decrease of manganese bearing minerals with increasing fractional crystallisation and therefore increasing acidity.

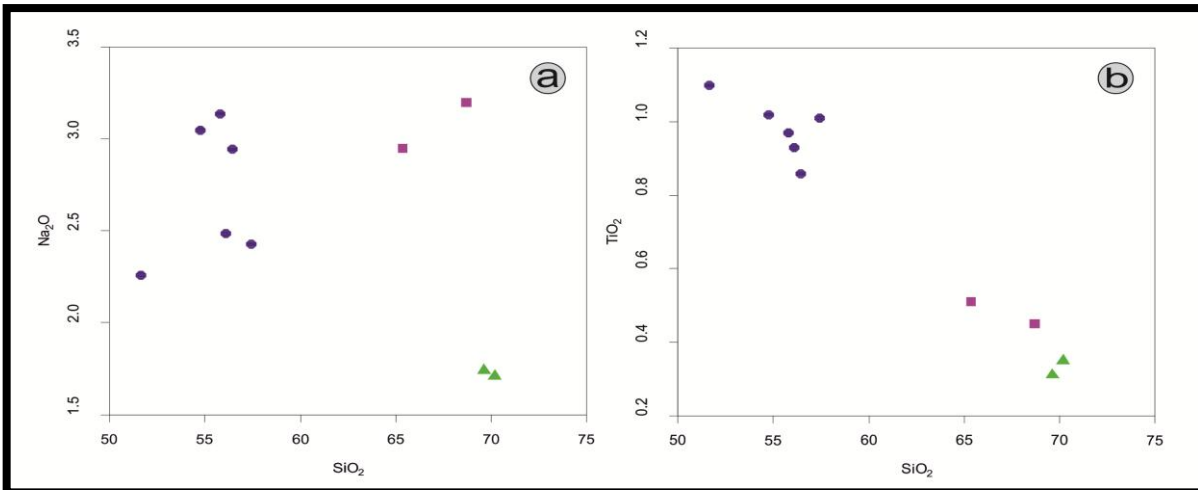


Figure 8.7: Harker binary plots of SiO₂ versus main elements. (a) Binary plot of SiO₂ versus Na₂O (after Harker, 1909). The trend is distinctly positive as in most cases of fractional crystallisation (after Harker, 1909). (b) Binary plot of SiO₂ versus TiO₂, where the trend is, expectedly, distinctly negative (after Harker, 1909).

In the SiO₂ versus Na₂O plot (Figure 8.7a) there is a clear positive trend for the samples of the Skoutaros and the Sikaminea Units. Indeed, sodium content increases, up to a point, with fractional crystallisation as more Na-rich plagioclase crystallises. The sharp drop noticed for the microgranite porphyry samples is attributed to the crystallisation of orthoclase, instead of plagioclase and the rising content of quartz. In the SiO₂ versus TiO₂ plot (Figure 8.7b), there is a clear negative trend as TiO₂ is hosted principally in amphiboles and pyroxenes, which are present in decreasing amounts with increasing SiO₂ contents. In the SiO₂ versus Sr plot (Figure 8.8a) and SiO₂ versus V plot (Figure 8.8b) the trend is clearly negative. This is consistent with the observation that Sr contents are higher in intermediate rocks in comparison to acidic rocks, since Sr substitutes for Ca and K in plagioclase and K-feldspar. Vanadium is moderately incompatible and may be preferentially enriched in pyroxenes and as a trace element in amphiboles. Vanadium also substitutes for Fe in magnetite and in silicates during the initial stages of magmatic evolution. Therefore, it is expected that more felsic rocks, which are more differentiated, will have lower V contents. This is clearly demonstrated in the relevant Harker plot. In the SiO₂ versus Ba plot (Figure 8.9a) and SiO₂ versus Y plot (Figure 8.9b) there is no clear trend. Rather a clustering of the Skoutaros Unit samples (blue circles) to the left side and of the Sikaminea Unit samples and microgranite porphyry samples to the right side of the diagramme is observed. Barium is concentrated preferentially in late stage magmatic products, Curiously, there is an almost stable barium content with increasing SiO₂ in this case. Yttrium, a Rare Earth Element (REE) is found in mediocre to low concentrations in andesites and more silicic rocks. As such rocks can follow many crystallisation paths, there seldom is a clear trend in SiO₂ versus Y plots (Randive *et al.*, 2014). In the SiO₂ versus Rb plot (Figure 8.10a) and the SiO₂ versus Zr plot (Figure 8.10b) the trend is positive, albeit not so well defined. In general, Rb and Zr are non-competitive elements and their concentrations are expected to rise along with increasing SiO₂ content.

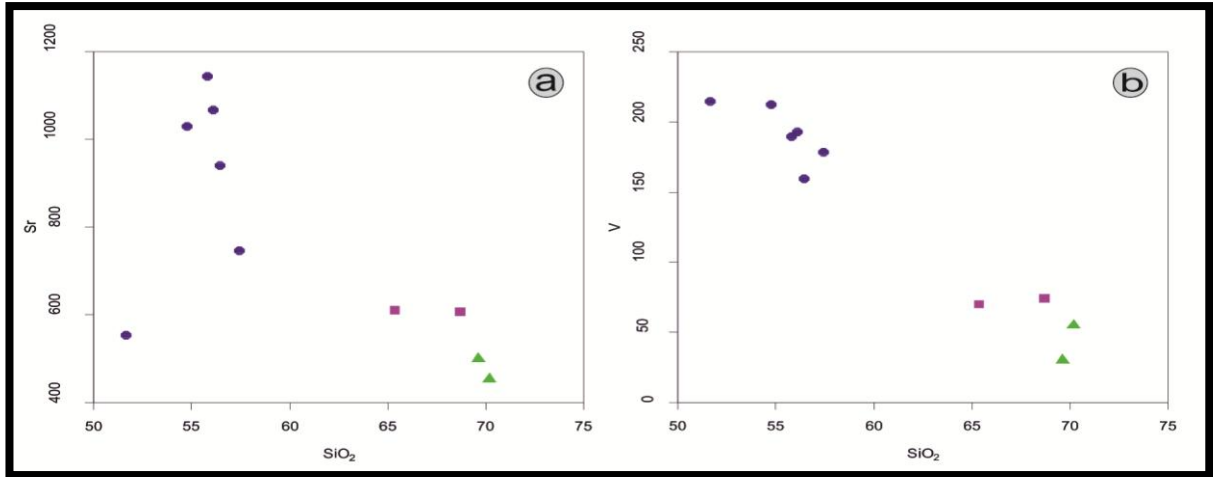


Figure 8.8: Harker binary plots of SiO₂ versus trace elements. (a) Binary plot of SiO₂ versus Sr. The trend is positive as in most cases of fractional crystallisation (after Harker, 1909). (b) Binary plot of SiO₂ versus V. The trend is distinctly positive, as V decreases with increasing SiO₂ content (after Harker, 1909).

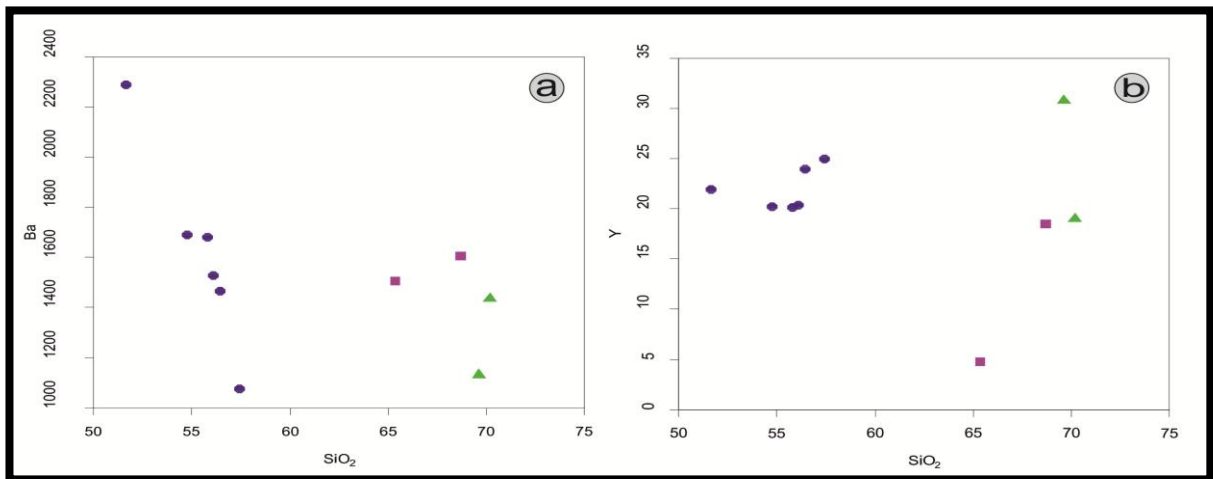


Figure 8.9: Harker binary plots of SiO₂ versus trace elements. (a) Binary plot of SiO₂ versus Ba (after Harker, 1909). (b) Binary plot of SiO₂ versus Y (after Harker, 1909). In both plots there is a distinct clustering of the samples from the Skoutaros Unit (blue circles) on one side and from the Sikaminea Unit (purple rectangles) and microgranite porphyry (green triangles) on the other side.

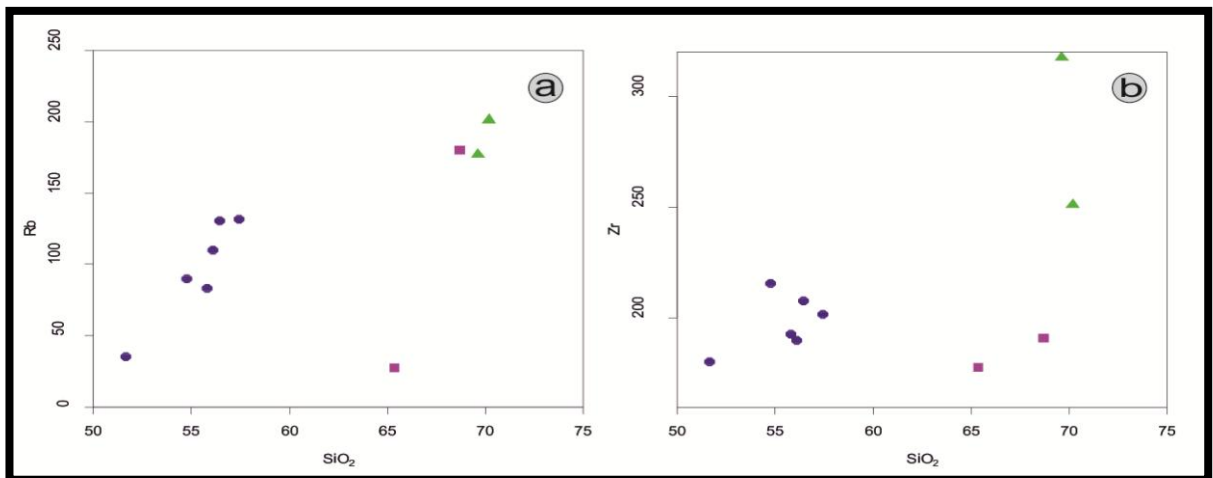
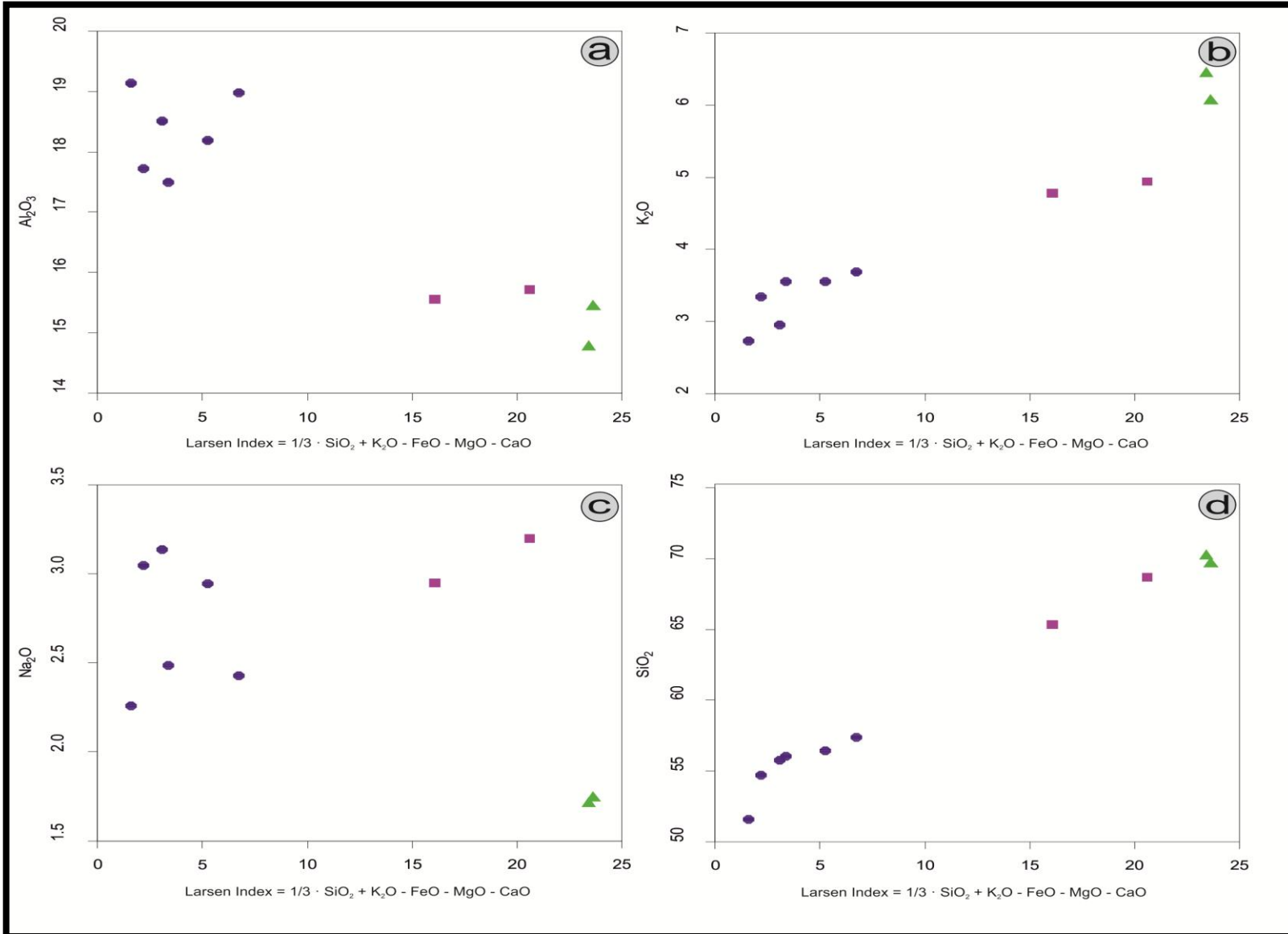


Figure 8.10: Harker binary plots of SiO₂ versus trace elements. (a) Binary plot of SiO₂ versus Rb, where a clear positive trend can be observed (Harker, 1909). (b) Binary plot of SiO₂ versus Zr, where there is a loosely defined positive trend (after Harker, 1909).

8.1.3: Larsen Variation Plots

The Larsen Variation Plots (Larsen, 1938) take advantage of the regular variations of the major oxides with increasing SiO_2 content. Instead of the Harker variation plots, in which only one element at a time is plotted versus SiO_2 , the plotting of major elements against a sum of the major oxides eliminates by and large, any analytical errors. This sum is called the **Larsen Index** and corresponds to the aggregation $\left[\frac{1}{3} \cdot (\text{SiO}_2) + \text{K}_2\text{O} - \text{FeO} - \text{MgO} - \text{CaO} \right]$. It will be observed that in the following series of Larsen variation plots (Figures 8.11a, 8.11b, 8.11c, 8.11d and 8.12a, 8.12b, 8.12c, 8.12d) the trends mirror closely those of the corresponding Harker plots but are better defined. So, it is evident that they corroborate the results of the previous plots.

Figure 8.11 (following page): Larsen binary plots of Larsen Index versus main elements. (a) Binary plot of L.I. versus Al_2O_3 . The trend is negative with increasing L.I. (after Larsen, 1938). (b) Binary plot of L.I. versus K_2O . The trend is positive with increasing L.I. (after Larsen, 1938). (c) Binary plot of L.I. versus Na_2O . There is a vague positive trend for the samples of the Skoutaros and the Sikaminea Units (after Larsen, 1938). (d) Binary plot of L.I. versus SiO_2 . The trend is clear and distinctly positive (after Larsen, 1938).



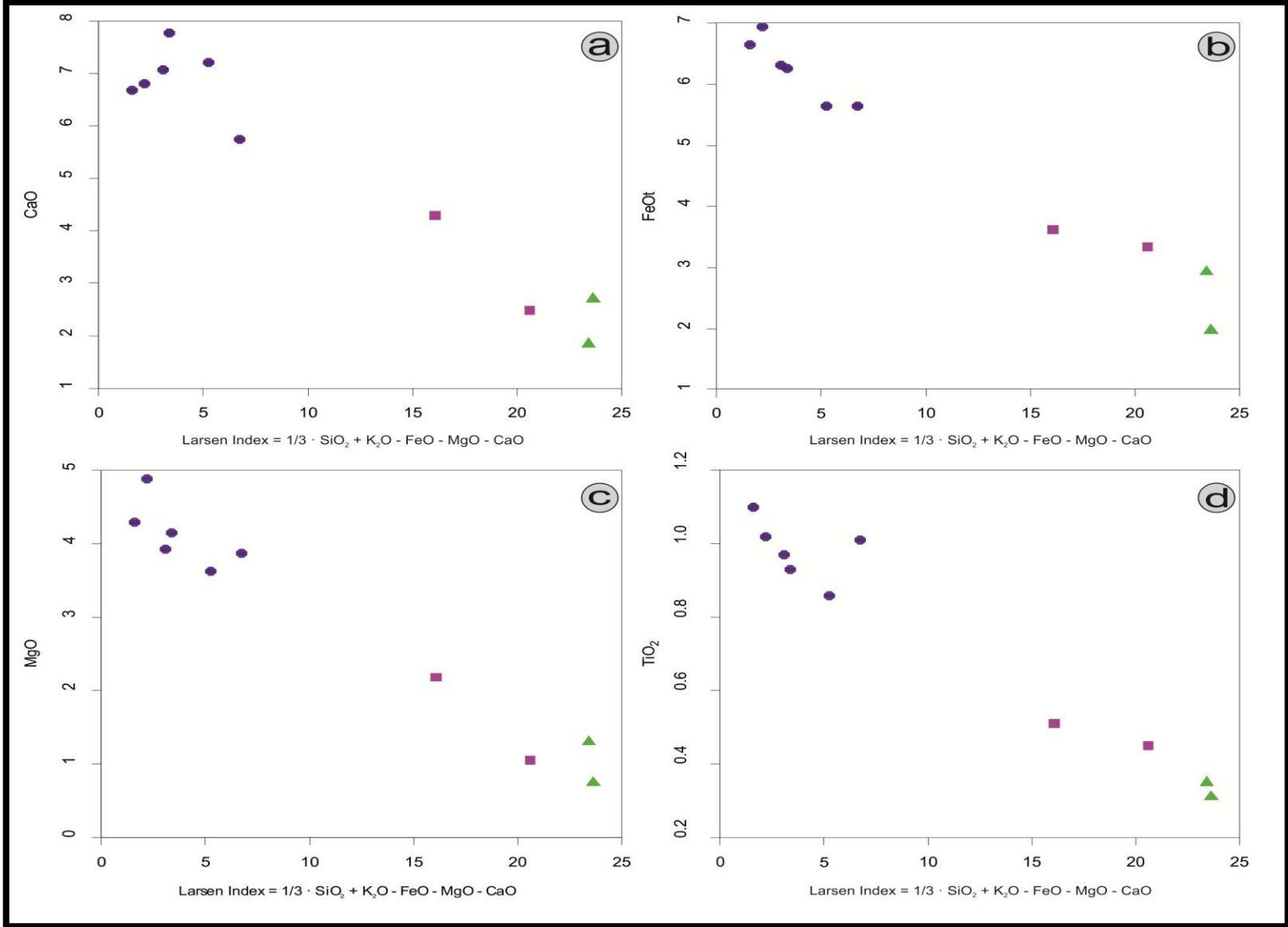


Figure 8.12 (previous page): Larsen binary plots of Larsen Index versus main elements. (a) Binary plot of L.I. versus CaO. The trend is distinctly negative (after Larsen, 1938). (b) Binary plot of L.I. versus FeO. The trend is expectedly negative (after Larsen, 1938). (c) Binary plot of L.I. versus MgO. The trend is clearly negative with increasing L.I. (after Larsen, 1938). (d) Binary plot of L.I. versus TiO₂. The trend is again distinctly negative (after Larsen, 1938).

8.1.4: Magma Series and Magma Calc/Alkali Indices

In order to determine with certainty, the geochemical relationship between the three different «magmatic series», another parameter, the **magma series index** must be used (Rittmann, 1957). This index is calculated by the following formula:

$$\sigma = \frac{(\text{Na}_2\text{O} + \text{K}_2\text{O})^2}{(\text{SiO}_2 - 43)}$$

In the following table (Table 8.3) the magma series index for each one of the fresh samples is calculated. From this it is possible to calculate the median magma series index for each of three «sample populations», in the following way:

$$\overline{\sigma_{\text{Sk.U.}}} = \frac{(3.50 + 2.90 + 2.89 + 2.80 + 3.16 + 2.58)}{6} = 2.97$$

$$\overline{\sigma_{\text{Sik.U.}}} = \frac{(2.57 + 2.67)}{2} = 2.62$$

$$\overline{\sigma_{\text{Mic.P.}}} = \frac{(2.29 + 2.44)}{2} = 2.36$$

It is obvious that, in accordance to relevant literature (e.g. Rittmann, 1957) the magma series index is indicative of the relevant geochemical character of each sample population. The Skoutaros Unit, which is of intermediate affinity is characterised by the highest index, while the more acidic samples are characterised by lower indices. However, the three indices differ by less than 1, thereby implying a common provenance. Taking into account spatial and temporal constraints, as well as previously published data (Pe-Piper & Piper, 1992, 1993), it can be concluded that both the Skoutaros and the Sikaminea Unit rocks and the microgranite porphyry are the result of the fractional crystallisation of the same magmatic source. This genetical and geochemical relationship is also graphically demonstrated (Figure 8.13).

Table 8.3: Rittmann Magma Series Index Calculation Table

Sample	Na ₂ O*	K ₂ O*	SiO ₂ *	(SiO ₂ - 43)	(Na ₂ O + K ₂ O) ²	σ
ST 20	1.74	6.06	69.62	26.62	60.84	2.29
ST 21	3.05	3.35	54.71	11.71	40.96	3.50
ST 25	3.14	2.95	55.77	12.77	37.09	2.90
ST 28	1.71	6.44	70.18	27.18	66.42	2.44
ST 32	2.26	2.73	51.61	8.61	24.90	2.89
ST 34	3.20	4.94	68.70	25.70	66.26	2.57
ST 35	2.49	3.56	56.06	13.06	36.60	2.80
Ar 100b	2.95	4.78	65.36	22.36	59.75	2.67
LS 1	2.95	3.56	56.42	13.42	42.38	3.16
LS 2	2.43	3.69	57.38	14.38	37.09	2.58

*The values for Na₂O, K₂O and SiO₂ are given in wt. %

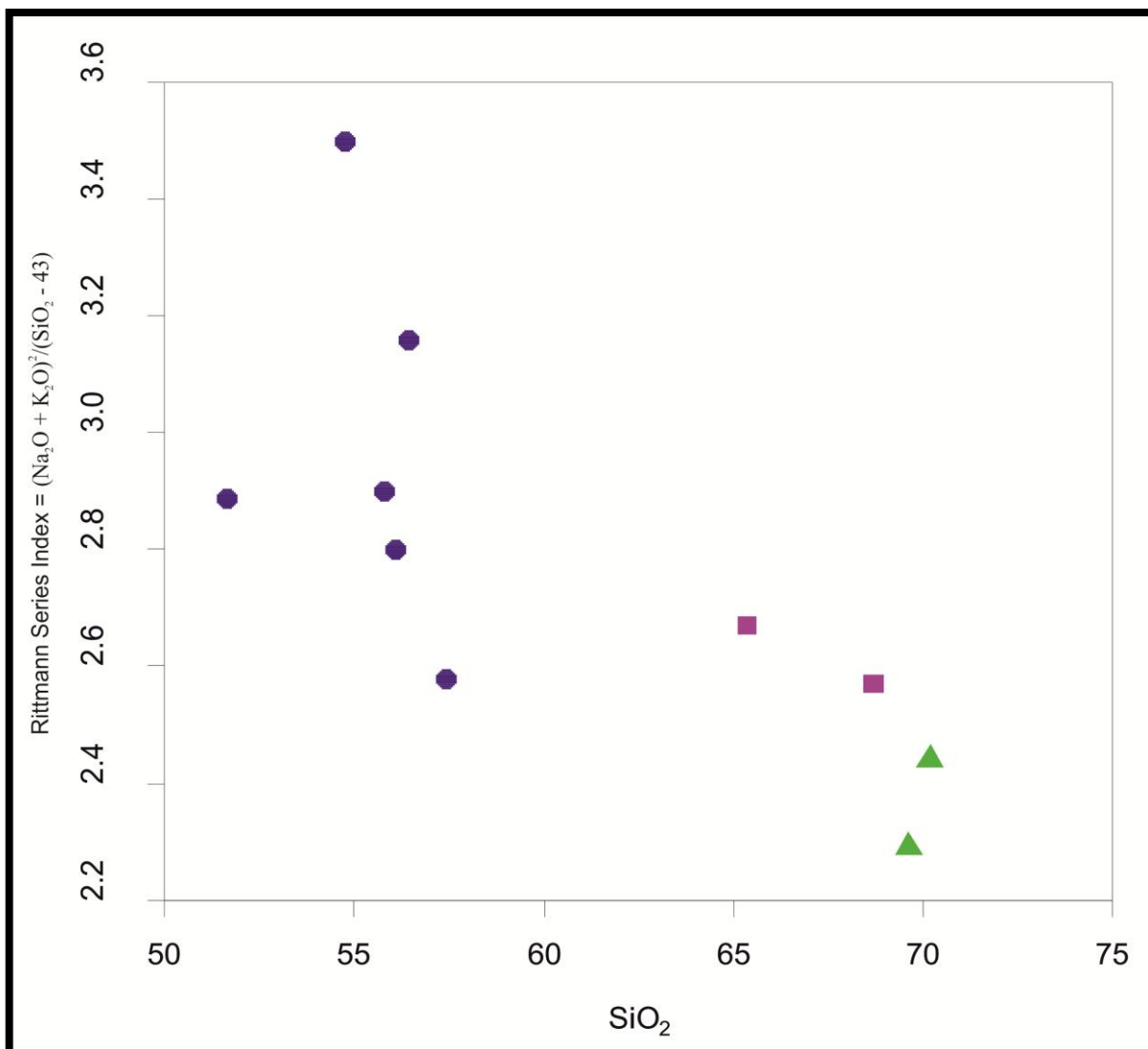


Figure 8.13: Binary plot of Rittmann Series Index versus SiO₂. The distinct clustering of samples reveals the existence of three different types of igneous rocks. In particular, the proximity of the Sikaminea Unit Samples (purple rectangles) and the microgranite porphyry samples (green triangles) indicates their similar geochemical affinities (after Rittmann, 1957).

Finally, regarding the geochemical character of the fresh samples discussed so far, and for reasons of verification of existing results, the calculation of the **calc/alkaline index** (Christiansen & Lipman, 1972) is deemed necessary. The calc/alkaline index is defined as the value of SiO₂ which corresponds to the quotient $\left[\frac{\text{CaO}}{(\text{Na}_2\text{O} + \text{Ca}_2\text{O})} \right]$ when it is equal to 1. This is calculated graphically (Figure 8.14b) and the data for plotting the corresponding diagram (Figure 8.14a) is provided below (Table 8.4).

Based on the least squares curves, for each of the sample populations, it is calculated that the calc/alkaline index is 58.29 for the Skoutaros Unit, 58.25 for the Sikaminea Unit and 66.33 for the microgranite porphyry. According to the theory of Christiansen & Lipman (1972), the samples from the Skoutaros and the Sikaminea Units are calc-alkaline and the samples from the microgranite porphyry are calcic. These findings support the hypothesis that all three types of rock are the result of successive fractional crystallisation of a single magmatic source.

Table 8.4: Calk/alkaline Index Calculation Table						
Sample	CaO*	Na ₂ O*	K ₂ O*	SiO ₂ *	Na ₂ O + K ₂ O	$\frac{\text{CaO}}{\text{Na}_2\text{O} + \text{K}_2\text{O}}$
ST 20	2.70	1.74	6.06	69.62	7.80	0.36
ST 21	6.81	3.05	3.35	54.71	6.40	1.06
ST 25	7.08	3.14	2.95	55.77	6.09	1.16
ST 28	1.84	1.71	6.44	70.18	8.15	0.23
ST 32	6.69	2.26	2.73	51.61	4.99	1.34
ST 34	2.49	3.20	4.94	68.70	8.14	0.31
ST 35	7.79	2.49	3.56	56.06	6.05	1.29
Ar 100b	4.29	2.95	4.78	65.36	7.73	0.55
LS 1	7.23	2.95	3.56	56.42	6.51	1.11
LS 2	5.76	2.43	3.69	57.38	6.12	0.94

*The values for Na₂O, K₂O, CaO and SiO₂ are given in wt. %

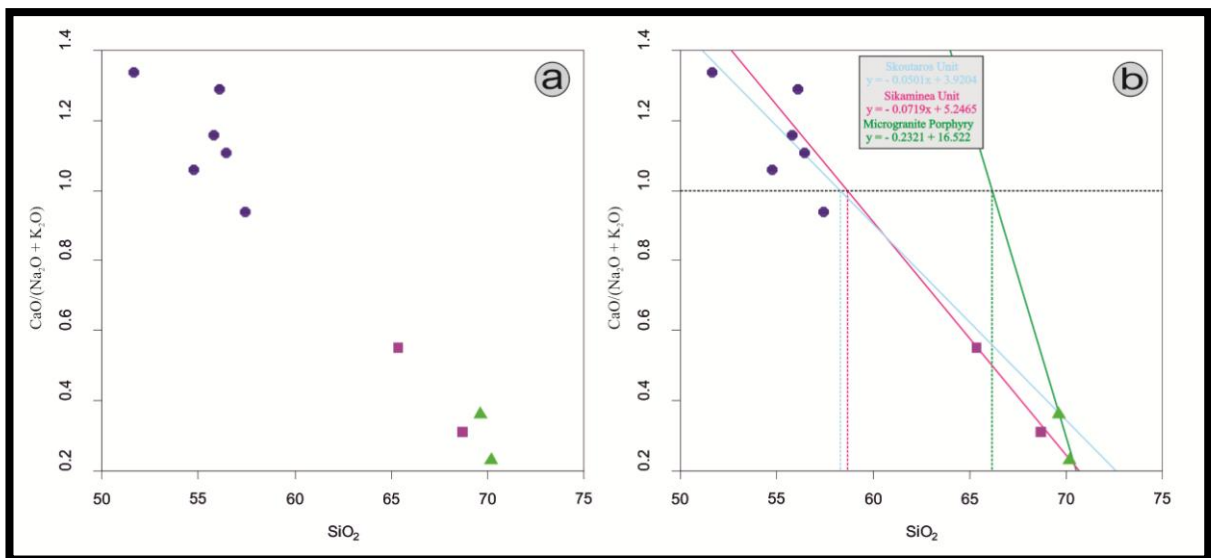


Figure 8.14: Binary plot of SiO₂ versus [CaO/(Na₂O + K₂O)]. (a) The plot, where the positions of the samples relative to the axes and to each other are presented. (b) The same plot with the least squares lines drawn for the three sample populations and the projection on the x axis for each one, corresponding to the value 1 of the y axis (after Christiansen & Lipman, 1972).

8.1.5: Geotectonic Discrimination Plots

On the Ta/Yb versus Th/Yb plot (Figure 8.15a) the samples plot into the oceanic arcs field and in the Ta versus Th plot (Figure 8.15b) they plot into the active continental margin field. This result is mirrored in the Ta/Hf versus Th/Hf plot (Figure 8.15c) It must be noted that the two latter plots do not distinguish between active continental margins and oceanic arcs. In the Yb versus Th/Ta the samples (Figure 8.15d) again plot into the oceanic arcs field. In general, the increase in Th, which behaves incompatibly, reflects an increasing arc component. The same applies for Ta, which is almost as incompatible as Th, whereas the more compatible Yb is gradually depleted (Gorton & Schandl, 2000; Schandl & Gorton, 2002).

On the Nb/Yb versus Th/Yb plot (Figure 8.16a) all the samples plot into the volcanic array field, thus corroborating their origin. On the Nb/Yb versus TiO₂/Yb plot (Figure 8.17b) the microgranite porphyry samples plot outside the basalt fields, while the other samples plot

nearer to the basaltic fields, since they have a basaltic component, as indicated by previous studies (Pe-Piper, 1978, 1980a, 1980b; Pe-Piper & Piper, 1992, 1993). On the Hf versus $(3 \cdot Ta)$ versus $(Rb/30)$ ternary plot (Figure 8.17a) the samples plot into the volcanic arc field. On the R_1 versus R_2 multivariate geotectonic discrimination plot (Figure 8.17b) the samples from the microgranite porphyry plot into the syn-collision field and the rest into the pre-plate collision field. This is in accordance with data presented earlier and confirmations that the microgranite porphyry postdates the other volcanics.

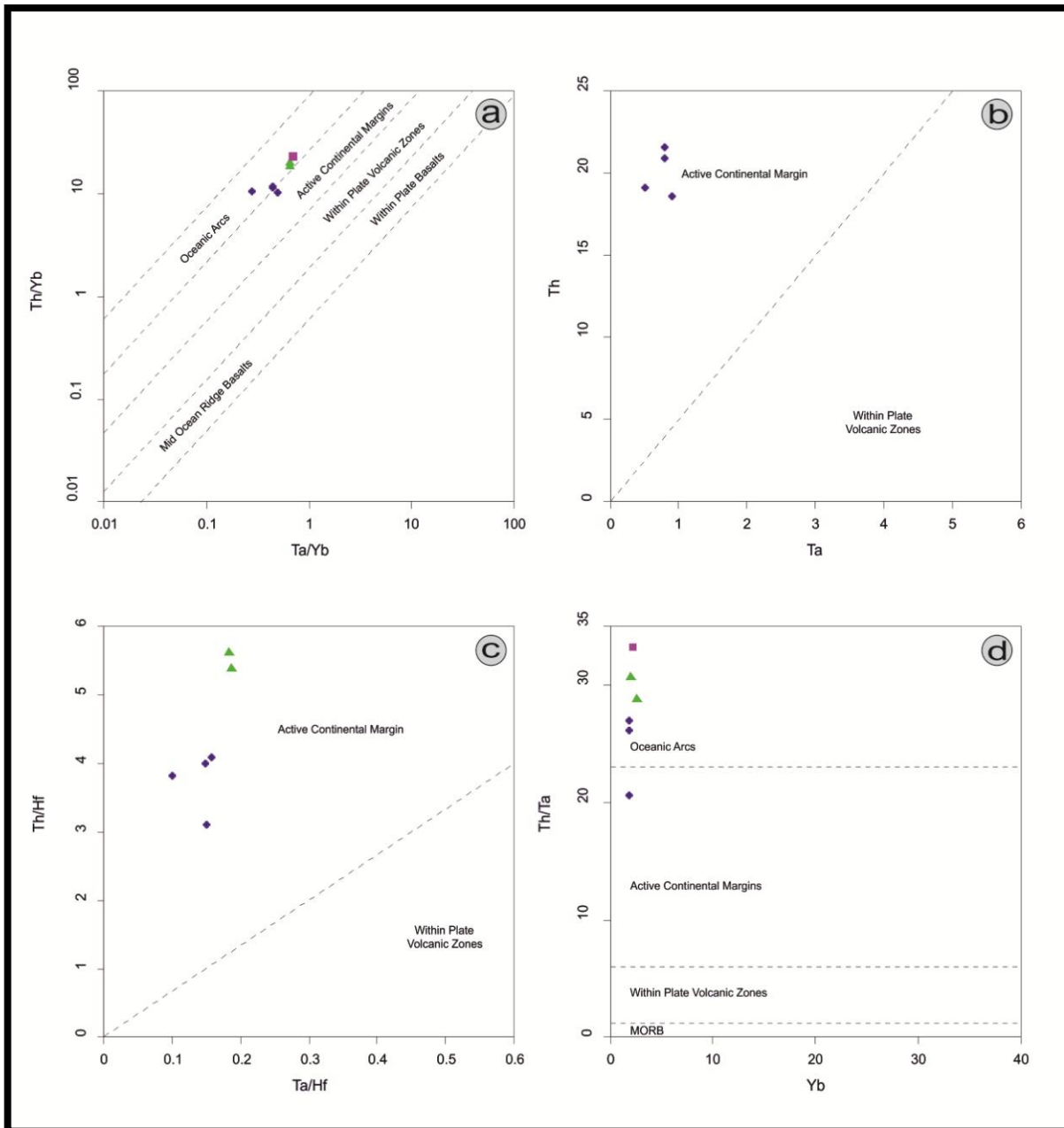


Figure 8.15: Geotectonic discrimination plots. (a) Ta/Yb versus Th/Yb plot. Most samples plot into the oceanic arcs field, while one sample from the Skoutaros Unit plots into the active continental margins field (after Gorton & Schandl, 2000). (b) Ta versus Th plot, where all the samples plot into the active continental margins field (after Schandl & Gorton, 2002). (c) Ta/Hf versus Th/Hf plot, where all the samples plot again into the active continental margin field (after Schandl & Gorton, 2002). (d) Yb versus Th/Ta plot. Most samples plot into the oceanic arcs field, and one sample from the Skoutaros Unit plots into the active continental margins field (after Gorton & Schandl, 2000).

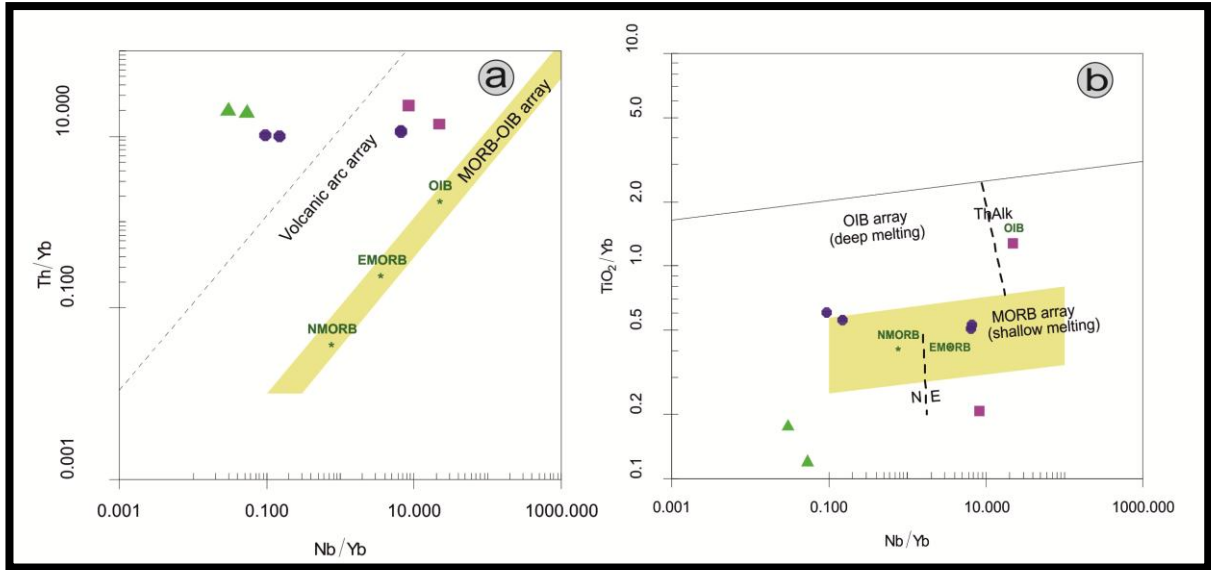


Figure 8.16: Geotectonic discrimination plots. (a) Nb/Yb versus Th/Yb, where all the samples plot into the volcanic arc array series (after Pearce, 2008). (b) Nb/Yb versus TiO_2/Yb plot, where the samples from the microgranite porphyry plot away from the basalt fields, whereas the other samples, which have a basaltic component, plot nearer the basalt fields. Their slight scattering may be attributed to slight alteration or weathering (after Pearce, 2008).

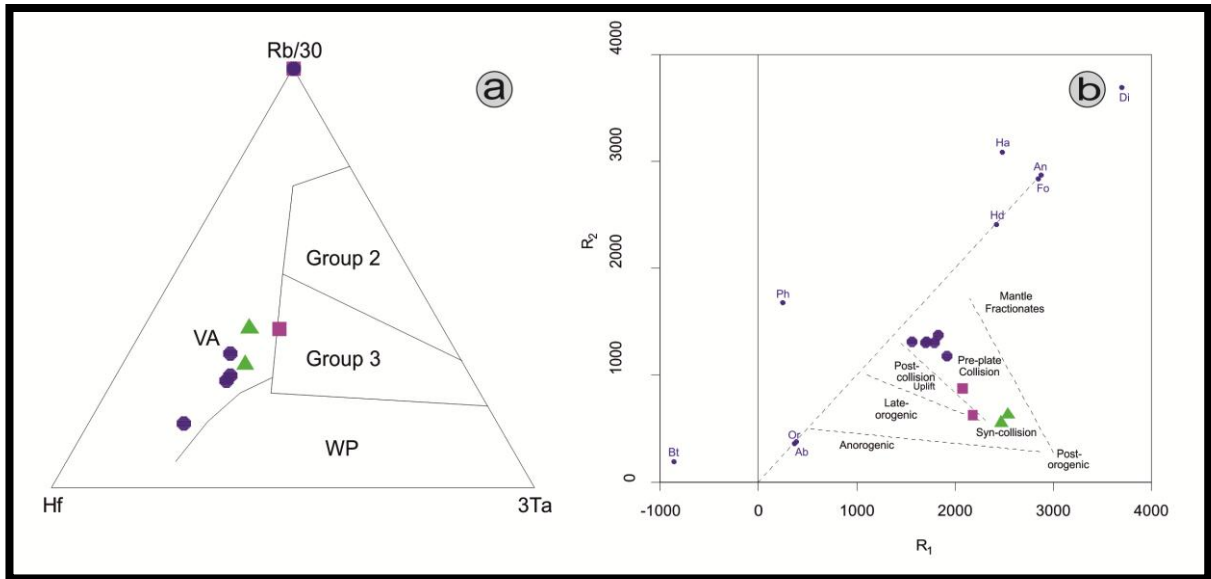


Figure 8.17: Geotectonic discrimination plots. (a) Hf versus $(3 \cdot \text{Ta})$ versus $(\text{Rb}/30)$ ternary plot, where all the samples plot into the volcanic arc field. The one exception is the sample from Sikamina Unit (the other one is not plotted because no Hf analysis is available) which due to slight weathering plots in the boundary with Group 3: post-collision calc-alkaline intrusions. Group 2 corresponds to syn-collision peraluminous intrusions, while WP corresponds to within plate rocks (after Harris *et al.*, 1986). (b) Multivariate geotectonic discrimination plot of $R_1 = 4 \cdot \text{Si} - 11 \cdot (\text{Na} + \text{K}) - 2 \cdot (\text{Fe} + \text{Ti})$ versus $R_2 = 6 \cdot \text{Ca} + 2 \cdot \text{Mg} + \text{Al}$. All the fresh samples plot in the pre-plate collision field, whereas the samples from the microgranite porphyry plot into the syn-collision field. This in effect indicates that they postdate the rest of the volcanics, a fact confirmed by the geochemical classification, Harker plots and magma series indices mentioned above (after Batchelor & Bowden, 1985).

To summarise, the samples from the Skoutaros and the Sikaminea Units along with the samples from the microgranite porphyry plot into the volcanic arc field in the relevant diagrams, thereby corroborating their geotectonic setting, already discussed by previous authors (Pe-Piper, 1978, 1980a, 1980b; Pe-Piper & Piper, 1992, 1993). Also, from the data relating to magmatic fractionation and the temporal relationship between the time of genesis

of different rocks, as shown in the R_1 versus R_2 multivariate geotectonic discrimination plot (Figure 8.17b), it is evident that the microgranite porphyry postdates the other volcanics.

8.1.6: Spider Plots

In the primitive mantle normalised plot (Figure 8.18), the relative enrichment in Cs in some of the fresh samples may be indicative of sediment addition and is a characteristic of many rocks of volcanic arcs. The same applies for Rb and Ba. The severe negative anomaly in Nb is a strong indicator of volcanic arc magmatic processes, as well as the pronounced positive Pb anomaly and the pronounced negative anomaly of Ti. In the REE chondrite normalised plot (Figure 8.19), the similarity between the geochemical signatures of samples from different igneous rocks of the Stypsi area is more apparent. In general, all samples are characterised by LREE enrichment, relative to HREE, as well as negative Eu anomalies.

To summarise, the conclusions from the following spider plots are in agreement with existing data (Pe-Piper, 1980b; Pe-Piper & Piper, 1992, 1993), in that the melts which gave rise to these igneous rocks were calc alkaline to shoshonitic, with enrichment in K, Nb, Th and F. In addition, based on existing data, as well as the geochemical and geodynamic constraints mentioned above, it is evident that all the rocks were derived from the progressive crystallisation of a melt derived from a single magmatic source.

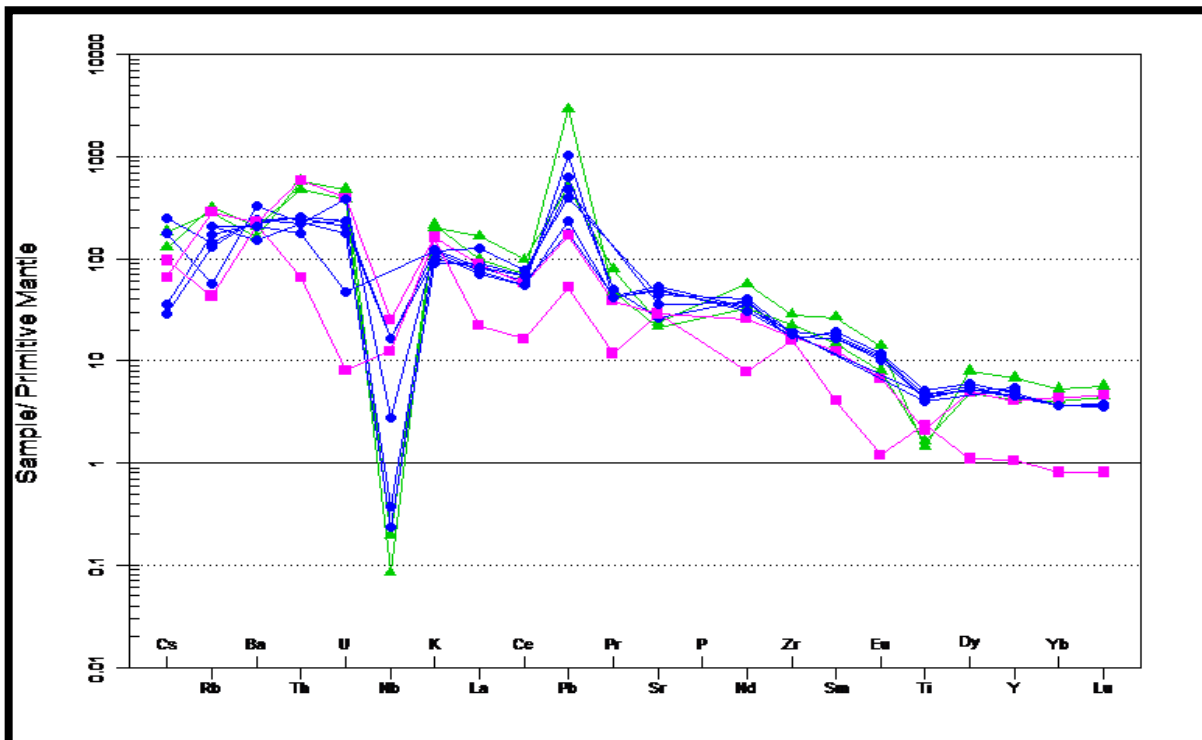


Figure 8.18: Primitive mantle normalised plot, for the fresh samples from the Skoutaros Unit (blue circles), Sikaminea Unit (purple rectangles) and the microgranite porphyry (green triangles). The microgranite porphyry samples exhibit the most negative anomaly in Nb and Ti, and the most positive ones in K, La, Ce, Pr, Zr, Eu, Dy, Y, Yb and Lu. In general, such a pattern is in conformity with the geochemical and the geotectonic classification of the volcanic rocks, and supports the conclusion that the microgranite porphyry is a more fractionated, later product, of the same magmatic source (after Sun & McDonough, 1989).

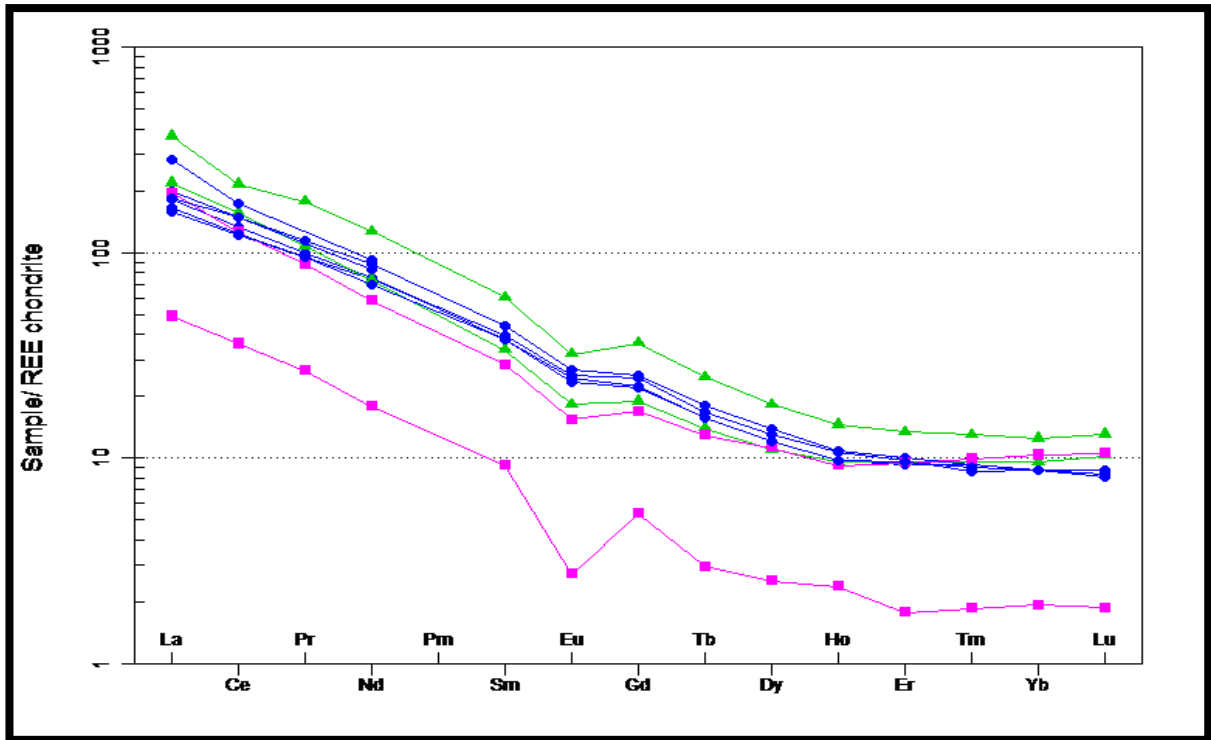


Figure 8.19: REE chondrite normalised plot, for both the fresh samples from the Skoutaros Unit (blue circles), Sikaminea Unit (purple rectangles) and the microgranite porphyry (green triangles). The Skoutaros Unit are more enriched in all elements compared to those of the Sikaminea Unit, while the microgranite porphyry samples have a similar geochemical signature to the Skoutaros lavas. All samples exhibit enrichment in LREE in comparison to HREE (after Boynton, 1984).

8.2: BULK ORE GEOCHEMISTRY

The Stypsi prospect has not been drilled or subjected to other modern exploration techniques. Bulk ore analyses of surface samples from porphyry style ore (D-type veins and banded quartz veins) indicate up to 842.64 ppm Cu, up to 76.19 ppm Mo, up to 120 ppb Au, up to 339.02 ppm Pb, up to 815.90 ppm Zn, up to 2.30 ppm Se, up to 3.46 ppm Te, 4.28 ppm Bi, and up to 15.00 ppm Sn. The Cu/Mo ratios range between 11.05 and 60 in porphyry style ores. The results of Voudouris & Alfieris (2005) for the Stypsi prospect were 0.48 ppm Au, 1330 ppm Cu, 170 ppm Mo, 1020 ppm Pb, 1.70 ppm Ag, 21 ppb Ag, 21 ppm Sn and 16 ppm Se. The bulk ore correlation diagrams reveal positive correlations between Ag, Mo, Re, Cu, Pb, and Zn (Figures 8.20, 8.21, 8.22, 8.23, 8.24, 8.25, 8.26, 8.27).

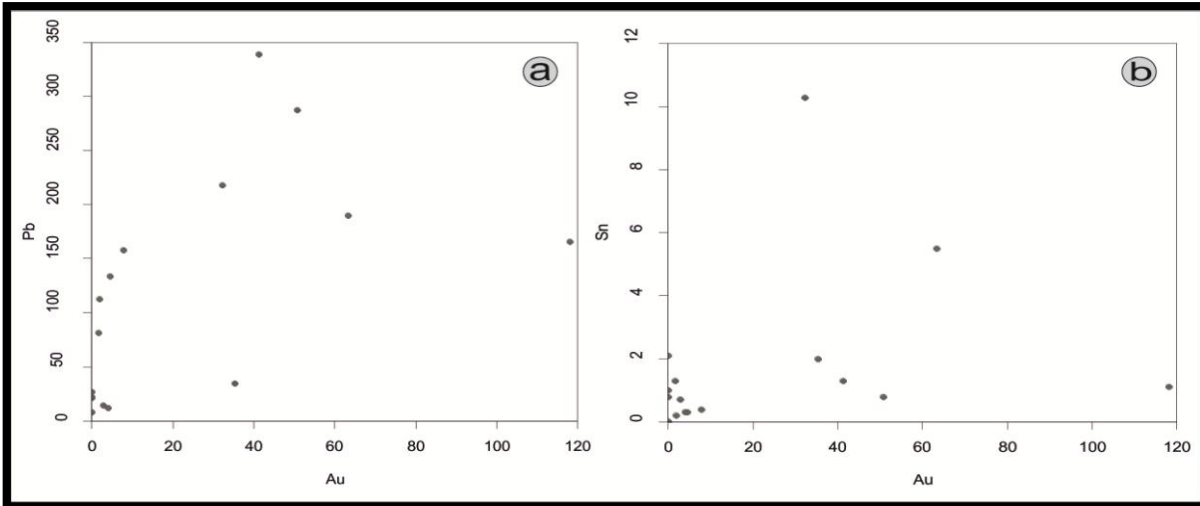


Figure 8.20: Bulk ore analyses plots. (a) Au versus Pb plot where the positive correlation is evident. (b) Au versus Sn plots where the positive correlation is more evident than in the previous diagramme.

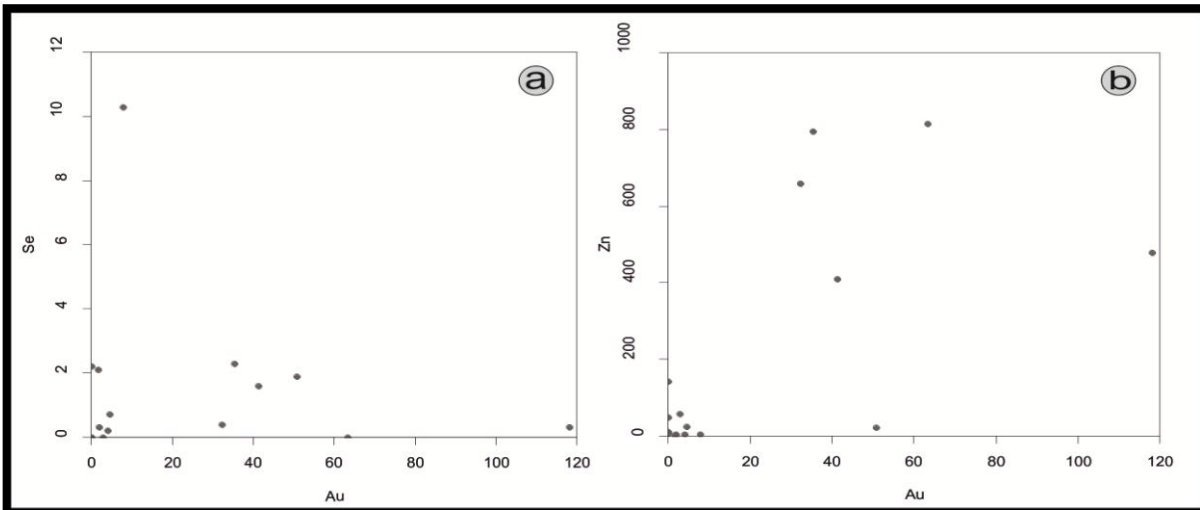


Figure 8.21: Bulk ore analyses plots. (a) Au versus Se plot where the positive correlation is evident. (b) Au versus Zn plot where the positive correlation is more evident than in the previous diagramme.

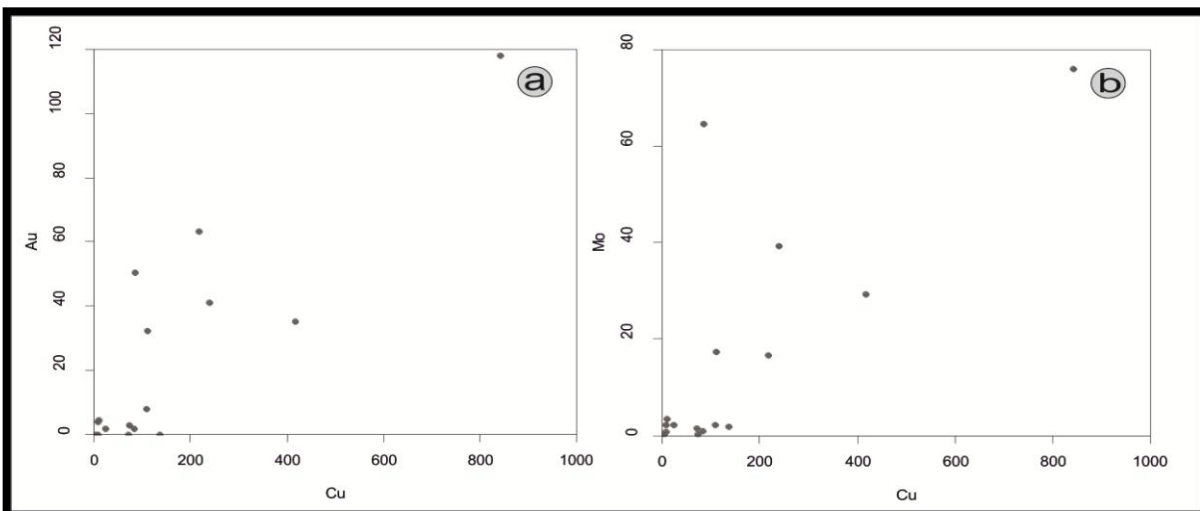


Figure 8.22: Bulk ore analyses plots. (a) Binary plot of Cu versus Au, where the positive correlation is evident for some samples. (b) Binary plot of Cu versus Mo where the the positive correlation is evident for most of the samples.

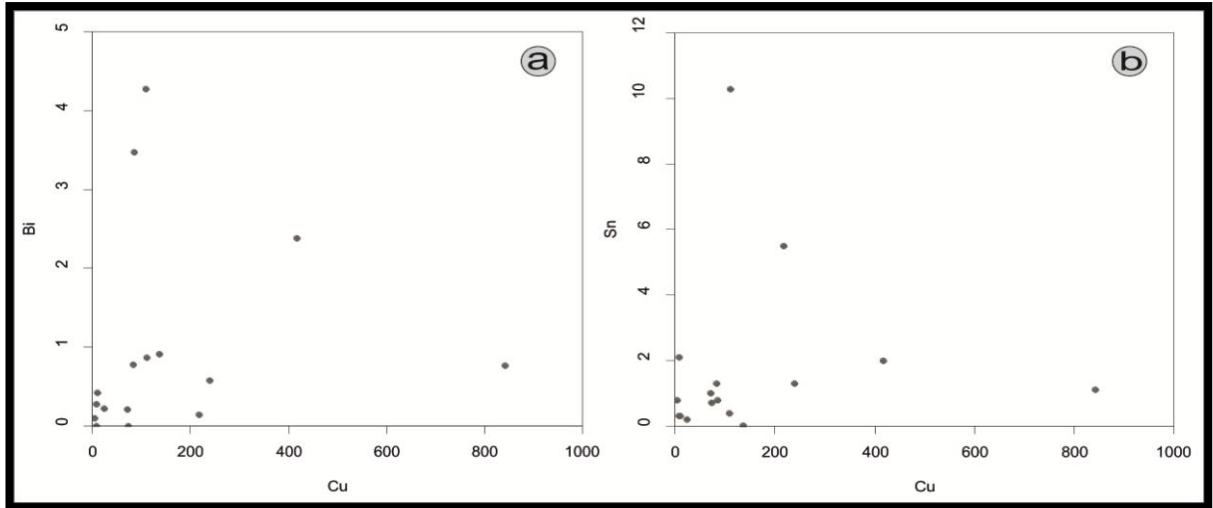


Figure 8.23: Bulk ore analyses plots. (a) Binary plot of Cu versus Bi, where the positive correlation is evident for some samples. (b) Binary plot of Cu versus Mo where the the positive correlation is evident for most of the samples.

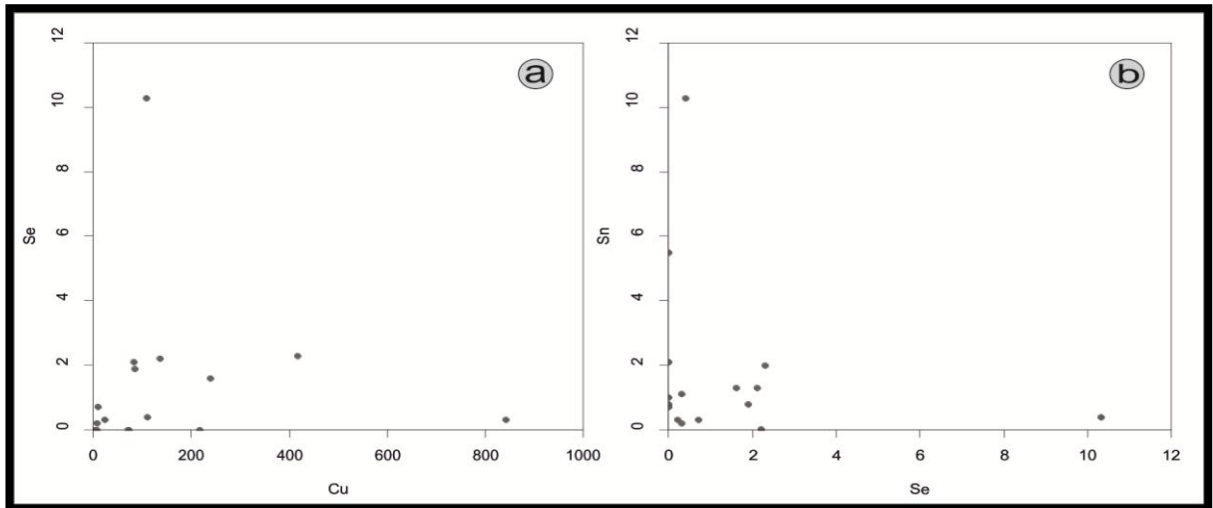


Figure 8.24: Bulk ore analyses plots. (a) Binary plot of Cu versus Se, where the positive correlation is evident for the majority of the samples. (b) Binary plot of Se versus Sn where the the positive correlation is evident for most of the samples.

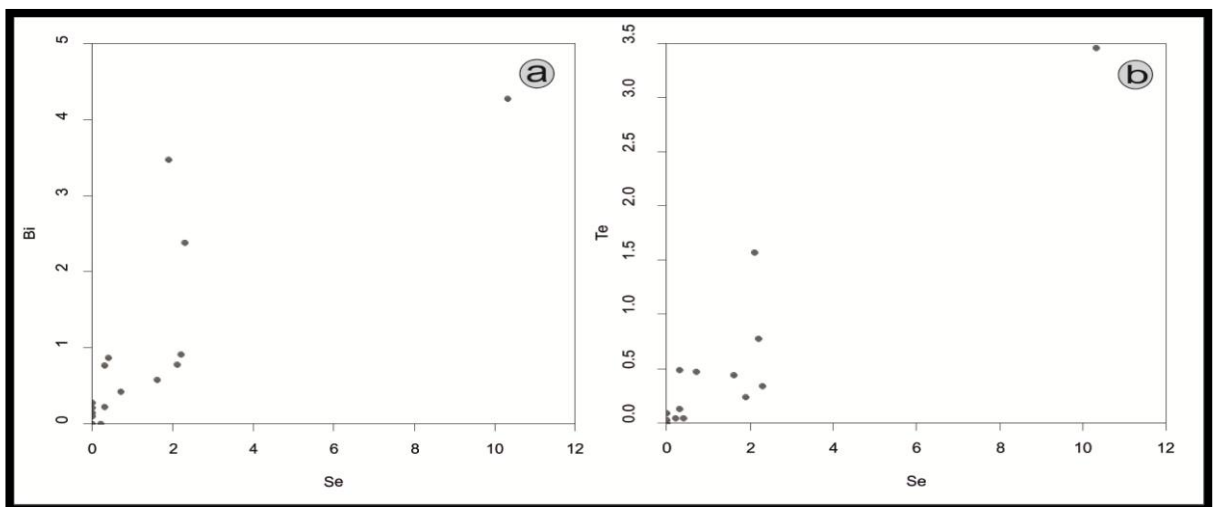


Figure 8.25: Bulk ore analyses plots. (a) Binary plot of Se versus Bi, where the positive correlation is evident for some samples. (b) Binary plot of Se versus Te where the the positive correlation is evident for the majority of the samples.

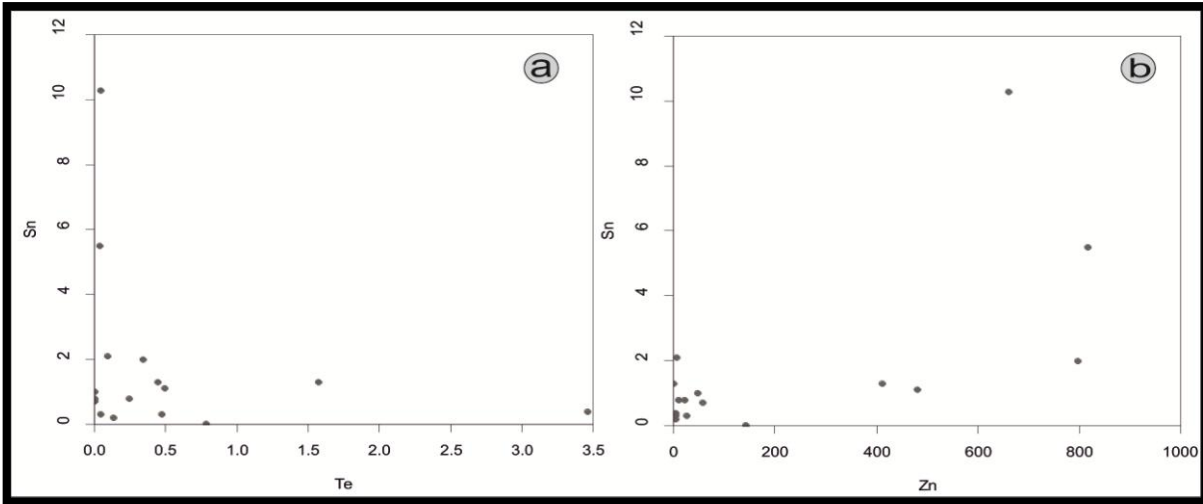


Figure 8.26: Bulk ore analyses plots. (a) Binary plot of Te versus Zn, where the positive correlation is evident for some samples. (b) Binary plot of Zn versus Sn where the positive correlation is evident for most of the samples.

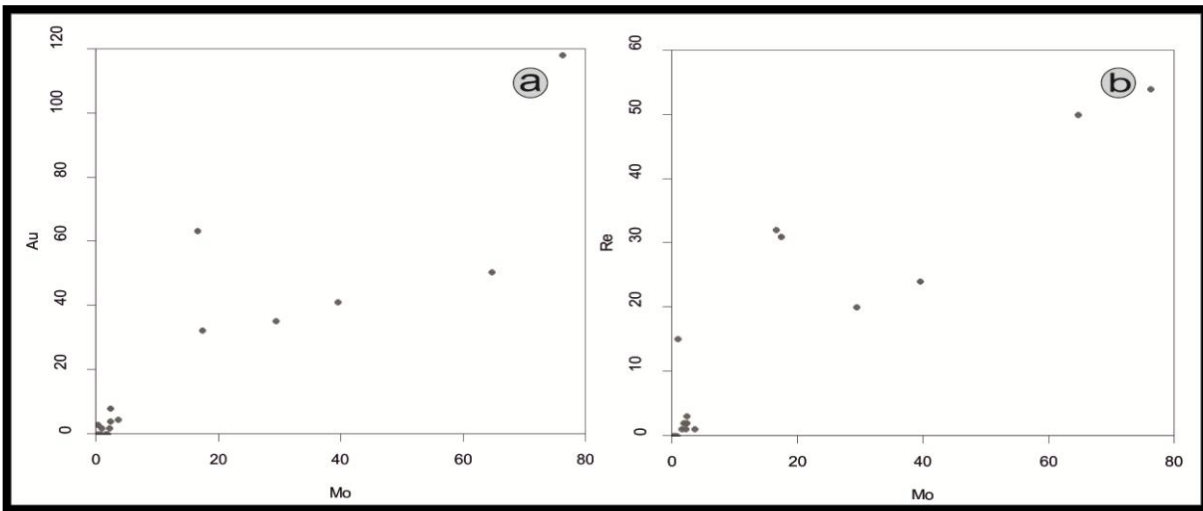


Figure 8.27: Bulk ore analyses plots. (a) Binary plot of Mo versus Au, where the positive correlation is evident for some samples. (b) Binary plot of Mo versus Re where the positive correlation is evident for some samples.

CHAPTER 9: PETROGRAPHY AND ORE MINERALOGY

Petrographical Description ~ Ore Mineralogy

The caldera of Stypsi comprises the Skoutaros Lower Lavas and the Sikaminea Upper Lavas, along with the microgranite porphyry and a small elongated body of pyroclastics of the Acid Volcanics Unit, to the NE of Stypsi. Depending upon their proximity to the focal point of the porphyry-epithermal system, the rocks are either fresh to propylitically altered or affected by Na-Ca, silicic or advanced argillic alteration. In an extended area there is also a phyllic epithermal overprint.

9.1: PETROGRAPHICAL DISCRIPTION

The Lower Lavas of the Skoutaros Unit appear dark grey when fresh or only slightly altered. They are very fine grained and contain clinopyroxene, K-feldspar and plagioclase. Sometimes, hornblende grains and iron oxides can be observed. The Upper Lavas of the Sikaminea Unit appear dark red to whitish red when fresh or only slightly altered. Quartz, K-feldspar and plagioclase constitute the groundmass, with abundant biotite grains and some grains of hornblende. The pyroclastics consist of lapilli tuff and breccia and are dominated by a quartz and feldspar assemblage.

The microgranite porphyry, which is associated with the creation of the porphyry system, intrudes the Lower Lavas of the Skoutaros Unit. A fine grained matrix of quartz and K-feldspar contains large K-feldspar phenocrysts. In all outcrops of the microgranite, the rock is heavily altered. There is a spatial and temporal association between the microgranite and the NNE trending fault running through the Stypsi area towards Megala Therma (Voudouris *et al.*, 2019).

Where the Na-Ca alteration affects the microgranite porphyry, the mineral assemblage of chlorite + albite + actinolite + plagioclase gives the rock a greenish colour. In places the alteration is so intense that it has obliterated the original textural features of the rocks. In addition, there is a sericitic overprint upon the Na-Ca altered microgranite to the SE of Stypsi. The Na-Ca alteration gradually grades outward to propylitic alteration, which affects all the volcanic rocks of the area. The characteristic mineral assemblage is quartz + calcite + chlorite + sericite + apatite + epidote + hematite, in varying amounts, according to the intensity of the alteration (Figure 9.1d, 9.1e, 9.1f) and the original mineralogy of the fresh rock (Voudouris *et al.*, 2019). Sericitic alteration overprints the majority of the central part of the system, obliterating earlier alteration textures and is characterised by a quartz + sericite mineral assemblage (Figure 9.1j). The silicic and advanced argillic alteration zones are observed at higher topographic levels, in the lithocap, to the East of Stypsi. The advanced argillic alteration zone is characterised mainly by kaolinite while the silicic alteration zone is characterised by large quartz crystals.

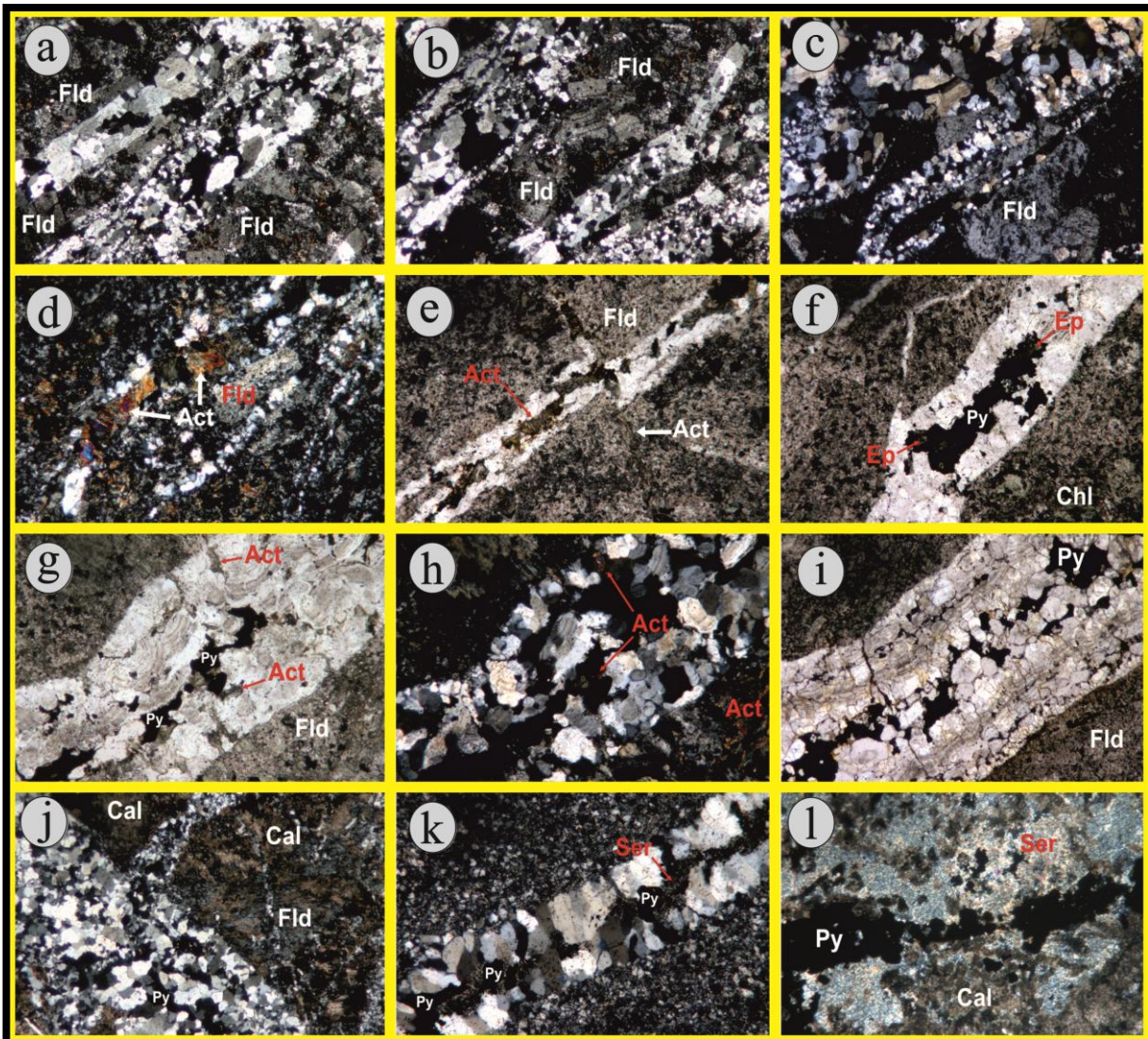


Figure 9.2: Photomicrographs of veins, associated hydrothermal alteration and gangue minerals, from the Stypsi system. (a, b, c) Quartz veins with granular quartz within K-feldspar altered microgranity porphyry. (d, e) Quartz + actinolite veinlets from the Na-Ca alteration of the microgranite porphyry. (f) Quartz + pyrite + epidote veinlets within the microgranite porphyry. (g, h, i) Banded quartz vein with granular quartz and botryoidal textures within K-feldspar, albite and actinolite altered trachyandesite. Metallic minerals occur in the marginal and central parts of the vein. Pyrite associated with actinolite \pm chlorite occurs mostly in the centre of the veins and also crosscuts quartz in the vein, thus suggesting late deposition. (j) Sericitisation, which has overprinted an earlier alteration event. (k) Granular quartz vein with molybdenite + pyrite + chalcocite + molybdenite. (l) D-type veinlet associated with phyllic alteration. The mineral abbreviations are as follows: Fld: feldspar; Act: actinolite; Ep: epidote; Py: pyrite; Chl: chlorite; Cal: calcite; Ser: sericite; and are taken after Whitney & Evans (2010). Photomicrographs e, f, g, i and l are taken under PPL and the rest under XPL.

9.2: ORE MINERALOGY

One of the principal aims of this study is the study of the chemical composition of the ore minerals, of the Stypsi porphyry and epithermal system. The ore minerals of this system are sulfides, sulfosalts and oxides. Sulfides constitute the dominant ore minerals and as such are dealt with in the first part of this chapter, followed by sulfosalts and oxides.

9.2.1: Sulfides

Pyrite can be observed as euhedral grains of various sizes, between 1-2 μm and 60-70 μm , with a typical yellow or whitish yellow colour. In some pyrite grains, inclusions of magnetite and molybdenite can be observed. Pyrite grains are ubiquitous in both early and late stage veins (Figure 9.1a, 9.1b, 9.1c).

Molybdenite is found as usually elongated euhedral grains, ranging from a few μm to about 100 μm . The grains of molybdenite are abundant in the late stage D-type veins, which are associated with phyllic alteration (Figure 9.1l). Some molybdenite grains exhibit enrichment in Re of up to 1.9 wt %, (Figure 9.4) but as evidenced from back-scattered microphotographs (Figures 9.2a, 9.2b, 9.3a, 9.3b, 9.5), Re content fluctuates even within the same crystal (Figure 9.2b). This phenomenon is similar to the variable Re contents of molybdenite grains from other porphyry deposits in Greece (Voudouris *et al.*, 2009, 2013a). In early black banded quartz veins some isolated molybdenite grains can be observed. Molybdenite grains are usually found in close contact with pyrite (Figure 9.1k).

Sphalerite grains are large and are found sometimes in contact with pyrite and always in a quartz groundmass (Figure 9.6a, 9.6b, 9.6c). Sphalerite is abundant in the black banded quartz veins. Microanalyses data indicate that sphalerite is Fe-poor, as the Fe content reaches up to 3.19 mol %. Galena is observed in black banded quartz veins and according to microanalyses results contains up to 0.13 wt. % Te, 0.05 wt. % Ag and 0.33 wt. % Bi. The grains of galena are found inside a quartz groundmass, in contact with pyrite and sphalerite (Figure 9.6d, 9.6e).

In the banded quartz veinlets (Figure 9.1g, 9.1h, 9.1i), chalcopyrite can be observed, intergrown either with sphalerite, galena or molybdenite. It postdates the formation of magnetite and pyrite. Chalcopyrite can also be observed as inclusions in sphalerite and in pyrite. In D-type quartz veins of the late stage, pyrite occurs along with molybdenite and pyrite. Bornite exists as small inclusions inside pyrite in the black banded quartz veins and is characterised by a relative enrichment in Sb.

Galena also occurs in the first two stages at Stypsi, and it can be observed surrounding pyrite in the banded quartz veins (Figure 9.6c). According to microanalyses data (Table 9.3), galena grains contain up to 0.046 wt. % Ag, 0.333 wt. % Bi, and 0.084 wt. % Te. Inside the banded quartz veins, bornite can also be observed, in contact with chalcopyrite.

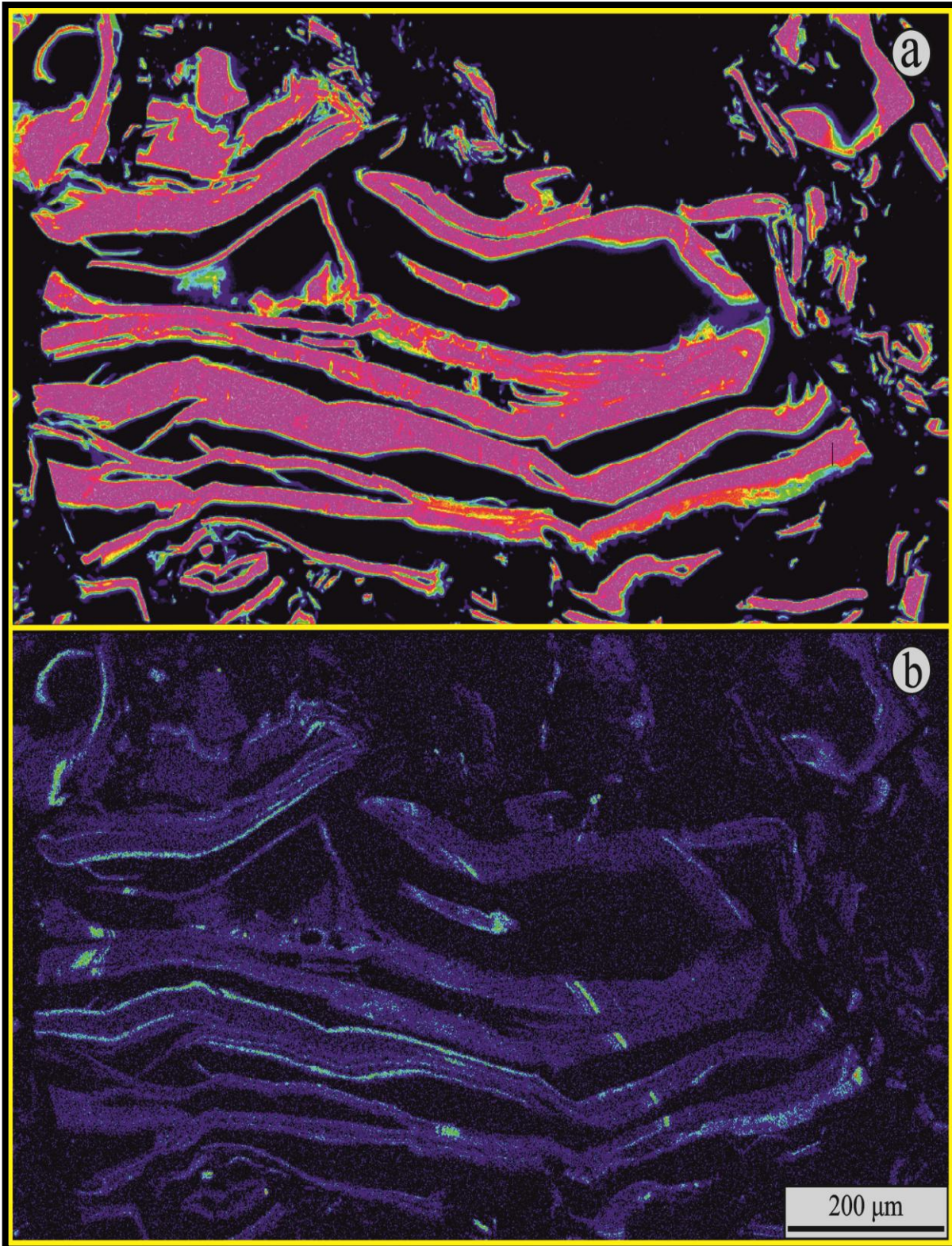


Figure 9.2: Back scattered electron images of molybdenite from the second stage of mineralisation of the Stypsi deposit. (a) Electron microprobe mapping of Mo distribution within the molybdenite grains (after Voudouris *et al.*, 2019). (b) Electron microprobe mapping of Re distribution within the molybdenite grains (after Voudouris *et al.*, 2019).

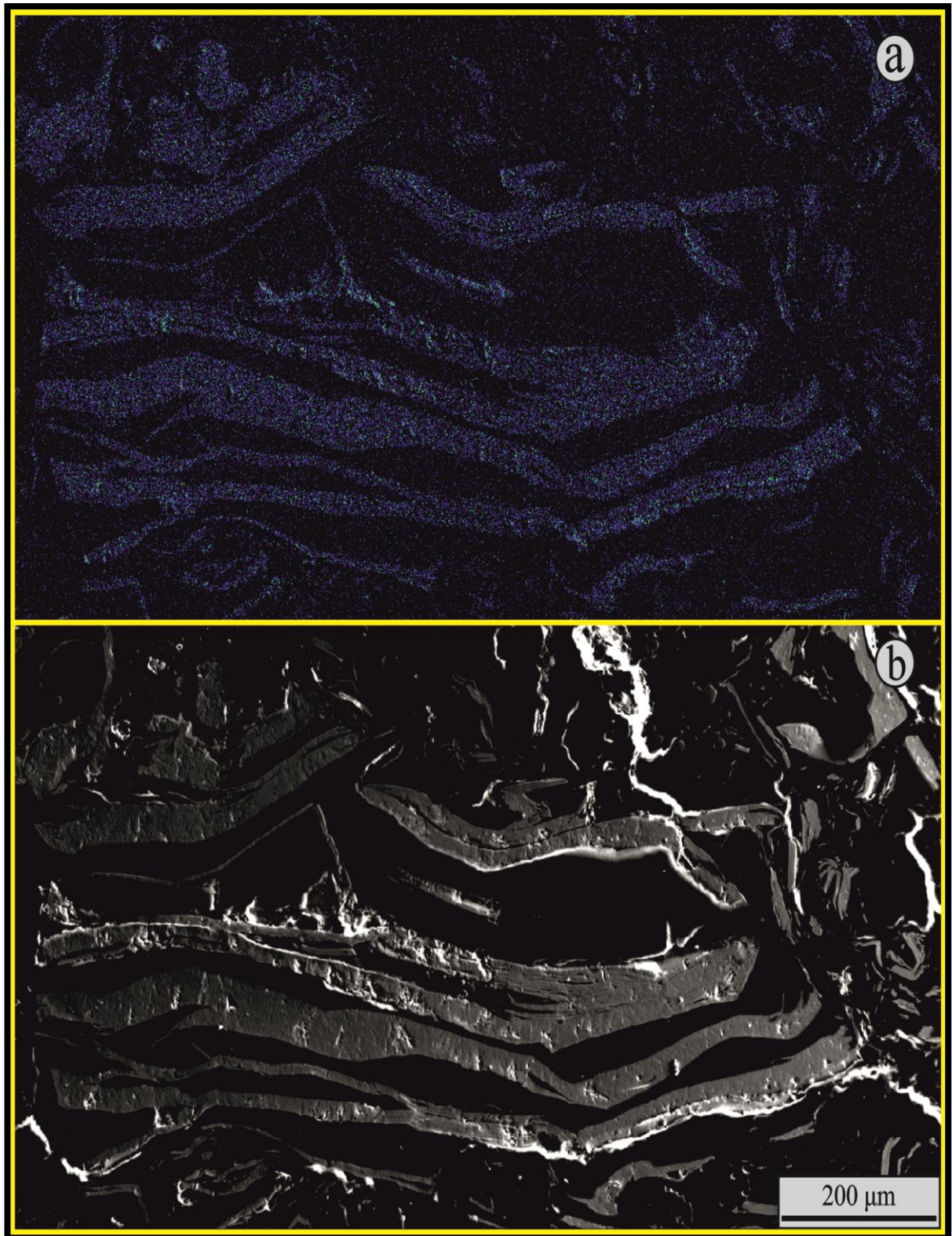


Figure 9.3: Back scattered electron images of molybdenite from the second stage of mineralisation of the Stypsi deposit. (a) Electron microprobe mapping of W distribution within the molybdenite grains (after Voudouris *et al.*, 2019). (b) Electron microprobe mapping of the relief of molybdenite grains (after Voudouris *et al.*, 2019).

Table 9.1: Molybdenite Microanalyses Data and Chemical Formula

EPMA Data (wt. %)																				
Sample Element	1	2	3	4	5	6	7	8	9	10	11	12	13	14	15	16	17	18	19	20
Mo	59.963	59.961	58.972	58.361	58.907	57.628	58.449	59.961	60.076	59.586	59.729	59.987	58.037	59.738	59.728	59.526	60.063	60.253	60.092	60.310
Re	0.019	0.000	0.049	0.055	0.144	0.203	0.308	0.000	0.017	0.104	0.190	0.212	0.087	0.052	0.100	0.000	0.146	0.118	0.049	0.282
Fe	0.666	0.789	0.095	0.290	0.050	0.053	0.066	0.087	0.059	0.551	0.567	0.553	0.240	0.162	0.132	0.915	1.007	1.036	0.097	0.183
Cu	0.003	0.009	0.005	0.028	0.012	0.000	0.010	0.000	0.000	0.029	0.017	0.000	0.000	0.000	0.000	0.019	0.007	0.000	0.015	0.037
W	0.064	0.064	0.016	0.002	0.000	0.000	0.062	0.135	0.034	0.000	0.016	0.040	0.000	0.048	0.049	0.000	0.026	0.000	0.000	0.074
S	41.111	39.613	39.845	39.204	38.696	38.773	38.929	39.358	39.842	39.088	41.219	39.082	37.691	39.067	39.443	39.443	39.358	39.506	39.131	39.761
Total	101.83	100.167	98.982	97.940	97.809	96.617	97.824	99.541	100.03	99.358	101.74	99.874	96.055	99.067	99.903	99.903	100.61	100.91	99.384	100.65
Sample Element	21	22	23	24	25	26	27	28	29	30	31	32	33	34	35	36	37	38	39	40
Mo	60.536	60.717	61.002	60.842	60.450	60.522	60.053	60.332	60.174	60.247	59.969	60.787	61.002	60.411	61.005	60.068	60.134	58.661	58.663	58.104
Re	0.121	0.085	0.054	0.015	0.066	0.043	0.044	0.075	0.039	0.01	0.041	0.013	0.02	0.004	0.004	0.021	0.004	0.000	0.000	0.001
Fe	0.297	0.336	0.054	0.546	0.547	1.048	0.000	0.000	0.000	0.022	0.008	0.013	0.02	0.004	0.004	0.021	0.004	0.000	0.000	0.001
Cu	0.030	0.014	0.018	0.013	0.000	0.000	0.016	0.000	0.000	0.001	0.000	0.014	0.017	0.000	0.000	0.000	0.000	0.000	0.000	0
W	0.012	0.040	0.009	0.092	0.080	0.000	0.030	0.022	0.004	0.021	0.000	0.000	0.034	0.014	0.000	0.000	0.000	0.000	0.000	0.025
S	38.849	39.05	39.027	38.913	39.727	39.227	39.146	39.084	39.446	39.417	39.724	39.552	39.492	39.599	39.457	38.617	39.127	37.97	38.788	38.459
Total	99.845	100.24	100.16	100.42	100.87	100.84	99.289	99.513	99.663	99.718	99.742	100.441	100.675	100.09	100.605	98.76	99.35	97.996	98.833	98.393
Sample Element	41	42	43	44	45	46	47	48	49	50	51	52	53	54	55	56	57	58	59	60
Mo	60.101	61.120	60.308	60.396	60.282	59.502	56.743	55.189	58.663	58.399	57.025	53.339	59.568	60.22	60.333	60.387	60.147	60.566	58.791	59.481
Re	0.419	0.155	0.056	0.121	0.027	0.115	1.517	0.731	1.918	1.858	1.549	1.524	0.814	0.028	1.487	0.055	0.014	0.071	0.006	0.019
Fe	0.089	0.000	0.008	0.001	0.016	0.000	0.024	0.016	0.001	0.007	0.002	0.012	0.001	0.011	0.015	0.644	0.157	0.034	1.856	0.59
Cu	0.015	0.015	0.009	0.007	0.000	0.005	0.000	0.008	0.002	0.007	0.011	0.000	0.000	0.007	0.000	0.372	0.011	0.016	0.000	0.009
W	0.000	0.000	0.000	0.000	0.000	0.000	0.000	0.000	0.042	0.000	0.008	0.000	0.037	0.000	0.000	0.000	0.000	0.000	0.000	0.000
S	38.421	40.571	39.253	39.069	39.559	38.681	37.348	36.68	38.095	38.448	37.163	38.417	38.945	38.967	38.559	39.424	39.12	39.119	39.326	38.988
Total	99.045	101.861	99.634	99.594	99.884	98.303	95.632	92.624	98.721	98.719	95.758	93.292	99.365	99.233	100.394	100.882	99.449	99.806	99.979	99.087
Chemical Formula – Calculated on 3 Atoms per Formula Unit																				
Sample Element	1	2	3	4	5	6	7	8	9	10	11	12	13	14	15	16	17	18	19	20
Mo	0.977	0.997	0.994	0.992	1.011	0.995	1.000	1.010	1.004	1.006	0.973	1.011	1.017	1.013	1.006	0.997	1.003	1.002	1.016	1.006
Re	0.000	0.000	0.000	0.000	0.002	0.002	0.003	0.000	0.000	0.002	0.002	0.002	0.000	0.000	0.002	0.000	0.002	0.0001	0.000	0.003
Fe	0.019	0.022	0.003	0.008	0.002	0.002	0.003	0.003	0.002	0.016	0.016	0.016	0.007	0.005	0.003	0.026	0.029	0.030	0.003	0.005
Cu	0.000	0.000	0.000	0.000	0.000	0.000	0.000	0.000	0.000	0.000	0.000	0.000	0.000	0.000	0.000	0.000	0.000	0.000	0.000	0.002

W	0.000	0.000	0.000	0.000	0.000	0.000	0.000	0.002	0.000	0.000	0.000	0.000	0.000	0.000	0.000	0.000	0.000	0.000	0.000	0.000
S	2.004	1.981	2.005	1.998	1.985	2.001	1.994	1.985	1.994	1.976	2.009	1.971	1.976	1.982	1.989	1.977	1.966	1.981	1.981	1.984
Total	3	3	3	3	3	3	3	3	3	3	3	3	3	3	3	3	3	3	3	3
Sample Element	21	22	23	24	25	26	27	28	29	30	31	32	33	34	35	36	37	38	39	40
Mo	1.024	1.023	1.029	1.023	1.006	1.011	1.017	1.021	1.013	1.015	1.006	1.018	1.023	1.013	1.021	34.189	1.018	1.016	1.002	1.011
Re	0.002	0.000	0.000	0.000	0.000	0.000	0.000	0.000	0.000	0.000	0.000	0.000	0.000	0.000	0.002	0	0	0.012	0.013	0.017
Fe	0.008	0.01	0.002	0.016	0.016	0.03	0.000	0.000	0.000	0.000	0.000	0.000	0.000	0.000	0.000	0.000	0.000	0.000	0.000	0.000
Cu	0.000	0.000	0.000	0.000	0.000	0.000	0.000	0.000	0.000	0.000	0.000	0.000	0.000	0.000	0.000	0.000	0.000	0.000	0.000	0.000
W	0.000	0.000	0.000	0.002	0.000	0.000	0.000	0.000	0.000	0.000	0.000	0.000	0.000	0.000	0.000	0.000	0.000	0.000	0.000	0.000
S	1.966	1.967	1.969	1.959	1.978	1.959	1.983	1.979	1.987	1.985	1.994	1.982	1.977	1.987	1.977	65.811	1.982	1.972	1.985	1.981
Total	3	3	3	3	3	3	3	3	3	3	3	3	3	3	3	3	3	3	3	3
Sample Element	41	42	43	44	45	46	47	48	49	50	51	52	53	54	55	56	57	58	59	60
Mo	1.027	1.004	1.018	1.021	1.013	1.018	1.005	1.001	1.013	1.005	1.012	0.947	1.013	1.022	1.026	1.006	1.017	1.022	0.982	1.008
Re	0.003	0.002	0.000	0.002	0.000	0.002	0.014	0.007	0.017	0.017	0.014	0.014	0.007	0.000	0.013	0.000	0.000	0.000	0.000	0.000
Fe	0.003	0.000	0.000	0.000	0.000	0.000	0.000	0.000	0.000	0.000	0.000	0.000	0.000	0.000	0.000	0.019	0.005	0.002	0.053	0.016
Cu	0.000	0.000	0.000	0.000	0.000	0.000	0.000	0.000	0.000	0.000	0.000	0.000	0.000	0.000	0.000	0.01	0.000	0.000	0.000	0.000
W	0.000	0.000	0.000	0.000	0.000	0.000	0.000	0.000	0.000	0.000	0.000	0.000	0.000	0.000	0.000	0.000	0.000	0.000	0.000	0.000
S	1.967	1.994	1.982	1.977	1.987	1.981	1.981	1.992	1.97	1.979	1.974	2.04	1.981	1.978	1.961	1.965	1.978	1.976	1.965	1.976
Total	3	3	3	3	3	3	3	3	3	3	3	3	3	3	3	3	3	3	3	3

Table 9.2: Sphalerite Microanalyses Data and Chemical Formula

EPMA Data (wt. %)																		
Sample Element	1	2	3	4	5	6	7	8	9	10	11	12	13	14	15	16	17	18
Zn	65.381	65.170	65.110	63.501	63.953	65.946	64.926	64.613	64.510	64.561	65.022	54.911	64.439	63.252	65.038	63.887	65.343	64.388
Fe	1.596	1.468	1.564	1.836	1.387	0.600	1.218	0.954	1.702	1.684	1.472	4.742	0.262	0.256	0.473	1.414	1.322	1.442
Mn	0.044	0.055	0.048	0.017	0.010	0.032	0.050	0.039	0.036	0.058	0.069	0.000	0.000	0.003	0.026	0.018	0.047	0.068
Cd	0.273	0.360	0.381	0.331	0.354	0.346	0.317	0.359	0.312	0.334	0.281	0.311	0.340	0.419	0.554	0.413	0.413	0.397
Sn	0.000	0.000	0.010	0.000	0.000	0.000	0.000	0.011	0.005	0.000	0.016	0.000	0.000	0.000	0.000	0.000	0.000	0.000
Cu	0.059	0.047	0.121	0.978	0.542	0.057	0.044	0.435	0.008	0.018	0.066	5.715	0.776	1.090	0.023	0.218	0.000	0.004
In	0.000	0.001	0.028	0.021	0.056	0.010	0.021	0.000	0.006	0.014	0.000	0.000	0.000	0.000	0.025	0.009	0.000	0.000
Hg	0.000	0.000	0.101	0.076	0.000	0.000	0.045	0.070	0.000	0.035	0.010	0.079	0.000	0.112	0.000	0.121	0.174	0.000
Ge	0.000	0.000	0.008	0.007	0.000	0.008	0.000	0.000	0.000	0.000	0.000	0.000	0.000	0.017	0.000	0.000	0.000	0.000
S	32.616	32.663	32.539	32.705	33.068	32.248	32.164	31.975	32.486	32.482	32.534	33.140	31.252	32.549	33.124	32.803	32.274	32.574
Total	99.969	99.773	99.910	99.472	99.370	99.247	98.785	98.456	99.065	99.182	99.470	98.898	97.069	97.698	99.263	98.883	99.673	98.873
Chemical Formula – Calculated on 2 Atoms per Formula Unit																		
Sample Element	1	2	3	4	5	6	7	8	9	10	11	12	13	14	15	16	17	18
Zn	0.976	0.974	0.974	0.924	0.956	0.993	0.982	0.981	0.970	0.970	0.975	0.819	0.995	0.963	0.975	0.961	0.980	0.969
Fe	0.028	0.025	0.027	0.031	0.024	0.011	0.021	0.017	0.030	0.030	0.026	0.083	0.005	0.005	0.008	0.025	0.024	0.026
Mn	0.001	0.001	0.001	0.000	0.000	0.001	0.001	0.001	0.001	0.001	0.001	0.000	0.000	0.000	0.000	0.000	0.001	0.001
Cd	0.002	0.003	0.003	0.003	0.003	0.003	0.003	0.003	0.003	0.003	0.002	0.003	0.003	0.004	0.005	0.004	0.004	0.004
Sn	0.000	0.000	0.000	0.000	0.000	0.000	0.000	0.000	0.000	0.000	0.000	0.000	0.000	0.000	0.000	0.000	0.000	0.000
Cu	0.001	0.0001	0.002	0.014	0.009	0.001	0.001	0.007	0.000	0.000	0.001	0.087	0.012	0.017	0.000	0.003	0.000	0.000
In	0.000	0.000	0.000	0.000	0.000	0.000	0.000	0.000	0.000	0.000	0.000	0.000	0.000	0.000	0.000	0.000	0.000	0.000
Hg	0.000	0.000	0.001	0.000	0.000	0.000	0.000	0.000	0.000	0.000	0.000	0.000	0.000	0.001	0.000	0.001	0.001	0.000
Ge	0.000	0.000	0.000	0.000	0.000	0.000	0.000	0.000	0.000	0.000	0.000	0.000	0.000	0.000	0.000	0.000	0.000	0.000
S	0.992	0.996	0.992	1.028	1.008	0.991	0.992	0.991	0.996	0.996	0.995	1.008	0.985	1.010	1.012	1.006	0.990	1.000
Total	2	2	2	2	2	2	2	2	2	2	2	2	2	2	2	2	2	2
Cation Sum	1.008	1.004	1.008	0.972	0.992	1.009	1.008	1.009	1.004	1.004	1.005	0.992	1.015	0.990	0.988	0.994	1.010	1.000
Fe mol %	2.778	2.490	2.679	3.189	2.419	1.090	2.083	1.685	2.988	2.988	2.587	8.367	0.493	0.505	0.810	2.515	2.376	2.600

Table 9.3: Galena Microanalyses Data and Chemical Formula							
EPMA Data (wt. %)							
Sample Element	1	2	3	4	5	6	7
Pb	85.976	86.843	85.952	87.593	87.361	86.930	87.335
Fe	0.059	0.228	0.275	0.877	0.219	0.141	0.179
Cu	0.053	0.019	0.014	0.000	0.044	0.025	0.009
Ag	0.014	0.017	0.007	0.034	0.000	0.000	0.046
Bi	0.220	0.205	0.333	0.182	0.235	0.157	0.243
Te	0.048	0.084	0.053	0.095	0.049	0.129	0.034
S	13.504	13.051	13.182	13.557	13.607	13.452	13.382
Total	99.874	100.447	99.816	102.338	101.515	100.834	101.228
Chemical Formula – Calculated on 2 Atoms per Formula Unit							
Sample Element	1	2	3	4	5	6	7
Pb	0.990	1.008	0.996	0.979	0.992	0.994	1.001
Fe	0.002	0.010	0.012	0.038	0.009	0.008	0.008
Cu	0.002	0.000	0.000	0.000	0.002	0.000	0.000
Ag	0.000	0.000	0.000	0.000	0.000	0.000	0.000
Bi	0.002	0.002	0.005	0.002	0.002	0.002	0.002
Te	0.000	0.002	0.000	0.002	0.000	0.002	0.000
S	1.004	0.978	0.987	0.979	0.995	0.994	0.989
Total	2	2	2	2	2	2	2

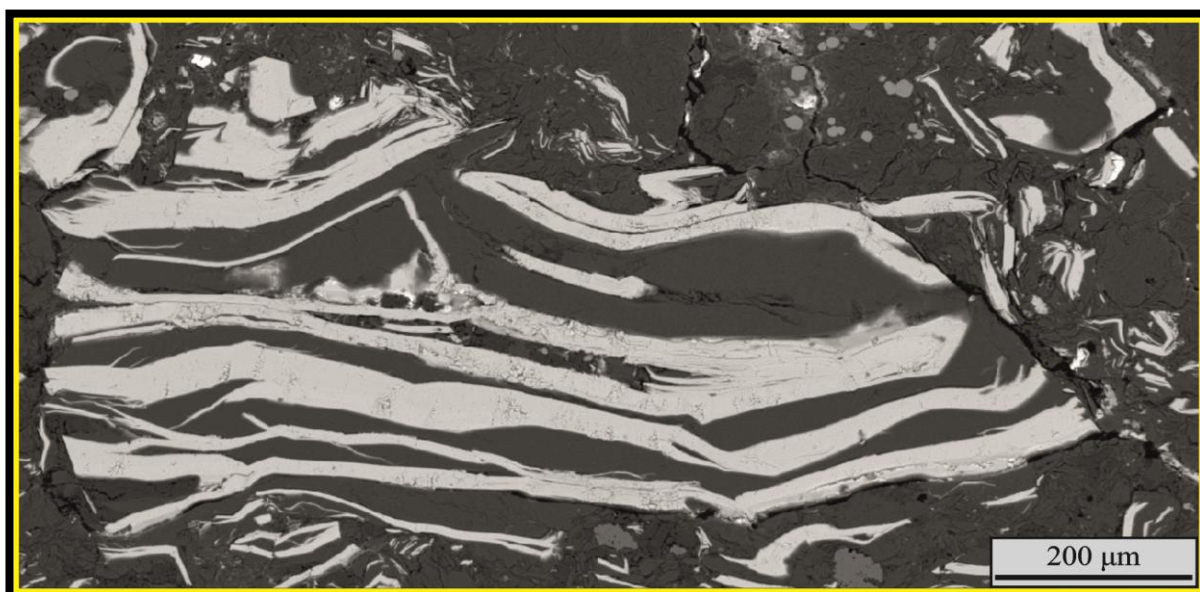


Figure 9.4: Back scattered electron image of molybdenite grains from the second stage of mineralisation of the Stypsi deposit.

9.2.2: Sulfosalts and Oxides

Both sulfosalts and oxides are minor mineral phases in the Stypsi mineralisation, so they are presented together. Fahlores (tennantite-tetrahedrite) appear during later mineralisation stages – i.e. they postdate D-type veins (Figure 9.6f). Microanalyses data from fahlores indicate enrichment in Sb (up to 9.424 wt. %) and Bi (up to 0.177 wt. %).

Regarding the oxides, magnetite is associated with early Na-Ca alteration and with the banded quartz veinlets. It can be observed associated with pyrite, chalcopyrite, bornite and molybdenite.

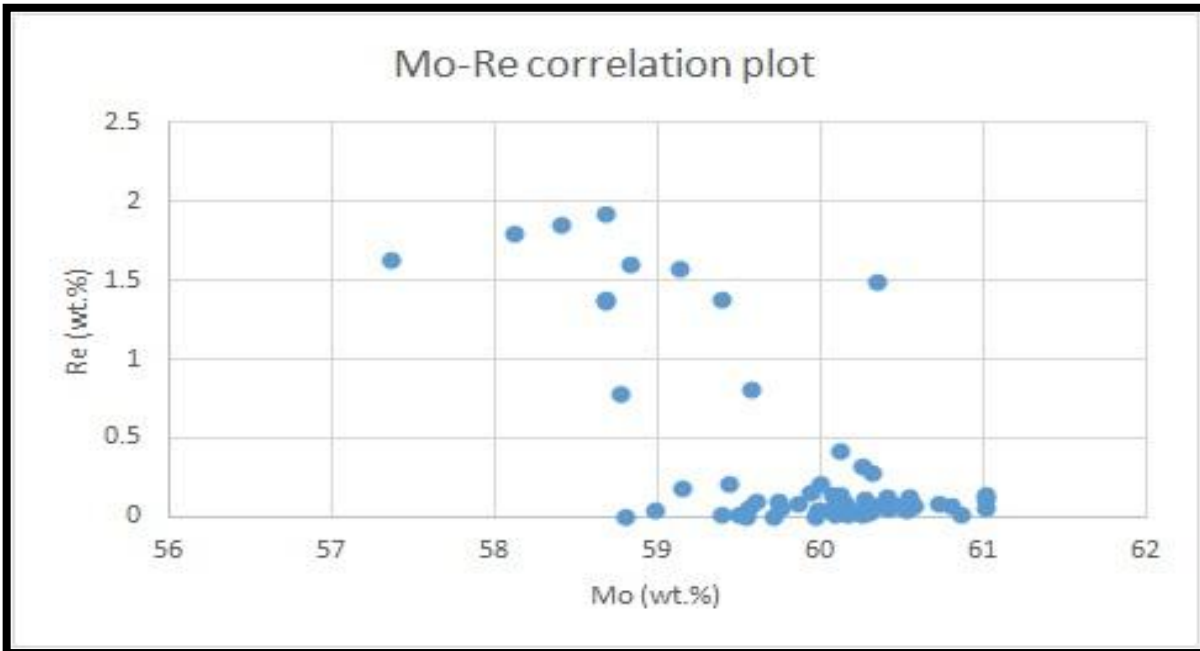


Figure 9.5: Mo versus Re correlation plot based on the EPMA data, as presented in Table 9.1, from the molybdenite of the samples from Stypsi.

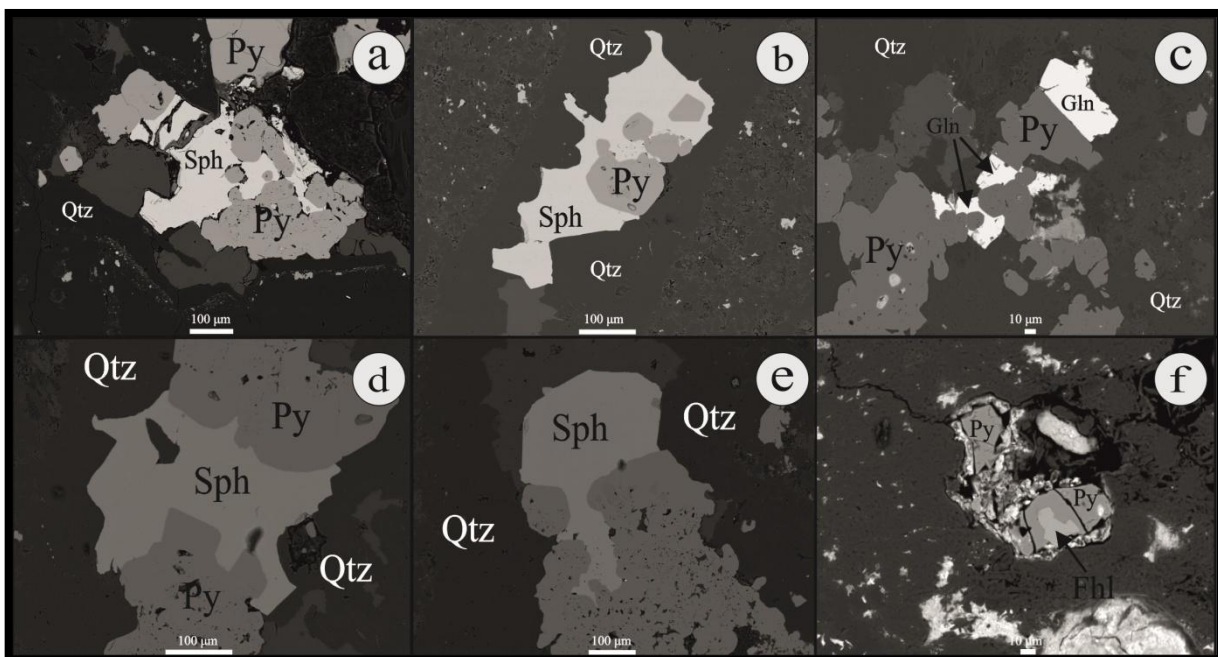


Figure 9.6: Photomicrographs of opaque mineral assemblages inside porphyry-type quartz (Qtz) veins. (a) and (b), sphalerite (Sph) in contact with pyrite (Py); (c) galena (Gln) in contact with pyrite (py); (d) and (e), sphalerite (Sph) inside pyrite (Py); (f) Fahlores (Fhl) inside pyrite (Py). Mineral abbreviations are taken after Whitney & Evans (2010).

CHAPTER 10: DISCUSSION AND CONCLUSIONS

The Stypsi porphyry and epithermal deposit can be regarded as the Eastern extension of the metallogenetic belt of the Hellenides, whose these systems were active during Meiocene. According to Jolivet *et al.* (2013), during the Meiocene, the Aegean and Western Anatolia region were regarded as a back-arc setting, where the slab retreat caused an extremely potent extensional tectonic regime. The Miocene magmatism of the area was synchronous with the entrance of the Mediterranean Ocean in the subduction zone of the Hellenides.

For the specific case of Lesvos Island, existing geochemical data (Pe-Piper, 1978, 1980a, 1980b; Pe-Piper & Piper, 1992, 1993, 2002) indicate the existence of calc alkaline to shoshonitic magmatism with a sub-continental lithospheric mantle contribution, with a degree of sediment contamination. The geochemical investigation confirmed previous existing data, regarding the derivation of the volcanic rocks of Skoutaros and Sikaminea from a single volcanic source. The Lower Lavas of the Skoutaros Unit were the first to crystallise, followed by the Upper Lavas of the Sikaminea Unit. The microgranite porphyry postdates these lithologies, but it is the product of the same magmatic source. Based on geochemical and temporal constraints it can unequivocally be stated that the microgranite porphyry belongs to the Acid Volcanics Unit. Helbling-Marschall (2011) proved that the magmatic source of the Tertiary volcanic rocks of Lesvos Island was in fact enriched by slab derived fluids, with no assimilation of crustal material.

So, the porphyry-epithermal system in Stypsi can be thought of as being roughly in the middle of the metallogenetic belt of the Hellenides to the West and of the Biga peninsula and Menderes metallogenetic belt to the East (Periferakis, 2014). All these systems represent the Tethyan metallogenetic belt (Delibaş *et al.*, 2017). The geodynamic setting of the Aegean Sea area is ideal for the creation of abundant Cu ± Au ± Mo and Pb ± Zn deposits. These are associated with metamorphic domes and back arc magmatic provinces (Oygür, 1997; Arikas & Voudouris, 1998; Oygür & Erler, 2000; Marchev *et al.*, 2005; Voudouris *et al.*, 2013a, 2018a; Sánchez *et al.*, 2016).

The Tethys metallogenetic belt comprises back arc Cu ± Mo ± Au porphyry mineralisations, from Rhodope through to Anatolia and to the Lesser Caucasus, which were created between Middle and Late Cenozoic (Voudouris *et al.*, 2019). Characteristic examples are the Konos porphyry Cu-Mo system Skouries porphyry Cu-Au-Mo system, the Pagoni Rachi Cu-Mo-Ag-Au system, the Kisladag porphyry Au-Mo system and the Kerman Cu-Mo porphyry belt in Iran. There is also a link between the metamorphic dome province of Rhodope and the Aegean Sea which has been addressed by previous authors (Arikas & Voudouris, 1998; Marchev *et al.*, 2005; Márton *et al.*, 2010; Kaiser-Rohrmeier *et al.*, 2013; Moritz *et al.*, 2014, 2016).

The Stypsi porphyry-epithermal deposit is a telescoped porphyry-epithermal IS system which shares similarities with other deposits of the Aegen Area and of Anatolia (Periferakis *et al.*,

2017, 2018; Voudouris *et al.*, 2018). There is significant enrichment in Au, Ag, Te, Sn, Zn and Pb (Voudouris *et al.*, 2019). Zn and Pb are unrelated to the epithermal overprint. It is believed that the Stypsi porphyry and epithermal system formed inside the collapsed Stypsi caldera, in accordance with the proposed method of formation for such deposits (Sillitoe, 1994). The Cu:Mo ratios of the system vary, between 11 and 60, hindering the system's classification.

The area of Stypsi is characterised by intense hydrothermal alteration, ranging from phyllic, to propylitic to silicic and advanced argillic. In the centre of the system, Na-Ca alteration has overprinted the host rocks and is associated with black banded quartz veinlets. The molybdenite + pyrite veins, termed D veins, are associated with phyllic alteration and postdate the black banded quartz veins. The porphyry system at Stypsi is associated with a microgranite porphyry, which has intruded the trachyandesitic Lower Lavas of the Skoutaros Unit. The area of Stypsi is, in reality, the caldera of a Miocene stratovolcano. The NNE trending fault zone, with a total length of about 5 Km, from Stypsi to Megala Therma, is associated with magma emplacement and the subsequent circulation of hydrothermal fluids. The repetitive reactivation of this fault resulted in the strong telescoping of the Stypsi porphyry-epithermal system.

The whole system is not of economic importance, insofar as the bulk ore contents of D-type and E-type veins are concerned. However, late stage molybdenite in the porphyry D veins is Re-rich in comparison to early stage molybdenite in the banded quartz veins (Voudouris *et al.*, 2019). This feature is in accordance with the late stage molybdenites of Pagoni Rachi, Greece (Voudouris *et al.*, 2013a) and Agua Rica, Argentina (Franchini *et al.*, 2011). According to relevant data the early stage magmatic molybdenite is Re poor and the late stage epithermal molybdenite is Re rich, probably because of sediment contamination of hydrothermal fluids. It must be born in mind that the spider plot patterns of altered samples exhibit indications of upper crustal rocks' contamination. One possible interpretation of Re enrichment is the interaction of hydrothermal fluids with the ophiolites of Lesvos. This assertion however raises some spatial and temporal constraints, regarding the path followed by the ascending hydrothermal fluids, given that the bulk of ophiolites is found some 15 Km to the SE of the porphyry-epithermal system at Stypsi. Xiong & Wood (2002) concluded that Re-enrichment is associated with oxidised mineralising fluids, so this must be the case at Stypsi (Voudouris *et al.*, 2019). Although there is a slight Te enrichment at Stypsi (up to a maximum of 3.46 ppm) there are no identifiable Te minerals.

The fluid inclusion analyses point to fluids boiling at a shallow level, a common fact of subvolcanic magmatic reservoirs according to the data presented by Voudouris *et al.* (2019). According to Henley & McNabb (1978) and Hedenquist *et al.* (1998) such a procedure is responsible for host rock fracturing, thereby increasing the volume of hydrothermal fluids able to permeate the rock. Thus are new veins created and older veins mineralised. Additional fluid inclusion data indicate the rapid decompression of the whole system at moderately high temperatures (between 440 °C and 520 °C). Based on the assertions of Monecke *et al.* (2018) this is probably the impetus for the creation of the banded quartz veins (Voudouris *et al.*,

2019). Cu and Mo can be precipitated by the condensation of brines, a fact already acknowledged by Seo *et al.* (2012). At Stypsi, the hypersaline fluid inclusions contain chalcopyrite which confirms the assumption of transportation of Cu through the brines (Voudouris *et al.*, 2019). It can therefore be presumed that the Cu-Mo mineralising event was associated with boiling events.

Further research is required for a final classification of the Stypsi system and for establishing a definite link between the Stypsi and Megala Therma deposits. Also, the microscopic examination of more samples could lead to the discovery of Te bearing minerals at the Stypsi deposit. Future research could establish the depth of emplacement of the microgranite at Stypsi as a parametre for establishing a complete genetic model for the system.

APPENDIX I: TERMINOLOGY USED IN THE DESCRIPTION OF PORPHYRY DEPOSITS

Veins are defined as fractures in the host rock, containing a distinct mineral or mineral assemblage. Typical veins have widths of less than a few centimetres while most are only a few millimetres wide. In many cases, there is an alteration envelope around the veins, which is developed symmetrically on both sides. This envelope, which is called **alteration halo** or **selvage**, is created by the diffusion of pore fluids, containing reactive elements, into the host rock (Seedorff *et al.*, 2005). While some haloes can be monomineralic, Meyer & Hemley (1967) document the existence of zoned haloes.

Texture in general refers to the way the grains or crystals are arranged, as well as their size relative to one another (Pellant, 1992). In particular, it must be mentioned that the textures produced by the hydrothermal alteration are distinct from those of magmatic origin (Seedorff *et al.*, 2005). For example, Carson & Jambor (1974) and Brimhall *et al.*, (1985) document the particular appearance of secondary biotite⁴¹ after magmatic hornblende. There appears the so-called «**shreddy biotite**», consisting of a series of randomly oriented aggregates, intermixed with rutile, magnetite and anhydrite. In contrast, Seedorff *et al.* (2005) describe a characteristic magmatic reaction texture, caused by the shift from the stability field of hornblende to this of biotite, in the presence of melt. The end result is an optically continuous crustal of biotite, overgrowing and variably replacing hornblende. The preservation of the original texture depends upon the environment of formation and the intensity of the alteration.

A group of minerals, which appear to have formed together and to be stable, is called a **hydrothermal mineral assemblage** (Seedorff *et al.*, 2005). Mineral assemblages give valuable information regarding the local equilibrium thermodynamics and the physicochemical conditions of their creation.

The aforementioned term is not to be confused with the term **hydrothermal mineral association**. Minerals belonging in a mineral assemblage have not necessarily formed together, regardless of their joint occurrence. This term is vital in describing alteration and sulfide zones, which are based on individual minerals or mineral associations (Seedorff *et al.*, 2005). So, it can be said that while each mineral assemblage corresponds to a single event, each mineral association is the result of time-integration of a number of events.

⁴¹ The term «**secondary biotite**» is used to describe hydrothermal biotite.

APPENDIX II: MINERALOGY OF STANDARD ALTERATIONS IN PORPHYRY SYSTEMS

Table II.1: Mineralogy of Standard Alterations in Porphyry Systems			
Alteration type	Mineralogy		
	Silicates	Sulfides & Oxides	Carbonates, Fluorides, Sulfates, Phosphates
Potassic (K-silicate)	K-feldspar, biotite, tourmaline ± albite, topaz, chlorite	Bornite + digenite + magnetite; bornite + magnetite; chalcopyrite + pyrite; magnetite + chalcopyrite; molybdenite + ilmenite + titanite + rutile ± pyrrhotite, pyrite, arsenopyrite + loellingite + wolframite + scheelite	Calcite + fluorite + anhydrite + apatite
Transitional potassic-sericitic	K-feldspar, biotite, sericite ± albite, topaz, tourmaline, chlorite	Bornite + chalcopyrite + magnetite; chalcopyrite + magnetite; chalcopyrite + pyrite; molybdenite + titanite + rutile ± cassiterite, wolframite, scheelite	Calcite + fluorite + anhydrite + apatite
Sericitic (phyilic, quartz-sericite-pyrite)	Sericite, chlorite ± albite, topaz, tourmaline, epidote, clinozoisite	Chalcopyrite + pyrite + molybdenite; pyrite; tennantite + sphalerite + galena + stannite + bismuthinite + cassiterite + magnetite + hematite + rutile ± pyrrhotite, bornite, arsenopyrite	Fluorite + apatite ± calcite, anhydrite
Transitional potassic-advanced argillic	K-feldspar, biotite, andalusite, albite ± corundum, topaz, tourmaline, cordierite	Chalcopyrite + molybdenite + magnetite + ilmenite	Anhydrite
Transitional potassic-sericitic-advanced argillic	K-feldspar, biotite, sericite, andalusite ± corundum, albite, topaz, tourmaline	Bornite + chalcopyrite ± magnetite; chalcopyrite + pyrite ± magnetite; molybdenite ± chalcopyrite ± pyrite; titanite	Anhydrite ± calcite
Transitional sericitic-advanced argillic	Sericite, andalusite, pyrophyllite, kaolinite-dickite, diaspore, alunite ± corundum, albite, topaz, dumortierite	Pyrite + bornite; chalcopyrite + pyrite + enargite + rutile	Al-phosphates ± Al-sulfates ± scorzalite ± lazulite

Advanced argillic (high T)	Andalusite, diaspore ± corundum, albite, topaz, dumortierite, cordierite	Pyrite + rutile	Al-phosphates ± Al-sulfates ± scorzalite ± lazulite
Advanced argillic (medium T)	Pyrophyllite, diaspore, topaz, dumortierite, zunyite ± albite	Covellite + digenite + chalcocite + bornite + enargite + pyrite + specular hematite + rutile	Alunite + Al-phosphates + Al-sulfates + scorzalite + lazulite + barite
Advanced argillic (low T)	Kaolinite-dickite, diaspore ± albite, topaz, dumortierite, zunyite	Covellite + digenite + chalcocite + bornite + enargite + pyrite + marcasite + specular hematite + rutile + anatase ± brookite	Alunite + Al-phosphates + Al-sulfates + barite
Intermediate argillic	Sericite-illite, kaolinite, montmorillonite, chlorite	Chalcopyrite + pyrite + hematite + sphalerite + cassiterite + stannite + bismuthinite + franckeite + rutile ± pyrrhotite, wolframite, arsenopyrite	Calcite + rhodochrosite + fluorite + barite
Propylitic	Albite, sericite-illite, montmorillonite, chlorite, epidote, relict K-feldspar, zircon ± actinolite, biotite	Bornite ± chalcopyrite ± pyrite ± pyrrhotite ± molybdenite ± sphalerite ± galena ± tennantite-tetrahedrite ± hematite ± titanite ± rutile	Calcite + ankerite ± relict apatite
Silicic	Quartz, tourmaline	Molybdenite ± ilmenorutile ± zircon	Fluorite ± apatite, monazite
Sodic-calcic	Actinolite, epidote ± plagioclase	Titanite ± rutile	Apatite ± calcite
Sodic	Albite, chlorite, tourmaline, vermicullite	Pyrite + rutile + titanite	Calcite + apatite
Calcic-potassic	K-feldspar, biotite, garnet, diopside, actinolite, epidote ± albite	Bornite + magnetite + bornite ± rutile	Calcite + anhydrite + apatite
Sodic-ferric	Amphibole, plagioclase	Magnetite; magnetite + bornite; chalcopyrite + ilmenite + titanite	Apatite
Mineralogy and alteration types as mentioned by Seedorff <i>et al.</i> (2005)			

APPENDIX III: DISTINGUISHING FEATURES OF PORPHYRY SYSTEMS' ALTERATIONS

Table III.1: Distinguishing Features of Porphyry Systems' Alterations			
Alteration Type	Chemical Process	Commonly Associated Vein Types	Examples and Associated References
Potassic (K-silicate)	Cooling of magmatic-hydrothermal fluids	Biotitic veinlets, A-type veinlets, B-type veinlets with molybdenite; veins with potassic and silicic envelopes	Refugio (Muntean & Einaudi, 2000); Bajo de la Alumbrera (Proffett, 2003a); El Salvador (Gustafson & Hunt, 1975)
Transitional potassic-sericitic *	Hydrolysis	Gray banded quartz veinlets; greisen veins and B-type veinlets with molybdenite	Refugio (Muntean & Einaudi, 2000); El Salvador (Gustafson & Hunt, 1975); Hall (Shaver, 1991)
Sericitic (phyllitic, quartz-sericite-pyrite) †	Hydrolysis	D-type veins; greissen veins	Bingham (Parry <i>et al.</i> , 2002); El Salvador (Gustafson & Hunt, 1975); Henderson (Seedorff & Einaudi, 2004a)
Transitional potassic-advanced argillic	Hydrolysis	A-type veinlets	El Salvador (Gustafson & Hunt, 1975; Gustafson & Quiroga, 1995)
Transitional potassic-sericitic-advanced argillic	Hydrolysis	EB-type veinlets; C-type and EDM-type veinlets	El Salvador (Gustafson & Quiroga, 1995); Los Pelambres (Atkinson <i>et al.</i> , 1996)
Transitional sericitic-advanced argillic	Hydrolysis	Sulfide veins	El Salvador (Gustafson & Hunt, 1975; Watanabe & Hedenquist, 2001); Resolution (Troutman, 2001)
Advanced argillic (high T)	Hydrolysis	Sulfide veins and massive replacements	Qonyrat (Nakovnik, 1968; Kudryavtsev, 1996)
Advanced argillic (medium T)	Hydrolysis	Sulfide veins and massive replacements	Butte (Meyer <i>et al.</i> , 1968); El Salvador (Gustafson & Hunt, 1975; Watanabe & Hedenquist, 2001)
Advanced argillic (low T)	Hydrolysis	Sulfide veins and massive replacements	El Salvador (Watanabe & Hedenquist, 2001); Island Copper (Arancibia & Clark, 1996)

Intermediate argillic	Hydrolysis	Pyrite veins and base metal veins	Refugio (Muntean & Einaudi, 2000); Bingham (Parry <i>et al.</i> , 2002); Henderson (Seedorff & Einaudi, 2004a)
Propylitic[‡]	Volatile addition	Calcite-chalcopyrite-hematite-chlorite veins	Adhedarán (Muntean & Einaudi, 2001); Bajo de la Alumbrera (Proffett, 2003a); El Salvador (Gustafson & Hunt, 1975)
Silicic[*]	Silica addition	Quartz veins with silicic and/or potassic envelopes	Robinson (Seedorff, 1993); Henderson (Carten <i>et al.</i> , 1988)
Sodic-calcic	Alkali exchange	Actinolite and epidote veins with sodic-calcic envelopes	Ann-Mason (Dilles & Einaudi, 1992); Yerington mine (Carten, 1986)
Sodic	Alkali exchange	Quartz-pyrite-tourmaline veins with albite-chlorite envelopes	Yerington mine (Carten, 1986); Ridgeway (Wilson <i>et al.</i> , 2003)
Calcic-potassic[°]	Alkali exchange	Calc-silicate-rich veins	Galore Creek (Enns <i>et al.</i> , 1995); Ridgeway (Wilson <i>et al.</i> , 2003)
Sodic-ferric	Alkali exchange	M-type veins	Tanamá (Cox, 1985); Koloula (Chivas, 1978); Panguna (Ford, 1978)
<p>* The existence of tourmaline in this alteration zone is most prominently associated with porphyry Cu deposits. [†] The existence of tourmaline in this alteration zone is most prominently associated with porphyry Cu and porphyry Sn deposits. [‡] Propylitic alteration can be observed in all types of porphyry deposits. [*] Silicic alteration is rare in porphyry Cu systems. [°] This alteration is observed only in alkalic porphyry Cu deposits, especially those associated with syenitic intrusions.</p>			
Table data from Seedorff <i>et al.</i> (2005)			

APPENDIX IV: BRECCIA FORMATION AND SIGNIFICANCE IN PORPHYRY SYSTEMS

Breccias are fragmental rocks, which can be found in most porphyry deposits, and in order to characterise and classify them it is essential to record the composition of the matrix, the characteristics of the cement, the nature of the fragments and the geometry and dimensions of the breccias' body (Seedorff *et al.*, 2005). Breccias are the result of rock fragmentation, which happens from the mechanical energy released by the separation of an aqueous fluid from a water-saturated magma and by the expansion of already exsolved magmatic hydrothermal fluids.

Hydrothermally cemented breccias which result from open-space filling are a common occurrence in porphyry systems. Many ore minerals can be found in their cementing material but sometimes the bulk of the ore is located in veinlets inside superimposed low grade breccias (Zweng & Clark, 1995). Sillitoe (1985) notes that cementing material and rock fragments alike are subject to alteration. These breccias are not believed to have formed at the later, lower temperature stages of a deposit (Seedorff *et al.*, 2005; Cline & Bodnar, 1994; Vargas *et al.*, 1999).

According to Burnham & Ohmoto (1980), Burnham (1985), and Fournier (1999) the separation of an aqueous fluid from a water-saturated magma and the expansion⁴² of already exsolved magmatic fluids which, as a result, undergo liquid-vapour saturation create a mechanical energy excess, which fractures the host rocks, creating the associated breccias. Despite the aforementioned common mechanisms it is possible for breccias to be created, even if new fluids are not introduced in the hydrothermal system. Fournier (1999) has proposed that the introduction of a hot water-poor intrusion may cause pre-existing brine to expand rapidly, thus fracturing the rock. This process is followed by boiling of the brine.

The existence of aquifers in the region of an intrusion, and their direct interaction between them and the ascending intrusives, may lead to the formation of a **heterolithic matrixsupported breccia**, which contain both broken and unbroken phenocrysts. The vast difference between the temperatures of the aquifer and the magma leads to an explosion which brecciates the surrounding rock. As Seedorff *et al.* (2005) report, the clasts in breccias can provide samples of deeper parts of a system, which may not be exposed in the surface.

⁴² This expansion is caused by the reduction of pressure, as the fluid goes from lithostatic to hydrostatic conditions.

APPENDIX V: HYDROTHERMAL FLUID GEOCHEMISTRY

Hydrothermal fluids are low density fluids which are exsolved from a more saline magmatic fluid which is located above or to the sides of the magmatic chamber. The exsolution of such fluids causes the partitioning of metals, metalloids and volatile gases into the vapour phases (Hedenquist & Lowenstern, 1994; Heinrich *et al.*, 1999). According to Holland (1972), Seward (1981), Keppler & Wyllie (1991) and Hemley & Hunt (1992), if the fluid's composition is appropriate, then most ore metals can be partitioned strongly into a magmatic hydrothermal fluid, as chloride, bisulfide and hydroxyacid complexes.

Noll *et al.* (1996) studied the concentrations of chalcophile and siderophile elements in arc lavas and concluded that these elements are fluid-mobile in subduction and moved into the magma source region by hydrothermal fluids derived from the slab. Holland (1972), Ryabchikov *et al.* (1980, 1981), Khitarov *et al.* (1982), Candela & Holland (1984) and Urabe (1985) proved that it is feasible for many metals – relevant to the origin of porphyry deposits – to be extracted from a granitic melt through equilibration with a fluid. Keppler & Wyllie (1991) mention that complexing agents, and most importantly Cl, are paramount in metal transport, such as Pb and Cu. Additionally, F as a complexing agent, is linked to mineralisations of Sn, U and Th (Ashley, 1984; Pollard *et al.*, 1987; Štemprok, 1982, 1984). On the other hand, it must be stressed that the field association of a metal with a potential ligand does not necessary imply that the metal has been complexed with that particular ligand.

Henley & McNabb (1978) assert that at shallower depths metal partitioning becomes relatively complicated, as the magma contains more than one non-silicate phase. Anyhow, the aqueous vapour separating from the magma contains SO₂, CO₂, H₂S and HCl, and has a tendency to ascend upon formation, either being discharged to the surface, as volcanic fumaroles, or becoming absorbed at depth, forming an acidic water that can subsequently leach the host rock. After the formation of the aqueous low density vapour a dense hypersaline liquid forms, which will be richer in Cu and other chalcophile elements. These two fluids are immiscible and evidence of their existence and immiscibility is abundant in intrusive rocks and some volcanic products, as mentioned by Roedder (1992).

V.1: SULFIDE AS A LIGAND

Sulfide (S²⁻) is an essential ligand in metal transporting fluids as it enhances the solubility of Au and possibly of Cu, forming stable metal-sulfide complexes⁴³ (Mountain & Seward, 2003; Stefánsson & Seward, 2004) in subcritical aqueous solutions.

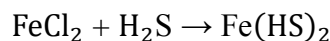
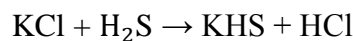
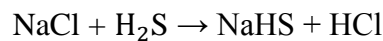
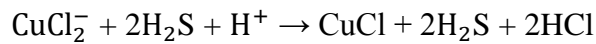
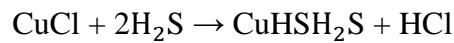
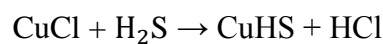
Sulfur and sulfide complexes as a consequence, are a salient feature of magmatic-hydrothermal systems and experimental data from various researchers (Candela & Piccoli,

⁴³ Evidence for the association of the importance of metal-sulfide complexes exists in bonanza-grade epithermal Au deposits as mentioned by Ronacher *et al.* (2004).

1995; Williams-Jones & Heinrich, 2005; Simon *et al.*, 2006) suggest that S has a pronounced effect on the ability of volatile phases to scavenge Cu from silicate melt.

According to Seo *et al.* (2009) chloride and sulfide species exhibit differences in thermodynamic stability, which are particularly important for selective metal transport in saline two phase hydrothermal systems, where hypersaline brine coexists with a lower salinity vapour phase – from which it may physically separate.

The relative importance of Cl and S as complexing agents can be demonstrated if the appropriate phase equilibria, for the four main cations (Na, K, Fe and Cu) in the aforementioned fluid phase, are considered. The corresponding chemical reactions are the following (Seo *et al.*, 2009):



According to Williams-Jones *et al.* (2002) and Palmer *et al.* (2004), neutral species will be dissociated to variable degrees, depending upon relative concentrations, pressure, temperature and pH. It then reasonable to propose that the low water density as well as the weak dielectric properties of the vapour phase will lead to stabilisation of neutral species. The same factors also suppress all those components whose stability depends upon metal hydration and their adjacent ligands.

The high chloride concentration of the dense brine will increasingly favour chloride species like NaCl, CuCl and FeCl₂, in the liquid phase at high temperatures, according to Seward & Barnes (1997) and Simon *et al.* (2004). In a silicate melt where volatile saturation has occurred early, in the case of crystallisation induced water saturation, the Cu ore potential of this particular melt is enhanced (Simon *et al.*, 2006). It is therefore evident that the partitioning of the four major cations, between the coexisting fluid phases is governed by their relative tendency to complex with the two competing ligand components, Cl and S.

V.2: CHLORIDE AS A LIGAND

Chloride (Cl⁻) is essential for the extraction of Cu from the melt and it has no noticeable effect on the behaviour of Mo. In a chlorine bearing system, an element with an affinity for chlorine could concentrate preferentially in the aqueous phase. Uranium but not thorium can be mobilised by chloride, and the different complexing behaviour of U and Th means that

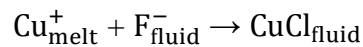
hydrothermal fluids of different compositions should have very different effects on the U-Th-Pb during hydrothermal alteration (Keppler & Wyllie, 1991).

V.2.1: Copper Partition Coefficient and its Relation to Chloride

According to Candela & Holland (1984) it is possible for copper to exist either as Cu^+ or as Cu^{2+} in a silicate melt. It is probable that Cu^+ is the only first row transition metal which is present in the univalent state in silicate magmas at high oxygen fugacities (Keppler & Wyllie, 1991).

This can probably be attributed to the fact that Cu^{2+} possesses a $3d^9$ electronic configuration and is therefore easily reduced to Cu^+ , whose stability is in turn enhanced by its $3d^{10}$ closed shell configuration (Keppler & Wyllie, 1991). A similar effect stabilises Fe^{3+} which possesses a filled half shell configuration. Candela & Holland (1984) postulated that Cu^{2+} bearing components in the melt and crystalline phases are unstable relative to Cu^+ bearing components, at the oxygen fugacity values typically prevailing in the Earth's crust and the upper mantle.

Field and experimental studies (Candela & Holland, 1984; Keppler & Wyllie, 1991) are conclusive in that only Cl and not F has any effect on the partitioning of Cu. The increase of $K_D^{f/m}$ is incremental when CuCl complexes form, as described by the following chemical reaction:



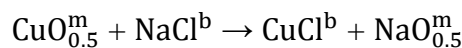
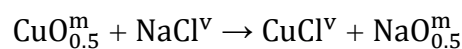
The equilibrium constant is:

$$K = \frac{C_{\text{CuCl}(f)}}{C_{\text{Cu}^+(m)} \cdot C_{\text{Cl}^-(m)}}$$

The dissolution constant for Cl is the following:

$$K_D^{f/m} = \frac{C_{\text{CuCl}(f)}}{C_{\text{Cu}^+(m)}}$$

From the aforementioned it can be deduced that there is a linear increase of the $K_D^{f/m}$ of Cu with the increase in $[\text{Cl}^-]$. Chemical partitioning data indicate that a complex with a stoichiometric ratio of Cu:Cl = 1 is present, in the magmatic fluid albeit with no data available on its precise constitution (Keppler & Wyllie, 1991). According to Simon *et al.* (2006), Cu and Na exchange between melt and vapour and melt and brine, is described by the following equilibria:



As the crystallising magma is cooling, it will eventually reach water saturation, and then the evolving fluid will concentrate on the available chloride (Kilinc & Burnham, 1972). As a result, Cu concentrates on the fluid phase and such a model explains the origin of porphyry Cu deposits (Keppler & Wyllie, 1991).

In a subcritical aqueous solution, Cu forms sulfide complexes such CuHS as and $\text{Cu}(\text{HS})_2^-$, which are the most stable. According to Giggenbach (1992), in moderately oxidised magmatic-hydrothermal systems, S is partially present as SO_2 . As postulated by Pokrovski *et al.* (2008), this gives rise to mixed sulfide-sulfite complexes with metals. This is also demonstrated experimentally by the preferential stabilisation of Cu in the vapour by addition of S. So there is a tendency of equilibria to shift towards Cu-S complexes in the vapour, compared to other such cases; thus K, Na and Fe are stabilised as chloride complexes in the brine (Heinrich *et al.*, 1999).

It can then be concluded that the partition coefficient of Cu is proportional to the chloride concentration of the vapour phase and Cl is important in promoting the partitioning of Cu into the aqueous phases from silicate melts. The initial chlorine concentration in magmatic systems and the behaviour of chlorine during magmatic evolution are important parameters in controlling the Cu/Mo ratio in magmatic aqueous fluids. The available experimental data (Simon *et al.*, 2006) indicate that Cu is strongly coupled to Cl with the concentration of Cu in the aqueous phase increasing linearly with Cl.

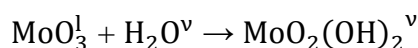
V.2.2: Aluminum Partition Coefficient and its Relation to Chloride

There is clear evidence for the complexing of Al with Cl, but the low partition coefficients measured for Cl concentrations lower than 2 M make it questionable whether a similar mechanism can account for the porphyry Al deposits. Even highly fractionated magmatic melts only reach Cl contents of about 1000 ppm, according to experimental data by Congdon & Nash (1988). Kilinc & Burnham (1972) have noted that a fluid in equilibrium with such a melt contains about 1 M of Cl.

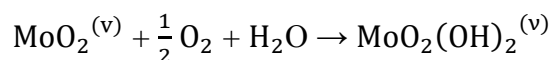
In a theoretical level, it is possible to assert that for the effective extraction of Al from a melt there would exist the need for a recycling chlorine containing fluid, between the magma and the ore deposit. According to Štemprok (1982) and Keppler & Wyllie (1991) the absence of any experimental evidence for complexing Al or W with Cl is not easy to understand, considering the characteristically high fluorine contents associated with this type of deposit.

V.2.3: Molybdenum and Wolfram Partition Coefficients and their Relation to Chloride

In the presence of alkali chloride solutions there is an increase in the $K_D^{f/m}$ for Mo, compared to chloride free systems (Candela & Holland, 1984). This however does not imply that the corresponding chloride complexes stable. Rather, the increase in the fluid's pH stabilises the corresponding hydroxy complexes, as the systems becomes more alkaline (Urabe, 1985). The simplest equation possible for describing the distribution of Mo between silicate melts and aqueous fluids is the following:



The ratio of fugacity of $\text{MoO}_2(\text{OH})_2$ to that of MoO_2 in the gas phase as a function of temperature, water fugacity and oxygen fugacity can be calculated. The equilibrium between these two chemical compounds is represented by the following reaction:



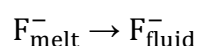
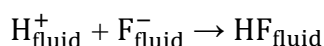
If the stoichiometry of the molybdenum bearing complexes in the melt differs from the stoichiometry of the molybdenum bearing complexes in the vapour phase, then the partition coefficient ($D_{\text{Mo}}^{v/l}$) is a function of molybdenum concentration (Candela & Holland, 1984).

When there is no fluorine in the system, then the partitioning coefficient of Mo appears to be essentially independent of the chloride concentration in the aqueous fluid. According to Holland (1972) and Kilinc & Burnham (1972), in a silicate-melt aqueous system, with a vapour to melt ratio of about 2, 99 % of chlorine is in the aqueous phase. The chlorine content is therefore insignificant in such a system, compared to the chlorine content in the aqueous phase. As for wolfram, Manning & Henderson (1984) have suggested that chloride complexes exist in magmatic hydrothermal fluids, based on their partitioning data. In general, the increasing concentration of HCl will lead to a rapid increase in $K_D^{f/m}$.

V.3: FLUORINE AS A LIGAND

According to experiments by Koster van Groos & Wyllie (1969) and Webster (1990) the presence of fluorine in fluid-melt systems strongly increases the content of dissolved silicates in the aqueous fluid, which therefore approaches the chemical composition of a silicate melt.

As the fluorine content decreases the system gradually becomes supercritical above a certain pressure. This, in turn, leads to a water rich critical fluid as the fractionation of crystals from the melt continues, which may lead to the enrichment of the residual melt in trace elements – such as Al and W – and F. According to Keppler & Wyllie (1991) this phase could then easily transport the ore forming fluid which forms porphyry Al and W deposits. Solutions containing fluoride seem to be able to transport some U and Th from a granitic magma, a fact confirmed by the numerous U and Th deposits associated with fluoride mineralisation (Chatterjee & Muecke, 1982; Ashley, 1984). The partitioning of fluorine between melt and fluid is determined by the following two equilibria (Keppler & Wyllie, 1991):

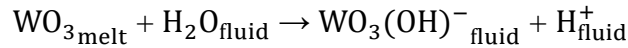


The second equilibrium determines the behaviour of fluorine in a peralkaline system with a low proton (H^+) concentration (Urabe, 1985). Conversely, any increase in proton concentration – which results in a decrease in pH – means that HF becomes the dominant species in the fluid. So, Keppler & Wyllie (1991) concluded that there is no single partition coefficient for

F, in a granitoid melt, and that the behaviour of F in such a system is predominantly controlled by the pH values.

V.3.1: Wolfram and Molybdenum Partition Coefficients and their Relation to Fluorine

The partition coefficient for W is fairly high if the only volatile present is H₂O and the dissolution reaction is the following:



The corresponding equilibrium and dissolution constants are the following:

$$K = \frac{C_{\text{WO}_3(\text{OH})^-_{\text{(f)}}} \cdot C_{\text{H}^+_{\text{(f)}}}}{C_{\text{WO}_3_{\text{(m)}}} \cdot C_{\text{H}_2\text{O}_{\text{(f)}}}}$$

$$K_D^{f/m} = \frac{C_{\text{WO}_3(\text{OH})^-_{\text{(f)}}}}{C_{\text{WO}_3_{\text{(m)}}}}$$

It is evident that any increase in [H⁺] will lead to a decrease in K_D^{f/m} and the available experimental evidence points to the existence of some hydroxy complex in the fluid (Keppler & Wyllie, 1991). Generally, the increasing concentration of HF will lead to a rapid decrease in K_D^{f/m}. The presence or absence of H₂O affects the partition coefficient of Mo in a manner very similar to that of W. Additionally, the value of K_D^{f/m} decreases when pH decreases, so there is a high probability of hydroxy chloride complexes⁴⁴.

According to the experiments of Koster van Groos & Wyllie (1968) fluorine partitions strongly into silicate melts while chlorine partitions strongly into aqueous fluids. In effect, the partition coefficient of fluorine between aqueous fluids and silicate melts is more than two orders of magnitude smaller than the partition coefficient of chlorine.

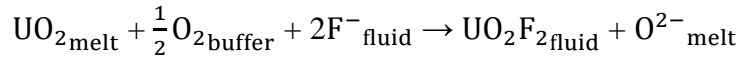
The experimental results of Candela & Holland (1984) indicate that the partition coefficient of Mo is independent of the fluorine content at least up to 1.7 wt. % in the melt. Despite this data, there is still the possibility that F and Mo complex with each other in such small amounts as to be practically, as of yet, untraceable.

So, it has been established that fluorine has little, if any, effect on the partitioning of Mo into a magmatic aqueous phase. Then, the close association of molybdenum and F bearing mineral, observed in many deposits, cannot be attributed to the complexation between Mo and F. According to Candela & Holland (1984), it must be concluded that the geological processes which concentrate Mo are most probably responsible for concentrating F.

⁴⁴ It should be noted however that F containing systems, in contrast to Cl containing ones, have somewhat higher K_D^{f/m} values.

V.3.2: Uranium and Thorium Partition Coefficients and their Relation to Fluorine

In a melt, according to Keppler & Wyllie (1991), the oxidation state of uranium is assumed to be + 4, and the fluid/melt partition is described by the following reaction:



The resulting equilibrium and dissolution constants are the following:

$$K = \frac{C_{\text{UO}_2\text{F}_{2(\text{f})}} \cdot C_{\text{O}^{2-}_{\text{melt}}}}{C_{\text{UO}_{2\text{melt}}} \cdot (C_{\text{O}_{2\text{buffer}}})^{(1/2)} \cdot (C_{\text{F}^-_{\text{fluid}}})^2}$$

$$K_D^{f/m} = \frac{C_{\text{UO}_2\text{F}_{2(\text{f})}}}{C_{\text{UO}_{2\text{melt}}}}$$

From the above it can be seen that $K_D^{f/m}$ increases along with $f\text{O}_2$ and this is a direct result of the assumption that the oxidation state of U is higher in the fluid than in the melt (Keppler & Wyllie, 1991). It is probable that there is a complex with a stoichiometric ratio of F:U = 1:1. As for Th, its partition coefficient is very low in the presence of H_2O – if it is the only volatile – and does not increase in a system containing CO_2 and HCl (Keppler & Wyllie, 1991).

V.3.3: The Case of Au

The release of voluminous magmatic fluids rich in Au, from upper crustal magma chambers, should favour the formation of large Au deposits. Rapid cooling or depressurisation of such magma chambers promotes the release of saturated fluids.

According to McInnes & Evans (1996) the slow degassing procedure of magma chambers, during rapid cooling, uplift or sector collapse, most likely inhibits formation of immiscible sulfide liquids, which could sequester Cu and Au from the melt.

Sulphur and chlorine are highly effective ligands for hydrothermal Au transport and their presence can explain the enhanced possibility of alkaline and shoshonitic rocks to generate large Au deposits (Müller & Groves, 1993). Moreover, Candela & Piccoli (1995) note that high Cl contents favour increased Cl:H₂O ratios in exsolved fluids. Thus, the probability of base metal and Au transport is maximised, along with the development of relevant mineralisation.

Candela & Holland (1984) and Cline & Bodnar (1991) have postulated that the formation of Cu ± Au rich ore fluids, by exsolution from a hydrous magma, is previously controlled by the salinity of this fluid. This theory has since been proven wrong, according to the results of Seo *et al.* (2009).

V.3.4: A Concise View on the Controls of Ore Deposition

It is likely that the efficiency of Cu extraction from the magma is determined by the sulfur concentration in the exsolving fluids. According to Hattori (1993) this may in turn be

controlled by the presence and amount of a separate sulfide melt phase that decomposes at the time of fluid saturation in the magma.

The fluids in porphyry deposits originate from relatively oxidised and peralkaline magmas, and as such exhibit a weaker tendency for Cu, As and S to fractionate into the vapour (Beane & Titley, 1981). Thus the hydrothermal fluids will be oxidised and less acidic. Such a chemical environment favours the stabilisation of charged sulfide species, which are less volatile than their neutral analogues in the saline fluids.

Various authors (Henley & McNabb, 1978; Williams-Jones & Heinrich, 2005; Klemm *et al.*, 2007) have concluded that the vapour phase is generally more important for ore deposition. Indeed, upon cooling, brine and, most importantly, vapour can efficiently precipitate their Cu as chalcopyrite or bornite, the dominant ore mineral in porphyry Cu deposits. As the cooling continues, pyrite precipitates after bornite (Seo *et al.*, 2009).

At lower temperatures, the remaining sulfur in the fluids can act as a ligand and cause the precipitation of other sulfides at lower temperatures. It is notable that, while magmatic vapours, with an excess of sulfur, can transport Au at lower temperatures, this is not observed with analogous magmatic fluids (Heinrich *et al.*, 2004). According to Seo *et al.* (2009), such a process requires, most probably, an excess of S for extreme precious metal enrichment, so as to form giant epithermal deposits, such as Porgera in Papua New Guinea.

APPENDIX VI: QUARTZ TEXTURES IN EPITHERMAL VEINS

In epithermal veins, quartz is the dominant gangue mineral and it is the only mineral deposited throughout the life of the hydrothermal system. Consequently, the characteristics of quartz (morphology, crystal structure, chemical composition, physicochemical properties) are partly a reflection of the hydrothermal processes which lead to its creation (Figures VI.1, VI.2, VI.3). Quartz textures are distinguished based on mutual geometric relations between quartz crystals. The quartz textures of epithermal veins are the following (Dong *et al.*, 1999):

- 1) **Massive quartz texture:** this texture is observed in veins displaying a more or less homogenous appearance. No banding or shear fractures are typically present in such veins.
- 2) **Crustiform quartz texture:** this texture comprises successive narrow and subparallel bands, which can be distinguished by differences in colour, texture and mineral proportions. It is typical to observe this texture in fissures, developing symmetrically from both walls. It was first described by Adams (1920) and Shaub (1934), who termed it «**crustification banding**». Additionally, Adams (1920) and then Spurr (1926) described the **cockade quartz texture**, to describe the concentric crustiform bands surrounding isolated fragments of wallrocks or early vein materials. This is in effect a subtype of the crustiform quartz texture.
- 3) **Colloform quartz texture:** this is a characteristic feature of chalcedonic aggregates in fine rhythmic bands. In such a texture, the mineral surfaces combine to assume spherical, botryoidal, reniform and mamillary outlines. This texture was originally described by Rogers (1917).
- 4) **Moss quartz texture:** this term is used to describe the heterogenous turbid appearance of some silica aggregates which is similar to moss vegetation. It is possible for samples displaying moss quartz texture to graduate to colloform quartz texture. This texture was originally described as a «**micro-botryoidal gel structure**» (Adams, 1920).
- 5) **Comb quartz texture:** this term is used to describe the development of parallel or subparallel quartz crystals which are oriented perpendicular to vein walls – such an image resembles the teeth of a comb. The free ends of the crystals are most commonly euhedral. This structure was first recognised by Adams (1920) and then described further by Boyle (1959).
- 6) **Zonal quartz texture:** this texture is created when there are alternating clear and milky quartz zones, within individual quartz crystals. The milky zones are usually full of solid or milky inclusions.
- 7) **Mosaic quartz texture:** in this case the quartz crystals exhibit irregular and interpenetrating grain boundaries. Macroscopically this results in a vitreous and tightly packed appearance. Lovering (1972) described a similar texture, which he

- termed «**jigsaw texture**», and which is sometimes observed in epithermal deposits, according to Saunders (1990).
- 8) **Feathery quartz texture**: this texture can be observed under the microscope, using crossed polars. Quartz exhibiting this texture will have a splintery or feathery appearance, seen only as slight optical differences in maximum extinction positions. Adams (1920) described this texture first and Sander & Black (1988) have called it **plumose quartz texture**.
 - 9) **Flamboyant quartz texture**: another texture originally described by Adams (1920), this term is used to describe the radial or flamboyant extinction of individual quartz crystals with a more or less rounded crystal outline. This is another example of a quartz texture recognisable only microscopically.
 - 10) **Ghost sphere quartz texture**: this term is used to describe the internal features of microcrystalline quartz, characterised by a lot of impurities. It is sometimes considered as a special case of moss quartz texture, albeit it is only visible under the microscope.
 - 11) **Pseudobladed quartz texture**: in this texture, aggregates of quartz or chalcedony may be arranged in a platy or bladed form. The aggregates of quartz blades can assume different forms, so this texture exhibits the following subdivisions:
 - ❖ **Lattice bladed quartz texture**: this texture was first reported by Schrader (1912), who termed it «**pseudomorphic lamellar platy quartz**». Macroscopically, it appears as a network of intersecting silica blades with polyhedral cavities, partly filled with comb quartz crystals, can be discerned.
 - ❖ **Ghost bladed quartz texture**: in this case quartz blades, distinguished by concentrations of impurities, can be identified and there are no cavities between individual blades.
 - ❖ **Parallel bladed quartz texture**: in this case there are silica blades parallel within a group but different groups may have different orientations. The outline of the groups defines a roughly granular pattern in hand specimens.
 - 12) **Pseudoacicular quartz texture**: this texture was first described by Lindgren & Bancroft (1914), and, macroscopically, comprises aggregates of silica minerals – commonly associated with adularia or its weathering products (kaolinite and sericite) – displaying a radial acicular appearance. Under the microscope, linear arrangements of fine grained quartz crystals, and adularia, sericite or kaolinite can be observed.

It must be specified that the term «**texture**» is used to describe the general physical appearance of a rock and the mutual relations among its component minerals. On the other hand, the term «**structure**» relates to the larger features of a rock. So, it may be more fitting to say crustiform stucture instead of crustiform texture. However, colloform and comb can be used both as term to describe both texture and structure. So, the two terms can be used interchangeably, and in many cases textural features may parallel structural ones.

As the aforementioned classifications are based on several parametres, a specimen can be described using different structural terms by employing different criteria. In most cases it is best to described all textures observed in a sample.

VI.1: ORIGINS OF QUARTZ TEXTURES

The interpretation of the origin of quartz textures is a complicated subject, since it requires an exact knowledge of the solubilities of silica minerals and of the various kinetic processes⁴⁵. These processes have not been entirely understood in theory, let alone in the context of a complex hydrothermal environment. From a genetic point of view, quartz textures can be classified as follows (Dong *et al.*, 1999):

- **Primary growth textures:** these textures represent the morphologies formed during crystal growth or the deposition of amorphous silica. As proven by Buchanan (1981), the processes of cooling, mixing of two fluids, reactions between wall rocks and fluids, and boiling can lead to the formation of simple crustiform bands. More complex crustiform bands are caused by episodic pressure release (Buchanan, 1981). Adams (1920) proposed that hydrothermal brecciation precedes the formation of the cockade texture, as minerals form around rock fragments. For the creation of colloform and moss textures, Rogers (1917) and Adams (1920) proposed the precipitation of silica gel in free space, where the controlling factor is surface tension (Adamson, 1960). An alternative procedure is the segregation of impurities by recrystallisation from silica gel (Adams, 1920; Oehler, 1976). Comb texture is most probably created by efficient geometrical selection (Grigor'ev, 1961). Finally, zonal texture is created by a slightly saturated hydrothermal fluid with respect to quartz and more or less stable crystallisation conditions.
- **Recrystallisation textures:** these textures result from the recrystallisation of chalcedony or amorphous silica to quartz. With the exception of quartz, all silica minerals after deposition are metastable and show a tendency to convert to quartz. Feathery textures are created by epiaxial growth of quartz (Rimstidt & Cole, 1983), which requires the presence of large quartz crystals acting as nucleation centres. The final appearance of a feathery texture is controlled by the mutual relationships between small crystals and the host crystals (Dong *et al.*, 1995). Flamboyant textures are most likely created by fibrous aggregates of fibrous chalcedony with rounded external surfaces, originating from a silica gel. The recrystallisation of amorphous silica or chalcedony with a moss texture most probably results in a ghost sphere texture. According to Lovering (1972) the recrystallisation of massive chalcedony or amorphous silica can result in the creation of a mosaic texture.
- **Replacement textures:** these textures represent partial or complete pseudomorphs of other minerals by silica minerals within veins. Pseudobladed calcite and barite are the most common soluble phases that may be replaced by quartz in epithermal veins. The impurities of these minerals are preserved after their replacement⁴⁶ and most often define the original crystal outlines. As noted by Adams (1920) the most frequent plane along which replacement proceeds, is that of the lamellar parting, a prominent feature of pinacoid calcite crystals. This selective replacement yields a parallel bladed

⁴⁵ These kinetic processes are polymerisation, coagulation, nucleation, crystallisation, dissolution and recrystallisation.

⁴⁶ This preservation of impurities can be attributed to their low solubility.

texture, which has an overall granular outline. Variations of the parallel bladed texture are caused by the difference in the crystallographic orientations of the initial crystals, or variations in the replacement process. The saccharoidal texture is the result of the replacement of calcite, as noted by Lindgren (1901), Adams (1920) and Lovering (1972), proceeding along the randomly distributed crystallographic defects, instead of the lamellar partings. In some cases it is possible to observe remnants of the original calcite crystals in saccharoidal textures.

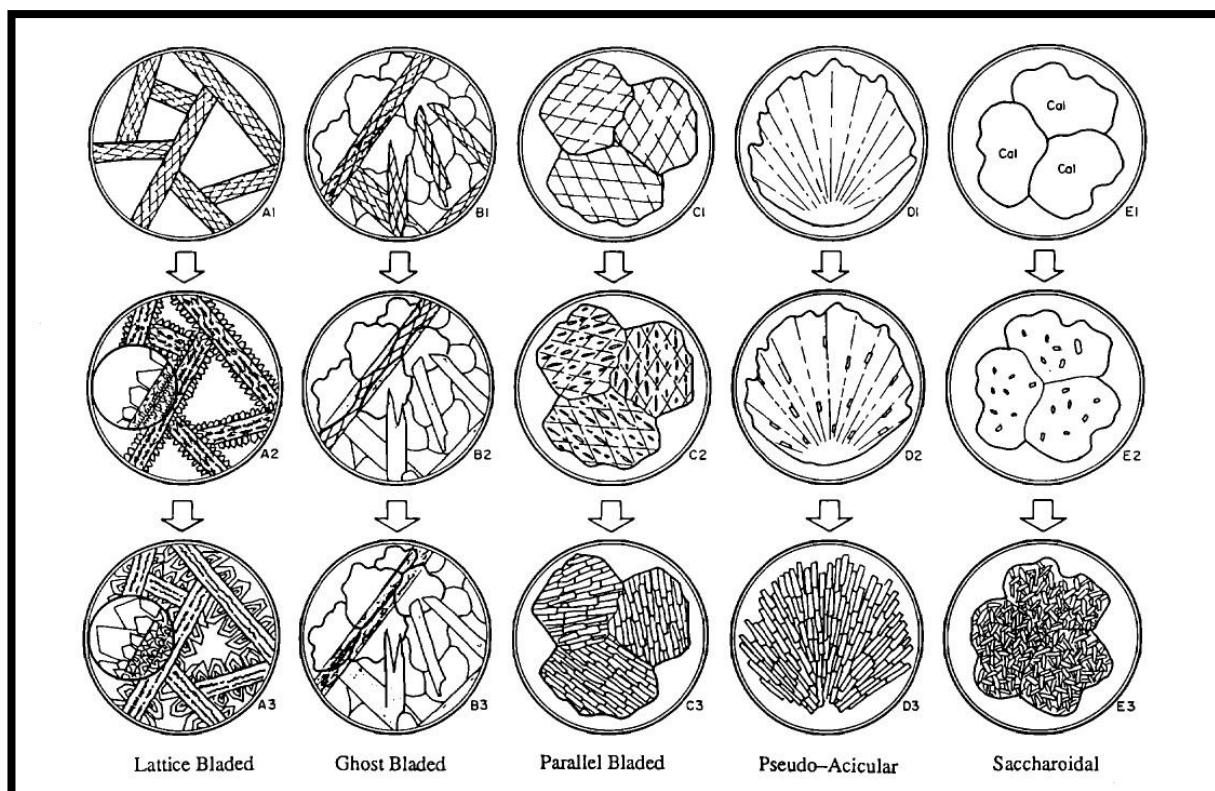


Figure VI.1: Interpretation of stages in the formation of various replacement quartz textures. The top row represents original forms of calcite. The middle row shows initial stage of replacement of calcite by quartz. The bottom row shows various quartz textures, formed after complete replacement of calcite (from Dong *et al.*, 1999).

Of the quartz textures described above, most of them fit into one of these categories. In the table of the next page (Table VI.1), the classification of quartz textures along with the proposed theories about their genesis are presented.

VI.2: IMPLICATIONS OF THE PRESENCE OF SPECIFIC QUARTZ TEXTURES

The most conspicuous textures in epithermal veins are those which indicate the presence of a silica gel precursor. Such textures are the flamboyant, ghost sphere, moss, colloform and pseudoacicular textures.

For silica gel to form, the hydrothermal fluid must be supersaturated with respect to amorphous silica. Fluid and silica gel equilibrium can be readily achieved in low temperatures. One way to achieve such an equilibrium is for a hydrothermal fluid to ascend fast enough so as to avoid silica precipitation during the ascend.

Table VI.1: Classification of Epithermal Quartz Textures

Texture Classification	Texture Type	Genesis	References
Primary growth textures	Crustiform texture	Formation of simple crustiform bands by cooling, two fluid mixing, wall and fluid reaction and boiling. Alternatively, formation of complex crustiform bands can be attributed to «episodic pressure release»	Buchanan (1981)
	Cockade texture	Hydrothermal brecciation and subsequent deposition of silica minerals around newly formed fragments	Adams (1920)
	Colloform texture	Precipitation of silica gel in free space, controlled by surface tension or segregation of impurities by crystallisation from a silica gel – this second process involves a very slow rate of impurity diffusion. The slight difference between the two textures may be attributed to initial differences on the occurrence of crystallisation nuclei.	Rogers (1917); Adams (1920); Oehler (1976)
	Moss texture		
	Comb texture	Effective geometrical selection between adjacent crystals. Directions of crystallisation perpendicular to the maximum rate of growth are preferred. Relative stable conditions during crystal growth are required.	Grigor'ev (1961)
	Zonal texture	Confined to quartz crystals growing directly from hydrothermal fluid. The hydrothermal fluid must be only slightly saturated in silica. Relatively stable crystallisation conditions are required.	Dong <i>et al.</i> (1995)
Recrystallisation textures	Feathery texture	Epiaxial growth of quartz and subsequent recrystallisation in approximate crystallographic continuity. Final appearance of the texture controlled by relation of small secondary crystals and the host crystal	Rimstidt & Cole (1983)
	Flamboyant texture	Aggregates of fibrous chalcedony with rounded surfaces, originating from a silica gel. Recrystallised materials follow the crystallographic direction of these chalcedony spheroids nuclei, microcrystalline quartz with radiating extinction is formed.	Dong <i>et al.</i> (1995)
	Ghost sphere texture	Recrystallisation of amorphous silica or chalcedony with a moss texture with preservation of initial spherically distributed impurities.	Dong <i>et al.</i> (1995)
	Mosaic texture	Recrystallisation of massive chalcedony or amorphous silica	Lovering (1972)
Replacement textures	Pseudobladed texture	Replacement of carbonate minerals by quartz and preservation of the original impurities of calcite. The replacement takes place along the lamellar parting of the basal pinacoid carbonate crystals.	Adams (1920)
	Saccharoidal texture	Replacement of calcite along randomly distributed crystallographic defects and not along the lamellar partings.	Lindgren (1901); Adams (1920); Lovering (1972)

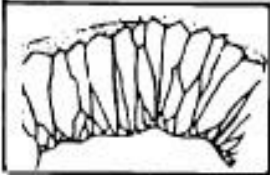
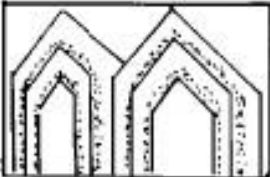
Texture Type	Sketch of Texture	Grain Size	Grain Form	Internal Feature of Individual Crystal	Morphology of Crystal Aggregate
Primary Growth Textures					
Massive		variable	anhedral	not applicable	homogenous
Crustiform		variable	variable	not applicable	successive banding
<u>Cockade</u>		variable	variable	not applicable	concentric banding
Colloform		fine	fibrous anhedral	not applicable	semi-spherical, reniform, mammillary
Moss		fine	variable	not applicable	spherical
Comb		variable	prismatic	not applicable	parallel-orientated
Zonal		variable	prismatic	zonal	not applicable

Figure VI.2: Schematic representation of the primary quartz textures in epithermal systems, along with their particular morphological characteristics (from Dong *et al.*, 1999).

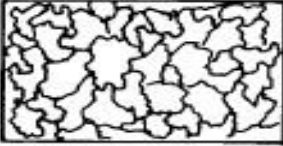
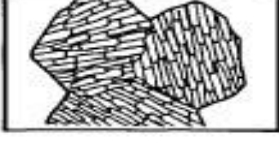
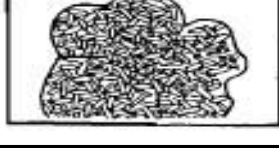
Texture Type	Sketch of Texture	Grain Size	Grain Form	Internal Feature of Individual Crystal	Morphology of Crystal Aggregate
Recrystallization Textures					
Mosaic		fine	anhedral	not applicable	interpenetrating
Feathery		variable	prismatic	plumose	not applicable
Flamboyant		variable	round	radial	not applicable
Ghost-sphere		fine	anhedral	spherical	not applicable
Replacement Textures					
<u>Pseudo-bladed</u> <u>Lattice-bladed</u>		fine	anhedral to prismatic	not applicable	intersecting bladed
<u>Ghost-bladed</u>		fine	anhedral	not applicable	intersecting bladed
<u>Parallel-bladed</u>		fine	anhedral to rectangular	not applicable	parallel bladed
Pseudo-acicular		fine	anhedral to rectangular	not applicable	acicular
Saccharoidal		fine	anhedral to prismatic	not applicable	interlocking

Figure VI.3: Schematic representation of the recrystallisation and replacement quartz textures in epithermal systems, along with their particular morphological characteristics (from Dong *et al.*, 1999).

Conversely, at relatively high temperatures the fluid can be made supersaturated in amorphous silica when it incurs adiabatic expansion, after boiling. This results in loss of water from the vapour phase and consequent increase in silica in the residual solution.

It is equally important to identify carbonate minerals in epithermal veins. According to Ellis (1959) calcite becomes soluble with decreasing temperature and increasing $p\text{CO}_2$. So it is possible for calcite to be dissolved or precipitated, depending on the boiling pressure, fluid components and temperature conditions. It is also important to know if the system is considered and open or a closed one.

Calcite can precipitate alone if the fluid becomes supersaturated with respect to calcite but undersaturated with respect to quartz. Then calcite is gradually replaced by silica minerals forming lattice bladed, parallel bladed or saccharoidal textures, depending on the morphology of carbonate precursors and the development of cleavages and fractures.

According to Bobis *et al.* (1995) and Worsley (1995) the textures associated with a silica gel precursor are widely distributed in mineralised epithermal systems. It is possible that the conditions favourable for the formation of silica gel also favour the precipitation of Au and other such ore metals. Another explanation was promulgated by Lindgren (1936) and Frondel (1938), who proposed that Au may be transported as colloidal particles, protected by colloidal silica. The two theories are not mutually exclusive.

APPENDIX VII: DETERMINATION OF MOLYBDENITES' CRYSTAL STRUCTURE AND DETAILS ON POLYTYPISM

VII.1: DETERMINATION OF MOLYBDENITE'S CRYSTAL STRUCTURE

A thorough investigation of molybdenite's crystal structure was performed by Dickinson & Pauling (1923), using X ray spectral photographs and Laue photographs⁴⁷. When assigning indices to Laue spots the structural unit containing only one MoS₂ molecule gave impossible values of $(n \cdot \lambda)$ while such values were not observed for the structural unit containing 2 MoS₂ molecules. Therefore, this is considered the smallest possible structural unit.

In the crystal structure proposed by Dickinson & Pauling (1923), each sulfur atom is equidistant from three molybdenum atoms and each molybdenum atom is surrounded by six equidistant sulfur atoms, at the corners of a small triangular prism, whose altitude is $3.17 \pm 0.10 \text{ \AA}$ and whose edge is $3.15 \pm 0.02 \text{ \AA}$. Then it can be calculated that the distance between the molybdenum atom and the nearest sulfur atoms is $2.41 \pm 0.06 \text{ \AA}$. This is consistent with the atomic radii of Mo (1.36 \AA) and S (1.05 \AA) as given by Bragg (1920). However, other sulfur atoms are at a distance of 3.49 \AA , while constant radii require 2.10 \AA .

So, according to the aforementioned, the structure of molybdenite contains 2 MoS₂ molecules in a hexagonal unit, having $d_{0001} = 12.30$ and an axial ratio of 3.90. The molybdenum atoms are at $\left(\frac{1}{3} \frac{3}{4} \frac{1}{4}\right) \left(\frac{2}{3} \frac{1}{3} \frac{3}{4}\right)$ and the sulfur atoms are at $\left(\frac{1}{3} \frac{2}{3} u\right) \left(\frac{2}{3} \frac{1}{3} \bar{u}\right) \left(\frac{1}{3} \frac{2}{3} \frac{1}{2} + u\right) \left(\frac{2}{3} \frac{1}{3} \frac{1}{2} - u\right)$ where $u = 0.621 \pm 0.004$ (Dickinson & Pauling, 1923). It must be mentioned that these data correspond to the 2H polytype (Figures VII.1) – polytypism was not recognised at the time (Figure VII.2).

VII.2: POLYTYPISM IN MOLYBDENITE

Despite extensive studies it is still not easy to ascertain the precise reasons for the existence of polytypes in nature. Trigunayat (1971) has proposed that the phenomenon can most probably be attributed to dislocation and growth processes as well as to differences in energies of different stacking sequences.

In the specific case of molybdenite, Clark (1970) has suggested the existence of a stoichiometric dissimilarity between the two polytypes, while polytypism has also been attributed to the existence of different trace element contents. Various authors have proposed other explanations, such as differences in formation pressures, formation temperatures or cooling rates during crystallisation (Chukhrov *et al.*, 1968).

⁴⁷ A Laue photograph taken with the incident beam normal to the basal plane possessed a hexagonal axis and six symmetry planes. Several photographs were made with the beam somewhat inclined to this position (Dickinson & Pauling, 1923).

The assumption of Clark (1970), that 3R molybdenite is present only in «exotic» low fS_2 environments, was disproven by Frondel & Wickman (1970), who demonstrated that 3R molybdenite exists in numerous deposits worldwide.

There is yet another question to be resolved. Since some studies (Clark, 1970; Hasan 1971) mention that 3R molybdenite is sulfur deficient – about 1 to 5 wt. % – and as such this polytype might be an indicator of low sulfidation states. If this assertion is proven correct then it is most likely that 2H, which is the most abundant, is transported by intermediate to high sulfidation mechanisms (Newberry, 1979a).

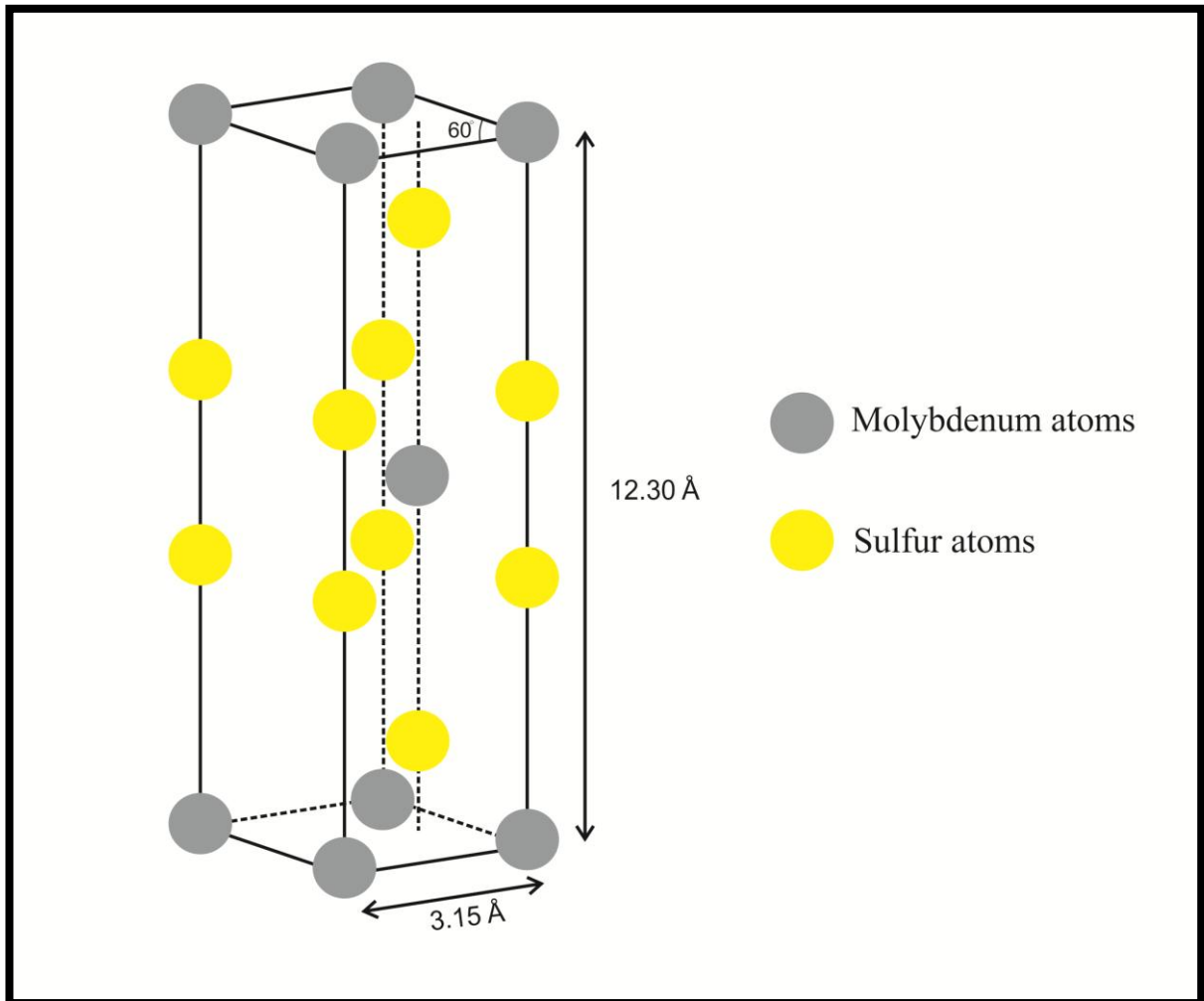


Figure VII.1: A schematic representation of the arrangement of atoms in a molybdenite crystal. This is the structure of the 2H polytype as polytypism was recognised after the first crystallographical study of molybdenite (after Dickinson & Pauling, 1923).

VII.2.1: Polytypism and Sulfidation States

Despite the existence of some studies correlating different polytypes' sulfur contents, as mentioned above, their conclusion is not verified by studies of the composition of both polytypes on a worldwide scale. Indeed, both polytypes have been reported with compositions ranging between 39.9 (Seebach, 1926) to 40.4 wt. % S (Zelikman *et al.*, 1961).

According to Newberry (1979a) literature data suggest that there is no quantifiable correlation between 3R/2H occurrences and the sulfidation states of the associated minerals, which would be necessary in order to corroborate the conclusions of Clark (1970) and Hasan (1971).

On the contrary, 3R molybdenite has been reported from low sulfidation (Petruk, 1964), intermediate sulfidation (Hasan, 1971) and high sulfidation environments (Znamenskiy *et al.*, 1969). The same applies to the 2H polytype (Newberry, 1979a), and it is essential to note that within the same specimen, both polytypes frequently coexist. The suggestion of Wildervanck & Jellinek (1964) that grain size is related to polytype abundance is not supported by any data.

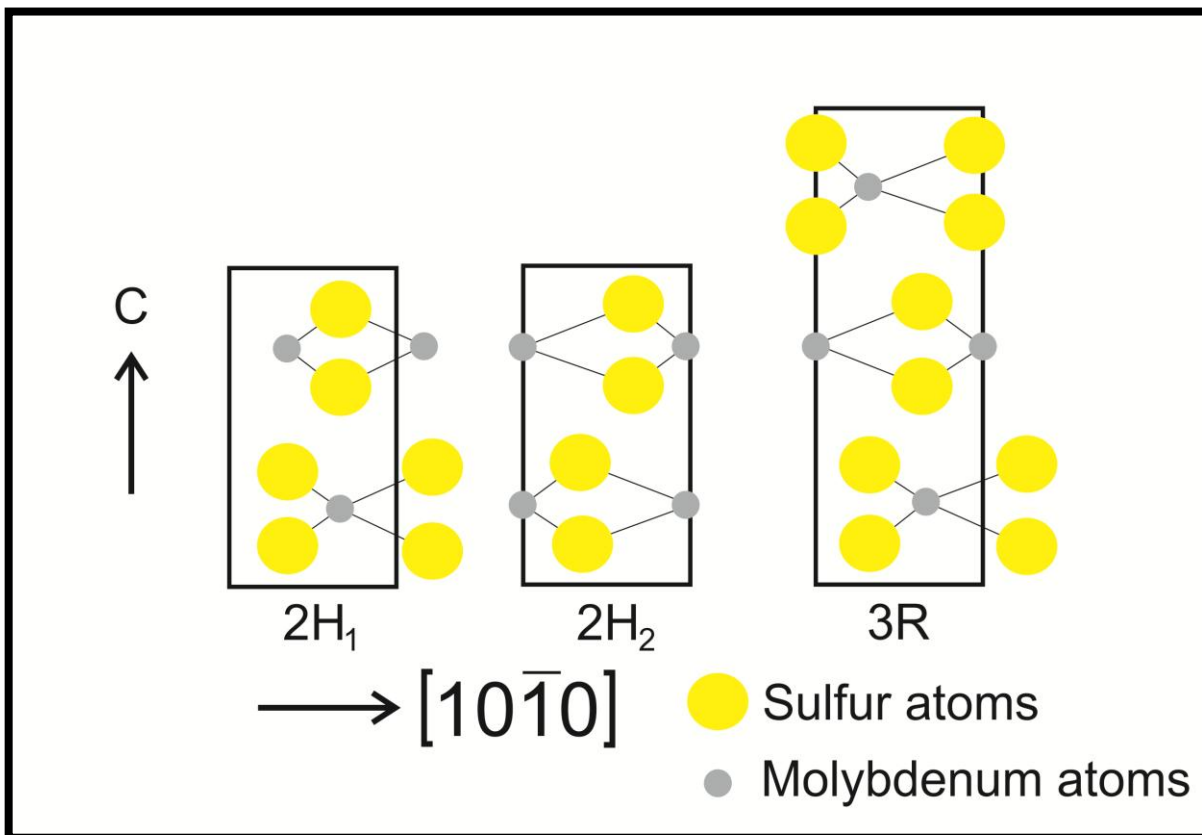


Figure VII.2: A schematic representation of the crystal structure of the two molybdenite polytypes. The 2H polytype is comprised of two different «types» of crystal structures, with slight differences. For the purposes of this study, no distinction between 2H₁ and 2H₂ polytypes is made. Instead they are referred to collectively as 2H polytypes (after Newberry, 1979a).

VII.2.2: Synthesis Studies of Molybdenite

According to the data published by Bell & Herfert (1957), it is possible to synthesise both polytypes. Also, Wildervanck & Jellinek (1964) have proven that the prolonged heating of 3R molybdenites, in temperatures greater than 500° C, results in their conversion to 2H molybdenites.

As is to be expected, lower temperatures – but still higher than the threshold of 500 ° C – will result in more prolonged conversion times (Clark, 1970). Zelikman *et al.* (1976) have

proven that the conversion of 3R to 2H can be accelerated and made more complete, in the presence of sulfur gas, and that the only possible mechanism for such a conversion is recrystallisation. There are two experimental procedures for molybdenite synthesis:

- Reaction of molybdenum with sulfur vapour or liquid sulfur, which results, most often, in a mixture of 2H and 3R polytypes (Newberry, 1979a). It is obvious that such a result contradicts the assumption that the 3R polytype forms only in comparatively sulfur-poor environments. However, as mentioned by Zelikman *et al.* (1976), the availability of sulfur affects the growth mechanisms of molybdenite formed at metal and sulfur interfaces.
- Reaction between MoS₂ and sulfur, which results in 2H molybdenite, while if there is an alkali carbonate flux present, the result is 3R molybdenite (Newberry, 1979a).

It must be mentioned, that according to Zelikman *et al.* (1961) the addition of an impurity, most notably Re, in molybdenite, affects the 2H to 3R conversion reaction. To summarise, it is evident from experimental results that the 3R polytype is unstable relative to 2H, under geologically common P-T conditions, which, according to Newberry (1979a) implies that polytypism is affected principally by growth processes and minimally, if at all, by equilibrium processes.

VII.2.3: Polytypism in Relation to the Structural Energy of the Crystal Lattice

The detailed examination of the geometry of the crystal structure of both polytypes indicates that, in a given S-Mo-S layer, the Mo ions can either be directly above and below of S ions of adjacent layers, or slightly offset.

It is obvious that in the first case, where ions are placed in a straight line so to speak, bonding should be stronger. Indeed, this theoretical assumption is corroborated by experimental data and the 2H polytype, which is harder and energetically more stable⁴⁸, relative to 3R, is of this configuration.

So, the weaker layer to layer bonding of the 3R polytype is the reason for its lower stability and consequent existence in nature. It must be stressed however that the 3R polytype does not adhere completely to the theoretical opposite geometry of the 2H polytype, as mentioned above. In effect, between three adjacent S-Mo-S layers, not both sulfur ions can be offset with respect to the molybdenum ion of the central layer (Newberry, 1979a).

VII.2.4: Polytypism and Crystal Growth Mechanisms

According to the research by Zelikman *et al.* (1976) it is most probable that the 3R polytype occurs due to a growth phenomenon accompanied by the lack of subsequent re-equilibration. Indeed, according to the same research there are differences between the growth mechanisms of the two polytypes but these cannot be yet quantified. A previous research (Jellinek, 1963) has considered the differences in orientation of successive S-Mo-S layers, concluding that 3R

⁴⁸ This is indicated by the exciton spectra of molybdenite, studied by Wilson & Yoffe (1969).

molybdenite forms by screw dislocation growth, a mechanism considered impossible for the 2H polytype.

VII.2.5: Polytypism in Relation to the Presence of Impurities

In nature, there are a lot of different trace elements which can be found as impurities in most minerals. Variations in the impurity content of a given mineral can be attributed to the following factors (Newberry, 1979a):

- Availability of impurity elements in the hydrothermal system
- Availability of impurities with the correct oxidation state in the hydrothermal system
- Sufficient insolubility of the impurity elements at the time of the mineral's deposition

In the specific case of molybdenite, the most common impurities are the elements Re, Sn, Ti, Bi⁴⁹ and W⁵⁰. All of these elements form sulfides, whose crystal structure comprises S-M-S layers, where M is any of the aforementioned metals (Table VII.1).

All of the aforementioned elements are of approximately the correct size, electronegativity and charge, to fit into the molybdenite structure, albeit with some strain⁵¹, as these parameters are roughly the same, but not identical with those of Mo.

Table VII.1: Structural and Chemical Parameters of MS_n Layer Sulfides

Chemical Formula	Mineral	M-S Coordination	Structure	M-S bond length (Å)	Metal electronegativity	Metal ion charge
MoS ₂	Molybdenite	Trigonal prismatic	Layer	2.42	1.8	4+
WS ₂	Tungstenite	Trigonal prismatic	Layer	2.41	1.7	4+
ReS ₂	Rheniite	Distorted octahedral	Layer	2.28-2.56	1.9	4+
TiS ₂	-	Octahedral	Layer	2.43	1.5	4+
SnS ₂	Berndtite	Octahedral	Layer	2.52	1.8	4+
Bi ₂ S ₃	Bismuthinite	Square prismatic	Layered ribbons	2.56-3.05	1.9	3+

Table modified after Newberry (1979a)

VII.2.6: Polytypism and Recrystallisation

It has been already mentioned that high temperature recrystallisation is the paramount mechanism for the 3R to 2H conversion. This fact is attributed to the high amount of energy required for the rotation and translation of the S-Mo-S layers. The moving of these layers in particular requires the highest amount of energy due to the significant bonding between them. Furthermore, there is a strong electromagnetic repulsion between adjacent S ions which are forced to come in close contact, albeit temporally, during the moving of layers. For these

⁴⁹ According to various researchers (Petruk, 1964; Mandarino & Gait, 1970; Ayres, 1974) bismuth and bismuthinite are associated many times with 3R molybdenite.

⁵⁰ In some high titanium deposits, Ti bearing molybdenites have been reported.

⁵¹ The amount of strain depends on the particular element. For example, between equal amounts of W and Al, the former causes much more strain (Newberry, 1979a).

reasons, the conversion of the 3R to the 2H polytype is particularly difficult⁵² and 3R molybdenites will be metastably maintained if the energy sufficient for their conversion is not available. This process will be also hindered by the presence of impurities⁵³.

⁵² This process is more difficult than in other polytypes, where there are simple displacive mechanisms (Newberry, 1979a).

⁵³ This, however, does not mean that recrystallisation is impossible and this is the reason why many 2H polytypes are characterised by high levels of impurities.

APPENDIX VIII: MOLYBDENITE IN GREEK ORE DEPOSITS

Molybdenite has been found in many porphyry style deposits and prospects in Greece (Table VIII.1). Re enrichment in molybdenite was observed in several cases (Voudouris *et al.*, 2013a), including Skouries in Chalkidiki (average of 900 gr/t), Sardes and Fakos in Limnos Island (average of 3785 gr/t and 1396 gr/t respectively) and Stypsi in Lesvos Island (average of 2460 gr/t). The cases of Re enriched molybdenite are summed up in the following table (Table VIII.1) and presented in Figure VIII.1.

Table VIII.1: Major Molybdenite Bearing Greek Ore Deposits and Prospects

Deposit/ Prospect	System Description	Molybdenite Localisation	References
Porphyry Mo-Cu and Cu-Au deposits			
Pagoni Rachi/Kirki	This Mo-Cu-Te-Ag-Au prospect is genetically related to an Oligocene dacite porphyry stock.	Molybdenite-rheniite-pyrite-bearing quartz stockworks which are related to the sericitic alteration of the intrusion	Arikas (1981); Voudouris <i>et al.</i> (2009, 2013b)
Konos/Sapes	In this area there are two mineralising events, which are genetically related to a microdiorite and a granite porphyry.	Molybdenite is found in veins, surrounded by rheniite, lead oxides and native Sn	Voudouris <i>et al.</i> (2006); Orтели <i>et al.</i> (2009); Orтели (2009)
Myli/Esymi	This is a Cu-Mo prospect quite similar to that of Pagoni Rachi, related to a dacite porphyry stock. Molybdenite-pyrite bearing quartz stockwork is related to sericite-carbonate alteration of the dacite.	Molybdenite is found as laths surrounding pyrite	Arikas (1985)
Ktismata/Maronia	There is a microgranite porphyry body nearby, to which this Cu-Mo mineralisation is genetically related. This body intrudes the Middle Oligocene shoshonitic intrusive complex of Maronia.	Molybdenite occurs within quartz stockworks crosscutting sericitically altered microgranite and is associated with pyrite, chalcopyrite, base metal sulfides and sulfosalts	Papadopoulou (2002); Melfos <i>et al.</i> (2002)
Melitena	This is a Mo porphyry prospect, hosted within a Tertiary intrusion of dacitic composition. The main ore and paragenetic ore minerals are pyrite, pyrrotite, sericite, pyrophyllite, diaspore and A-phosphate-sulfate minerals	Molybdenite forms disseminations and fissure fillings and is associated with quartz veinlets crosscutting the sericitic altered porphyry body.	Michailidis <i>et al.</i> (1993); Melfos <i>et al.</i> (2001)
Stypsi/Lesvos Island	This a porphyry Cu-Mo prospect, overprinted by a IS epithermal system. It is hosted by a high K-calc alkaline microgranite porphyry	Grey to black silica veinlets contain pyrite, chalcopyrite, bismuthinite, molybdenite and galena	Voudouris & Alfieris (2005); Periferakis (2014); Periferakis <i>et al.</i> (2017); present study
Sardes & Fakos/Limnos Island	The Sardes and Fakos prospects are telescoped porphyry-epithermal systems	Molybdenite occurs within a stockwork of quartz + pyrite veinlets, crosscutting sericite-tourmaline altered monzonite and sedimentary rocks and overprinting earlier K-silicate alteration	Voudouris & Alfieris (2005)
Skouries/Chalkidiki	This is a porphyry Cu-Au-Pd deposit, hosted by a least four monzonite porphyry phases	Molybdenite occurs in late pyrite veinlets related to sericite-carbonate alteration of the porphyry stocks	Eliopoulos & Economou-Eliopoulos (1991); Kroll <i>et al.</i> (2002); Frei (1995)
Reduced Intrusion-Related Mo-W Deposits			
Kimmeria/Xanthi	This is an intrusion-related polymetallic system, which crosscut sericite-carbonate altered granodiorite and skarn ores, with pyrite, chalcopyrite, pyrrotite and magneite	Molybdenite is found along with the other ore minerals	Walenta & Pantartzis (1969); Vavelidis <i>et al.</i> (1990)
Plaka/Lavrion	This polymetallic deposit consists of pyrite, molybdenite, chalcopyrite and pyrrotite	Molybdenite is found in veins and stockwork, crosscutting the Plaka granodiorite	Bonsall <i>et al.</i> (2007); Voudouris <i>et al.</i> (2008)

Pigi/Axiopolis	This deposit is related to the Upper Jurassic Fanos pluton. The ore minerals are wolframite, pyrite and galena	Molybdenite is found within the leucogranite as disseminations	Marakis & Skounakis (1992); Michailidis <i>et al.</i> (1993)
Seriphos Island	There is an undeformed leucogranite in the Southern part of the Island	Molybdenite occurs together with pyrite as disseminations and fracture fillings within the fresh host rock	Voudouris <i>et al.</i> (2010)
Shear Zone-Related Cu-Au-Bi-Mo Mineralisation			
Stanos/Chalkidiki	This mineralisation is emplaced within a shear zone hosted in two mica gneisses of the Serbomacedonian massif. The gneisses bear evidence of strong mylonitisation and Fe-K alteration, with muscovite, biotite and siderite	Molybdenite can be found in the second stage of mineralisation, along with associated chalcopyrite, galena, and Bi-Au-Te minerals. This stage was contemporaneous with lower amphibolite and/or greenschist metamorphism	Voudouris & Sakellaris (2008)
Table data after Voudouris <i>et al.</i> (2013a)			

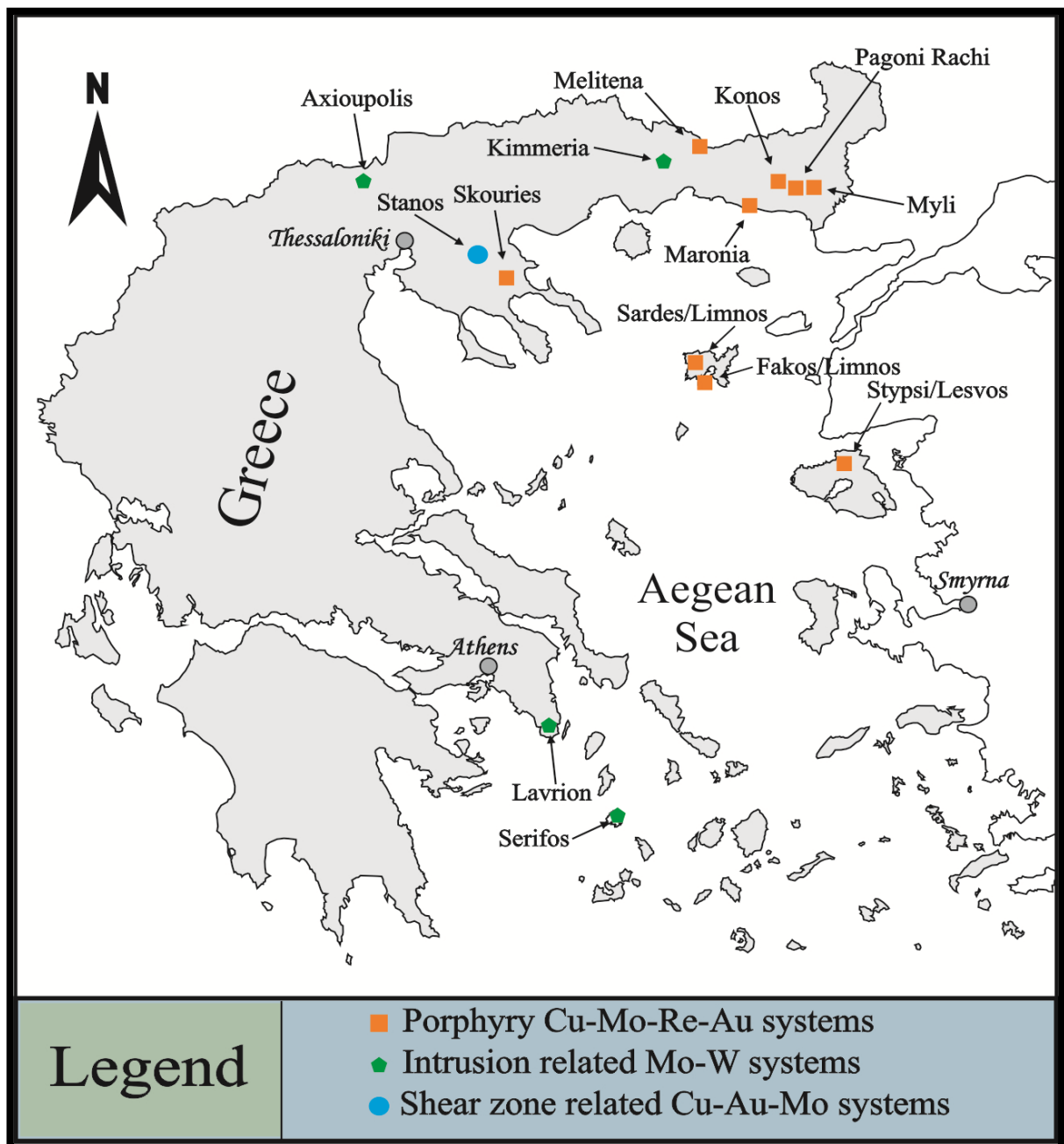


Figure VIII.1: A schematic map of Greece, where all the molybdenite occurrences are presented, according to deposit type and location (from Voudouris *et al.*, 2013a).

The structural analysis, of four molybdenite crystals, with the highest Re content ever reported in nature, showed that Re actually enters the molybdenite structure as an isovalent substituent for Mo. This observation is corroborated by the progressive shortening of the Mo-S bond distance, as well as by the decrease of the unit cell values with the increase of Re (Voudouris *et al.*, 2009). It can be concluded that the heterogeneity with up to 4.7 wt % Re in molybdenite is the result of a solid solution (Voudouris *et al.*, 2013a), thus expanding on the results of Drábek *et al.* (1993). Inversely, pure rheniite and Mo-rich rheniite, with up to 6 wt % Mo occurs at Pagoni Rachi and Konos porphyry systems (Voudouris *et al.*, 2009; 2010). However, these Re values are much lower than those from molybdenite in porphyry deposits, in NE Greece (Voudouris *et al.*, 2010; 2013b).

The strong variation in the Re concentration of molybdenite grains has been a subject of many studies (Stein *et al.*, 2001; Kosler *et al.*, 2003; Selby & Creaser, 2001; Selby *et al.*, 2004; Grabezhev & Shagalov, 2010). On the basis of their Re content, four molybdenite categories in Greece can be distinguished (Table VIII.2).

Table VIII.2: Molybdenite Categories According to Rhenium Content in Greek Ore Deposits				
Molybdenite Type	Re Content			Molybdenite Location
	Re_{min}	Re_{max}	$\overline{\text{Re}}$	
Re free molybdenite	—	—	—	Stanos/Chalkidiki
Very low Re-molybdenite	10	1310	206	Lavrion
Intermediate to high Re-molybdenite	300	10600	2302	Stypsi, Sardes, Fakos, Skouries, Myli
Ultra-high Re-molybdenite	379	46900	13182	Pagoni Rachi, Konos/Sapes, Melitena, Maronia
Table data after Voudouris <i>et al.</i> (2013a)				

APPENDIX IX: THE ALPINE OROGENY

The development of the **Plate Tectonics Theory** was of prime importance in understanding the dynamic processes which shaped the Earth's crust and in explaining adequately the formation of mountain ranges, volcanoes, islands and other geological features. The basic principles of this theory⁵⁴ can be stated as follows (Dewey *et al.*, 1973):

- The lithospheric shell of the Earth consists of a number of torsionally rigid plates, each being in motion, in relation to adjacent plates.
- Most tectonic activity results from extension, compression or strike slip motions, which are the three basic types of motion. Accordingly, boundaries between tectonic plates are defined as **divergent plate boundaries**, **convergent plate boundaries** and **transform plate boundaries**.
- Seafloor spreading (plate accretion) occurs at extensional boundaries and results in the formation of oceanic crust and mantle. The purely strike-slip boundaries are considered as **transform faults**. Finally, convergent plate boundaries result in three types of tectonic features:
 - ❖ Simple trench-island arc systems, such as the Aleutians and the Tonga-Kermadec island arc.
 - ❖ More complex trench-volcanic arc continental margin systems, such as the Peru-Chile trench and the landward complex of the Andes.
 - ❖ Compressional interaction between two continental portions of plates, such as the India-Asia collision which produced the Himalayan orogeny.

IX.1: THE ALPINE OROGENY

From early works (Argand, 1916; Heim, 1919; Staub, 1924) it was suggested that the creation of the **Alpine orogeny** was some kind of compressional motion between Asia and Europe. However, despite the early identification of the cause of this orogeny and the development of the Plate Tectonics Theory, there were, until relatively recently, two main problems, hindering the analysis of the mechanism of the Alpine orogeny (Dewey *et al.*, 1973).

At first, the geological history of the drift of the Atlantic was not known and, as a result, it was not possible to determine the pattern of relative motion between Europe and Asia. Additionally, in the general area of the Alpine orogeny, there are numerous microplates, each having different relative motions to each other (McKenzie, 1970).

⁵⁴ It is beyond the scope of this study to present the details and the complete chronology of the development of the Plate Tectonics Theory. The first publications regarding this Theory were made by Wegener (1912, 1920). For a modern approach and detailed explanation of this Theory the reader is referred to McKenzie (1970) and Smith (1971).

As Dewey *et al.* (1973) have deduced there was never one single plate boundary, between Europe and Africa. It is more probable that there was a network of convergent, divergent and transform boundaries.

The interpretation of the Alpine orogeny, using a single plate boundary, as made by Smith (1971) was not adequate, as it could not explain the existence of all the geological features. However, even if it is impossible to explain the orogeny using a single plate boundary, it is also difficult to work out the original position of the microplates. It must also be mentioned that many of the tectonic zones of the Alpine orogenic system are terminated by transform faults, which means that not all of these zones are interconnected.

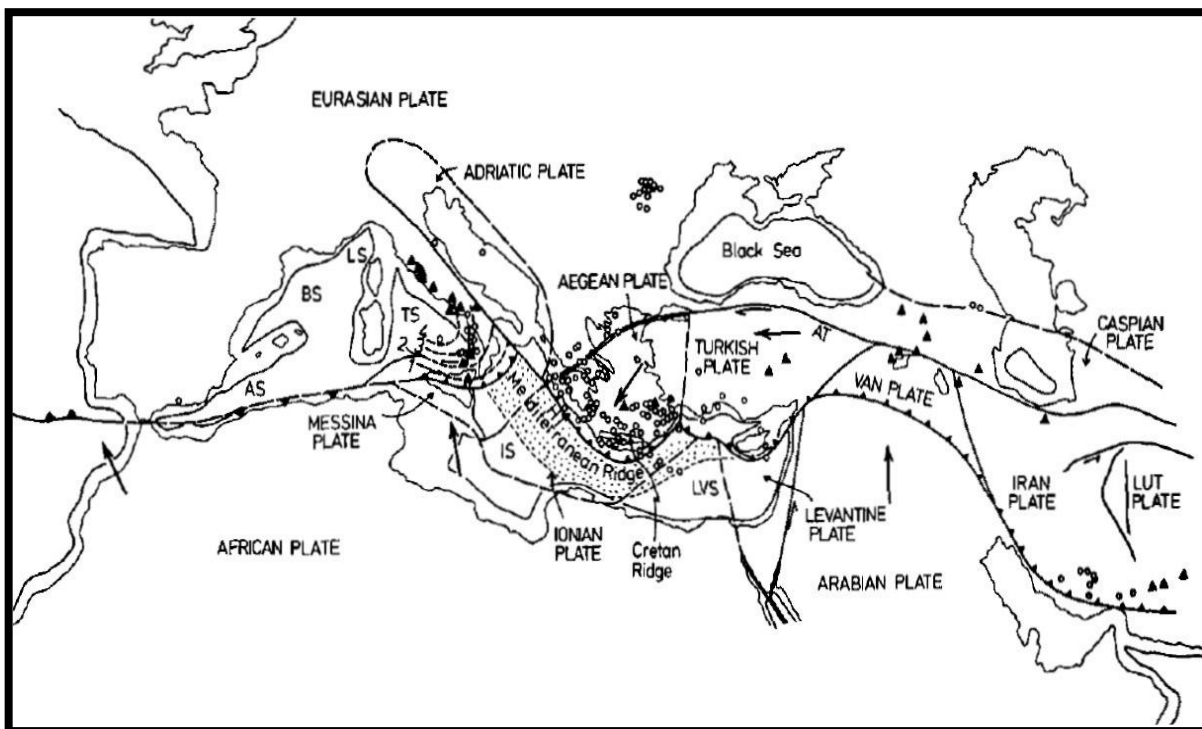


Figure IX.1: The neotectonic regime of the Alpine System where the major active microplates are presented, based mainly on Bogdanoff *et al.* (1964), Choubert (1968), Stöcklin (1968), McKenzie (1970) and Ryan *et al.* (1971). Key to symbols: triangles: volcanoes of Quaternary and Holocene age; circles: epicentres of earthquakes deeper than 100 Km; arrows: slip directions of plates with respect to the Eurasian plate; dashed lines: contours on Benioff zone in hundreds of kilometres. Key to abbreviations: AS: Alboran Sea; AT: Anatolian Transform; BS: Balearic Sea; HT: Hellenic Trench; IS: Ionian Sea; LS: Ligurian Sea; LVS: Levantine Sea; TS: Tyrrhenian Sea (from Dewey *et al.*, 1973).

It is possible to identify active plates (Figure IX.1) by the seismic activity at their margins, and inactive plates by the presence of suture zones. It is even possible to discern smaller plates welded together to form larger ones, using palaeomagnetism or other methods (Dewey *et al.*, 1973). In any case, regardless of the number of microplates, the dominant motion between Eurasia and Africa, has been continuously compressive since 180 my ago (Figure IX.2).

To determine the palaeogeographic position of a microplate it is possible to utilise facies similarities – between two or more microplates – and palaeomagnetic pole position determination. A characteristic example is that of Sardinia and Corsica, which, during the

Miocene, were rifted from Southern France and rotated into their present position. However, this is a relatively easy case, as ample palaeomagnetic data as well as data on facies similarities with other microplates exist. A more complicated problem is that of the Rhodope Massif, where different theories have been proposed, due to the absence of any conclusive facies similarities and relevant palaeomagnetic data. The criteria for determining microplates' motion are the determination of the original and final position of each microplate – the former being always speculative – and the type, age and length of relative motion between microplates and/or major plates. It is also possible, for a microcontinental fragment to be lifted out of a margin characterised by compressive motion (Dewey *et al.*, 1973).

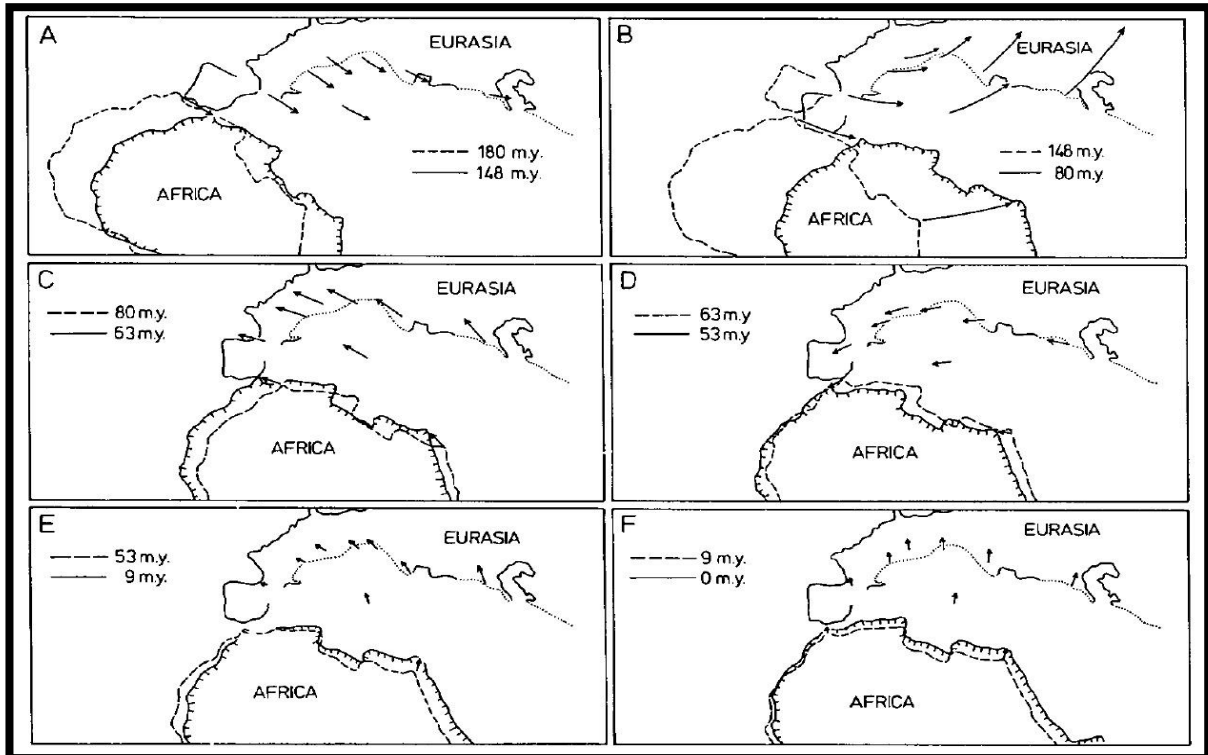


Figure IX.2: A representation of the position of Africa relative to Europe, at 180 my, 148 my, 80 my, 63 my, 53 my, 9 my and present. In A through F, the dashed and hachured lines are the outline of Africa, taken as present-day shoreline, before and after the continents rotation, as determined by palaeomagnetic data. The arrows are finite slip vectors representing the simplest path Africa could have taken to move from its position, relative to Europe, at 180 my, to successive positions at 148 my, 80 my and so on (from Dewey *et al.*, 1973).

IX.2: THE MOUNTAIN BELT OF THE EUROPEAN ALPS

The **European Alps** comprise a mountain chain (Figure IX.3) which stretches from Nice to Vienna, with elevations almost as high as 5000 m. The highest peak is that of Mont Blanc, whose elevation is 4807 m. The predominant feature of the Alpine mountain range is the granite belt, from the Pelvoux Massif in France to the High Tauern in Austria. The Alpine belt is characterised by many valleys, some of which run parallel to the mountains (Figures IX.4 and IX.5). The Molasse Basin, which is the North Alpine foreland basin, occupies the North side of the Alps, and was filled by sediments, transported by rivers, between 34 and 10 my ago. The rivers draining the Alps to the South transported sediments to the Po Basin. Both of these basins formed during the building of the Alpine mountains (Pfiffner, 2005).

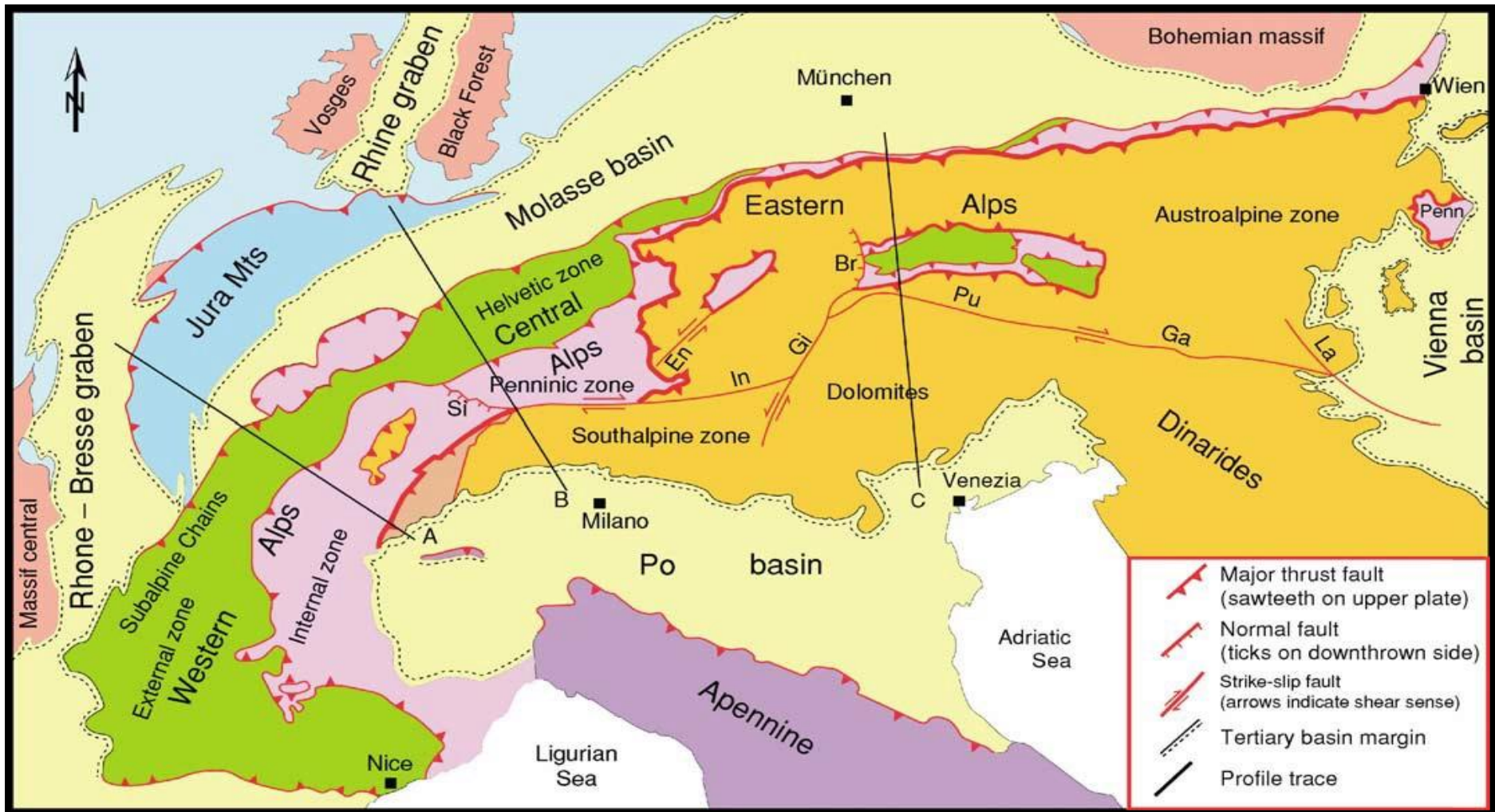


Figure IX.4: A modern tectonic map of the Western and Central Alps, showing the major tectonic units. Site A, B and C correlate to the corresponding transects in Figure IX.5. Key to abbreviations of fault names: Br: Brenner; Si: Simplon; En: Engadine; In: Insubric; Gi: Giudicarie; Pu: Pustertal; Ga: Gailtal; La: Lavanttal (from Pfiffner, 2005).

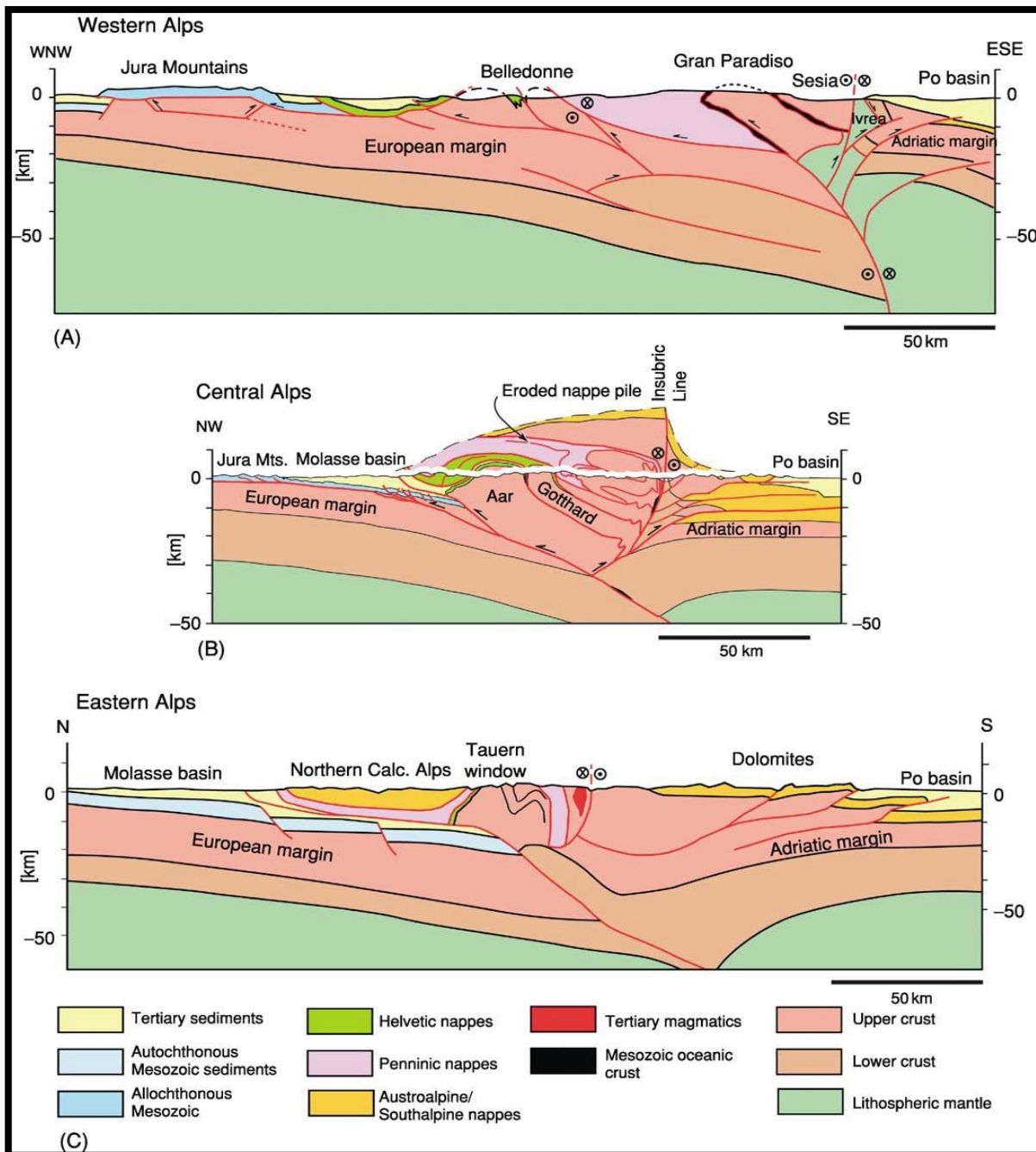


Figure IX.5: Three profiles through the Alpine Mountain Range, illustrating the deep structure of the orogen. The profile sites A, B and C, are those shown in Figure IX.4. (a) Transect through the Western Alps of France and Italy. (b) Transect through the Central Alps of Switzerland and Italy. (c) Transect through the Eastern Alps of Austria and Italy (from Pfiffner, 2005).

The shallow seas which exist in the Mediterranean region were formed when the weight of the mountain chain caused the concave bending of the tectonic plates. The detailed study of the accumulated sediments has revealed that the erosion⁵⁵ of the growing chain was roughly equalised by the vertical uplift⁵⁶.

⁵⁵ In fact, about 35 Km of rocks are calculated to have been eroded from the Alpine mountains (Pfiffner, 2005).

⁵⁶ Practically, this fact means it is unlikely that the Alpine mountains ever reached significantly higher elevations, compared to their modern ones.

It is well established that before 100 my ago, the Eurasian and African Continents were separated by ocean basins. The subsequent approach of these plates closed the ocean basins and resulted in their ultimate collision. It is then to be expected that the rock suites in modern day Alps may belong to the Eurasian margin, or to the African margin, or to an ocean basin situated between them, before their convergence. For example the Helvetic zone, Jura Mountains and the areas to the North and the West of the Alps belong to the former European margin of the Eurasian plate. On the other hand, the Austroalpine and Southalpine zones are parts of the former Adriatic margin of the African plate (Pfiffner, 2005).

IX.2.1: Rock Types of the Alpine Geological Setting

When describing the Alpine geology, the rocks are firstly classified according to their relative ages. The oldest rocks are called the **prealpine basement**. This petrologic group comprises two major units, the crystalline rock unit and the Palaeozoic sequence⁵⁷. The highest peaks of the Alps are mostly covered by granites, which are resistant to erosion.

So, in essence, rocks in the area of the Alps are divided between those older than the opening of the Piemonte and Valais basins and those contemporary or younger than them. The younger rocks of the Alps are of Mesozoic and Cenozoic age, ranging from 225 to 10 my ago.

Of particular note in the Alpine geologic setting are the carbonate rocks, which often form high cliffs. In general, large quantities of carbonates formed along the continental margins, which were shallow seas. The carbonates reach sometimes 1 Km in thickness. In the continental slopes, sandstones and shales formed, and the extensive faulting in some areas lead to breccias accumulating at the foot of the steep fault scarps. The basalts of the oceanic crust were gradually covered by radiolarian cherts (Pfiffner, 2005).

IX.2.2: The Alpine Nappes

In the collision zone, between the two continents, there was extensive folding and fracturing of the rocks. The large scale compressional forces lead to the development of thrust faults, which resulted in the transport of crustal blocks upwards on fault surfaces of low incline. Those displaced blocks are called **nappes**. Most often they have a length of about 50 to 100 Km, a width of several hundred kilometres and a thickness of a few kilometres. Besides the presence of nappes, a prominent feature of the deformation characteristic in Alpine rocks is the presence of faults from millimetre to kilometre scale.

Inside the nappes themselves there can also be significant internal deformation. Of course, the type of deformation depends upon the nature and mechanical characteristics of the rocks involved. Folds are a common enough feature in sedimentary sequences while if there are mechanically weak layers, thrust faults may develop inside a nappe. The existence of a type of deformation does not preclude the existence of others inside the same nappe (Pfiffner, 2005).

⁵⁷ The crystalline rocks unit comprises granites and gneisses and schists, while the Palaeozoics unit comprises volcanic and sedimentary rocks, formed between 300 and 400 my ago.

IX.2.3: The Creation of the Alpine Mountain Range

One of the first realisations of geologists in the Alps was that the observed oceanic sediments were created within the Mountain Range, and were subsequently juxtaposed with continental rocks. A cardinal feature of the Alpine geology was the creation of the Piemont Ocean, initiated by the divergent motion between Eurasia and Africa. All the stages of the Alpine orogeny correspond to different phases of relative movements between those two continents. Obviously, all ocean basins between the plates were closed due to their convergence. The Piemont Ocean closed in the Cretaceous (~ 100 my ago) and the Valais Ocean closed in the Tertiary (~ 35 my ago). This closure also involved, besides compression, strike-slip movements between the European and Adriatic margins.

During the Cretaceous, the general direction of convergence was East and West, and the European margin was approaching the Adriatic one, where there existed a pre-Alpine mountain range. At this stage, as mentioned above, the Piemont Ocean had already been subducted. There occurred then a process known as «**underplating**». Small fragments of the descending plate were scrapped off and attached to the upper plate. The Briançonnais microcontinent, which was then being subducted, has also some of its parts being scrapped off (Pfiffner, 2005).

The next major phase of the Alpine orogeny started at about 40 my ago, with the change of the convergence's direction to a N-S orientation. As a result, the Valais Ocean disappeared into a South-dipping subduction zone, with some underplating taking place. At 35 my ago, the collision between the two margins happened. In the Central and Eastern Alps⁵⁸, the margins were compressed and there was a stacking of crustal pieces, resulting in horizontal shortening and vertical stretching.

Finally, the deformation of the two continental margins pushed crustal fragments in greater elevations, through thrust faults, and parts of the orogen were uplifted through extensive large scale folding and vertical stretching. The whole land surface of the ancestral Alps was uplifted, and the high elevations caused in turn precipitation and increased rate of erosion. Rivers with extensive fan deltas gradually formed. Deep crustal fragments were in the process revealed, due to erosion, and rocks lying tens of kilometres deep were exposed to the surface. Thus came about the modern day geodynamic setting of the Alps (Pfiffner, 2005).

⁵⁸ The Western Alps, where there was already an older mountain range, were characterised by strike-slip movements at this stage.

APPENDIX X: TECTONICS OF THE CENTRAL AND EASTERN MEDITERRANEAN REGION

Before the introduction of the Theory of Plate Tectonics, many researchers had tried to interpret the Alpine orogeny, using the pre-plate geosynclinal models⁵⁹. However, due to the intrinsic shortcomings of the geosynclinal models, such attempts were always characterised by their inability to fully interpret all geologic features.

In the special case of the Eastern Mediterranean the Plate Tectonics Model was first applied by McKenzie (1972, 1978) and Le Pichon & Angelier (1979). Additionally, the Tethys Project, by the International Correlation Geological Project (ICGP), was a major promoter of the elucidation of the area's palaeogeography.

Regarding the Tethys, the original interpretation was that of an ocean dating from the Triassic time, bordered by the African and European continents. The ophiolites of Mesozoic age were believed to have formed at mid-ocean ridges, and it was believed that the Tethyan Ocean was subducted northwards beneath Eurasia. However, other models were later proposed (Robertson & Mountrakis, 2006). Smith *et al.* (1975) and Smith (1993) considered that the ophiolite belt of western Greece was separate from the ophiolite belt from further East. In addition to that, the distribution of ophiolites within Turkey suggested the presence of Mesozoic ocean basins (Figure X.1).

Sengör & Yilmaz (1981) proposed another model for Turkey which mentioned the interaction of several microcontinents and small ocean basins. Further works, such as the paper by Sengör (1984) introduced the term «**Palaeotethys**», referring to a Palaeozoic-Early Mesozoic ocean and «**Neotethys**», referring to a Jurassic ocean basin. In the same year, Robertson & Dixon (1984) combined the theory of microcontinents with the formation of many Mesozoic ophiolites in intra-oceanic subduction zones.

The most thorough and complete analysis of the geology of the Tethys was given by the ICGP No. 276, entitled «**Terrane Maps and Terrane Descriptions**». Of special importance in regional interpretations were the palaeomagnetic studies conducted by Morris & Tarling (1996). A major breakthrough in the elucidation of regional tectonic settings and relation between different such settings, was the realisation, made firstly in the South Aegean Region, was that tectonic contacts thought to be thrusts – related to nappe emplacement – were in reality extensional faults – which are called «**extensional detachments**» – related to Tethyan exhumation.

⁵⁹ Characteristic examples of such approaches are those of Suess (1875), Fuchs (1882) and Steinmann (1905).

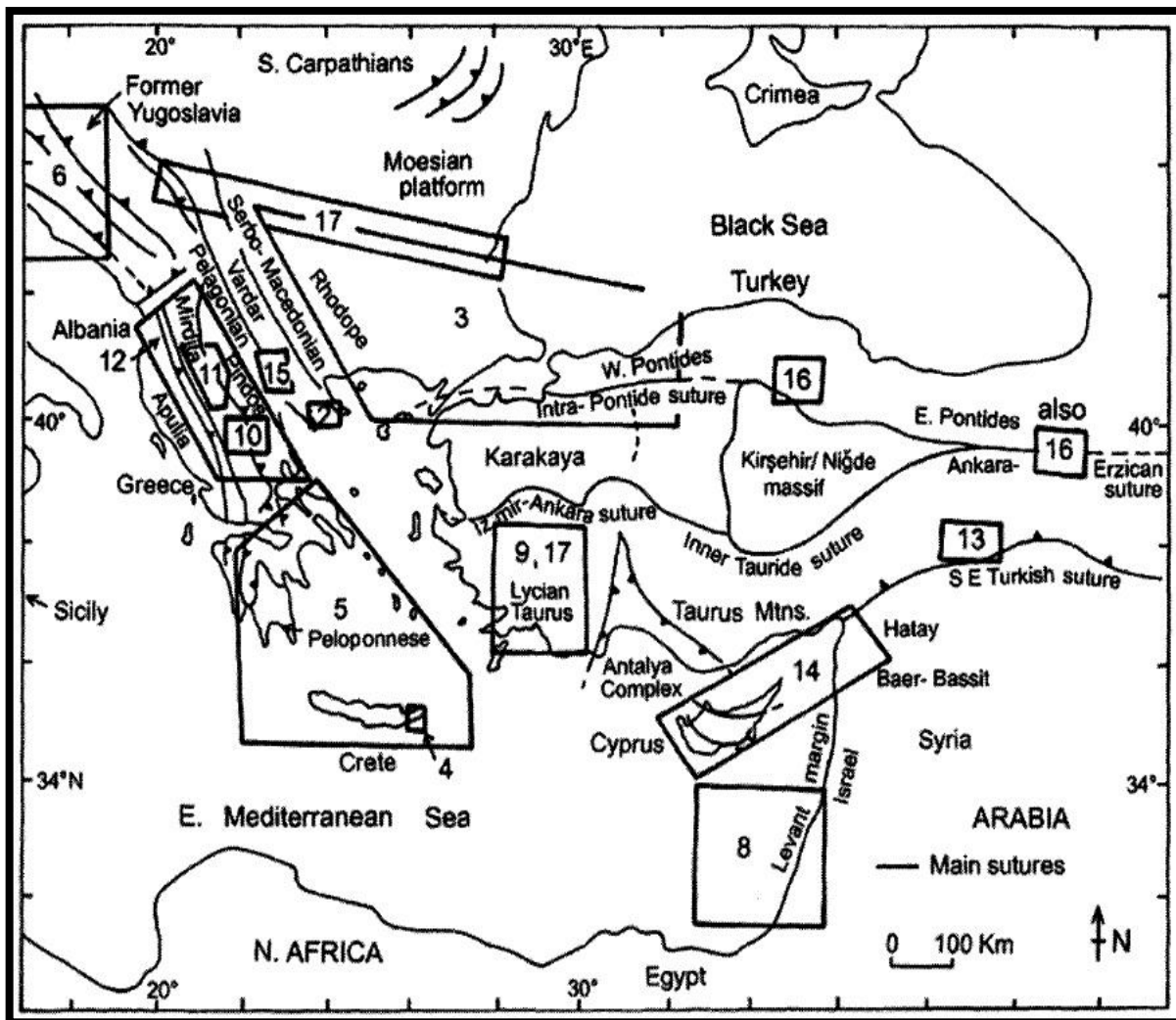


Figure X.1: Outline map delineating the main ophiolite suture zones, and showing the locations of studies concerned mainly with the Palaeozoic and Mesozoic development of the Eastern Mediterranean region. Key to numbers (each number corresponds to a study): 1: Smith (1993); 2: Himmerkus *et al.* (2006); 3: Yanev (2003); 4: Romano *et al.* (2006); 5: Robertson (2002); 6: Karamata (2006); 7: Kazmin & Tikhonova (2006); 8: Gardosh & Druckman (2006); 9: Danelian *et al.* (2006); 10: Rassios & Moores (2006); 11: Koller *et al.* (2006); 12: Garfunkel (2006); 13: Rizaoglu *et al.* (2006); 14: Morris *et al.* (2006); 15: Sharp & Robertson (1998); 16: Rice *et al.* (2006); 17: Rimmelé *et al.* (2006). Studies 1 to 7 cover the whole area (from Robertson & Mountrakis, 2006).

X.1: TECTONIC SETTING

In modern scientific literature (e.g. Kazmin & Tikhonova, 2006) the existence of the Palaeotethys Ocean is widely accepted. However, there is widespread disagreement, regarding the emergence and disappearance of this Ocean (Robertson & Mountrakis, 2006).

Yanev *et al.* (2003) and Karamata (2006) postulate that some of the extensive allochthonous terranes of Late Palaeozoic or earlier originated along the Northern margin of the Gondwana. These were later accreted to Eurasia, at different times. Some terranes containing igneous and/or metamorphic rocks – termed «**exotic terranes**» – are thought to have remained along the northern margin of the Gondwana along their entire history (Romano *et al.*, 2006; Karamata, 2006).

According to Smith (2006), Rassios & Moores (2006) and Garfunkel (2006), most Mesozoic ophiolites are believed to have formed above intra-subduction zones. Despite this conclusion, there is still an ongoing debate, since others believe that these ophiolites have formed in mid-ocean ridges. Robertson & Mountrakis (2006) mention that there is no consensus regarding subduction timing and the number of subduction zones. The progressive nature of continental collision does not allow for precise temporal and spatial constraints. The Upper Mesozoic-Early Cenozoic deep water basin can either represent intra-continental rifting or back-arc basins related to subduction, and as of yet there is no uniform opinion amongst researchers.

Miocene and recent tectonics are better understood (Figure X.2). Le Pichon & Angelier (1979) have deduced that a Tethyan Ocean in the South Aegean region (e.g. Ionian basin) was subducted northwards, accompanied by back arc extension, which affected the whole of the Aegean region and western Turkey. Mountrakis *et al.* (2006), Tranos *et al.* (2006) and Westaway (2006) have all found evidence of the existence of an extensional regime as far as Northern Greece and Bulgaria.

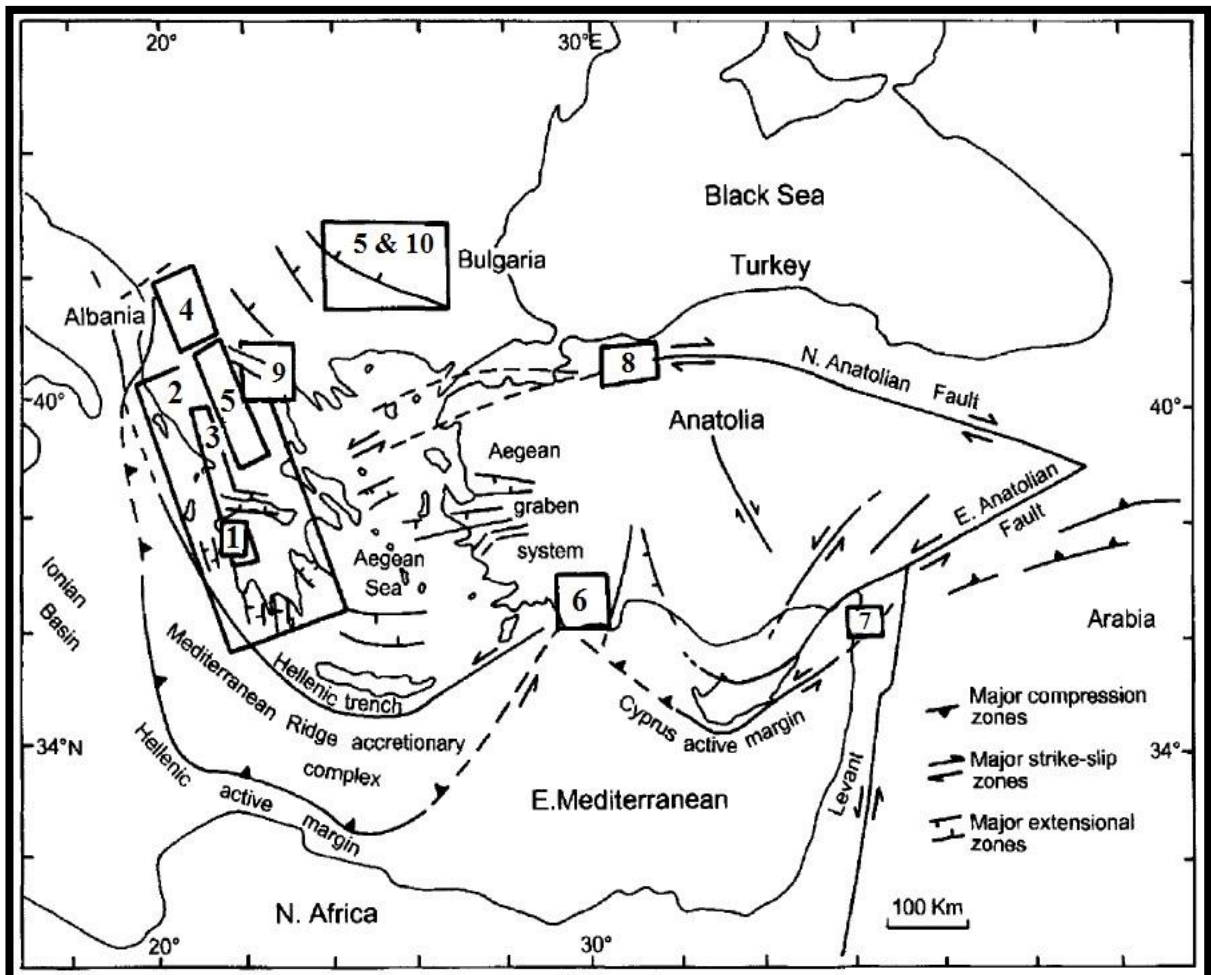


Figure X.2: Outline map delineating the main neotectonic features and presenting the locations of studies mainly concerning the Cenozoic-recent tectonic development of the Eastern Mediterranean region. Key to numbers (each number corresponds to a study): 1: Degan & Robertson (2006); 2: Doutsos *et al.* (1993); 3: Vamvaka *et al.* (2006); 4: Muceku *et al.* (2006); 5: Westaway (2006); 6: Alçiçek *et al.* (2006); 7: Boulton *et al.* (2006); 8: Pavlides *et al.* (2006); 9: Mountrakis *et al.* (2006); 10: Tranos *et al.* (2006). Papazachos *et al.* (2006) cover the whole area (from Robertson & Mountrakis, 2006).

X.2: TECTONIC RECONSTRUCTION

The palaeomagnetic studies by Morris & Tarling (1996) have shown that continental separation between Gondwana and Eurasia has evolved through time. However, as Robertson *et al.* (1996) attest there are many different theories for the placement and movements of each microplate relative to each other. The following are the predominant models:

- A model involving Northward extension for which many variations exist (Robertson *et al.*, 1991, 1996, 2004; Ricou, 1996).
- The model of the Southern Neotethyan basins as proposed by Sengör (1984).
- A model involving the final closure of back-arc basins in early Cenozoic time (Stampfli *et al.*, 2001; Stampfli & Borel, 2002).

The possible correlation of the Palaeotethys with the Hercynian orogeny was also proposed by Romano *et al.* (2006).

Robertson & Mountrakis (2006) summarised the modern reconstructions in a model of a continuous northward subduction of the African plate below the Southern margin of Eurasia, from the Late Cretaceous suture of the Tethys Ocean to the present situation. Such a tectonic regime has resulted in an abundance of HP-LT metamorphic rocks. Jolivet & Brun (2010) summarised the geologic development of these rocks, as occurring in the following stages:

- Subduction within the sinking plate
- First exhumation within the subduction channel
- Post-orogenic exhumation below low-angle normal faults in extensional metamorphic domes

The available tomographic models of Spakman *et al.* (1993) and Wortel & Spakman (2000) indicate that there indeed was one subduction zone, which was active through most of the Mesozoic and the entire Cenozoic. Of course, as Jolivet *et al.* (2003) such a model presupposes that there was an effective delamination process and a decoupling between the lower crust and the upper mantle, below the main decollement and the upper crust above it.

REFERENCES

- Adams S., 1920, *A microscopic study of vein quartz*, Economic Geology, vol. 15, issue 8, pp. 623-644.
- Adamson A., 1960, *Physical Chemistry of Surfaces*, John Wiley and Sons, New York.
- Albinson T., Norman D., Cole D., and Chomiak B., 2001, *Controls on formation of low-sulfidation epithermal deposits in Mexico: Constraints from fluid inclusion and stable isotope data*. In: Albinson T. & Nelson C. (Eds.), *New Mines and Discoveries in Mexico and Central America*, Society of Economic Geologists, Special Publication, No. 8, pp. 1-32.
- Alçıçek M., ten Veen J., and Özkul M., 2006, *Neotectonic development of the Çameli Basin, southwestern Anatolia, Turkey*. In: Robertson A. & Mountrakis D. (Eds.), *Tectonic Development of the Eastern Mediterranean Region*, Geological Society of London, Special Publication, No. 260, pp. 591-611.
- Alderton D. & Fallick A., 2000, *The nature and genesis of gold-silver-tellurium mineralization in the Metaliferi Mountains of western Romania*, Economic Geology, vol. 95, issue 3, pp. 495-516.
- Aleinikoff J., Creaser R., Lowers H., Magee Jr. C., and Grauch R., 2012, *Multiple age components in individual molybdenite grains*, Chemical Geology, vol. 300-301, pp. 55-60.
- Algeo T. & Lyons T., 2006, *Mo-total organic carbon covariation in modern anoxic marine environments: implications for analysis of paleoredox and paleohydrographic conditions*, Paleogeography and Paleoclimatology, vol. 21, issue 1, pp. 1-23.
- Aminzadeh B., Shahabpour J., and Maghami M., 2011, *Variation of rhenium contents in molybdenites from the Sar Cheshmeh porphyry Cu-Mo deposit in Iran*, Resource Geology, vol. 61, issue 3, pp. 290-295.
- Arancibia O. & Clark A., 1996, *Early magnetite-amphibole-plagioclase alteration-mineralization in the Island Copper porphyry copper-gold-molybdenum deposit, British Columbia*, Economic Geology, vol. 91, issue 2, pp. 402-438.
- Argand E., 1916, *Sur l' arc des Alpes occidentales*, Eclogae Geologicae Helveticae, vol. 14, issue 1, pp. 145-191. [in French]
- Arikas K. & Voudouris P., 1998, *Hydrothermal alterations and mineralizations of magmatic rocks in the southern Rhodope massif*, Acta Vulcanologica, vol. 10, pp. 353-365.
- Arikas K., 1981, *Subvolcanic hydrothermal Mo-Cu-Pb-Zn mineralization in S.E. Rhodopes, Northern Greece: petrology and geochemistry*, Tschermaks Petrographische und Mineralogische Mitteilungen, vol. 28, issue 3, pp. 189-205. [in German]
- Arikas K., 1985, *Hydrothermal alteration of subvolcanic rocks in Myli/ Esymi area: Mineralogy and geochemistry*, Internal Report, I.G.M.E. Xanthi Branch, Xanthi. [in Greek]
- Arnorrsson S. & Oskarsson N., 2007, *Molybdenum and tungsten in volcanic rocks and in surface and < 100 °C ground waters in Iceland*, Geochimica et Cosmochimica Acta, vol. 71, issue 2, pp. 284-304.
- Arribas Jr. A., 1995, *Characteristics of high-sulfidation epithermal deposits, and their relation to magmatic fluid*, Mineralogical Association of Canada, Short Course, No. 23, pp. 419-454.
- Arribas Jr. A., Cunningham C., Rytuba J., Rye R., Kelly W., Podwysocki M., McKee E., and Tosdal R., 1995, *Geology, geochronology, fluid inclusions, and isotope geochemistry of the Rodalquilar gold-silver deposit, Spain*, Economic Geology, issue 4, vol. 90, pp. 795-822.
- Ashleman J., Taylor C., and Smith P., 1997, *Porphyry molybdenum deposits of Alaska, with emphasis on the geology of the Quartz Hill deposit, southeastern Alaska*. In: Goldfarb R. & Miller L. (Eds.), *Mineral Deposits of Alaska*, Economic Geology, Monograph, No. 9, pp. 334-354.
- Ashley P., 1984, *Sodic granitoids and felsic gneisses associated with uranium-thorium mineralisation, Crocker's Well, South Australia*, Mineralium Deposita, vol. 19, issue 1, pp. 7-18.
- Atkinson Jr. W., Souviron A., Vehrs T., and Faunes G., 1996, *Geology and mineral zoning of the Los Pelambres porphyry copper deposit, Chile*. In: Camus F., Sillitoe R., and Petersen R., (Eds.). *Andean Copper Deposits: New Discoveries, Mineralization, Styles and Metallogeny*, Society of Economic Geologists, Special Publication, No. 5, pp. 131-156.
- Aubouin J., 1959, *Contribution à l' étude de la Grèce septentrionale: les confins de l' Epire et de la Thessalie*, Annales Geologiques des Pays Helleniques, vol. 1, pp. 1-484. [in French]

- Audétat A., 2010, *Source and evolution of molybdenum in the porphyry Mo(-Nb) deposit at Cape Peak, Texas*, *Journal of Petrology*, vol. 51, issue 8, pp. 1739-1760.
- Audétat A., Dolejš D., and Lowenstern J., 2011, *Molybdenite saturation in silicic magmas: occurrence and petrological implications*, *Journal of Petrology*, vol. 52, issue 5, pp. 891-904.
- Axen G., Taylor W., and Bartley J., 1993, *Space-time patterns and tectonic controls of Tertiary extension and magmatism in the Great Basin of the western United States*, *Geological Society of America Bulletin*, vol. 105, issue 1, pp. 56-76.
- Ayres D., 1974, *Distribution and occurrence of some naturally occurring polytypes of molybdenite in Australia and Papua New Guinea*, *Journal of the Geological Society of Australia*, vol. 21, issue 3, pp. 273-278.
- Ayres L., Averill S., and Wolfe W., 1982, *An Archean molybdenite occurrence of possible porphyry type at Setting Net Lake, northwestern Ontario, Canada*, *Economic Geology*, vol. 77, issue 5, pp. 1105-1119.
- Bailey D. & Hampton C., 1990, *Volatiles in alkaline magmas*, *Lithos*, vol. 26, issues 1-2, pp. 157-165.
- Ballard J., Palin J., Williams I., Campbell I., and Faunes A., 2001, *Two ages of porphyry intrusion resolved for the super-giant Chuquibambilla copper deposit of northern Chile by ELA-ICP-MS and SHRIMP*, *Geology*, vol. 29, issue 5, pp. 383-386.
- Barr S., Temperley S., and Tarney S., 1999, *Lateral growth of the continental crust through deep level subduction initiation of central Greek Rhodope*, *Lithos*, vol. 46, pp. 69-94.
- Barton Jr. P., 1970, *Sulfide petrology*, *Mineral Society of America*, Special Paper, No. 3, pp. 187-198.
- Barton Jr. P., Bethke P., and Roedder E., 1977, *Environment of ore deposition in the Creede mining district, San Juan Mountains, Colorado; Part III, Progress toward interpretation of the chemistry of the ore-forming environment*, *Economic Geology*, vol. 72, issue 1, pp. 1-24.
- Barton M., 2000, *Overview of the lithophile element-bearing magmatic-hydrothermal system at Birch Creek, White Mountains, California*. In: Dilles J., Barton M., Johnson D., Proffett M., Einaudi M., and Crafford E. (Eds.), Part I. Contrasting Styles of Intrusion-Associated Hydrothermal Systems: Part II. *Geology & Gold Deposits of the Getchell Region*, *Society of Economic Geologists, Guidebook Series*, vol. 32, p. 9-26.
- Barton M., Ilchik R., and Marikos M., 1991, *Metasomatism*, *Reviews in Mineralogy*, vol. 26, issue 1, pp. 321-350.
- Batchelor R. & Bowden P., 1985, *Petrogenetic interpretation of granitoid rock series using multicationic parameters*, *Chemical Geology*, vol. 48, issues 1-4, pp. 43-55.
- Bates T., 1989, *Bald Hill molybdenum prospect*. In: Kear D. (Ed.), *Mineral Deposits of New Zealand*, Australasian Institute of Mining and Metallurgy, Monograph, No. 13, pp. 137-138.
- Battles D. & Barton M., 1995, *Arc-related sodic hydrothermal alteration in the western United States*, *Geology*, vol. 23, issue 10, pp. 913-916.
- Beane R. & Titley S., 1981, *Porphyry copper deposits, Part II: Hydrothermal alteration and mineralization*, *Economic Geology*, 75th Anniversary Volume, pp. 236-269.
- Bell R. & Herfert R., 1957, *Preparation and characterization of a new crystalline form of molybdenum disulfide*, *Journal of the American Chemical Society*, vol. 79, issue 13, pp. 3351-3354.
- Berzina A., Sotnikov V., Economou-Eliopoulos M., and Eliopoulos D., 2005, *Distribution of rhenium in molybdenite from porphyry Cu-Mo and Mo-Cu deposits of Russia (Siberia) and Mongolia*, *Ore Geology Reviews*, vol. 26, issues 1-2, pp. 91-113.
- Bingen B. & Stein H., 2003, *Molybdenite Re-Os dating of biotite dehydration melting in the Rogaland high-temperature granulites, S.Norway*, *Earth and Planetary Science Letters*, vol. 208, issues 3-4, pp. 181-195.
- Bissig T., Clark A., Lee J., and Hodgson C., 2002, *Miocene landscape evolution and geomorphologic controls on epithermal processes in the El Indio-Pascua Au-Ag-Cu belt, Chile and Argentina*, *Economic Geology*, vol. 97, issue 5, pp. 971-996.
- Blevin P. & Chappell B., 1992, *The role of magma sources, oxidation states and fractionation in determining granite metallogeny of eastern Australia*, *Transactions of the Royal Society of Edinburgh on Earth Sciences*, vol. 83, issues 1-2, pp. 305-316.
- Blevin P., 2009, *The primacy of magma compositions in determining the Re and W contents of molybdenite*. In: Lentz D., Thorne K., and Beal K.L. (Eds.), *Proceedings of the 24th International Applied Geochemistry Symposium*, vol. 1, Fredericton, Canada, pp. 119-122.
- Bobis R., Morrison G., and Jaireth S., 1995, *Anatomy of a Carboniferous epithermal ore shoot at Pajingo, Queensland: setting, zoning, alteration, and*

- geochemistry, *Economic Geology*, vol. 90, issue 6, pp. 1776-1798.
- Bogdanoff A., Mouratov M., and Schatsky N., 1964, *Tectonique de l'Europe: notice explicative pour la carte tectonique internationale de l' Europe au 1:2.500.000*, Maison d'édition Nedra Moscow, Moscow. [in French]
- Bohnhoff M., Makris J., Papanikolaou D., and Stavrakakis G., 2001, *Crustal investigation of the Hellenic subduction zone using wide aperture seismic data*, *Tectonophysics*, vol. 343, issues 3-4, pp. 239-262.
- Bonev N., Burg J., and Ivanov Z., 2006a, *Mesozoic-Tertiary structural evolution of an extensional gneiss dome - the Kesebir-Kardamos dome, E. Rhodope, Bulgaria*, *International Journal of Earth Sciences*, vol. 95, issue 2, pp. 318-340.
- Bonev N., Marchev P., and Singer B., 2006b, $^{40}\text{Ar}/^{39}\text{Ar}$ geochronology constraints on the Middle Tertiary basement extensional exhumation, and its relation to ore-forming and magmatic processes in the Eastern Rhodope (Bulgaria), *Geodinamica Acta*, vol. 19, issue 5, pp. 265-280.
- Bonham Jr. H., 1969, *Geology and mineral deposits of Washoe and Storey Counties, Nevada, with a section on Industrial rock and mineral deposits by Papke K.*, Nevada Bureau of Mines and Geology, Bulletin, Nevada, USA, No. 70.
- Bonham Jr. H., 1988, *Models for volcanic-hosted precious metal deposits: A review*. In: Schafer R. & Cooper J., and Vikre P., (Eds.), *Bulk mineable precious metal deposits of the western United States*, Reno, Geological Society of Nevada, Reno, pp. 259-271.
- Bonsall T., Spry P., Voudouris P., St. Seymour K., Tombros S., and Melfos V., 2007, *Fluid inclusion and stable isotope characteristics of carbonate replacement Pb-Zn-Ag deposit in the Lavrion district, Greece*. In: Andrews C. (Ed.), *Mineral Exploration and Research: Digging Deeper*, Proceedings of the IX Biennial Meeting of the Society for Geology Applied to Mineral Deposits, Dublin, Ireland, 20th-23rd August 2007, Millpress Editions, Rotterdam, pp. 283-286.
- Boulton S., Robertson A., and Ünlügenç U., 2006, *Tectonic and sedimentary evolution of the Cenozoic Hatay Graben, Southern Turkey: a two-phase model for graben formation*. In: Robertson A. & Mountrakis D. (Eds.), *Tectonic Development of the Eastern Mediterranean Region*, Geological Society of London, Special Publication, No. 260, pp. 613-634.
- Bowman J., Parry W., Kropp W., and Krueger S., 1987, *Chemical and isotopic evolution of hydrothermal solutions at Bingham, Utah*, *Economic Geology*, vol. 82, issue 3, pp. 395-428.
- Boyle R.W., 1959, *The geochemistry of gold and its deposits*, Canada Geological Survey Bulletin, vol. 280.
- Boynton W.V., 1984, *Geochemistry of the rare earth elements: meteorite studies*. In: Henderson P. (Ed.), *Rare Earth Element Geochemistry*, Elsevier Publications, pp. 63-114.
- Bragg L., 1920, *The arrangement of atoms in crystals*, The London, Edinburgh, and Dublin Philosophical Magazine and Journal of Science, Series 6, vol. 40, issue 236, pp. 169-189.
- Brimhall Jr. G., 1977, *Early fracture-controlled disseminated mineralization at Butte, Montana*, *Economic Geology*, vol. 72, issue 1, pp. 384-409.
- Brimhall Jr. G., Agee C., and Stoffregen R., 1985, *The hydrothermal conversion of hornblende to biotite*, *Canadian Mineralogist*, vol. 23, issue 3, pp. 369-379.
- Brookins D., 1986, *Rhenium as analog for fissiogenic technetium: Eh-pH diagram (25° C, 1 bar) constraints*, *Applied Geochemistry*, vol. 1, issue 4, pp. 513-517.
- Brooks C., Engell J., Larsen L., and Pedersen A., 1982, *Mineralogy of the Werner Bjerger alkaline complex, East Greenland, Meddelelser om Grønland*, *Geoscience*, vol. 7, p. 1-35.
- Brun J.P. & Sokoutis D., 2007, *Kinematics of the Southern Rhodope Core Complex (North Greece)*, *International Journal of Earth Sciences*, volume 96, issue 6, pp. 1079-1099.
- Buchanan L., 1981, *Precious metal deposits associated with volcanic environments in the Southwest*. In: Dickinson W. & Payne W. (Eds.), *Relations of Tectonics to Ore Deposits in the Southern Cordillera*, Digest, Arizona Geological Society, vol. 14, Tucson, pp. 237-262.
- Burg J.P., Godfriaux I., and Ricou L.E., 1995, *Extension of the Mesozoic Rhodope thrust units in the Vertiskos-Kerdilion massifs (Northern Greece)*, *Comptes Rendus de l' Académie des Sciences, Paris*, vol. 320, pp. 889-896.
- Burke K. & Kidd W., 1980, *Volcanism on Earth through time*, Geological Association of Canada, Special Paper, No. 20, pp. 503-522.
- Burnham C. & Ohmoto H., 1980, *Late-stage processes of felsic magmatism*, *Mining Geology*, Special Issue No. 8, pp. 1-11.
- Burnham C., 1985, *Energy release in subvolcanic environments: implications for breccia formation*, *Economic Geology*, vol. 80, issue 6, pp. 1515-1522.

- Candela P. & Holland H., 1984, *The partitioning of copper and molybdenum between silicate melt and aqueous fluids*, *Geochimica et Cosmochimica Acta*, vol. 48, issue 2, pp. 373-380.
- Candela P. & Holland H., 1986, *A mass transfer model for copper and molybdenum in magmatic hydrothermal systems; the origin of porphyry-type ore deposits*, *Economic Geology*, vol. 81, issue 1, pp. 1-19.
- Candela P. & Piccoli P., 1995, *Model ore-metal partitioning from melts into vapor and vapor/brine mixtures*. In: Thompson J. (Ed.), *Magmas, Fluids and Ore Deposits*, Mineralogical Association of Canada Short Course, No. 23, pp. 101-128.
- Candela P. & Piccoli P., 2005, *Magmatic processes in the development of porphyry-type ore systems*, *Economic Geology 100th Anniversary Volume*, pp. 25-37.
- Candela P., 1989, *Magmatic ore-forming fluids: thermodynamic and mass transfer calculations of metal concentrations*. In: Whitney J. & Naldrett A. (Eds.), *Ore Deposits Associated with Magmas*, *Reviews in Economic Geology*, vol. 4, pp. 203-232.
- Candela P., 2004, *Ores in the earth's crust*. In: Holland H. & Turekian D. (Eds.), *Treatise on Geochemistry*, Elsevier Publications, Amsterdam, vol. 3, pp. 411-432.
- Capitant M., Francotte J., Picot P., and Troly G., 1963, *Hautes teneurs en rhénium dans une molybdénite de Kipushi*, *Comptes Rendus de l'Académie des Sciences*, Paris, vol. 257, issue 6, pp. 3443-3444. [in French]
- Carman G., 2003, *Geology, mineralization, and hydrothermal evolution of the Ladolam gold deposit, Lihir Island, Papua New Guinea*. In: Simmons S. & Graham I. (Eds.), *Volcanic, Geothermal, and Ore-Forming Fluids: Rulers and Witnesses of Processes within the Earth*, *Society of Economic Geologists, Special Publication*, vol. 10, pp. 247-284.
- Carson D. & Jambor J., 1974, *Mineralogy, zonal relationships and economic significance on hydrothermal alteration at porphyry copper deposits, Babine Lake area, British Columbia*, *Canadian Institute of Mining and Metallurgy Bulletin*, vol. 67, pp. 110-133.
- Carten R., 1986, *Sodium-calcium metasomatism: chemical, temporal, and spatial relationships at the Yerington, Nevada, porphyry copper deposit*, *Economic Geology*, vol. 81, issue 6, pp. 1495-1519.
- Carten R., Geraghty E., Walker B., and Shannon J., 1988, *Cyclic development of igneous features and their relationship to high-temperature hydrothermal features in the Henderson porphyry molybdenum deposit, Colorado*, *Economic Geology*, vol. 83, issue 2, pp. 266-296.
- Carten R., Walker B., Geraghty E., and Gunow A., 1988, *Comparison of field-based studies of the Henderson porphyry molybdenum deposit, with experimental and theoretical models of porphyry systems*, *Canadian Institute of Mining and Metallurgy, Special Volume, No. 39*, pp. 351-366.
- Carten R., White W., and Stein H., 1993, *High-grade granite-related molybdenum systems: classification and origin*. In: Kirkham R., Sinclair W., Thorpe R., and Duke J. (Eds.), *Mineral Deposit Modelling*, *Geological Association of Canada, Special Papers, No. 40*, pp. 521-554.
- Casselmann M., McMillan W., and Newman K., 1995, *Highland Valley porphyry copper deposits near Kamloops, British Columbia: a review and update with emphasis on the Valley deposit*, *Canadian Institute of Mining, Metallurgy and Petroleum Special Volume, No. 46*, pp. 161-191.
- Cathles L., 1981, *Fluid flow and genesis of hydrothermal ore deposits*, *Economic Geology, 75th Anniversary Volume*, pp. 424-457.
- Čech F., Rieder M., and Vrána S., 1973, *Drysdallite, MoSe₂, a new mineral*, *Neues Jahrbuch für Mineralogie, Monatshefte No. 10*, pp. 433-442.
- Chamot-Rooke N., Rangin C., Le Pichon X., Rabate A., Laurent O., Ego F., Lallemand S., Nielsen C., Pagot P., Tsang Hin Sun D., Walcott R., and Bousquet R., 2005, *DOTMED: Deep Offshore Tectonics of the Mediterranean. A synthesis of deep marine data in eastern Mediterranean*, *Mémoires de la Société Géologique de France*, vol. 177.
- Chappell B. & Stefens W., 1988, *Origin of I-type granites*, *Transactions of the Royal Society of Edinburgh on Earth Sciences*, vol. 79, pp. 71-86.
- Chappell B. & White A., 1974, *Two contrasting granite types*, *Pacific Geology*, vol. 8, pp. 173-174.
- Chappell B., 1979, *Granites as images of their source rocks*, *Geological Society of America, Abstracts with Programs*, vol. 11, pp. 400.
- Chappell B., 1999, *Aluminium saturation and I- and S-type granites and the characterisation of fractionated haplogranites*, *Lithos*, volume 46, issue 3, pp. 535-551.
- Chappell B., Bryant C., Wyborn D., White A., Williams S., 1998, *High and low temperature I-type granites*, *Resource Geology*, vol. 48, issue 4, pp. 225-235.
- Chappell W., White A., and Wyborn D., 1987, *The importance of residual source material (restitute) in*

- granite petrogenesis, *Journal of Petrology*, vol. 28, issue 6, pp. 1111-1138.
- Chatterjee A. & Muecke G., 1982, *Geochemistry and the distribution of uranium and thorium in the granitoid rocks of the South Mountain Batholith, Nova Scotia: some genetic and exploration implications*, Geological Survey of Canada, Paper 81-23, pp. 11-17.
- Chatzipetros A., Kiratzi A., Sboras S., Zouros N., and Pavlides S., 2013, *Active faulting in the North Aegean Islands*, *Tectonophysics*, vol. 106, pp. 106-122.
- Chivas A., 1978, *Porphyry copper mineralization at the Koloula igneous complex, Guadalcanal, Solomon Islands*, *Economic Geology*, vol. 73, issue 5, pp. 645-677.
- Chivas A., O'Neil J., and Katchan G., 1984, *Uplift and submarine formation of some Melanesian porphyry copper deposits: stable isotope evidence*, *Earth and Planetary Science Letters*, vol. 68, issue 2, pp. 326-334.
- Choubert, G., 1968, *International tectonic map of Africa – scale 1:5.000.000*, UNESCO, Paris.
- Christiansen R. & Lipman P., 1972, *Cenozoic volcanism and plate tectonic evolution of the western United States, Pt. II: Late Cenozoic*, *Philosophical Transactions of the Royal Society of London, Series A: Mathematical and Physical Sciences*, vol. 271, issue 1213, pp. 249-284.
- Christiansen R. & Lipman P., 1972, *Cenozoic Volcanism and Plate-Tectonic Evolution of the Western United States. II. Late Cenozoic*, *Philosophical Transactions of The Royal Society, Series B: Biological Sciences*, vol. 271, pp. 249-284.
- Christofides G., Soldatos T., Eleftheriadis G., and Koroneos A., 1998, *Chemical and isotopic evidence for source contamination and crustal assimilation in the Hellenic Rhodope plutonic rocks*, *Acta Vulcanologica*, vol. 10, pp. 305-318.
- Chukhrov, F., Zvyagin B., Yermilova L., Soboleva S., and Khitrov V., 1968, *Polytypes of molybdenite and their occurrences in ores*, *Geologiya Rudnykh Mestorozhdenii*, vol. 10, issue 1, pp. 12-20.
- Ciobanu C., Cook N., and Stein H., 2002, *Regional setting and geochronology of the Late Cretaceous Banatitic magmatic and metallogenic belt*, *Mineralium Deposita*, v. 37, issue 6-7, pp. 541-567.
- Ciobanu C., Cook N., Kelson C., Guerin R., Kalleske N., and Danyushevs K., 2013, *Trace element heterogeneity in molybdenite fingerprints stages of mineralisation*, *Chemical Geology*, vol. 347, pp. 175-189.
- Clark A. 1970, *Compositional differences between hexagonal and rhombohedral molybdenite*, *Neues Jahrbuch für Mineralogie, Monatshefte*, pp. 33-38.
- Clark A., 1993, *Are outsize porphyry copper deposits either anatomically or environmentally distinctive?*. In: Whiting B., Hodgson C., and Mason R. (Eds.), *Giant Ore Deposits*, Society of Economic Geologists, Special Publication, No. 2, pp. 213-283.
- Clark G., 1990, *Panguna copper-gold deposit*, Australian Institute of Mining and Metallurgy, Monograph, No. 14, pp. 1807-1816.
- Clarke D., 1992, *Granitoid Rocks*, Topics in the Earth Sciences Series, No. 7, Chapman & Hall Editions, London.
- Claveria R., 2001, *Mineral paragenesis of the Lepanto copper and gold and the Victoria gold deposits, Mankayan mineral district, Philippines*, *Resource Geology*, vol. 51, issue 2, p. 97-106.
- Cline J. & Bodnar R., 1991, *Can economic porphyry copper mineralization be generated by a typical calc-alkaline melt?*, *Journal of Geophysical Research*, vol. 96, issue B5, pp. 8113-8126.
- Cline J. & Bodnar R., 1994, *Direct evolution of brine from a crystallizing silicic melt at the Questa, New Mexico, molybdenum deposit*, *Economic Geology*, vol. 89, issue 8, pp. 1780-1802.
- Cline J., 1995, *Genesis of porphyry copper deposits: The behavior of water, chloride, and copper in crystallizing melts*. In: Pearce F. & Bolm J. (Eds.), *Arizona Geological Society, Digest*, No. 20, pp. 69-82.
- Clode C., Proffett Jr. J., Mitchell P., and Munajat I., 1999, *Relationships of intrusion, wall-rock alteration and mineralisation in the Batu Hijau copper-gold porphyry deposit*, PACRIM '99, Australasian Institute of Mining and Metallurgy Congress, Bali, Indonesia, 10-13 October 1999, Conference Proceedings, pp. 485-498.
- Congdon R. & Nash W., 1988, *High-fluorine rhyolite: an eruptive pegmatite magma at the Honeycomb Hills, Utah*, *Geology*, vol. 16, issue 11, pp.1018-1021.
- Cooke D. & Simmons S., 2000, *Characteristics and genesis of epithermal gold deposits*. In: Hagemann S. & Brown P. (Eds.), *Gold in 2000, Reviews in Economic Geology*, vol. 13, pp. 221-244.
- Cox D., 1985, *Geology of the Tanamá and Helecho porphyry copper deposits and vicinity, Puerto Rico, U.S.* Geological Survey, Professional Paper, No. 1327.

- Cox K., Bell J., and Pankhurst R., 1979, *The Interpretation of Igneous Rocks*, Allen and Unwin Editions, London.
- Crusius J., Calvert S., Pederson T., and Sage D., 1996, *Rhenium and molybdenum enrichments in sediments as indicators of oxic, suboxic and sulfidic conditions of deposition*, Earth and Planetary Science Letters, vol. 145, issues 1-4, pp. 65-78.
- Danelian T., Robertson A., Collins A., and Poisson A., 2006, *Biochronology of Jurassic and Early Cretaceous radiolarites from the Lycian Mélange (SW Turkey) and implications for the evolution of the northern Neotethyan ocean*. In: Robertson A. & Mountrakis D. (Eds.), *Tectonic Development of the Eastern Mediterranean Region*, Geological Society of London, Special Publication, No. 260, pp. 229-236.
- Davies J. & von Blackenburg F., 1995, *Slab breakoff: a model of lithosphere detachment and its test in the magmatism and deformation of collisional orogens*, Earth and Planetary Science Letters, vol. 129, issues 1-4, pp. 85-102.
- de la Roche H., Leterrier J., Granclaude P., and Marchal M., 1980, *A classification of volcanic and plutonic rocks using R_1R_2 -diagram and major-element analyses — Its relationships with current nomenclature*, Chemical Geology, vol. 29, issues 1-4, pp. 183-210.
- de Launay L., 1898, *La géologie de l'île de Mételin (Lesbos), Lemnos et Thasos*, P.Vincq-Dunod et C^{ie} Éditeurs, Paris. [in French]
- Deditius A., Utsunomiya S., Ewing R., Chyrssoulis S., Venter D., and Kesler S., 2009, *Decoupled geochemical behavior of As and Cu in hydrothermal systems*, Geology, vol. 37, issue 8, pp. 707-710.
- Deen J., Rye R., Munoz, J., and Drexler J., 1994, *The magmatic hydrothermal system at Julcani, Peru: Evidence from fluid inclusions and hydrogen and oxygen isotopes*, Economic Geology, vol. 89, issue 8, pp. 1924-1938.
- Degnan P. & Robertson A., 2006, *Synthesis of the tectonic-sedimentary evolution of the Mesozoic-Early Cenozoic passive margin evolution of the Pindos ocean; evidence from NW Peloponnese, Greece*. In: Robertson A. & Mountrakis D. (Eds.), *Tectonic Development of the Eastern Mediterranean Region*, Geological Society of London, Special Publication, No. 260, pp. 467-491.
- Delibaş O., Moritz R., Chiaradia M., Selby D., Ulianov A., and Revan M., 2017, *Post-collisional magmatism and ore-forming systems in the Menderes massif: new constraints from the Miocene porphyry Mo-Cu Pınarbaşı system, Gediz-Kütahya, western Turkey*, Mineralium Deposita, vol. 52, issue 8, pp. 1157-1178.
- Dewey J., Pitman III W., Ryan W., and Bonnin J., 1973, *Plate tectonics and the evolution of the Alpine system*, Geological Society of America Bulletin, vol. 84, issue 10, pp. 3137-3180.
- Dickinson R. & Pauling L., 1923, *The crystal structure of molybdenite*, Journal of the American Chemical Society, vol. 45, issue 6, pp. 1446-1471.
- Dilles J., & Einaudi M., 1992, *Wall-rock alteration and hydrothermal flow paths about the Ann-Mason porphyry copper deposit, Nevada — a 6-km vertical reconstruction*, Economic Geology, vol. 87, issue 8, pp. 1963-2001.
- Dilles J., 1987, *Petrology of the Yerington batholith, Nevada: evidence for evolution of porphyry copper ore fluids*, Economic Geology, vol. 82, issue 7, pp. 1924-1938.
- Dilles J., Einaudi M., Proffett J., and Barton M., 2000, *Overview of the Yerington porphyry copper district: magmatic to nonmagmatic sources of hydrothermal fluids; their flow paths and alteration effects on rocks and Cu-Mo-Fe-Au ores*, Society of Economic Geologists, Guidebook Series, vol. 32, pp. 55-66.
- Dilles J., Farmer G., and Field C., 1995, *Sodium-calcium alteration by non-magmatic saline fluids in porphyry copper deposits: results from Yerington, Nevada*, Mineralogical Association of Canada, Short Course, vol. 23, pp. 309-338.
- Dilles J., Solomon G., Taylor Jr. H., and Einaudi M., 1992, *Oxygen and hydrogen isotope characteristics of hydrothermal alteration at the Ann-Mason porphyry copper deposits, Yerington, Nevada*, Economic Geology, vol. 87, issue 1, pp. 44-63.
- Dong G., Morrison G., and Jaireth S., 1995, *Quartz textures in epithermal veins, Queensland; classification, origin and implication*, Economic Geology, vol. 90, issue 6, pp. 1841-1856.
- Doutsos T., Pe-Piper G., Boronkay K., and Koukouvelas I., 1993, *Kinematics of the central Hellenides*, Tectonics, vol. 12, issue 4, pp. 936-953.
- Drábek M., 1995, *The Mo-Se-S and Mo-Te-S systems*, Neues Jahrbuch für Mineralogie, vol. 169, issue 3, pp. 255-263.
- Drábek M., Drábková E., and Kvaček M., 1993, *Distribution of rhenium, tungsten and selenium in molybdenites of the Bohemian Massif*, Věstník Ústředního Ústavu Geologického, vol. 68, pp.11-17.
- Duermeijer C., Nyst M., Meijer P., Langereis C., and Spakman W., 2000, *Neogene evolution of the Aegean arc: paleomagnetic and geodetic evidence for a rapid*

- and young rotation phase, *Earth and Planetary Science Letters*, vol. 176, issues 3-4, pp. 509-525.
- Eastoe C., 1978, *A fluid inclusion study of the Panguna porphyry copper deposit, Bougainville, Papua New Guinea*, *Economic Geology*, vol. 73, issue 5, pp. 721-748.
- Eaton P. & Setterfield T., 1993, *The relationship between epithermal and porphyry hydrothermal systems within the Tavua caldera, Fiji*, *Economic Geology*, vol. 88, issue 5, pp. 1053-1083.
- Economou-Eliopoulos M. & Eliopoulos D., 2000, *Palladium, platinum and gold concentration in porphyry copper systems of Greece and their genetic significance*, *Ore Geology Reviews*, vol. 16, issues 1-2, pp. 59-70.
- Eichelberger J., Chertkoff D., Dreher S., and Nye C., 2000, *Magmas in collision: rethinking chemical zonation in silicic magmas*, *Geology*, vol. 28, issue 7, pp. 603-606.
- Einaudi M., 1977, *Environment of ore deposition at Cerro de Pasco, Peru*, *Economic Geology*, vol. 72, issue 6, pp. 893-924.
- Einaudi M., 1982, *Description of skarns associated with porphyry copper plutons, southwestern North America*. In: Titley S. (Ed.), *Advances in Geology of the porphyry copper deposits, southwestern North America*, University of Arizona Press, Tucson, pp. 139-182.
- Einaudi M., Hedenquist J., and Inan E., 2003, *Sulfidation state of fluids in active and extinct hydrothermal systems: transition from porphyry to epithermal environments*. In: Simmons S. & Graham I. (Eds.), *Volcanic, Geothermal and Ore-Forming Fluids, Rulers and Witnesses of Processes Within the Earth*, Society of Economic Geologists, Special Publication, No. 10, pp. 285-313.
- Einaudi M., Meinert L., and Newberry R., 1981, *Skarn deposits*, *Economic geology* 75th Anniversary volume, pp. 317-391.
- Einsle O., Tezcan F., Andrade S., Schmid B., Yoshida M., Howard J., and Rees D., 2002, *Nitrogenase MoFe-protein at 1.16 Å resolution: a central ligand in the MoFe-cofactor*, *Science*, vol. 297, issue 5587, pp. 1696-1700.
- Eliopoulos D. & Economou-Eliopoulos M., 1991, *Platinum-group element and gold contents in the Skouries porphyry copper deposit, Chalkidiki peninsula, N. Greece*, *Economic Geology*, vol. 86, issue 8, pp. 740-749.
- Ellis A., 1959, *The solubility of calcite in carbon dioxide solutions*, *American Journal of Science*, vol. 257, issue 5, pp. 354-365.
- Enns S., Thompson J., Stanley C., and Yarrow E., 1995, *The Galore Creek porphyry copper-gold deposits, northwestern British Columbia*. In: Schroeter T. (Ed.), *Porphyry Deposits of the Northwestern Cordillera of North America*, Canadian Institute of Mining, Metallurgy, and Petroleum, Special Volume, No. 46, pages 630-644.
- Etoh J., Izawa E., and Taguchi S., 2002, *A fluid inclusion study on columnar adularia from the Hishikari low sulfidation epithermal gold deposit, Japan*, *Resource Geology*, vol. 52, issue 1, p. 73-78.
- Faure, K., Matsuhisa, Y., Metsugi, H., Mizota, C., and Hayashi, S., 2002, *The Hishikari Au-Ag epithermal deposit, Japan: Oxygen and hydrogen isotope evidence in determining the source of paleohydrothermal fluids*, *Economic Geology*, vol. 97, issue 3, pp. 481-498.
- Field C., Zhang L., Dilles J., Rye R., and Reed M., 2005, *Sulfur and oxygen isotope record in sulfate and sulfide minerals of early, deep, pre-Main Stage porphyry Cu-Mo and late Main Stage base-metal mineral deposits, Butte district, Montana*, *Chemical Geology*, vol. 215, issues 1-4, pp. 61-93.
- Fleischer M., 1959, *The geochemistry of rhenium, with special reference to its occurrence in molybdenite*, *Economic Geology*, vol. 54, issue 8, pp. 1406-1413.
- Floyd P. & Winchester J., 1978, *Identification and discrimination of altered and metamorphosed volcanic rocks using immobile elements*, *Chemical Geology*, vol. 21, issues 3-4, pp. 291-306.
- Ford J., 1978, *A chemical study of alteration at the Panguna porphyry copper deposit, Bougainville, Papua New Guinea*, *Economic Geology*, vol. 73, issue 5, pp. 703-720.
- Fournier R., 1987, *Conceptual models of brine evolution in magmatic-hydrothermal systems*. In: Decker R., Wright T., and Stauffer P. (Eds), *Volcanism in Hawaii*, United States Geological Survey, Professional Paper, No. 1350, vol. 2, pp. 1487-1506.
- Fournier R., 1999, *Hydrothermal processes related to movement of fluid from plastic into brittle rock in the magmatic-epithermal environment*, *Economic Geology*, vol. 94, issue 8, pp. 1193-1211.
- Franchini M., Impiccini A., Lentz D., Rios F., O'Leary S., Pons J., and Schalamuk A., 2011, *Porphyry to epithermal transition in the Agua Rica polymetallic deposit, Catamarca, Argentina: an integrated petrologic analysis of ore and alteration parageneses*, *Ore Geology Reviews*, vol. 41, issue 1, pp. 49-74.

- Franco S., Puente N., Varela C., and Gemuts I., 1999, *Mineralización aurífera en el distrito Los Menucos, Río Negro*. In: Zappettini E. (Ed.), Recursos minerales de la República Argentina, Instituto de Geología y Recursos Minerales, Buenos Aires, vol. 1, pp. 893-894. [in Spanish]
- Frei P., 1995, *Evolution of mineralizing fluid in the porphyry copper system of the Skouries deposit, northern Chalkidiki (Greece): evidence from combined Pb-Sr and stable isotope data*, *Economic Geology*, vol. 90, issue 4, pp. 746-762.
- FrondeL C., 1938, *Stability of colloidal gold under hydrothermal conditions*, *Economic Geology*, vol. 33, issue 1, pp. 1-20.
- FrondeL J. & Wickman F., 1970, *Molybdenite polytypes in theory and occurrence; II: some naturally occurring polytypes of molybdenite*, *American Mineralogist*, vol. 55, issues 11-12, pp. 1857-1875.
- Fuchs T., 1882, *Welche Ablagerungen haben wir als Tiefsee-bildungen zu betrachten?*, *Neues Jahrbuch für Geologie und Paläontologie*, vol. 2, Beilage Band, pp. 487-584. [in German]
- Gaál G. & Isohanni M., 1979, *Characteristics of igneous intrusions and various wall rocks in some Precambrian porphyry copper-molybdenum deposits in Pohjanmaa, Finland*, *Economic Geology*, vol. 74, issue 5, pp. 1198-1210.
- Gannoun A., Vlastelic I., and Schiano P., 2015, *Escape of unradiogenic osmium during sub-aerial lava degassing: evidence from fumarolic deposits, Piton de la Fournaise, Reunion Island*, *Geochimica et Cosmochimica Acta*, vol. 166, pp. 312-326.
- Gardosh M. & Druckman Y., 2006, *Seismic stratigraphy, structure and tectonic evolution of the Levantine basin, offshore Israel*. In: Robertson A. & Mountrakis D. (Eds.), *Tectonic Development of the Eastern Mediterranean Region*, Geological Society of London, Special Publication, No. 260, pp. 201-227.
- Garfunkel Z., 2006, *Neotethyan ophiolites: formation and obduction within the life cycle of the host basins*. In: Robertson A. & Mountrakis D. (Eds.), *Tectonic Development of the Eastern Mediterranean Region*, Geological Society of London, Special Publication, No. 260, pp. 301-326.
- Gautier P. & Brun J.P., 1994a, *Crustal-scale geometry and kinematics of late-orogenic extension in the central Aegean (Cyclades and Evvia island)*, *Tectonophysics*, vol. 238, issues 1-4, pp. 1180-1194.
- Gautier P. & Brun J.P., 1994b, *Ductile crust exhumation and extensional detachments in the Central Aegean (Cyclades and Evvia islands)*, *Geodinamica Acta*, vol. 7, issue 2, pp. 31-72.
- Georgalas G., 1949, *Contribution à la connaissance des roches éruptives de l'île de Mételin*, *Bulletin Vulcanologique*, vol. 9, issue 1, pp. 31-63. [in French]
- Giggenbach W., 1992, *Magma degassing and mineral deposition in hydrothermal systems along convergent plate boundaries*, *Economic Geology*, vol. 87, issue 1, pp. 1927-1944.
- Giggenbach W., 1995, *Variations in the chemical and isotopic composition of fluids discharged from the Taupo Volcanic Zone, New Zealand*, *Journal of Volcanology and Geothermal Research*, vol. 68, issues 1-3, pp. 89-116.
- Giggenbach W., 1997, *The origin and evolution of fluids in magmatic-hydrothermal systems*. In: Barnes H. (Ed.), *Geochemistry of hydrothermal ore deposits*, John Wiley and Sons, New York, 3rd Edition, pp. 737-796.
- Giles D. & Thompson T., 1972, *Petrology and mineralization of a molybdenum-bearing alkalic stock, Sierra Blanca, New Mexico*, *Geological Society of America, Bulletin*, vol. 83, issue 8, pp. 2129-2148.
- Giles D. and Schilling J., 1972, *Variation in rhenium content of molybdenite*, *Proceedings of the 24th International Geological Congress, Montreal, Canada*, vol. 10, pp. 145-152.
- Gill J., 1980, *Orogenic Andesites and Plate Tectonics*, Springer Editions, Berlin.
- Golden J., McMillan M., Downs R., Hystad G., Goldstein I., Stein H., Zimmerman A., Sverjensky D., Armstrong J., and Hazen R., 2013, *Rhenium variations in molybdenite (MoS₂): evidence for progressive subsurface oxidation*, *Earth and Planetary Science Letters*, vol. 366, pp. 1-5.
- Goldsmith R., 1980, *The melting and breakdown reactions of anorthite at high temperatures and pressures*, *American Mineralogist*, vol. 65, issues 3-4, pp. 272-284.
- Gorton M. & Schandl E., 2000, *From continents to island arcs: a geochemical index of tectonic setting for arc-related and within-plate felsic to intermediate volcanic rocks*, *The Canadian Mineralogist*, vol. 38, issue 5, pp. 1065-1073.
- Grabezhev A. & Shagalov E., 2010, *Rhenium distribution in molybdenite: results of microprobe scanning (Copper Porphyry Deposits, the Urals)*, *Doklady Earth Sciences*, vol. 431, issue 1, pp. 351-355.

- Grant J., Halls C., Sheppard S., and Avila W., 1980, *Evolution of the porphyry tin deposits of Bolivia*. In: Ishihara S. & Takenouchi S. (Eds.), *Granitic Magmatism and Related Mineralization, Mining Geology, Special Issue, No. 8*, p. 151-173.
- Grigor'ev D., 1961, *Ontogeny of minerals*, Israel Program of Scientific Translations Limited, Jerusalem (1965 Translation).
- Gustafson L. & Hunt J., 1975, *The porphyry copper deposit at El Salvador, Chile*, *Economic Geology*, vol. 70, issue 5, pp. 857-912.
- Gustafson L. & Quiroga J., 1995, *Patterns of mineralization and alteration below the porphyry copper orebody at El Salvador, Chile*, *Economic Geology*, vol. 90, issue 1, pp. 2-16.
- Hamlyn P. & Keays R., 1986, *Sulfur saturation and second-stage melts; application to the Bushveld platinum metal deposits*, *Economic Geology*, vol. 81, issue 6, pp. 1431-1445.
- Harker A., 1909, *The Natural History of Igneous Rocks*, Methuen & Co. Publishers, London.
- Harris N., Pearce J., and Tindle A., 1986, Geochemical characteristics of collision-zone magmatism. In: Coward M. & Ries A. (Eds.), *Collision Tectonics*, Geological Society London, Special Publication, No. 19, pp 67-81.
- Harry D. & Leeman W. 1995, *Partial melting of melt-metasomatized subcontinental mantle and the magma source potential of the lower lithosphere*, *Journal of Geophysical Research*, vol. 100, issue 86, pp. 10255-10269.
- Hasan Z., 1971, *Supracrustal rocks and Mo-Cu bearing veins in Dalen*, *Norsk Geologisk Tidsskrift*, vol. 51, pp. 287-310.
- Hastie A., Kerr A., Pearce J., and Mitchell S., 2007, *Classification of altered volcanic island arc rocks using immobile trace elements: development of the Th-Co discrimination diagram*, *Journal of Petrology*, vol. 48, issue 12, pp. 2341-2357.
- Hattori K. & Keith J., 2001, *Contribution of mafic melts to porphyry copper mineralization: Evidence from Mount Pinatubo, Philippines, and Bingham Canyon, Utah, USA*, *Mineralium Deposita*, vol. 36, issue 8, pp. 799-806.
- Hattori K., 1993, *High-sulfur magma, a product of fluid discharge from underlying mafic magma: evidence from Mount Pinatubo, Philippines*, *Geology*, vol. 21, issue 12, pp. 1083-1086.
- Hatzipanagiotou K. & Pe-Piper G., 1995, *Ophiolitic and sub-ophiolitic metamorphic rocks of the Vatera area, southern Lesbos (Greece): geochemistry and geochronology*, *Ofioliti*, vol. 20, issue 1, pp. 17-29.
- Heald P., Foley N., and Hayba D., 1987, *Comparative anatomy of volcanic-hosted epithermal deposits: acid sulfate and adularia-sericite types*, *Economic Geology*, vol. 82, issue 1, pp. 1-26.
- Hecht J., 1970, *Zur Geologie von Südost-Lesbos (Griechenland)*, Ph.D. Thesis, University of Munich, Munich. [in German]
- Hecht J., 1972a, *Zur Geologie von Südost-Lesbos (Griechenland)*, *Zeitschrift der Deutschen Geologischen Gesellschaft*, vol. 123, pp. 423-432. [in German]
- Hecht J., 1972b, *Geological Map of Greece, 1:50000, Lesbos Island – Plomari/Mytilene Sheet*, The National Institute of Geological and Mining Research, Athens.
- Hecht J., 1973, *Geological Map of Greece, 1:50000, Lesbos Island – Agia Paraskevi Sheet*, The National Institute of Geological and Mining Research, Athens.
- Hecht J., 1974a, *Geological Map of Greece, 1:50000, Lesbos Island – Polychnitos Sheet*, The National Institute of Geological and Mining Research, Athens.
- Hecht J., 1974b, *Geological Map of Greece, 1:50000, Lesbos Island – Mithimna Sheet*, The National Institute of Geological and Mining Research, Athens.
- Hecht J., 1975, *Geological Map of Greece, 1:50000, Lesbos Island – Eressos Sheet*, The National Institute of Geological and Mining Research, Athens.
- Hedenquist J. & Henley R., 1985, *Hydrothermal eruptions in the Waiotapu geothermal system, New Zealand; their origin, associated breccias, and relation to precious metal mineralization*, *Economic Geology*, vol. 80, issue 6, pp. 1379-1406.
- Hedenquist J. & Lowenstern J., 1994, *The role of magmas in forming hydrothermal ore deposits*, *Nature*, vol. 370, pp. 519-527.
- Hedenquist J., 1995, *The ascent of magmatic fluid: discharge versus mineralization*, *Mineralogical Association of Canada, Short Course*, No. 23, p. 263-289.
- Hedenquist J., Arribas Jr. A., and Gonzalez-Urien E., 2000, *Exploration for epithermal gold deposits*. In: Hagemann S. & Brown P. (Eds.), *Gold in 2000, Reviews in Economic Geology*, vol. 13, pp. 245-277.
- Hedenquist J., Arribas Jr. A., and Reynolds T., 1998, *Evolution of an intrusion-centered hydrothermal system: Far Southeast-Lepanto porphyry and epithermal Cu-Au*

- deposits, *Philippines*, *Economic Geology*, vol. 93, issue 4, pp. 373-404.
- Hedenquist J., 1987, Mineralization associated with volcanic-related hydrothermal systems in the Circum-Pacific Basin. In: Horn M. (Ed.), *Circum Pacific Energy and Mineral Resources 4th Conference*, Singapore, 1986, Transactions, American Association of Petroleum Geologists, Tulsa, USA, pp. 513-524.
- Heim A., 1919, *Geologie de Schweiz*, Tauchnitz Publishers, Leipzig, vol. 2. [in German]
- Heinrich C., Driesner T., Stefánsson A, and Seward T., 2004, *Magmatic vapor contraction and the transport of gold from the porphyry environment to epithermal ore deposits*, *Geology* vol. 32, issue 9, pp.761-764.
- Heinrich C., Günther D., Audétat A., Ulrich T., and Frischknecht R., 1999, *Metal fractionation between magmatic brine and vapor, determined by microanalysis of fluid inclusions*, *Geology*, vol. 27, issue 8, pp. 755-758.
- Helbling-Marschall A., 2011, *Lithium, Beryllium and Boron in High-K Rhyolites from Lesbos Island, Greece*, PhD Thesis, Ruprecht Karls Universität, Heidelberg.
- Hemley J. & Hunt J., 1992, *Hydrothermal ore-forming processes in the light of studies in rock-buffered systems; II. Some general geologic applications*, *Economic Geology*, vol. 87, issue 1, pp. 23-43.
- Hemley J., Cygan G., Fein J., Robinson G., and d'Angelo W., 1992, *Hydrothermal ore-forming processes in the light of studies in rock-buffered systems; I. Iron-copper-zinc-lead sulfide solubility relations*, *Economic Geology*, vol. 87, issue 1, pp. 1-22.
- Henley R. & Ellis A., 1983, *Geothermal systems, ancient and modern*, *Earth Science Reviews*, vol. 19, issue 1, pp. 1-50.
- Henley R. & McNabb A., 1978, *Magmatic vapor plumes and ground-water interaction in porphyry copper emplacement*, *Economic Geology*, vol. 73, issue 1, pp. 1-20.
- Henley R., 1990, *Ore transport and deposition in epithermal ore environments*. In: Herbert, H. & Ho S. (Eds.), *Stable isotopes and fluid processes in mineralization*, University of Western Australia, Publication of the Geology Department, No. 23, Perth, pp. 51-69.
- Herd C., 2008, *Basalts as probes of planetary interior redox state*. In: McPherson G., Mittlefehldt D. and Jones J., (Eds.), *Oxygen in the Solar System*, Mineralogical Society of America and Geochemical Society, *Reviews in Mineralogy and Geochemistry*, vol. 68, pp. 527-553.
- Hildreth, W., 1981, *Gradients in silicic magma chambers: Implications for lithospheric magmatism*, *Journal of Geophysical Research*, v. 86, issue B11, p. 10153–10192.
- Hillemeier F., Johnson M., and Kern R., 1991, *Geology, alteration and mineralization of the Modoc hot springs gold prospect, Imperial County, California*. In: McKibben (Ed.), *The Diversity of Mineral and Energy Resources of Southern California*, Society of Economic Geologists Guidebook Series, vol. 12, pp. 139-155.
- Himmerkus F., Reischmann T., and Kostopoulos D., 2006, *Late Proterozoic and Silurian basement units within the Serbo-Macedonian Massif, northern Greece: the significance of terrane accretion in the Hellenides*. In: Robertson A. & Mountrakis D. (Eds.), *Tectonic Development of the Eastern Mediterranean Region*, Geological Society of London, Special Publication, No. 260, pp. 35-50.
- Holland H., 1972, *Granites, solutions and base metal deposits*, *Economic Geology*, vol. 67, issue 3, pp. 281-301.
- Hunt J., 1991, *Porphyry copper deposits*. In: Hutchinson R. & Grauch R. (Eds.), *Historical Perspectives of Genetic Concepts and Case Histories of Famous Discoveries*, *Economic Geology Monograph*, No. 8, pp. 192-206.
- Irvine T. & Baragar W., 1971, *A guide to the chemical classification of the common volcanic rocks*, *Canadian Journal of Earth Sciences*, vol. 8, issue 5, pp. 523-548.
- Isuk E., 1976, *Solubility of Molybdenite in the System Na₂O-K₂O-SiO₂-MoS₂-H₂O-CO₂ with Geologic Application*, Ph.D. Thesis, Iowa University, Iowa.
- Ito E., Harris D., and Anderson Jr. A., 1983, *Alteration of oceanic crust and geologic cycling of chlorine and water*, *Geochimica et Cosmochimica Acta*, vol. 47, issue 9, pp. 1613-1624.
- Ivascanu, P.M., Rosu, E., and Udubasa, G., 2002, *Geodynamic control of magma emplacement and ore deposit formation: Case study of South Apuseni Mts. Neogene calc-alkaline magmatic belt, Romania*, Study Centre on Geodynamics and Ore Deposit Evolution, Grenoble, Working Group Discussion Paper, pp. 3.
- Jellinek F., 1963, *Sulfides of the transition metals of Groups IV, V, and VI*, *Arkiv för Kemi*, vol. 20, pp. 447-448.
- Jensen E. & Barton M., 2000, *Gold deposits related to alkaline magmatism*. In: Hagemann S. & Barton M. (Eds.), *Gold in 2000*, *Reviews in Economic Geology*, vol. 13, pp. 279-314.

- Jensen L., 1976, *A new cation plot for classifying subbalkalic volcanic rocks*, Miscellaneous Paper, No. 66, Ministry of Natural Resources, Division of Mines, Ontario, pp. 1-22.
- John D., 2001, *Miocene and early Pliocene epithermal gold-silver deposits in the northern Great Basin, western USA: characteristics, distribution, and relationship to magmatism*, Economic Geology, vol. 96, issue 8, pp. 1827-1853.
- John E., 1978, *Mineral zones in the Utah Copper orebody*, Economic Geology, vol. 73, issue 7, pp. 1250-1259.
- Jolivet L. & Brun J., 2010, *Cenozoic geodynamic evolution of the Aegean region*, International Journal of Earth Sciences, vol. 99, issue 1, pp. 109-138.
- Jolivet L. & Faccena C., 2000, *Mediterranean extension and the Africa-Eurasia collision*, Tectonics, vol. 19, issue 6, pp. 1095-1106.
- Jolivet L. & Patriat M., 1999, *Ductile extension and the formation of the Aegean Sea*. In: Durand B., Jolivet L., Horváth F., and Séranne M. (Eds.), *The Mediterranean Basins: Tertiary Extension within the Alpine Orogen*, Geological Society of London, Special Publication, No. 156, pp. 427-456.
- Jolivet L., Faccenna C., Goffé B., Burov E., and Agard P., 2003, *Subduction tectonics and exhumation of high-pressure metamorphic rocks in the Mediterranean orogens*, American Journal of Science, vol. 303, issue 5, pp. 353-409.
- Jolivet L., Faccenna C., Huet B., Labrousse L., Le Pourhiet L., Lacombe O., Lecomte E., Burov E., Denéle Y., and Brun J., 2013, *Aegean tectonics: strain localisation, slab tearing and trench retreat*, Tectonophysics, vol. 597-598, pp. 1-33.
- Jolivet L., Famin V., Mehl C., Parra T., Auburg C., Hébert R., and Philippot P., 2004, *Progressive strain localisation, boudinage and extensional metamorphic complexes, the Aegean Sea case*. In: Whitney D., Teyssier C., and Siddoway C. (Eds.), *Gneiss Domes in Orogeny*, Geological Society of America, Boulder Editions, pp. 185-210.
- Jones C., Tarney J., Baker J., and Gerouki F., 1992, *Tertiary granitoids of Rhodope, northern Greece: magmatism related to extensional collapse of the Hellenic Orogen?*, Tectonophysics 210, issues 3-4, pp. 295-314.
- Kaiser-Rohrmeier M., von Quadt A., Driesner T., Heinrich C., Handler R., Ovtcharova M., Ivanov Z., Petrov P., Sarov S., and Peytcheva I., 2013, *Post-orogenic extension and hydrothermal ore formation: high-precision geochronology of the central Rhodopian metamorphic core complex (Bulgaria-Greece)*, Economic Geology, vol. 108, issue 4, pp. 691-718.
- Kamilli R. & Ohmoto H., 1977, *Paragenesis, zoning, fluid inclusion, and isotopic studies of the Finlandia vein, Colqui district, central Peru*, Economic Geology, vol. 72, issue 6, pp. 950-982.
- Karamata S., 2006, *The geological development of the Balkan Peninsula related to the approach, collision and compression of Gondwanan and Eurasian units*. In: Robertson A. & Mountrakis D. (Eds.), *Tectonic Development of the Eastern Mediterranean Region*, Geological Society of London, Special Publication, No. 260, pp. 155-178.
- Kazmin V. & Tikhonova N., 2006, *Evolution of Early Mesozoic back-arc basins in the Black Sea-Caucasus segment of a Tethyan active margin*. In: Robertson A. & Mountrakis D. (Eds.), *Tectonic Development of the Eastern Mediterranean Region*, Geological Society of London, Special Publication, No. 260, pp. 179-200.
- Keith J., Shanks III W., Archibald D., and Farrar E., 1986, *Volcanic and intrusive history of the Pine Grove porphyry molybdenum system, southwestern Utah*, Economic Geology, vol. 81, issue 3, pp. 553-577.
- Kelepertsis A. & Esson J., 1987, *Major- and trace-element mobility in altered volcanic rocks near Stypsi, Lesbos, Greece and genesis of a kaolin deposit*, Applied Clay Science, vol. 2, issue 1, pp. 11-28.
- Kelley K., Romberger S., Beaty D., Pontius J., Snee L., Stein H., and Thompson T.B., 1998, *Geochemical and geochronological constraints on the genesis of Au-Te deposits at Cripple Creek, Colorado*, Economic Geology, vol. 93, issue 7, pp. 981-1012.
- Keppler & Wyllie P., 1991, *Partitioning of Cu, Sn, Mo, W, U, and Th between melt and aqueous fluid in the systems haplogranite-H₂O-HCl and haplogranite-H₂O-HF*, Contributions to Mineralogy and Petrology, vol. 109, issue 2, pp. 139-150.
- Kesler S. & Wilkinson B., 2009, *Resources of gold in Phanerozoic epithermal deposits*, Economic Geology, vol. 104, issue 5, pp. 623-633.
- Kesler S., 1973, *Copper, molybdenum, and gold abundances in porphyry copper deposits*, Economic Geology, vol. 68, issue 1, pp. 106-112.
- Khitarov N., Malinin S., Lebedev Y., and Shibayeva N., 1982, *The distribution of Zn, Cu, Pb, and Mo between a fluid phase and a silicate melt of granitic composition at high temperatures and pressures*, Geochemistry International, vol. 19, issue 4, pp. 123-136.

- Kilinc I. & Burnham C., 1972, *Partitioning of chloride between a silicate melt and coexisting aqueous phase from 2 to 8 kilobars*, Economic Geology, vol. 67, issue 2, pp. 231-235.
- Kirkham R. & Sinclair W., 1996, *Porphyry copper, gold, molybdenum, tungsten, tin, silver*. In: Eckstrand O., Sinclair W., and Thorper R. (Eds.), *Geology of Canadian Mineral Deposit Types*, Geological Survey of Canada, No.8, pp. 421-446.
- Klemm L., Pettke T., Heinrich C., and Campos E., 2007, *Hydrothermal evolution of the El Teniente deposit, Chile: porphyry Cu–Mo ore deposition from low-salinity magmatic fluids*, Economic Geology, vol. 102, issue 6, pp. 1021-1045.
- Koglin N., Kostopoulos D., and Reischmann T., 2009, *The Lesvos mafic-ultramafic complex, Greece: ophiolite or incipient rift?*, Lithos, vol. 108, issues 1-4, pp. 243-261.
- Koller F., Hoeck V., Meisel T., Ionescu C., Onuzi K., and Ghega D., 2006, *Cumulates and gabbros in southern Albanian ophiolites: their bearing on regional tectonic setting*. In: Robertson A. & Mountrakis D. (Eds.), *Tectonic Development of the Eastern Mediterranean Region*, Geological Society of London, Special Publication, No. 260, pp. 267-299.
- Kontis E., Keleperdis A., and Skounakis S., 1994, *Geochemistry and alteration facies associated with epithermal precious metal mineralization in an active geothermal system, northern Lesvos, Greece*, Mineralium Deposita, vol. 29, issue 5, pp. 430-433.
- Kontis, E., 1997, *Lithochemical study and metallogenesis of Au, Ag and other metals of north Lesvos*, PhD Thesis, Athens, National and Kapodestrian University of Athens, Athens.
- Kooiman G., McLeod M., and Sinclair W., 1986, *Porphyry tungsten-molybdenum orebodies, polymetallic veins and replacement bodies and tin-bearing greisen zones in the Fire Tower zone, Mount Pleasant, New Brunswick*, Economic Geology, vol. 81, issue 6, pp. 1356-1373.
- Koski, R.A., and Cook, D.S., 1982, *Geology of the Christmas porphyry copper deposit, Gila County, Arizona*. In: Titley, S.R., (Ed.), *Advances in Geology of the Porphyry Copper Deposits, Southwestern North America*, University of Arizona Press, Tucson, Arizona, pp. 353-374.
- Kosler J., Simonetti A., Sylvester P., Cox R., Tubrett M., and Wilton D., 2003, *Laser ablation ICP-MS measurements of Re/Os in molybdenite and implications for Re-Os geochronology*, Canadian Mineralogist, vol. 41, issue 2, pp. 307-320.
- Koster van Groos A. & Wyllie P., 1968, *Melting relations in the system $\text{NaAlSi}_3\text{O}_8\text{-NaF-H}_2\text{O}$ to 4 kilobars pressure*, Journal of Geology, vol. 76, issue 1, pp. 50-70.
- Kovalenker V., Safonov Y., Naumov V., and Rusinov V., 1997, *The epithermal gold-telluride Kochbulak deposit (Uzbekistan)*, Geology of Ore Deposits, vol. 39, issue 2, pp. 107-128.
- Krohe A. & Boskos E., 2002, *Multiple generations of extensional detachments in the Rhodope mountains (northern Greece): evidence of episodic exhumation of high-pressure rocks*. In: Brundell D., Neubauer F., von Quadt A. (Eds.), *The timing and location of major ore deposits in an evolving orogen*, Geological Society of London, Special Publication, vol. 204, pp. 151-178.
- Kroll T., Mueller D., Seifert T., Herzig P., and Schneider A., 2002, *Petrology and geochemistry of the shoshonite-hosted Skouries porphyry Cu-Au deposit, Chalkidiki, Greece*, Mineralium Deposita, vol. 37, issue 1, pp. 137-144.
- Kudryavtsev Y., 1996, *The Cu-Mo deposits of central Kazakhstan*. In: Shatov V., Seltmann R., Kremenetsky A., Lehmann B., Popov V., and Ermolov P. (Eds.), *Granite-related Ore Deposits of Central Kazakhstan and Adjacent Areas*, Glagol Publishing House, St. Petersburg, pp. 119-144.
- Kuhlemann J., Frisch W., Dunkl I., Kázmér M., and Schmiel G., 2004, *Miocene siliciclastic deposits of Naxos Island: geodynamic and environmental implications for the evolution of the southern Aegean Sea (Greece)*. In: Bernet M. & Spiegel C. (Eds.), *Detrital Thermochronology – Provenance Analysis, Exhumation and Landscape Evolution of Mountain Belts*, Geological Society of America, vol. 378, pp. 51-65.
- Lamb S., Hoke L., Kennan L., and Dewey J., 1997, *Cenozoic evolution of the Central Andes in Bolivia and northern Chile*. In: Burg J.P. (Ed.), *Orogeny Through Time*, Geological Society of London, Special Publication, No. 121, pp. 237-264.
- Lang J. & Titley S., 1998, *Isotopic and geochemical characteristics of Laramide magmatic systems in Arizona and implications for the genesis of porphyry copper deposits*, Economic Geology, vol. 93, issue 2, pp. 138-170.
- Langton J. & Williams S., 1982, *Structural, petrological and mineralogical controls for the Dos Pobres orebody: Lone Star mining district, Graham County, Arizona*. In: Titley S. (Ed.), *Advances in Geology of the Porphyry Copper Deposits, Southwestern North America*, University of Arizona Press, Tucson, pp. 335-352.

- Larsen E., 1938, *Some new variation diagrams for groups of igneous rocks*, Journal of Geology, vol. 46, issue 3, pp. 505-520.
- Lasmanis R. & Utterback W., 1995, *The Mount Tolman porphyry molybdenum-copper deposit, Ferry County, Washington*, Canadian Institute of Mining, Metallurgy and Petroleum, Special Volume, No. 46, pp. 718-731.
- le Bas M., le Maitre R., Streckeisen A., and Zanettin B., 1986, *A chemical classification of volcanic rocks based on the total alkali silica diagram*, Journal of Petrology, vol. 27, issue 3, pp. 745-750.
- Le Pichon X. & Angelier J., 1979, *The Hellenic arc and trench system: a key to the neotectonic evolution of the Eastern Mediterranean area*, Tectonophysics, vol. 60, issues 1-2, pp. 1-42.
- Le Pichon X. & Angelier J., 1981, *The Aegean Sea*, Philosophical Transactions of the Geological Society of London, Series A: Mathematical and Physical Sciences, vol. 300, issue 1454, Extensional Tectonics Associated with Convergent Plate Boundaries, pp. 357-372.
- Lehmann B., 1982, *Metallogeny of tin: magmatic differentiation versus geochemical heritage*, Economic Geology, vol. 77, issue 1, pp. 50-59.
- Łętowski F., Serkies J., and Niemiec J., 1966, *Application of potential-ph diagrams for determination of the occurrence forms of trace elements in some economic mineral deposits*, Economic Geology, vol. 61, issue 7, pp. 1272-1279.
- Li X., Bock G., Vafidis A., Kind R., Harjes H.P., Hanka W., Wylegalla K., van der Meijde M., and Yuan X., 2003, *Receiver function study of the Hellenic subduction zone: imaging crustal thickness variations and the oceanic Moho of the descending African lithosphere*, Geophysical Journal International, vol. 155, issue 2, pp. 733-748.
- Li Y. & Audétat A., 2015, *Effects of temperature, silicate melt composition, and oxygen fugacity on the partitioning of V, Mn, Co, Ni, Cu, Zn, As, Mo, Ag, Sn, Sb, W, Au, Pb and Bi between sulfide phases and silicate melt*, Geochimica et Cosmochimica Acta, vol. 162, issue 1, pp. 25-45.
- Li Y., 2014, *Comparative geochemistry of rhenium in oxidised arc magma and MORB and rhenium partitioning during magmatic differentiation*, Chemical Geology, vol. 386, pp. 101-114.
- Lickfold V., Cooke D., Smith S., and Ulrich T., 2003, *Endeavour Cu-Au porphyry deposits, Northparkes, New South Wales - Intrusive history and fluid evolution*, Economic Geology, vol. 98, issue 8, pp. 1607-1636.
- Lindgren W. & Bancroft H., 1914, *The ore deposits of the Republic mining district*, US Geological Survey Bulletin, vol. 550.
- Lindgren W., 1901, *Metasomatic processes in fissure veins*, American Institute of Mining Engineers, Transactions, vol. 30, pp. 578-692.
- Lindgren W., 1936, *Succession of minerals and temperatures of formation in ore deposits of magmatic affiliations*, American Institute of Mining and Metallurgical Engineers, Technical Publications, vol. 713.
- Linnen R., Williams-Jones A., Leitch C., and Macauley T., 1995, *Molybdenum mineralization in a fluorine-poor system: the Trout Lake stockwork deposit, southeastern British Columbia*. In: Schroeter T. (Ed.), *Porphyry Deposits of the Northwestern Cordillera of North America*, Canadian Institute of Mining, Metallurgy and Petroleum, Special Volume, No. 46, pp. 771-780.
- Lodders K. & Fegley B., 1998, *The Planetary Scientist's Companion*, Oxford University Press, Oxford.
- Lodders K. & Palme H., 1991, *On the chalcophile character of molybdenum: determination of sulfide/silicate partition coefficients of Mo and W*, Earth and Planetary Science Letters, vol. 103, issues 1-4, pp. 311-324.
- Lorand J.P., 1989, *Mineralogy and chemistry of Cu-Fe-Ni sulfides in orogenic-type spinel peridotite bodies from Ariège (Northeastern Pyrenees, France)*, Contributions to Mineralogy and Petrology, vol. 103, issue 3, pp. 335-345.
- Lorand J.P., 1990, *Are spinel Iherzolite xenoliths representative of the abundance of sulfur in the upper mantle?*, Geochimica et Cosmochimica Acta, vol. 54, issue 5, pp. 1487-1492.
- Lovering T., 1972, *Jasperoid in the United States - its characteristics, origin and economic significance*, US Geological Survey, Professional Paper, No. 710.
- Lowell J. & Guilbert J., 1970, *Lateral and vertical alteration-mineralization zoning in porphyry ore deposits*, Economic Geology, vol. 65, issue 4, pp. 373-408.
- Lowell J., 1968, *Geology of the Kalamazoo orebody, San Manuel district, Arizona*, Economic Geology, vol. 63, issue 6, pp. 645-654.
- Lowenstern J., Mahood G., Hervig R., and Sparks J., 1993, *The occurrence and distribution of Mo and molybdenite in unaltered peralkaline rhyolites from Pantelleria, Italy*, Contributions to Mineralogy and Petrology, vol. 114, issue 1, pp. 119-129.

- MacKenzie W. & Bookstrom A., 1976, *Geology of the Majuba Hill area, Pershing County, Nevada*, Nevada Bureau of Mines and Geology, Bulletin, Nevada, No. 86.
- MacLean W., 1969, *Liquidus phase relations in the FeS-FeO-Fe₃O₄-SiO₂ system, and their application in geology*, Economic Geology, vol. 64, issue 8, pp. 865-884.
- Maher D., 1996, *Stratigraphy, structure, and alteration of igneous and carbonate wall rocks at Veteran Extension in the Robinson (Ely) porphyry copper district, Nevada*, Geology and Ore Deposits of the American Cordillera, Geological Society of Nevada Symposium, Reno/Sparks Nevada, April 1995, Proceedings, vol. 3, pp. 1595-1621.
- Makris J., Papoulia J., Papanikolaou D., and Stavrakakis G., 2001, *Thinned continental crust below northern Evoikos Gulf, central Greece detected from deep seismic soundings*, Tectonophysics, vol. 341, issues 1-4, pp. 225-236.
- Mallmann G. & O'Neill H., 2007, *The effect of oxygen fugacity on the partition of Re between crystals and silicate melt during mantle melting*, Geochimica et Cosmochimica Acta, vol. 71, issue 11, pp. 2837-2857.
- Mandarino J. & Gait R., 1970, *Molybdenite polytypes in the Royal Ontario Museum*, Canadian Mineralogist, vol. 10, issue 4, pp. 723-729.
- Manning D. & Henderson P., 1984, *The behaviour of tungsten in granitic melt-vapour systems*, Contributions to Mineralogy and Petrology, vol. 86, issue 3, pp. 286-293.
- Marakis G. & Skounakis S., 1972, *The physical properties of wolframite from Axioupolis Mo occurrences and their significance in the genesis of the Mo paragenesis*, Annales Geologiques des Pays Helleniques, vol. 24, pp. 399-405. [in Greek]
- Marchev P., Kaiser-Rohrmeier B., Heinrich C., Ovtcharova M., von Quadt A., and Raicheva R., 2005, *Hydrothermal ore deposits related to post-orogenic extensional magmatism and core complex formation: the Rhodope massif of Bulgaria and Greece*, Ore Geology Reviews, vol. 27, issues 1-4, pp. 53-89.
- Margolis J., Reed M., and Albino G., 1991, *A process-oriented classification of epithermal systems: magmatic volatile-rich versus volatile-poor paths*, Geological Society of America, Abstracts with Programs, vol. 23, No. 5, San Diego, USA, pp. A230.
- Márton I., Moritz R., and Spikings R., 2010, *Application of low-temperature thermochronology to hydrothermal ore deposits: formation, preservation and exhumation of epithermal gold system from the eastern Rhodopes, Bulgaria*, Tectonophysics, vol. 483, issues 3-4, pp. 240-254.
- Matsuhisa Y. & Aoki M., 1994, *Temperature and oxygen isotope variations during formation of the Hishikari epithermal gold-silver veins, southern Kyushu, Japan*, Economic Geology, vol. 89, issue 7, pp. 1608-1613.
- McCandless T., Ruiz J., and Campbell A., 1993, *Rhenium behaviour in molybdenite in hypogene and near-surface environments: implications for Re-Os geochronology*, Geochimica et Cosmochimica Acta, vol. 57, issue 4, pp. 889-905.
- McInnes B. & Cameron E., 1994, *Carbonated, alkaline hybridizing melts from a sub-arc environment: mantle wedge samples from the Tabar-Lihir-Tanga-Feni arc, Papua New Guinea*, Earth and Planetary Science Letters, vol. 122, issues 1-2, pp. 125-141.
- McInnes B. & Evans N., 1996, *Cu- and Pd-rich immiscible sulphide liquids in submarine shoshonitic lavas from the Tabar-Lihir-Tanga-Feni island arc, Papua New Guinea*, Geological Society of Australia Abstracts, No. 41, Melbourne, Australia, pp. 288.
- McKenzie D., 1970, *Plate tectonics of the Mediterranean region*, Nature, vol. 226, pp. 239-243.
- McKenzie D., 1972, *Active tectonics of the Mediterranean region*, Geophysical Journal International, vol. 30, issue 2, pp. 109-185.
- McKenzie D., 1978, *Some remarks on the development of sedimentary basins*, Earth and Planetary Science Letters, vol. 40, issue 1, pp. 25-32.
- McLennan S., 2001, *Relationships between the trace element composition of sedimentary rocks and upper continental crust*, Geochemistry, Geophysics, Geosystems, vol. 2, issue 4, doi:10.1029/2000GC000109.
- McMillan W. & Panteleyev A., 1980, *Ore deposit models – I. Porphyry copper deposits*, Geoscience Canada, vol. 7, issue 2, pp. 52-63.
- McMillan W. & Panteleyev A., 1995, *Porphyry copper deposits of the Canadian Cordillera*, In: Pearce F. & Bolm J. (Eds.), Arizona Geological Society, Digest, No. 20, pp. 203-218.
- Melfos V., Vavelidis M., Christofides G. and Seidel E., 2002, *Origin and evolution of the Tertiary Maronia porphyry copper-molybdenum deposit, Thrace, Greece*, Mineralium Deposita, vol. 37, issues 6-7, pp. 648-668.
- Melfos, V., Voudouris P., Arikas K., and Vavelidis M., 2001, *Rhenium-rich molybdenites in Thracian Mo±Cu porphyry occurrences, NE Greece*, Bulletin of the

- Geological Society of Greece, vol. 34, issue 3, pp. 1015-1022. [in Greek]
- Meyer C. & Hemley J., 1967, *Wall rock alteration*. In: Barnes H. (Ed.), *Geochemistry of hydrothermal ore deposits*, Holt, Rinehart and Winston Editions, New York, pp. 166-235.
- Meyer C., 1965, *An early potassic type of wall-rock alteration at Butte, Montana*, *American Mineralogist*, vol. 50, pp. 1717-1722.
- Meyer C., Shea E., Goddard Jr. C., and staff of the Anaconda Company, 1968, *Ore deposits at Butte, Montana*. In: Ridge J. (Ed.), *Ore deposits of the United States, 1933-1967*, Grafton-Sales Series, New York, American Institute of Mining, Metallurgical and Petroleum Engineers, New York, vol. 2, pp. 1373-1416.
- Meyer P., 1981, *Ore-forming processes in geologic history*, *Economic Geology 75th Anniversary Volume*, pp. 6-41.
- Michailidis K., Fillipidis A., and Kassoli-Fournaraki A., 1993, *Polytypism and rhenium contents of molybdenites from two Mo-deposits in northern Greece*. In: Fenoll Hach-Ali P., Torres-Ruiz J., Gervilla F. (Eds.), *Current Research in Geology Applied to Ore Deposits*, Proceedings of the second biennial SGA meeting, Granada, Spain, pp. 641-644.
- Middlemost E., 1994, *Naming materials in the magma/igneous rock system*, *Earth-Science Reviews*, vol. 37, issues 3-4, pp. 215-224.
- Migiros G., Hatzipanagiotou K., Gartzos E., Serelis K., and Tsikouras B., 2000, *Petrogenetic evolution of ultramafic rocks from Lesbos Island (NE Aegean, Greece)*, *Chemier der Erde*, vol. 60, issue 1, pp. 27-46.
- Miller C., Peucker-Ehrenbrink B., Walker B., and Marcantonio F., 2011, *Re-assessing the surface cycling of molybdenum and rhenium*, *Geochimica et Cosmochimica Acta*, vol. 75, issue 22, pp. 7146-7179.
- Minubayeva Z. & Seward T., 2010, *Molybdic acid ionisation under hydrothermal conditions to 300 °C*, *Geochimica et Cosmochimica Acta*, vol. 74, issue 15, pp. 4365-4374.
- Monecke T., Monecke J., Reynolds T., Tsuruoka S., Bennett M., Skewe W., and Palin, R., 2018, *Quartz solubility in the H₂O-NaCl system: a framework for understanding vein formation in porphyry copper deposits*, *Economic Geology*, vol. 113, issue 5, pp. 1007-1046.
- Morachevskii D. & Nechaeva A., 1960, *Characteristics of migration of rhenium from molybdenites*, *Geokhimiya*, vol. 1970, pp. 648-645.
- Morelli R., Creaser R., Selby D., Kontak D., and Horne R., 2005, *Rhenium-osmium geochronology of arsenopyrite in Meguma Group gold deposits, Meguma terrane, Nova Scotia, Canada: evidence for multiple gold-mineralizing events*, *Economic Geology*, vol. 100, issue 6, pp. 1229-1242.
- Morette A., 1942, *Sur le système binaire tellure-mollybdène: tellurures de mollybdène Te₂Mo et Te₃Mo₃*, *Compte Rendus hebdomadaires de l'Academie des Sciences, Paris*, issue 2, pp. 86-88. [in French]
- Moritz R., Noverraz C., Márton I., Marchev P., Spikings R., Fontignie D., Spangenberg J., Vennemann T., Kolev K., and Hasson S., 2014, *Sedimentary-rock-hosted epithermal systems of the tertiary eastern Rhodopes, Bulgaria: new constraints from the Stremtsi gold prospect*. In: Garofalo P. & Ridley J. (Eds.), *Gold-transporting Hydrothermal Fluids in the Earth's Crust*, Geological society of London, Special Publication, No. 402, pp. 207-230.
- Moritz R., Rezeau H., Ovtcharova M., Tayan R., Melkonyan R., Hovakimyan S., Ramazanov V., Selby D., Ulianov A., Chiaradia M., and Putlitz B., 2016, *Long-lived, stationary magmatism and pulsed porphyry systems during Tethyan subduction to post-collision evolution in the southernmost lesser Caucasus, Armenia and Nakhitchevan*, *Gondwana Research*, vol. 37, pp. 465-503.
- Morris A. & Tarling D., 1996, *Palaeomagnetism and tectonics of the Mediterranean region: an introduction*. In: Fleet A. (Ed.), *Palaeomagnetism and Tectonics of the Mediterranean Region*, Geological Society of London, Special Publication, No. 105, pp. 1-18.
- Morris A., Anderson M., Inwood J., and Robertson A., 2006, *Palaeomagnetic insights into the evolution of Neotethyan oceanic crust in the eastern Mediterranean*. In: Robertson A. & Mountrakis D. (Eds.), *Tectonic Development of the Eastern Mediterranean Region*, Geological Society of London, Special Publication, No. 260, pp. 351-372.
- Morris D. & Short E., 1969, *Rhenium*. In: Wedepohl K. (Ed.), *Handbook of Geochemistry*, Springer Verlag Editions, New York.
- Mountain B. & Seward T., 2003, *Hydrosulfide complexes of copper (I): experimental confirmation of the stoichiometry and stability of Cu(HS)₂ to elevated temperatures*, *Geochimica et Cosmochimica Acta*, vol. 67, issue 16, pp. 3005-3014.
- Mountrakis D., Tranos M., Papazachos C., Thomaidou E., Karagianni E., and Vamvakaris D., 2006, *Neotectonic and seismological data concerning major active faults, and stress regimes of Northern Greece*. In: Robertson A. & Mountrakis D. (Eds.), *Tectonic Development of the*

- Eastern Mediterranean Region, Geological Society of London, Special Publication, No. 260, pp. 649-670.
- Muceku B., Mascle G., and Tashko A., 2006, *First results of fission track thermochronology in the Albanides*. In: Robertson A. & Mountrakis D. (Eds.), Tectonic Development of the Eastern Mediterranean Region, Geological Society of London, Special Publication, No. 260, pp. 539-556.
- Müller D. & Groves D., 1993, *Direct and indirect associations between potassic igneous rocks, shoshonites and gold-copper deposits*, Ore Geology Reviews, vol. 8, issue 5, pp. 383-406.
- Müller D., Kaminski K., Uhlig S., Graupner T., Herzig P.M., and Hunt S., 2002, *The transition from porphyry- to epithermal-style gold mineralization at Ladolam, Lihir Island, Papua New Guinea, A reconnaissance study*, Mineralium Deposita, vol. 37, issue 1, p. 61-74.
- Muntean J. & Einaudi M., 2000, *Porphyry gold deposits of the Refugio district, Maricunga belt, northern Chile*, Economic Geology, vol. 95, issue 7, pp. 1445-1472.
- Muntean J. & Einaudi M., 2001, *Porphyry-epithermal transition: Maricunga belt, northern Chile*, Economic Geology, vol. 96, issue 4, pp. 742-772.
- Mutschler F., Ludington S., and Bookstrom A., 1999, *Giant porphyry-related metal camps of the world; a database*, US Geological Survey Open File Report No. 99-556.
- Nakovnik N., 1968, *Secondary quartzites of the U.S.S.R. and related mineral deposits*, Izdatel'stvo Nedra, Moscow, pp. 335. [in Russian]
- Naney M., 1983, *Phase equilibria of rock-forming ferromagnesian silicates in granitic systems*, American Journal of Science, vol. 283, issue 10, pp. 993-1033.
- Newberry R., 1979a, *Polytypism in molybdenite (I): a non-equilibrium impurity induced phenomenon*, American Mineralogist, vol. 64, issues 7-8, pp. 758-767.
- Newberry R., 1979b, *Polytypism in molybdenite (II): relationships between polytypism, ore deposition/alteration stages and rhenium contents*, American Mineralogist, issues 7-8, pp. 768-775.
- Noble D., McCormack J., McKee E., Silberman M., and Wallace A., 1988, *Time of mineralization in the evolution of the McDermitt caldera complex, Nevada-Oregon, and the relation of middle Miocene mineralization in the northern Great basin to coeval regional basaltic magmatic activity*, Economic Geology, vol. 83, issue 4, pp. 859-863.
- Noll Jr. P., Newsom H., Leeman W., and Ryan J., 1996, *The role of hydrothermal fluids in the production of subduction zone magmas; evidence from siderophile and chalcophile trace elements and boron*, Geochimica et Cosmochimica Acta, vol. 60, issue 4, p. 587-611.
- Nunes P. & Ayres L., 1982, *U-Pb zircon age of the Archean Setting Net Lake porphyry molybdenum occurrence, northwestern Ontario*, Economic Geology, vol. 77, issue 5, pp. 1236-1239.
- Oehler J., 1976, *Hydrothermal crystallisation of silica gel*, Geological Society of America Bulletin, vol. 87, issue 8, pp. 1143-1152.
- Ohmoto H. & Rye R., 1967, *Isotopes of sulfur and carbon*. In: Barnes H. (Ed.), Geochemistry of Hydrothermal Ore Deposits, John Wiley and Sons Editions, New York, 2nd Edition, pp. 509-567.
- Okay A. & Göncüoğlu M., 2004, *The Karakaya Complex: a review of data and concepts*, Turkish Journal of Earth Sciences, vol. 13, issue 2, pp. 77-95.
- O'Neil R. & Chappell B., 1977, *Oxygen and hydrogen isotope relations in Berridale Batholith*, Journal of the Geological Society of London, vol. 133, issue 6, pp. 559-571.
- Ortelli M., Moritz R., Voudouris P., and Spangenberg J., 2009, *Tertiary porphyry and epithermal association of the Sapes-Kassiteres district, eastern Rhodopes, Greece*. In: Williams P. (Ed.), Smart Science for Exploration and Mining, Proceedings of the 10th Biennial SGA Meeting, Townsville, Australia, 17-20 August 2009, Economic Geology Research Unit, James Cook University, Douglas, pp. 536-538.
- Ortelli, M. 2009, *Tertiary Porphyry and Epithermal Association of the Sapes/Kassiteres District, Eastern Rhodopes, Greece*, MSc Thesis, University of Geneva, Geneva.
- Osatenko M. & Jones M., 1976, *Valley Copper*, Canadian Institute of Mining and Metallurgy, Special Volume, No. 15, pp. 130-143.
- Ossandón C., Fréaut C., Gustafson L., Lindsay D., and Zentilli M., 2001, *Geology of the Chuquicamata mine: a progress report*, Economic Geology, vol. 96, issue 2, pp. 249-270.
- Oygür V. & Erler A., 2000, *Metallogeny of Simav graben (inner-western Anatolia, Turkey)*, Geological Bulletin of Turkey, vol. 43, issue 1, pp. 7-19.
- Oygür V., 1997, *Anatomy of an epithermal mineralization: Mumcu (Balıkesir-Sındırgı), inner-western Anatolia, Turkey*, Bulletin of the Mineral Research and Exploration, vol. 119, pp. 29-39.

- Padilla Garza R., Titley S., and Pimentel B., 2001, *Geology of the Escondida porphyry copper deposit, Antofagasta region, Chile*, Economic Geology, vol. 96, issue 2, pp. 307-324.
- Palmer D., Simonson J., and Jensen J., 2004, *Partitioning of electrolytes to steam and their solubilities in steam*. In: Palmer D., Fernández-Prini R., and Harvey A. (Eds.), *Aqueous Systems at Elevated Temperatures and Pressures: Physical Chemistry in Water, Steam and Hydrothermal Solutions*, Elsevier, pp. 407-439.
- Panteleyev A., Drummond A., and Beaudoin P., 1976, *Berg*, Canadian Institute of Mining and Metallurgy, Special Volume, No. 15, pp. 274-283.
- Papadopoulou L., 2002, *Mineral phase equilibria, crystallization conditions and evolution of the Maronia pluton, Thrace, Greece*, PhD thesis, University of Thessaloniki. [in Greek]
- Papanikolaou D., 1984, *The three metamorphic belts of the Hellenides: a review and a kinematic interpretation*. In: Dixon J. & Robertson A. (Eds.), *The Geological Evolution of the Eastern Mediterranean*, Geological Society of London, Special Publication, No. 17, pp. 551-561.
- Papanikolaou D., 1989, *Are the medial crystalline massifs of the Eastern Mediterranean drifted Gondwanan fragments?*, Geological Society of Greece, Special Publication, No. 1, pp. 63-90.
- Papanikolaou D., 1993, *Geotectonic evolution of the Aegean*, Bulletin of the Geological Society of Greece vol. 28, issue 1, pp. 33-48.
- Papanikolaou D., 1997, *Introduction to the terrane descriptions of the Alpine Tethyan belt*, Annales Géologiques des Pays Helléniques, vol. 37, pp. 195-197.
- Papanikolaou D., 1999, *The Triassic ophiolites of Lesbos Island within the Cimmeride Orogenic event*, European Union of Geosciences, Conference Abstracts, EUG 10, Journal of Conference Abstracts, vol. 4, pp. 315.
- Papanikolaou D., 2009, *Timing of tectonic emplacement of ophiolites and terrane paleogeography in the Hellenides*, Lithos, vol. 108, issues 1-4, pp. 262-280.
- Papanikolaou D., Elbargathi H., Dabovski C., Dimitriu R., El-Hawat A., Ioane D., Kranis H., Obeidi A., Oaie G., Seghedi A., Zagorchev I., 2004, *TRANSMED Transect VII: East European Craton-Scythian Platform-Dobrogea-Balkanides-Rhodope Massif-Hellenides-East Mediterranean-Cyrenaica*. In: Cavazza W., Roure F., Spakman W., Stampfli G., and Zeigler P. (Eds.), *The TRANSMED Atlas – The Mediterranean Region from Crust to Mantle*, Springer Editions, Berlin, pp. 78-79.
- Papazachos B., Karakaisis G., Papazachos C., and Scordilis E., 2006, *Perspectives for earthquake prediction in the Mediterranean and contribution of geological observations*. In: Robertson A. & Mountrakis D. (Eds.), *Tectonic Development of the Eastern Mediterranean Region*, Geological Society of London, Special Publication, No. 260, pp. 689-707.
- Parry W., Jasumback M., and Wilson P., 2002, *Clay mineralogy of phyllic and intermediate argillic alteration at Bingham, Utah*, Economic Geology, vol. 97, issue 2, pp. 221-239.
- Pašava J., Svojtka M., Veselovský F., Ďurišova J., Ackerman L., Pour O., Drábek M., Halodová P., and Haluzová E., 2016, *Laser ablation ICPMS study of trace element chemistry in molybdenite coupled with scanning electron microscopy (SEM) – An important tool for identification of different types of mineralization*, Ore Geology Reviews, vol. 72, issue 1, pp. 874-895.
- Pavlidis S., Chatzipetros A., Tutkun Z., Özaksoy V., and Doğan B., 2006, *Evidence for late Holocene activity along the seismogenic fault of the 1999 Izmit earthquake, NW Turkey*. In: Robertson A. & Mountrakis D. (Eds.), *Tectonic Development of the Eastern Mediterranean Region*, Geological Society of London, Special Publication, No. 260, pp. 635-647.
- Pearce J., 1996, *A user's guide to basalt discrimination diagrams*. In: Wyman D. (Ed.), *Trace Elements Geochemistry of Volcanic Rocks: Applications for Massive sulphide Exploration*, Geological Association of Canada, Short Course Notes, No. 12, pp. 79-113.
- Pearce J., 2008, *Geochemical fingerprinting of oceanic basalts with applications to ophiolite classification and the search for Archean oceanic crust*, Lithos, vol. 100, issues 1-4, pp. 14-48.
- Pearce J., Harris N., and Tindle A., 1984, *Trace element discrimination diagrams for the tectonic interpretation of granitic rocks*, Journal of Petrology, vol. 25, issue 4, pp. 956-983.
- Peccerillo, A. & Taylor S.R., 1976, *Geochemistry of eocene calc-alkaline volcanic rocks from the Kastamonu area, Northern Turkey*, Contributions to Mineralogy and Petrology, vol. 58, issue 1, pp. 63-81.
- Pellant C., 1992, *Rocks and Minerals*, Dorling Kindersley Handbooks, Dorling Kindersley Limited, London.
- Penniston-Dorland S., 2001, *Illumination of vein quartz textures in a porphyry copper ore deposit using scanned cathodoluminescence: Grasberg Igneous Complex, Irian Jaya, Indonesia*, American Mineralogist, vol. 86, issues 5-6, pp. 652-666.

- Pe-Piper G. & Piper D., 1992, *Geochemical variation with time in the Cenozoic high-K volcanic rocks of the island of Lesbos, Greece: significance for shoshonite petrogenesis*, Journal of Volcanology and Geothermal Research, vol. 53, issues 1-4, pp. 371-387.
- Pe-Piper G. & Piper D., 1993, *Revised stratigraphy of the Miocene volcanic rocks of Lesbos, Greece*, Neues Jahrbuch für Geologie und Paläontologie, vol. 229, issue H2, pp. 97-110.
- Pe-Piper G. & Piper D., 2002, *The Igneous Rocks of Greece: The Anatomy of an Orogen*, Schweizerbart Scientific Publications, Stuttgart.
- Pe-Piper G., 1978, *The Cenozoic Volcanic Rocks of Lesbos*, Lectureship Thesis, University of Patras, Patras. [in Greek]
- Pe-Piper G., 1980a, *Geochemistry of Miocene shoshonites, Lesbos, Greece*, Contributions to Mineralogy and Petrology, vol. 72, issue 4, pp. 387-396.
- Pe-Piper G., 1980b, *The Cenozoic volcanic sequence of Lesbos, Greece*, Zeitschrift der Deutschen Geologischen Gesellschaft, vol. 131, pp. 889-901.
- Pe-Piper G., Piper D., Matarangas D., and Varti-Matarangas M., 2001, *The sub-ophiolitic melange of the island of Lesbos, Greece*, Neues Jahrbuch für Mineralogie, vol. 176, issue 6, pp. 241-260.
- Periferakis A., 2014, *Epithermal and Porphyry Ore Systems in Stypsi and Megala Therma Areas in Lesvos: a Mineralogical and Chemical Study and its Implications*, Diplomats Thesis, National and Kapodistrian University of Athens, Athens, Greece.
- Periferakis A., Voudouris P., Melfos V., Kolodziejczyk J., Mavrogonatos C., and Alfieris D., 2018, *New Mineralogical Data and Geochemical Constraints on the Stypsi-Megala Therma Porphyry-Epithermal Mineralisation, Lesvos Island, Greece*. In: Uysal I. (Ed.), 8th Geochemistry Symposium Abstracts Book, Trabzon, Turkey, pp. 189.
- Periferakis A., Voudouris P., Melfos V., Mavrogonatos C., and Alfieris D., 2017, *The Stypsi-Megala Therma porphyry-epithermal mineralisation, Lesvos Island, Greece: new mineralogical and geochemical data*, EGU General Assembly, Geophysical Research Abstracts, vol. 19, EGU2017-12950.
- Petford, N. & Atherton M., 1994, *Cretaceous-Tertiary volcanism and syn-subduction crustal extension in northern central Peru*, In: Smellie J. (Ed.), Volcanism Associated with Extension and Consuming Plate Margins, Geological Society of London, Special Publication, No. 81, pp. 233-248.
- Petruk W., 1964, *Mineralogy of the Mount Pleasant tin deposit, New Brunswick, Ottawa*, Department of Mines Technical Survey, Technical Bulletin, vol. 56.
- Pettke T., Oberli F., and Heinrich C., 2010, *The magma and metal source of giant porphyry-type ore deposits, based on lead isotope microanalysis of individual fluid inclusions*, Earth and Planetary Science Letters, vol. 296, issues 3-4, pp. 267-277.
- Pfiffner O.A., 2005, *The Alps*. In: Selley R., Cocks L., and Plimer I. (Eds.), Encyclopedia of Geology, Academic Press Books, vol. 2, pp. 125-135.
- Piomallo C. & Morelli A., 2003, *P wave tomography of the mantle under the Alpine-Mediterranean area*, Journal of Geophysical Research, vol. 108, issue 82, pp. 1-23.
- Pitcher W., 1993, *The Nature and Origin of Granite*, Springer Editions, London.
- Pokalov V., 1977, *Deposits of molybdenum*. In: Smirnov (Ed.), Ore Deposits of the U.S.S.R., Vol. III (translated), Pitman Publications, London, pp. 125-179.
- Pokrovski G., Borisova A., and Harrichoury J., 2008, *The effect of sulfur on vapor-liquid fractionation of metals in hydrothermal systems*, Earth and Planetary Science Letters, vol. 266, issues 3-4, pp. 345-362.
- Pollard P., Pichavant M., and Charoy B., 1987, *Contrasting evolution of fluorine and boron-rich tin systems*, Mineralium Deposita, vol. 22, issue 4, pp. 315-321.
- Power M., Pirrie D., Jedwab J., and Stanley C., 2004, *Platinum-group element mineralization in an As-rich magmatic sulfide system, Talnoy, southwest Scotland*, Mineralogical Magazine, vol. 68, issue 2, pp. 395-411.
- Proffett Jr. J., 2003a, *Geology of the Bajo de la Alumbrera porphyry copper-gold deposit, Argentina*, Economic Geology, vol. 98, issue 8, pp. 1535-1574.
- Proffett Jr. J., 2003b, *Maps to accompany geology of the Bajo de la Alumbrera porphyry copper-gold deposit, Argentina*, Supplement to Economic Geology, vol. 98, issue 8, 4 maps.
- Randive K., Vijaya Kumar J., Bhondwe A., and Lanjewar S., 2014, *Understanding the behaviour of Rare Earth Elements in minerals and rocks*, Gondwana Geological Magazine, vol. 29, issues 1-2, pp. 29-37.
- Rassios A. & Moores E., 2006, *Heterogenous mantle complex, crustal processes and obduction kinematics in a unified Pindos-Vourinos ophiolitic slab (northern Greece)*. In: Robertson A. & Mountrakis D. (Eds.), Tectonic Development of the Eastern Mediterranean

- Region, Geological Society of London, Special Publication, No. 260, pp. 237-246.
- Rathkopf C., Mazdab F., Barton I., and Barton M., 2017, *Grain-scale and deposit-scale heterogeneity of Re distribution in molybdenite at the Bagdad porphyry Cu-Mo deposit, Arizona*, Journal of Geochemical Exploration, vol. 178, pp. 45-54.
- Redmont P., Einaudi M., Inan E., Landtwing M., and Heinrich C., 2004, *Copper deposition by fluid cooling in intrusion-centered systems: new insights from the Bingham porphyry ore deposit, Utah*, Geology, vol. 32, issue 3, pp. 217-220.
- Rees D., Tezcan F., Haynes C., Walton M., Andrade S., Einsle O., and Howard J., 2005, *Structural basis of nitrogen fixation*, Philosophical Transactions of the Royal Society of London, vol. A363, pp. 971-984.
- Rempel K., Migdisov A., and Williams-Jones A., 2006, *The solubility and speciation of molybdenum in water vapour at elevated temperatures and pressures: implications for ore genesis*, Geochimica et Cosmochimica Acta, vol. 70, issue 3, pp. 687-696.
- Rempel K., Williams-Jones A., and Migdisov A., 2008, *The solubility of molybdenum dioxide and trioxide in HCl-bearing water vapour at 350 °C and pressures up to 160 bars*, Geochimica et Cosmochimica Acta, vol. 72, issue 13, pp. 3074-3083.
- Requia K., Stein H., Fontbote L., and Chiaradia M., 2003, *Re-Os and Pb-Pb geochronology of the Archean Salobo iron oxide copper-gold deposit, Carajas mineral province, northern Brazil*, Mineralium Deposita, vol. 38, issue 6, pp. 727-738.
- Rice S., Robertson A., and Ustaömer T., 2006, *Late Cretaceous-Early Cenozoic tectonic evolution of the Eurasian active margin in the Central and Eastern Pontides, northern Turkey*. In: Robertson A. & Mountrakis D. (Eds.), Tectonic Development of the Eastern Mediterranean Region, Geological Society of London, Special Publication, No. 260, pp. 413-444.
- Richards J., 1995, *Alkalic-type epithermal gold deposits-a review*, Mineralogical Association of Canada, Short Course Series, vol. 23, pp. 367-400.
- Richards J., 2009, *Postsubduction porphyry Cu-Au and epithermal Au deposits: products of remelting of subduction-modified lithosphere*, Geology, vol. 37, issue 3, pp. 247-250.
- Richards J., 2011, *Magmatic to hydrothermal metal fluxes in convergent and collided margins*, Ore Geology Reviews, vol. 40, issue 1, pp. 1-26.
- Ricou L.E., 1996, *The plate tectonic history of the past Tethys ocean*, In: Nairn A., Ricou L.E., Vrielynck B., and Dercourt J. (Eds.), The Ocean Basins and Margins, No. 8, The Tethys Ocean, Plenum Editions, New York, pp. 3-62.
- Ricou L.E., Burg J.P., Godfriaux I., and Ivanov Z., 1998, *Rhodope and Vardar: the metamorphic and olisostromic paired belts related to the Cretaceous subduction under Europe*, Geodinamica Acta, vol. 11, issue 6, pp. 285-309.
- Richter K., Chesley J., Geist D., and Ruiz J., 1998, *Behaviour of Re during magma fractionation: an example from Volcan Alcedo, Galapagos*, Journal of Petrology, vol. 39, issue 4, pp. 785-795.
- Rimmelé G., Oberhänsli R., Candan O., Goffé B., and Jolivet L., 2006, *The wide distribution of HP-LT rocks in the Lycian Belt (Western Turkey): implications for accretionary wedge geometry*. In: Robertson A. & Mountrakis D. (Eds.), Tectonic Development of the Eastern Mediterranean Region, Geological Society of London, Special Publication, No. 260, pp. 447-466.
- Rimstidt J. & Cole D., 1983, *Geothermal mineralisation; Part I. The mechanism of formation of the Beowawe, Nevada, siliceous sinter, Nevada*, American Journal of Science, vol. 283, issue 8, pp. 861-875.
- Ring U., Glodny J., Will T., and Thomson S., 2010, *The Hellenic subduction system: high pressure metamorphism, exhumation, normal faulting, and large-scale extension*, Annual Review of Earth and Planetary Sciences, vol. 38, pp. 45-76.
- Rittmann A., 1957, *On the series character of igneous rocks*, Egyptian Journal of Geology, vol. 1, issue 1, pp. 23-48.
- Rizaoglu T., Parlak O., Höck V., and İşler F., 2006, *Nature and significance of Late Cretaceous ophiolitic rocks and its relation to the Baskil granitoid in Elazığ region*. In: Robertson A. & Mountrakis D. (Eds.), Tectonic Development of the Eastern Mediterranean Region, Geological Society of London, Special Publication, No. 260, pp. 327-350.
- Robertson A. & Dixon J., 1984, *Introduction: aspects of the geological evolution of the Eastern Mediterranean*. In: Robertson A. & Dixon J. (Eds.), The Geological Evolution of the Eastern Mediterranean, Geological Society of London, Special Publication, No. 17, pp. 1-74.
- Robertson A. & Mountrakis D., 2006, *Tectonic development of the eastern Mediterranean region: an introduction*. In: Robertson A. & Mountrakis D. (Eds.), Tectonic Development of the Eastern Mediterranean Region, Geological Society of London, Special Publication, No. 260, pp. 1-9

- Robertson A., 2002, *Overview of the genesis and emplacement of Mesozoic ophiolites in the Eastern Mediterranean Tethyan region*, Lithos, vol. 65, issues 1-2, pp. 1-67.
- Robertson A., Clift P., Degnan P., and Jones G., 1991, *Palaeogeographic and palaeotectonic evolution of the Eastern Mediterranean Neotethys*, Palaeogeography, Palaeoclimatology, Palaeoecology, vol. 87, issues 1-4, pp. 289-344.
- Robertson A., Ustaömer T., Pickett E., Collins A., Andrew T., and Dixon J., 2004, *Testing models of Late Palaeozoic-Early Mesozoic orogeny: support for an evolving one-Tethys model*, Journal of the Geological Society of London, vol. 161, issue 3, pp. 501-511.
- Robertson, A., Dixon, J., Brown S., Collins A., Morris A., Pickett E, and Sharp I., 1996, *Alternative tectonic models for the Late Palaeozoic-Early Tertiary development of Tethys in the eastern Mediterranean region*. In: Morris A. & Tarling D.M. (Eds.), Palaeomagnetism and Tectonics of the Mediterranean region, Geological society of London, Special Publication, No. 105, pp. 239-263.
- Roedder E., 1984, *The fluids in salt*, American Mineralogist, vol. 69, issues 5-6, pp. 413-439.
- Rogers A., 1917, *A review of amorphous minerals*, Journal of Petrology, vol. 25, issue 6, pp. 515-541.
- Romano S., Brix M., Dörr W., Fiala J., Krenn E., and Zulauf G., 2006, *The Carboniferous to Jurassic evolution of the pre-Alpine basement of Crete: constraints from U-Pb and U-(Th)-Pb dating of orthogneiss, fission-track dating of zircon, structural and petrological data*. In: Robertson A. & Mountrakis D. (Eds.), Tectonic Development of the Eastern Mediterranean Region, Geological Society of London, Special Publication, No. 260, pp. 69-90.
- Romero B., Kojima S., Wong C., Barra F., Véliz W., and Ruiz J., 2010, *Molybdenite mineralization and Re-Os geochronology of the Escondida and Escondida Norte porphyry deposits, Northern Chile*, Resource Geology, vol. 61, issue 1., pp. 91-100.
- Ronacher E., Richards J., Reed M., Bray C., Spooner E., and Adams P., 2004, *Characteristics and evolution of the hydrothermal fluid in the North zone high-grade area, Porgera gold deposit, Papua New Guinea*, Economic Geology, vol. 99, issue 5, pp. 843-867.
- Rusk B. & Reed M., 2002, *Scanning electron microscope-cathodoluminescence analysis of quartz reveals complex growth histories in veins from the Butte porphyry copper deposit, Montana*, Geology, vol. 30, issue 8, pp. 727-730.
- Ryabchikov I., Orlova G., Yefimov A., and Kalenchuk G., 1980, *Copper in a granite-fluid system*, Geochemistry International, vol. 17, issue 5, pp. 29-34.
- Ryabchikov I., Rekharskiy V., and Kudrin A., 1981, *Mobilization of molybdenum by fluids during the crystallization of granite melts*, Geochemistry International, vol. 18, issue 4, pp. 183-186.
- Ryan W., Stanley D., Hersey J., Fahlquist D., and Allan T., 1971, *The tectonics and geology of the Mediterranean Sea*. In: Maxwell A. (Ed.), The sea, vol. 4, part. 2, Interscience Editions, New York, USA, Pp. 387-492.
- Rye R., 1993, *The evolution of magmatic fluids in the epithermal environment: the stable isotope perspective*, Economic Geology, vol. 88, issue 3, pp. 733-752.
- Rye R., 2005, *A review of the stable-isotope geochemistry of sulfate minerals in selected igneous environments and related hydrothermal systems*, Chemical Geology, vol. 215, issues 1-4, pp. 5-36.
- Sánchez M., McClay K., and King A., 2016, *Crustal extension and its relationship to porphyry Cu-Au and epithermal Au mineralization in the Biga Peninsula, NW Turkey*. In: Richards J. (Ed.), Tectonics and Metallogeny of the Tethyan Metallogenic Belt, Society of Economic Geology, Special Publication, vol. 19, pp. 113-156.
- Sander, M. & Black J., 1988, *Crystallization and recrystallization of growth-zoned vein quartz crystals from epithermal systems – implications for fluid inclusion studies*, Economic Geology, vol. 83, issue 5, pp. 1052-1060.
- Saunders J. & Brueseke M., 2012, *Volatility of Se and Te during subduction-related distillation and the geochemistry of epithermal ores of the Western United States*, Economic Geology, vol. 107, issue 1, pp. 165-172.
- Saunders J., 1990, *Colloidal transport of gold and silica in epithermal precious-metal systems: evidence from the Sleeper deposits, Nevada*, Geology, vol. 18, issue 8, pp. 757-760.
- Saunders J., Unger D., Kamenov G., Fayek M., Hames W., and Utterback W., 2008, *Genesis of middle Miocene Yellowstone-hotspot-related bonanza epithermal Au-Ag deposits, Northern Great Basin region, USA*, Mineralium Deposita, v. 43, issue 7, p. 715-734.
- Sawkins F., 1984, *Metal deposits in relation to plate tectonics*, Springer Editions, London.
- Schandl E. & Gorton M., 2002, *Applications of high field strength elements to discriminate tectonic setting in VMS*

- environments, *Economic Geology*, vol. 97, issue 3, pp. 629-642.
- Scherkenbach D., Sawkins F., and Seyfried Jr. W., 1985, *Geologic, fluid inclusion, and geochemical studies of the mineralized breccias at Cumobabi, Sonora, Mexico*, *Economic Geology*, vol. 80, issue 6, pp. 1566-1592.
- Schmidt E., Broch M., and White R., 1983, *Geology of the Thompson Creek molybdenum deposit, Custer County, Idaho. The genesis of Rocky Mountain ore deposits: changes with time and tectonics*, Denver Region Exploration Geologists Society Symposium, 4-5 November 1982, Proceedings, Denver, USA, pp. 79-84.
- Schrader F., 1912, *A reconnaissance of the Jarbidge, Contact and Elk mountain mining districts, Elco County, Nevada*, US Geological Survey Bulletin, vol. 741.
- Schwartz G., Mendel R., and Ribbe M., 2009, *Molybdenum cofactors, enzymes and pathways*, *Nature*, vol. 460, pp. 839-847.
- Seebach M., 1926, *Molybdanglanz*. In: C. Doelter C. & Leitmeier H. (Eds.), *Handbuch der Mineralchemie, Band IV Erste Halfte*, Theoder Skinkop Editions, Dresden, pp. 67-74. [in German]
- Seedorff E. & Einaudi M., 2004a, *Henderson porphyry molybdenum system, Colorado, pt. I., sequence and abundance of hydrothermal mineral assemblages, flow paths of evolving fluids, and evolutionary style*, *Economic Geology*, vol. 99, issue 1, pp. 3-37.
- Seedorff E. & Einaudi M., 2004b, *Henderson porphyry molybdenum system, Colorado, pt. II., decoupling of introduction and deposition of metals during geochemical evolution of hydrothermal fluids*, *Economic Geology*, vol. 99, issue 1, pp. 39-72.
- Seedorff E., 1988, *Cyclic development of hydrothermal mineral assemblages related to multiple intrusions at the Henderson porphyry molybdenum deposit, Colorado*, Canadian Institute of Mining and Metallogeny, Special Volume, No. 39, pp. 367-393.
- Seedorff E., 1993, *Alteration logged in core holes from the Liberty pit, metal and alteration zoning in the Ruth-Ruth Extension arc, and implications for structural reconstructions*, Geological Society of Nevada, Special Publication, No. 17, pp. 28-31.
- Seedorff E., Dilles J., Proffett Jr. J., Einaudi M., Zurcher L., Stavast D., Johnson D., and Barton M., 2005, *Porphyry deposits: characteristics and origin of hypogene features*, *Economic Geology*, vol. 100, issue 1, pp. 251-298.
- Selby D. & Creaser R., 2001, *Re-Os geochronology and systematics in molybdenite from the Endako porphyry molybdenum deposit, British Columbia, Canada*, *Economic Geology*, vol. 96, issue 1, pp. 197-204.
- Selby D. & Creaser R., 2004, *Macroscale NTIMS and microscale LA-MC-ICP-MS Re-Os isotopic analysis of molybdenite: testing spatial restriction for reliable Re-Os age determinations, and implications for the decoupling of Re and Os within molybdenite*, *Geochimica et Cosmochimica Acta*, vol. 68, issue 19, pp. 3897-3908.
- Selby D., Nesbitt B., Muchlenbachs K., and Prochaska W., 2000, *Hydrothermal alteration and fluid chemistry of the Endako porphyry molybdenum deposit, British Columbia*, *Economic Geology*, vol. 95, issue 1, pp. 183-202.
- Sengor A. & Yilmaz Y., 1981, *Tethyan evolution of Turkey: a plate tectonic approach*, *Tectonophysics*, vol. 75, issues 3-4, pp. 81-241.
- Sengor A., 1984, *The Cimmeride Orogenic System and the Tectonics of Eurasia*, Geological Society of America, Special Paper, No. 195.
- Seo J., Guillong M., and Heinrich A., 2012, *Separation of molybdenum and copper: the roles of sulfur, redox and pH in ore mineral deposition at Bingham Canyon*, *Economic Geology*, vol. 107, issue 2, pp. 333-356.
- Seo J., Guillong M., and Heinrich C., 2009, *The role of sulfur in the formation of magmatic-hydrothermal copper-gold deposits*, *Earth and Planetary Science Letters*, vol. 282, issues 1-4, pp. 323-328.
- Serafica V. & Baluda R., 1977, *Geology of the Philex Santo Tomas II ore body*, 5th Symposium on Mineral Resources Development, Baguio City, Philippines, 24-26 November 1977, Section 1, Paper 3.
- Seward T. & Barnes H., 1997, *Metal transport by hydrothermal ore fluids*. In: Barnes H (Ed.), *Geochemistry of Hydrothermal Ore Deposits*, Wiley Editions, 3rd edition, pp. 435-486.
- Seward T. & Sheppard D., 1986, *Waimangu geothermal field*. In: Henley R., Roberts P., and Hedenquist J. (Eds.), *Guide to the Active Epithermal (Geothermal) Systems and Precious Metal Deposits of New Zealand*, Monograph Series on Mineral Deposits, vol. 26, Balogh Scientific Books, Champaign, Illinois, pp. 81-91.
- Seward T., 1981, *Metal complex formation in aqueous solutions at elevated temperatures and pressures*, *Physics and Chemistry of the Earth*, vol. 13 & 14, pp. 113-132.
- Shand S., 1927, *Eruptive Rocks, Their Genesis, Composition, Classification, and their Relation to Ore Deposits*, T.Murby & Company Publishers, London.

- Shand, S.J., 1943, *The Eruptive Rocks*, John Wiley and Sons, New York.
- Sharp I. & Robertson A., 1998, *Late Jurassic-Lower Cretaceous oceanic crust and sediments of the Eastern Almopias Zone, NW Macedonia (Greece); implications for the evolution of the Eastern 'Internal' Hellenides*, Bulletin of the Geological Society of Greece, vol. 30, issue 1, pp. 47-61.
- Sharp J., 1979, *Cave Peak, a molybdenum-mineralized breccia pipe complex in Culberson County, Texas*, Economic Geology, vol. 74, issue 3, pp. 517-534.
- Shaub B., 1934, *The cause of banding in fissure veins*, American Mineralogist, vol. 15, issue 9, pp. 393-402.
- Shaver S., 1991, *Geology, alteration, mineralization and trace element geochemistry of the Hall (Nevada Moly) deposit, Nye County, Nevada*, Geology and Ore Deposits of the Great Basin, Geological Society of Nevada Symposium, Reno/Sparks, April 1990, Proceedings, vol. 1, pp. 303-332.
- Sherlock R., Tosdal R., Lehrman N., Craney J., Losh S., Jowett E., and Kesler S., 1995, *Origin of the McLaughlin mine sheeted vein complex: metal zoning, fluid inclusion, and isotopic evidence*, Economic Geology, vol. 90, issue 8, pp. 2156-2181.
- Shinohara H., & Hedenquist J., 1997, *Constraints on magma degassing beneath the Far Southeast porphyry Cu-Au deposit, Philippines*, Journal of Petrology, vol. 38, issue 12, pp. 1741-1752.
- Shinohara H., Kazahaya K., and Lowenstern J., 1995, *Volatile transport in a convecting magma column: implications for porphyry Mo mineralization*, Geology vol. 23, issue 12, pp. 1091-1094.
- Shirey S. & Richardson S., 2011, *Start of the Wilson Cycle at 3 Ga shown from diamonds from the subcontinental mantle*, Science, vol. 333, issue 6041, pp. 434-436.
- Shirey S. & Walker R., 1998, *The Re-Os isotope system in cosmochemistry and high-temperature geochemistry*, Annual Reviews of Earth and Planetary Sciences, vol. 26, pp. 423-500.
- Signorelli S. & Carroll M., 2000, *Solubility and fluid-melt partitioning of Cl in hydrous phonolite melts*, Geochimica et Cosmochimica Acta, vol. 64, issue 16, pp. 2851-2862.
- Sillitoe R. & Gappe Jr. I., 1984, *Philippine porphyry copper deposits: geologic setting and characteristics: United Nations Economic Social Commission Asia-Pacific*, Committee for Coordination of Joint Prospecting for Mineral Resources in Asian Offshore Areas, Technical Publication No. 14.
- Sillitoe R. & Hedenquist J., 2003, *Linkages between volcanotectonic settings, ore-fluid compositions, and epithermal precious metal deposits*, In: Simmons S. & Graham I. (Eds.). Volcanic, Geothermal, and Ore-Forming Fluids: Rulers and Witnesses of Processes within the Earth, Society of Economic Geologists, Special Publication, No. 10, pp. 315-345.
- Sillitoe R. & Khan S., 1977, *Geology of Saindak porphyry copper deposit, Pakistan*, Institution of Mining and Metallurgy, Transactions, vol. 86, pp. B27-B42.
- Sillitoe R., 1972, *A plate tectonic model for the origin of porphyry copper deposits*, Economic Geology, vol. 67, issue 2, pp. 184-197.
- Sillitoe R., 1976, *Andean mineralisation: a model for the metallogeny of convergent plate margins*. In: Strong D. (Ed.), Metallogeny and Plate Tectonics, Geological Association of Canada Special Paper, No. 14, pp. 59-100.
- Sillitoe R., 1979, *Some thoughts on gold-rich porphyry copper deposits*, Mineralium Deposita vol. 14, issue 2, pp. 161-174.
- Sillitoe R., 1980, *Types of porphyry molybdenum deposits*, Mining Magazine, vol. 142, pp. 550-553.
- Sillitoe R., 1983, *Enargite-bearing massive sulfide deposits high in porphyry copper systems*, Economic Geology, vol. 78, issue 2, pp. 348-352.
- Sillitoe R., 1985, *Ore-related breccias in volcanoplutonic arcs*, Economic Geology, vol. 80, issue 6, pp. 1467-1514.
- Sillitoe R., 1989, *Gold deposits in western Pacific island arcs: the magmatic connection*. In: Keays R., Ramsay W., and Groves D. (Eds.), The Geology of Gold Deposits: the Perspective in 1988, Economic Geology Monograph, No. 6, pp. 274-291.
- Sillitoe R., 1993a, *Gold-rich porphyry copper deposits: geological model and exploration implications*. In: Kirkham R., Sinclair W., Thorpe R., and Duke J. (Eds.), Mineral Deposit Modeling, Geological Association of Canada, Special Paper No. 40, pp. 465-478.
- Sillitoe R., 1993b, *Epithermal models: genetic types, geometrical controls and shallow features*. In: Kirkham R., Sinclair W., Thorpe R., and Duke J. (Eds.), Mineral Deposit Modeling, Geological Association of Canada, Special Paper No. 40, pp. 403-418.

- Sillitoe R., 1994, *Erosion and collapse of volcanoes: causes of telescoping in intrusion-centered ore deposits*, *Geology*, vol. 22, issue 10, pp. 945-948.
- Sillitoe R., 1997, *Characteristics and controls of the largest porphyry copper-gold and epithermal gold deposits in the Circum-Pacific region*, *Australian Journal of Earth Sciences*, vol. 44, issue 3, pp. 373-388.
- Sillitoe R., 1998, *Major regional factors favouring large size, high hypogene grade, elevated gold content and supergene oxidation and enrichment of porphyry copper deposits*. In: Porter T. (Ed.), *Porphyry and Hydrothermal Copper and Gold Deposits: A Global Perspective*, Perth, 1998, Conference proceedings, Australian Mineral Foundation, Glenside, pp. 21-34.
- Sillitoe R., 1999, *Styles of high-sulphidation gold, silver and copper mineralization in the porphyry and epithermal environments*. In: Weber G. (Ed.), *Pacrim 1999 Congress, Bali, Indonesia, Conference Proceedings*, Australasian Institute of Mining and Metallurgy, Parkville, pp. 29-44.
- Sillitoe R., 2000, *Gold-rich porphyry deposits: descriptive and genetic models and their role in exploration and discovery*. In: Hagemann S. & Brown P. (Eds.), *Reviews in Economic Geology*, vol. 13, pp. 315-345.
- Sillitoe R., 2002, *Some metallogenic features of gold and copper deposits related to alkaline rocks and consequences for exploration*, *Mineralium Deposita*, vol. 37, issue 1, pp. 4-13.
- Sillitoe R., 2005, *Supergene oxidized and enriched porphyry copper and related deposits*, *Economic Geology*, 100th Anniversary Volume, pp. 723-768.
- Sillitoe R., Steele G., Thompson J., and Lang, J., 1998, *Advanced argillic lithocaps in the Bolivian tin-silver belt*, *Mineralium Deposita*, vol. 33, issue 6, pp. 539-546.
- Simmons S. & Brown K., 2007, *The flux of gold and related metals through a volcanic arc, Taupo Volcanic Zone, New Zealand*, *Geology*, vol. 35, issue 12, pp. 1099-1102.
- Simmons S., 1991, *Hydrologic implications of alteration and fluid inclusion studies in the Fresnillo district, Mexico: evidence for a brine reservoir and a descending water table during the formation of hydrothermal Ag-Pb-Zn orebodies*, *Economic Geology*, vol. 86, issue 8, pp. 1579-1601.
- Simmons S., Gemmill J., Sawkins F., 1988, *The Santo Nino silver-lead-zinc vein, Fresnillo District, Zacatecas, Mexico; Part II: Physical and chemical nature of ore-forming solutions*, *Economic Geology*, vol. 83, issue 8, pp. 1619-1641.
- Simmons S., White N., and John D., 2005, *Geological characteristics of epithermal precious metal and base metal deposits*, *Economic Geology*, 100th Anniversary volume, pp. 485-522.
- Simon A., Pettke T., Candela P., Piccoli P., and Heinrich C., 2004, *Magnetite solubility and iron transport in magmatic-hydrothermal environments*, *Geochimica et Cosmochimica Acta*, vol. 68, issue 23, pp. 4905-4914.
- Simon A., Pettke T., Candela P., Piccoli P., and Heinrich C., 2006, *Copper partitioning in a melt-vapor-brine-magnetite-pyrrhotite assemblage*, *Geochimica et Cosmochimica Acta*, vol. 70, issue 22, pp. 5583-5600.
- Sinclair D., Jonasson I., Kirkham R., Soregaroli A., 2009, *Rhenium and other platinum-group metals in porphyry deposits*, Open File Report 6181, Geological Survey of Canada, Ottawa, Canada.
- Sinclair W., 2007, *Porphyry Deposits*. In: Goodfellow W. (Ed.), *Mineral Deposits of Canada: A Synthesis of Major Deposit Types, District Metallogeny, the Evolution of Geological Provinces, and Exploration Methods*, Geological Association of Canada, Mineral Deposits Division, Special Publication, No 5, pp. 223-243.
- Singer D., Berger V., and Moring B., 2005, *Porphyry copper deposits of the world: database, map, and grade and tonnage models*, US Geological Survey Open-File Report, <http://pubs.usgs.gov/of/2005/1060>.
- Skewes C. & Stern M., 1996, *Late Miocene mineralized breccias in the Andes of Central Chile: Sr- and Nd-isotopic evidence for multiple magmatic sources*, *Society of Economic Geologists, Special Publication*, No. 5, pp. 33-41.
- Smith A., 1971, *Alpine deformation and the oceanic areas of the Tethys, Mediterranean and Atlantic*, *Geological Society of America Bulletin*, vol. 82, issue 8, pp. 2039-2070.
- Smith A., 1993, *Tectonic significance of the Hellenic-Dinaric ophiolites*. In: Prichard H., Alabaster T., Harris N., and Nance D. (Eds.), *Magmatic Processes and Plate Tectonics*, Geological Society of London, Special Publications, No. 76, London, pp. 213-243.
- Smith A., 2006, *Tethyan ophiolite emplacement, Africa to Europe motions, and Atlantic spreading*. In: Robertson A. & Mountrakis D. (Eds.), *Tectonic Development of the Eastern Mediterranean Region*, Geological Society of London, Special Publication, No. 260, pp. 11-34.
- Smith A., Hynes A., Menzies M., Nisbet E., Price I., Welland M., and Ferrière J., 1975, *The stratigraphy of the Othris Mountains, Eastern Central Greece: a*

- deformed Mesozoic continental margin sequence*, *Eclogae Geologicae Helvetiae*, vol. 68, issue 3, 463-481.
- Sokoutis D., Brun J., Driessche J., and Pavlides S., 1993, *A major Oligo-Miocene detachment in southern Rhodope controlling north Aegean extension*, *Journal of the Geological Society of London*, vol. 150, issue 2, pp. 243-246.
- Sonder L. & Jones C., 1999, *Western United States extension: how the west was widened*, *Annual Review of Earth and Planetary Sciences*, vol. 27, p. 417-462.
- Spakman W., 1990, *Tomographic images of the upper mantle below central Europe and the Mediterranean*, *Terra Nova*, vol. 2, issue 6, pp. 542-553.
- Spurr J.E., 1926, *Successive banding around rock fragments in veins*, *Economic Geology*, vol. 21, issue 6, pp. 519-537.
- Stampfli G. & Borel G., 2002, *A plate tectonic model for the Palaeozoic and Mesozoic constrained by dynamic plate boundaries and restored synthetic oceanic isochrones*, *Earth and Planetary Science Letters*, vol. 199, issues 1-2, pp. 17-33.
- Stampfli G., Mosar J., Fauré P., Pilleveit A., and Vannay J.C., 2001, *Permo-mesozoic evolution of the Western Tethys realm: the Neotethys East Mediterranean basin connection*. In: Ziegler P., Cavazza W., Robertson A., and Crasquinsoleau S. (Eds.), *Peri-Tethys Memoir No. 6: Peri-Tethyan Rift/Wrench Basins and Passive Margins*, *Mémoires du Muséum National d' Histoire Naturelle*, pp. 51-108.
- Staub R., 1924, *Der Bau des Alpen*, *Beiträge zur geologischen Karte der Schweiz*, No. 52. [in German]
- Steeffel C. & Atkinson Jr. W., 1984, *Hydrothermal andalusite and corundum in the Elkhorn district, Montana*, *Economic Geology*, vol. 79, issue 3, pp. 573-579.
- Stefánsson A. & Seward T., 2004, *Gold (I) complexing in aqueous sulfide solutions to 500 °C at 500 bar*, *Geochimica et Cosmochimica Acta*, vol. 68, issue 20, pp. 4121-4143.
- Stein H., 2006, *Low-rhenium molybdenite by metamorphism in northern Sweden: recognition, genesis and global implications*, *Lithos*, vol. 87, issues 3-4, pp. 300-327.
- Stein H., Marke R., Morgan J., Hannah J., and Scherstén A., 2001, *The remarkable Re-Os chronometer in molybdenite: how and why it works*, *Terra Nova*, vol. 13, issue 6, pp. 479-486.
- Stein H., Schersten A., Hannah J., and Markey R., 2003, *Subgrain-scale decoupling of Re and ¹⁸⁷O and assessment of laser ablation ICP-MS spot dating in molybdenite*, *Geochimica et Cosmochimica Acta*, vol. 67, issue 19, pp. 3673-3686.
- Steininger R., 1973, *Hydrothermal alteration in some quartz monzonite dikes at the Climax molybdenum deposit, Colorado*. In: Hamblin W. (Ed.), *Brigham Young University Geology Studies*, vol. 20, part 1, pp. 115-128.
- Steinmann G., 1905, *Geologische Beobachtungen in den Alpen. II; Die Scharf'sche Überfaltungstheorie und die geologische Bedeutung der Tiefseeabsätze und der ophiolithischen Massengesteine*, *Berichte der Naturforschenden Gesellschaft zu Freiburg im Breisgau*, vol. 16, Germany, pp. 18-67. [in German]
- Štemprok M., 1982, *Tin-fluorine relationships in ore-bearing assemblages*. In: Evans A. (Ed.) *Metallization Associated with Acid Magmatism*, Wiley Editions, New York, pp. 321-337.
- Štemprok M., 1984, *Alkaline trend in the differentiation of tin bearing granites*. In: Janelidze T. & Tvalchrelidze A. (Eds.), *Proceedings of the Sixth Quadrennial IAGOD Symposium*, Schweizerbarth, Stuttgart, pp. 449-455.
- Steven T. & Ratté J., 1960, *Geology of ore deposits of the Summitville district, San Juan Mountains, Colorado*, U.S. Geological Survey, Professional Paper, No. 343.
- Stöcklin J., 1968, *Structural history and tectonics of Iran: a review*, *American Association of Petroleum Geologists, Bulletin*, vol. 52, issue 7, pp. 1229-1258.
- Stoffregen R., 1987, *Genesis of acid sulfate alteration and Au-Cu mineralization at Summitville*, *Economic Geology*, vol. 82, issue 6, pp. 1575-1591.
- Stoiper E. & Newman S., 1993, *The role of water in the petrogenesis of Mariana trough magmas*, *Earth and Planetary Science Letters*, vol. 121, issue 3-4, pp. 293-325.
- Suess E., 1875, *Die Entstehung der Alpen*, Wilhelm Braumüller Publikationen, Wien. [in German]
- Sun S., McDonough W.F., 1989, *Chemical and isotope systematics of oceanic basalts: implications for mantle composition and processes*. In: Saunders, A., Norry, M. (Eds.), *Magmatism in the Ocean Basins*. Geological Society of London, Special Publication, No. 42, pp. 313-345.
- Sun W., Arculus R., Kamenetsky V., and Binns R., 2004, *Release of gold-bearing fluids in convergent margin magmas prompted by magnetite crystallisation*, *Nature*, vol. 431, pp. 975-978.

- Takada A., 1994, *The influence of regional stress and magmatic input on styles of monogenetic and polygenetic volcanism*, Journal of Geophysical Research, vol. 99, issue 7, pp. 13563-13573.
- Tarkian M. & Koopman G., 1995, *Platinum-group minerals in the Santo Tomas II (Philex) porphyry copper-gold deposit, Luzon Island, Philippines*, Mineralium Deposita, vol. 30, pp. 39-47.
- Taylor S. & McLennan S., 1985, *The Continental Crust: Its Composition and Evolution*, Blackwell Scientific Publications, London.
- Tessalina S., Yudovskaya M., Chaplygin I., Birck J.L., and Capmas F., 2008, *Sources of unique rhenium enrichment in fumaroles and sulphides at Kudryavy volcano*, Geochimica et Cosmochimica Acta, vol. 72, issue 3, pp. 889-909.
- Theodore T., Blake D., Loucks T., and Johnson C., 1992, *Geology of the Buckingham stockwork molybdenum deposit and surrounding area, Lander County, Nevada*, U.S. Geological Survey, Professional Paper, Series D, No. 798.
- Thompson A., 1996, *Fertility of crustal rocks during anatexis*, Transactions of the Royal Society of Edinburgh, vol. 87, issue 1-2, pp. 1-10.
- Tirel C., Gueydan F., Tiberi C., and Brun J.P., 2004, *Aegean crustal thickness inferred from gravity inversion. Geodynamical implications*, Earth and Planetary Science Letters, vol. 228, issues 3-4, pp. 267-280.
- Titley S. & Beane R., 1981, *Porphyry copper deposits, Part I: Geologic settings, petrology and tectogenesis*, Economic Geology 75th Anniversary Volume, pp. 214-234.
- Titley S., 1966, *Preface*. In: Titley S. & Hicks C. (Eds.), *Geology of the Porphyry Copper Deposits, Southwestern North America*, University of Arizona, Tucson, pp. ix-x.
- Titley S., 1982a, *The style and progress of mineralization and alteration in porphyry copper systems*, In: Titley S. (Ed.), *Advances in Geology of the porphyry copper deposits, southwestern North America*, University of Arizona Press, Tucson, Arizona, pp. 93-116.
- Titley S., 1982b, *Geologic setting of porphyry copper deposits*. In: Titley S. (Ed.), *Advances in Geology of the Porphyry Copper Deposits, Southwestern North America*, University of Arizona Press, Tucson, Arizona, pp. 37-58.
- Titley S., Thompson R., Haynes F., Manske S., Robison L., and White J., 1986, *Evolution of fractures and alteration in the Sierrita-Esperanza hydrothermal system, Pima County, Arizona*, Economic Geology, vol. 81, issue 2, pp. 343-370.
- Tosdal R. & Richards J., 2001, *Magmatic and structural controls on the development of porphyry Cu ± Mo ± Au deposits*. In: Richards J. & Tosdal R. (Eds.), *Structural Controls on Ore Genesis*, Reviews in Economic Geology, vol. 14, pp. 157-181.
- Tosdal R., Sherlock R., Nelson G., Enderlin D., and Lehrman N., 1996, *Precious metal mineralization in a fold and thrust belt: the McLaughlin hot spring deposit, northern California*. In: Coyner A. & Fahey P. (Eds.), *Geology and ore deposits of the American Cordillera*, Symposium proceedings, vol. 2, Geological Society of Nevada, pp. 839-854.
- Tranos M., Karakostas V., Papadimitriou E., Kachev V., Rangelov B., and Gospodinov D., 2006, *Major active faults of SW Bulgaria: implications of their geometry, kinematic and regional active stress regime*. In: Robertson A. & Mountrakis D. (Eds.), *Tectonic Development of the Eastern Mediterranean Region*, Geological Society of London, Special Publication, No. 260, pp. 671-688.
- Trigunayat G., 1971, *Progress in the study of polytypism in crystals (II)*, Physical Status Solidi (a), vol. 4, issue 2, pp. 281-303.
- Troutman S., 2001, *Advanced argillic alteration in the deeply buried Magma Porphyry Cu-Mo prospect, Superior, Arizona*, M.Sc. Thesis, Stanford University, Stanford.
- Tsikouras B., Beltas P., and Hatzipanagiotou K., 1994, *Petrography and geochemistry of basaltic rocks from the Vatera ophiolitic mélange (S. Lesvos, northern Aegean)*, Bulletin of the Geological Society of Greece, vol. 30, pp. 103-112.
- Urabe T., 1985, *Aluminous granite as a source magma of hydrothermal ore deposits: an experimental study*, Economic Geology, vol. 80, issue 1, pp. 148-157.
- Vamvaka A., Kiliass A., Mountrakis D., and Papaikononou J., 2006, *Geometry and structural evolution of the Mesohellenic Trough (Greece): a new approach*. In: Robertson A. & Mountrakis D. (Eds.), *Tectonic Development of the Eastern Mediterranean Region*, Geological Society of London, Special Publication, No. 260, pp. 521-538.
- Vamvoukakis C., 2009, *Epithermal Au-Ag mineralisation in Lesvos Island*, Ph.D. Thesis, University of Patras, Patras. [in Greek]
- Vamvoukakis C., St. Seymour K., Kouli M., Lamera S. and Denes G., 2005, *Investigation of non pristine volcanic structures acting as probable hosts to*

- epithermal gold mineralization in the back arc region of the active Aegean arc, using combined satellite imagery and field data: examples from Lesvos volcanic terrain*, Developments in Volcanology, Volume 7, 2005, pp. 329-343.
- van Hinsbergen D., Hafkenscheid E., Spakman W., Meulenkamp J., and Wortel R., 2005a, *Nappe stacking resulting from subduction of oceanic and continental lithosphere below Greece*, Geology, vol. 33, issue 4, pp. 325-328.
- van Hinsbergen D., Langereis C., Meulenkamp J., 2005b, *Revision of the timing, magnitude and distribution of Neogene rotations in the western Aegean region*, Tectonophysics, vol. 396, issue 1-2, pp. 1-34.
- van Kranendonk M., 2011, *Onset of plate tectonics*, Science, vol. 333, issue 6041, pp. 413-414.
- van Leeuwen T., Leach T., Hawke A., and Hawke M., 1990, *The Kelian disseminated gold deposit, east Kalimantan, Indonesia*, Journal of Geochemical Exploration, vol. 35, issues 1-3, pp. 1-61.
- Vargas R., Gustafson L., Vukasovic M., Tidy F., and Skewes M., 1999, *Ore breccias in the Rio Blanco-Los Bronces porphyry copper deposit, Chile*. In: Skinner B. (Ed.), *Geology and Ore Deposits of the Central Andes*, Society of Economic Geologists, Special Publication, No. 7, pp. 281-297.
- Vavelidis M., Michelidis K., Christofides G., and Boboti-Tsitlakides I., 1990, *Geochemical study of placer gold and the gold-bearing skarn-type mineralization of Kimmeria area, Xanthi district, NE Greece*, Geologica Rhodopica, vol. 2, 297-307.
- Vikre P., 1985, *Precious metal vein systems in the National district, Humboldt County, Nevada*, Economic Geology, vol. 80, issue 2, pp. 360-393.
- Vila T., and Sillitoe R., 1991, *Gold-rich porphyry systems in the Maricunga belt, northern Chile*, Economic Geology, vol. 86, issue 6, pp. 1238-1260.
- Vila T., Sillitoe R., Betzhold J., and Viteri E., 1991, *The porphyry gold deposit at Marte, northern Chile*, Economic Geology, vol. 86, issue 6, pp. 1271-1286.
- Vlasov K., 1966, *The Geochemistry of Rare Elements*, Israel Programme for Scientific Translations, Jerusalem.
- Voudouris P. & Alfieris D., 2005, *New porphyry-Cu±Mo occurrences in the north-eastern Aegean, Greece: Ore mineralogy and epithermal relationships*, In: Mao J. & Bierlein F. (Eds.), *Mineral Deposit Research: Meeting the Global Challenge*, VIII Biennial SGA Meeting, Beijing, China, pp. 473-476.
- Voudouris P. & Sakellaris G., 2008, *The Stanos shear zone-hosted Cu-Au-Bi deposit, Chalkidiki/N.Greece: new mineralogical and textural data*, In: Bortnikov N. (Ed.), *Proceedings of the XIII International conference on thermobarogeochemistry and IV APFIS symposium*, Moscow, vol. 1. pp. 247-250.
- Voudouris P., Mavrogonatos C., Melfos V., Spry P.G., Magganas A., Alfieris D., Soukis K., Tarantola A., Periferakis A., Kołodziejczyk J., Scheffer C., Repstock A., and Zeug M., 2019, *The geology and mineralogy of the Stypsi porphyry Cu-Mo-Au-Re prospect, Lesvos Island, Aegean Sea, Greece*, Ore Geology Reviews, vol. 112, <https://doi.org/10.1016/j.oregeorev.2019.103023>.
- Voudouris P., Melfos V., Moritz R., Spry P., Ortelli M., and Kartal T., 2010, *Molybdenite occurrences in Greece: mineralogy, geochemistry and rhenium content*. In: Christofides G., Kantiradis N., Kostopoulos D., and Chatzipetros A. (Eds.), *Scientific Annals of the School of Geology AUTH*, Proceedings of the XIX Congress of the Carpathian-Balkan Geological Association, Thessaloniki, pp. 369-378.
- Voudouris P., Melfos V., Spry P., Alfieris D., Mavrogonatos C., Repstock A., Djiba A., Stergiou C., Periferakis A., and Melfou M., 2018, *Porphyry and epithermal deposits in Greece: a review and new discoveries*. In: Uysal I. (Eds.), *8th Geochemistry Symposium Abstracts Book*, Trabzon, Turkey, pp. 181.
- Voudouris P., Melfos V., Spry P., Bindi L., Kartal T., Arikas K., Moritz R., and Ortelli M., 2009, *Rhenium-rich molybdenite and rheniite (ReS₂) in the Pagoni Rachi-Kirki Mo-Cu-Te-Ag-Au deposit in northern Greece: implications for the rhenium geochemistry of porphyry-style Cu-Mo and Mo mineralization*, Canadian Mineralogist, vol. 47, issue 5, pp. 1013-1036.
- Voudouris P., Melfos V., Spry P., Bindi L., Moritz R., Ortelli M., and Kartal T., 2013a, *Extremely Re-rich molybdenite from porphyry Cu-Mo-Au prospects in northeastern Greece: mode of occurrence, causes of enrichment, and implications for gold exploration*, Minerals, vol. 3, issue 2, pp. 165-191.
- Voudouris P., Melfos V., Spry P., Kartal T., Schleicher H., Moritz R., and Ortelli M., 2013b, *The Pagoni Rachi/Kirki Cu-Mo±Re±Au deposit, northern Greece: mineralogical and fluid inclusion constraints on the evolution of a telescoped porphyry-epithermal system*, The Canadian Mineralogist, vol. 51, issue 2, pp. 253-284.
- Voudouris P., Melfos V., Spry P., Bonsall T., Tarkian M. and Economou-Eliopoulos M., 2008, *Mineralogy and fluid inclusion constraints on the evolution of the Plaka intrusion-related ore system, Lavrion, Greece*, Mineralogy and Petrology, vol. 93, issue 1-2, pp. 79-110.

- Voudouris P., Tarkian M., and Arikas K., 2006, *Mineralogy of telluride-bearing epithermal ores in Kassiteres-Sappes area, western Thrace, Greece*, *Mineralogy and Petrology*, vol. 87, pp. 31-52.
- Walcott C. & White S., 1998, *Constraints on the kinematics of post-orogenic extension imposed by stretching lineations in the Aegean region*, *Tectonophysics*, vol. 298, issues 1-3, pp. 155-175.
- Walenta K. & Pantartzis P., 1969, *The molybdenite deposit of Kimmeria, Xanthi, northern Greece*, *Erzmetall*, vol. 22, pp. 272-278.
- Wallace A., 2003, *Geology of the Ivanhoe Hg-Au district, northern Nevada: influence of Miocene volcanism, lakes and active faulting on epithermal mineralisation*, *Economic Geology*, vol. 98, issue 2, pp. 409-424.
- Wallace S., 1995, *The Climax-type molybdenite deposits: what they are, where they are, and why they are [Presidential Address]*, *Economic Geology*, vol. 90, issue 5, pp. 1359-1380.
- Wallace S., Muncaster N., Jonson D., MacKenzie, W., Bookstrom A., and Surface V., 1968, *Multiple intrusion and mineralization at Climax, Colorado*. In: Ridge J. (Ed.), *Ore deposits of the United States, 1933-1967 (Graton-Sales Volume)*, American Institute Mining Metallurgy and Petroleum Engineers, New York, vol. 1, pp. 605-640.
- Wanhainen C., Broman C., and Martinsson O., 2003, *The Aitik Cu-Au-Ag deposit in northern Sweden: a product of high salinity fluids*, *Mineralium Deposita*, vol. 38, issue 6, pp. 715-726.
- Watanabe Y. & Hedenquist J., 2001, *Mineralogic and stable isotopic zonation at the surface over the El Salvador porphyry copper deposit, Chile*, *Economic Geology*, vol. 96, issue 8, pp. 1775-1797.
- Watanabe Y., 1995, *A tectonic model for epithermal Au mineralization in NE Hokkaido, Japan*, *Proceedings of the Sapporo International Conference on Mineral Resources of the NW Pacific Rim*, *Resource Geology*, Special Issue, No. 18, pp. 257-269.
- Watanabe Y., 2002, *Late Cenozoic metallogeny of southwest Hokkaido, Japan*, *Resource Geology*, vol. 52, issue 3, pp. 191-210.
- Waterman G. & Hamilton R., 1975, *The Sar Cheshmeh porphyry copper deposit*, *Economic Geology*, vol. 70, issue 3, p. 568-576.
- Webster J. & Mandeville C., 2007, *Fluid immiscibility in volcanic environments*. In: Liebscher A. & Heinrich C. (Eds.), *Fluid-Fluid Interactions, Reviews in Mineralogy and Geochemistry*, vol. 65, pp. 313-362.
- Webster J., 1990, *Partitioning of F between H₂O and CO₂ fluids and topaz rhyolite melt*, *Contributions to Mineralogy and Petrology*, vol. 104, issue 4, pp. 424-438.
- Wegener A., 1912, *Die Entstehung der Kontinente*, *Geologische Rundschau*, vol. 3, issue 4, pp. 276-292. [in German]
- Wegener A., 1922, *Die Entstehung der Kontinente und Ozeane*, Vieweg & Sohn Publikationen, Braunschweig. [in German]
- Westaway R., 2006, *Late Cenozoic extension in SW Bulgaria: a synthesis*. In: Robertson A. & Mountrakis D. (Eds.), *Tectonic Development of the Eastern Mediterranean Region*, Geological Society of London, Special Publication, No. 260, pp. 557-590.
- Westra G. & Keith S., 1981, *Classification and genesis of stockwork molybdenum deposits*, *Economic Geology*, vol. 76, issue 4, pp. 844-873.
- Westra, G., 1982, *Alteration and mineralization in the Ruth porphyry copper deposit near Ely, Nevada*, *Economic Geology*, vol. 77, issue 4, pp. 950-970.
- Whalen J., 1985, *Geochemistry of an Island-Arc Plutonic Suite: the Uasilau-Yau Yau Intrusive Complex, New Britain, P.N.G.*, *Journal of Petrology*, vol. 26, issue 3, pp. 603-632.
- White A. & Chappell B., 1983, *Granitoid types and their distribution in the Lachlan Fold Belt, southeastern Australia*. In: Roddick, J. (Ed.), *Circum-Pacific Plutonic Terranes*, Geological Society of America, Memoir, vol. 159, pp. 21-34.
- White A., 1979, *Sources of granite magmas*, Geological Society of America, Abstracts with Programs, vol. 11, pp. 539.
- White N., 1991, *High sulfidation epithermal gold deposits: characteristics, and a model for their origin*, Geological Survey of Japan, Report, No. 277, pp. 9-20.
- White W., Bookstrom A., Kamilli R., Ganster M., Smith R., Randa D., and Steininger E., 1981, *Character and origin of Climax-type molybdenum deposits*, *Economic Geology*, 75th Anniversary Volume, pp. 270-316.
- Whitney D. & Evans B., 2010, *Abbreviations for names of rock-forming minerals*, *American Mineralogist*, vol. 95, issue 1, pp. 185-187.

- Wildervanck J. & Jellinek F., 1964, *Crystallinity of molybdenum and tungsten sulfides*, Zeitschrift für Anorganische und Allgemeine Chemie, vol. 328, issues 5-6, pp. 309-318.
- Williams-Jones A. & Heinrich C., 2005, *Vapor transport of metals and the formation of magmatic-hydrothermal ore deposits*, Economic Geology, 100th Anniversary Volume, pp. 1287-1312.
- Williams-Jones A., Migdisov A., Archibald S., and Xiao Z., 2002, *Vapor transport of ore metals*. In: Hellmann R. & Wood S. (Eds.), *Water-Rock Interactions, Ore Deposits and Environmental Geochemistry, A Tribute to David A. Crerar*, The Geochemical Society, Special Publication, No. 7, pp. 279-305.
- Wilson A., Cooke D., and Harper B., 2003, *The Ridgeway gold-copper deposits: a high-grade alkaline gold deposit in the Lachlan fold belt, New South Wales, Australia*, Economic Geology, vol. 98, issue 8, pp. 1637-1666.
- Wilson J. & Yoffe A., 1969, *The transition metal dichalcogenides: discussion and interpretation of the observed optical, electrical and structural properties*, Advances in Physics, vol. 18, issue 73, pp. 193-335.
- Winter D., 2010, *Principles of Igneous and Metamorphic Petrology*, Pearson Prentice Hall Editions, New Jersey, 2nd Edition.
- Worsley M., 1995, *The controls on gold mineralisation at the Golden Plateau mine, Cracow, Queensland, Australia*, Ph.D. Thesis, James Cook University of North Queensland, Queensland.
- Wortel M. & Spakman W., 2000, *Subduction and slab detachment in the Mediterranean-Carpathian region*, Science, vol. 290, issue 5498, pp. 1910-1917.
- Xiong Y., Wood S., 2002, *Experimental determination of the solubility of ReS₂ and the Re-ReO₂ buffer assemblage and transport of rhenium under supercritical conditions*, Geochemical Transactions, vol. 3, issue 1, pp. 1-10.
- Yanev Y., 2003, *Mantle source of the Paleogene collision-related magmas of the Eastern Rhodopes (Bulgaria) and Western Thrace (Greece): characteristics of the mafic magmatic rocks*, Neues Jahrbuch für Mineralogie, vol. 178, issue 2, pp. 131-155.
- Yang J., 1991, *High rhenium enrichment in brown algae: a biological sink of rhenium in the sea?*, Hydrobiologia, vol. 211, issue 3, pp. 165-170.
- Zagorchev I., 1998, *Rhodope controversies*, Episodes, vol. 21, issue 3, pp. 159-166.
- Zajacz Z., Halter W., Pettke T., and Guillong M., 2008, *Determination of fluid/melt partition coefficients by LA-ICPMS analysis of coexisting fluid and silicate melt inclusions: controls on element partitioning*, Geochimica et Cosmochimica Acta, vol. 72, pp. 2169-2197.
- Zaluski G., Nesbitt B., and Muehlenbachs K., 1994, *Hydrothermal alteration and stable isotope systematics of the Babine porphyry Cu deposits, British Columbia; Implications for fluid evolution in porphyry systems*, Economic Geology, vol. 89, issue 7, pp. 1518-1541.
- Zehr J. & Ward B., 2002, *Nitrogen cycling in the ocean: new perspectives on processes and paradigms*, Applied Environmental Microbiology, vol. 68, issue 3, pp. 1015-1024.
- Zelikman A., Christyakov Y., Idenbaum G., and Krein O., 1961, *Crystal structure analysis of MoS₂ synthesized by various methods*, Kristallografya, vol. 6, pp. 389-394.
- Zelikman, A., Lobashev B., Makarov V., and Sevost'yanova G., 1976, *Kinetics and mechanism of the growth of molybdenum disulfide coatings on molybdenum*, Izvestiya Akademii Nauk SSSR, Seriya Khimicheskaya, vol. 12, pp. 1665-1667.
- Zen E., 1986, *Aluminum enrichment in silicate melts by fractional crystallisation: some mineralogical and petrographic constraints*, Journal of Petrology, vol. 27, issue 5, pp 1095-1117.
- Znamenskiy V., Lebedev L., and Sidorenko G., 1969, *Molybdenite from volcanic rocks of Quaternary age on Iturup Island, Kurile Islands*, Doklady Akademii Nauk SSSR, vol. 193, pp. 487-489.
- Zweng P. & Clark A., 1995, *Hypogene evolution of the Toquepala porphyry copper-molybdenum deposit, Moquegua, southeastern Peru*, Arizona Geological Society Digest, No. 20, pp. 566-612.